(6)

SOLID STATE ELECTRONICS LABORATORY

STANFORD ELECTRONICS LABORATORIES
DEPARTMENT OF ELECTRICAL ENGINEERING
STANFORD UNIVERSITY · STANFORD, CA 94305

STUDY OF THE ELECTRONIC SURFACE STATES OF III-V COMPOUNDS AND SILICON

Semi-Annual Technical Progress Report

1 October 1981 to 31 March 1982

Principal Investigators:

W. E. Spicer
I. Lindau

Telephone: (415) 497-4643

Office of Naval Research
Department of the Navy
Arlington, Virginia 22217

Sponsored by

DEFENSE ADVANCED RESEARCH PROJECTS AGENCY
DARPA Order No. 3564
Program Code No. HX1241
Contract No. N00014-79-C-0072

Effective: 1 October 1981 Expiration: 30 September 1982

STUDY OF THE ELECTRONIC SURFACE STATES OF III-V COMPOUNDS AND SILICON

Semi-Annual Technical Progress Report

1 October 1981 to 31 March 1982

Principal Investigators:

W. E. Spicer
I. Lindau

Telephone: (415) 497-4643

Office of Naval Research
Department of the Navy
Arlington, Virginia 22217

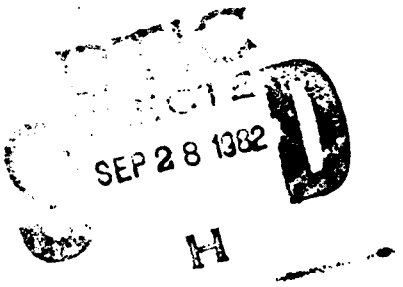

Sponsored by

Defense Advanced Research Projects Agency
DARPA Order No. 3564
Program Code No. HX1241

Contract No. N00014-79-C-0072

Effective: 1 October 1981 Expiration: 30 September 1982

Stanford Electronics Laboratories
Stanford University
Stanford, California 94305

TABLE OF CONTENTS:

states on III-V compounds'" to be published in Thin Solid Films.

K. I. Lindau and W. E. Spicer, "The Use of Synchrotron Radiation to Study Oxygen and Metal Overlayers on GaAs (110) Surfaces," in Electron Spectroscopy; Theory, Techniques, and Applications, Ed. C. R. Brundle and A. D. Baker (Academic, 1981), p. 197.

L. Stephen J. Eglash, Shihong Pan, William E. Spicer, and Douglas M. Collins, "Modified Schottky Barrier Heights by Interfacial Doped Layers: MBE Al on GaAs," submitted to Int. Conf. Solid St. Dev. (Tokyo, 1982).

M. Papers published during this period.

A. Introduction and Overview

Our work on the electronic and atomic structure of surfaces and interfaces of the III-V compound semiconductors and Si has proceeded in numerous directions. These include: 1) the interfaces of the column IV elemental semiconductors, Ge and Si, with various metals, especially the transition and noble metals; 2) studies of the III-V compound semiconductor surfaces, as well as the individual column III and column V constituents of the compounds; 3) the continued refinement of the unified defect model for surface and interface states formation on the III-V compound semiconductors (developed by our group), including a comphrehensive comparison between our results and the work of others; 4) the continued exploitation of synchrotron radiation in photoemission and other studies; 5) the successful application of fundamental studies by our group to useful and new electronic device structures; 6) the purchase of a laser for use in a wide range of surface studies which include surface recombination and enhanced oxidation behavior; and 7) the preparation and testing of an ultrahigh vacuum chamber for preliminary cleaving and photoluminescence studies.

Extensive discussion of many of these topics may be found in the following pages. Additional discussion of those and other subjects appears in our earlier progress reports and contract renewal proposals.

B. Summary review: Si/metal interfaces

We have extended our investigations of the valence band structure of Si/metal interfaces to the Si/Mo[1] (refractory metal) and Si/Yb[2] (rare earth) systems.

By applying the Cooper minimum method[3] of h dependent photoemission to the Si/Mo valence band we were able to distinguish the main features of the bonding mechanisms at this interface. In the coverage interval between 0.5 and 20 monolayers (ML), the room temperature (RT) deposition of Mo onto vacuum cleaved Si(111) 2 x 1 surfaces produced a mixed phase in which the electronic structure is a hybridization of Mo 4d and Si 3p electrons. This conclusion comes from the analysis of the Cooper minimum data, changes in the Si contributions to the valence band, and the $h\nu$ dependence of the different peaks having d-character. These results confirm our previous explanation of the Si/near-noble metal interfaces, and support that the main features of such a scheme[3] are valid also for the Si/refractory metal interfaces (i.e. d orbitals with a low occupation number). X-ray photoemission and Auger electron spectroscopies indicate intermixing and the changes in the Si $L_{2,3}VV$ lineshape also shows that the density-of-states (DOS) of the Si atoms in the mixed region is different from that of pure Si.

The Si/Yb system has been prepared in a similar way in ultra-high vacuum, and the evolution of the valence band (V.B.) energy distribution curves versus Yb coverage has been followed by synchrotron radiation photoemission of valence and core states, and photon stimulated Si $L_{2,3}VV$ Auger lineshape spectroscopy. The V. B. DOS is dominated by Yb 4f emission. The 4f peak shifts toward the bulk Yb binding energy position (close to E_F) with increasing coverage. At the 1 and 2 ML coverages evidence of a

B. Summary review: Si/metal interfaces

We have extended our investigations of the valence band structure of Si/metal interfaces to the Si/Mo[1] (refractory metal) and Si/Yb[2] (rare earth) systems.

By applying the Cooper minimum method[3] of h dependent photoemission to the Si/Mo valence band we were able to distinguish the main features of the bonding mechanisms at this interface. In the coverage interval between 0.5 and 20 monolayers (ML), the room temperature (RT) deposition of Mo onto vacuum cleaved Si(111) 2 x 1 surfaces produced a mixed phase in which the electronic structure is a hybridization of Mo 4d and Si 3p electrons. This conclusion comes from the analysis of the Cooper minimum data, changes in the Si contributions to the valence band, and the $h\nu$ dependence of the different peaks having d-character. These results confirm our previous explanation of the Si/near-noble metal interfaces, and support that the main features of such a scheme[3] are valid also for the Si/refractory metal interfaces (i.e. d orbitals with a low occupation number). X-ray photoemission and Auger electron spectroscopies indicate intermixing and the changes in the Si $L_{2,3}VV$ lineshape also shows that the density-of-states (DOS) of the Si atoms in the mixed region is different from that of pure Si.

The Si/Yb system has been prepared in a similar way in ultra-high vacuum, and the evolution of the valence band (V.B.) energy distribution curves versus Yb coverage has been followed by synchrotron radiation photoemission of valence and core states, and photon stimulated Si $L_{2,3}VV$ Auger lineshape spectroscopy. The V. B. DOS is dominated by Yb 4f emission. The 4f peak shifts toward the bulk Yb binding energy position (close to E_F) with increasing coverage. At the 1 and 2 ML coverages evidence of a

chemical reaction between Si and Yb are given both by the position and shape of the Yb 4f emission, and by the presence of a chemically shifted Si 2p peak along with the unshifted Si peak. The reaction kinetics appear to be low at RT, and a Yb rich layer is obtained by 4 monolayers. A higher thermal activation energy appears to be necessary to enhance mixing and compound formation.

Other Si/ and Ge/metal interfaces have been studied: Si/Ba and Ge/Au. The analysis of the data on these systems is in progress.

1. G. Rossi, I. Abbati, L. Braicovich, I. Lindau, and W. E. Spicer, to be published in J. Vac. Sci. Technol.
   L. Braicovich, S. Nenarone, V. del Pennino, W. E. Spicer, I. Lindau, I. Abbati, and G. Rossi, Abstract to the 16th International Conf. on the Physics of Semiconductors, Montpellier (1982).
2. G. Rossi, S. Nanarone, V. del Pennino, I. Abbati, L. Braicovich, I. Lindau, and W. E. Spicer to be published.
3. G. Rossi, I. Abbati, L. Braicovich, I. Lindau, and W. E. Spicer, Solid State Comm. 39, 195 (1980).

C. G. Rossi, I. Abbati, L. Braicovich, I. Lindau, and W. E. Spicer, "Ge-Ag interface at room temperature: An energy-dependent photo emission study," submitted to Physical Review B.

PHYSICAL REVIEW B VOLUME 25, NUMBER 6 15 MARCH 1982

Ge-Ag interface at room temperature: An energy-dependent photoemission study

G. Rossi, I. Abbati,* L. Braicovich,* I. Lindau, and W. E. Spicer†
Stanford Electronics Laboratory, Stanford University, Stanford, California 94305
(Received 28 August 1981)

The electronic structure of the Ge(111)-Ag interface has been studied using synchrotron radiation photoemission of the valence band at $h\nu$=40.8, 80, and 130 eV (Cooper minimum for Ag 4*d* electrons) and of the Ge 3*d* and Ag 3*d* core lines at $h\nu$=120 and 450 eV, respectively. By using extensively the Cooper-minimum techniques it was clearly demonstrated that in the first monolayers (2–3) a strong chemical interaction takes place between Ge and Ag at room temperature with incorporation of Ag into the Ge surface lattice. Further Ag growth on top of the intermixed region follows the Stransky-Krostanov mechanism with almost pure Ag island formation. The present data constitute the first evidence of intermixing at the Ge-Ag interface.
MS code no. BH2120 1977 PACS numbers: 73.40–c, 79.60.Eq

I. INTRODUCTION

The elemental semiconductor–noble-metal interface is a subject of great interest and a growing number of systematic studies have recently appeared in the literature.[1–7] One of the reasons for this interest is that no stable bulk compounds (i.e., stable silicides or germanides) are known for these systems, and contrary to the case of the reactive "*d*" metal-semiconductor systems,[8] the formation of an abrupt interface could be expected when the noble metal is deposited on top of a semiconductor surface, as the traditional model for the Schottky barrier assumes.[19] In the cases of Si + Au and Si + Cu,[1,2,7] however, it is clear that considerable intermixing takes place and the interface has a nonzero width that has been interpreted as an alloy phase whose extension is possibly connected with the heat of formation of the Si-metal bond.[10] The Si + Ag interface has been described as atomically abrupt in a photoemission report by McKinley *et al*,[3] whereas no spectroscopic information is available in the literature for Ge + Ag. The aim of the present paper is to present an extensive set of photoemission results on Ge + Ag. We show that on the scale of 1–3 monolayers a strong chemical reaction takes place with a severe intermixing at the interface. This new result has its counterpart in recent experimental observations for Si-Ag which are being published elsewhere[5,6] and implies a change in the generally accepted picture for elemental semiconductor-Ag interfaces.

The present results come from a photoemission investigation with synchrotron radiation (SR) in which considerable experimental efforts have been devoted to the growth of submonolayer films in order to follow, step by step, the formation of the first Ag monolayer. The most relevant changes in the interface chemistry are expected in this coverage interval.

Taking advantage of the unique tunability of synchrotron radiation (SR), we have exploited energy dependent photoemission, obtaining valence-band energy distribution curves (EDC's) at the Cooper minimum for the Ag 4*d* orbitals ($h\nu$=130 eV), where the *d* cross section for photoionization is strongly reduced and the substrate valence density of states can be revealed, and at two photon energies ($h\nu$=40.8 and 80 eV) where the metal *d* contribution is the dominant emission. This technique has been described earlier by Rossi *et al.*[11] and successfully applied to the reactive semiconductor–transition-metal interfaces and is of particular value in this case where the presence of a rather small amount of intermixing requires a high sensitivity to the details of the different contributions to the valence-band emission at the interface. The Cooper-minimum technique is complemented by an analysis based on the electron escape depth which has already been used in the Si–noble-metal cases (Cu and Au).[1,4]

The organization of the paper is as follows: Details on the experiment are given in Sec. II and a full review of the experimental results and their internal organization is given in Sec. III. The discussion of Sec. IV is divided into three coverage intervals showing different stages in the interface growth. The summary is given in the concluding paragraph.

II. EXPERIMENTAL

Medium doped, *n*-type, germanium single crystals were cleaved *in situ* along the (111) plane at an operative pressure of 5×10^{-11} Torr. The high reproducibility of the clean valence-band EDC provides us with a good assumption that no relevant differences are present among the various Ge(111) surfaces, although we had no independent technique to check the cleavage quality.

The thin overlayers of Ag were prepared by evaporation from a bead on a tungsten wire, and the thickness was obtained using two quartz crystal monitors. The first crystal monitor was very close to the evaporation source, behind the evaporator shield; the second one was on the sample carousel and could be put in the sample position. The first crystal monitor was carefully calibrated against the second one in order to have the exact geometric correction factor. The desired coverages were typically obtained during a few seconds of evaporation by operating a shutter in front of the source and continuously monitoring the evaporation rate by means of the first thickness monitor. With this procedure we estimated a maximum error of 20% for the very low submonolayer coverages, and 5% or less for the higher coverages. The photoemission spectra obtained at submonolayer coverages on different cleaves had high reproducibility and consistent phenomenological trends for the estimated coverages. The evaporation source was positioned more than 10 cm away from the sample surface to avoid heating of the substrate; also the heating problem was reduced because of the low power required for Ag evaporations. The maximum pressure during the evaporation was 1×10^{-10} Torr, with all the low coverages done at 9×10^{-11} Torr. The photoelectron spectra were taken in the retarding mode with a double pass cylindrical mirror analyzer having the axis normal to the sample surface. The radiation source was the two 4° beam lines at the Stanford Synchroton Radiation Laboratory[12] (SSRL) equipped with a "grasshopper" monochromator[13] providing an intense *p* polarized monochromatic beam in the range 35–500 eV. The spectra at $h\nu=40.8$ eV were taken on the "new" 4° beam line at SSRL covering the photon energy range 35–500; all the other measurements were taken on the "old" 4° line covering the region 65–900 eV. The light was impinging on the sample surface at grazing incidence (15°). Very high counting rates, typically on the order of 10^4 count/s, were obtained at all the energies used, giving high statistical quality to the data. More details on the experimental apparatus were published by Pianetta *et al.*[14].

The kinetic energies of all the measurements were in the range 35–120 eV which gives the maximum surface sensitivity [escape depth 5–6 Å (Ref. 15)]. All the data are in this way directly comparable, referring to the same sampled region of the interface.

III. RESULTS

This section summarized the experimental results discussed in Sec. IV. To make the discussion easier, we present relevant experimental trends in representative plots. Figures 1 and 2 give the coverage dependence of the valence band EDC's $h\nu=80$ eV and at the Cooper minimum ($h\nu$ 0 eV). Figure 3 gives the EDC's at $h\nu=40.8$ e selected low coverages and for the high cover

In the EDC's at $h\nu=40.8$ eV (Fig. 3) and $h\nu=80$ eV (Fig. 1), the Ag 4*d* contribution is inant over the Ge *sp* contribution due to the r tively much higher cross section for the photoionization of the 4*d* orbitals. This makes it possible to easily detect the role of Ag in the determination of the valence density of states even when at very low [0.03 monolayers (ML)] Ag coverages. At $h\nu=130$ eV (Fig. 2), the 4*d* cross section[16] has a deep minimum (Cooper minimum) so that the *d* contribution seen in the EDC is of the same order of magnitude as that due to the *sp* band of the Ge substrate. In this case the modification of the substrate electronic structure can be clearly followed. The physical information coming from Ge 3*d* and Ag 3*d* core lines are summarized as a function of the coverage in Figs. 4 and 5 (intensities versus coverage) and in Fig. 6 (binding energy versus coverage).

IV. DISCUSSION

In this section we discuss the results by making a division into three coverage regions which correspond to three different stages in the interface growth: the very low submonolayer coverages [Sec. IV A ($\theta\leq0.3$ ML)], the completion of the first monolayer [Sec. IV B (0.3 ML $<\theta<$ 1.08 ML)], and the high coverages interval extending up to 10 monolayers (Sec. IV C). This division into three regions is merely to provide a phenomenological frame for the discussion, since different dom-

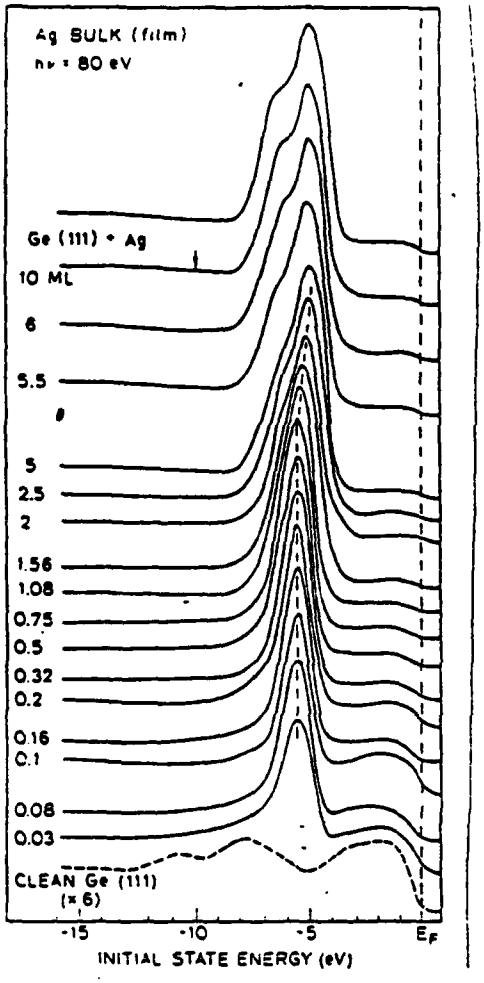

FIG. 1. Angle-integrated photoelectron energy distribution curves (EDC's) at $h\nu = 80$ eV for Ge(111) + Ag at increasing coverages at room temperature, and for bulk Ag (film). The Ag coverages θ quoted in the figure are in monolayer units.

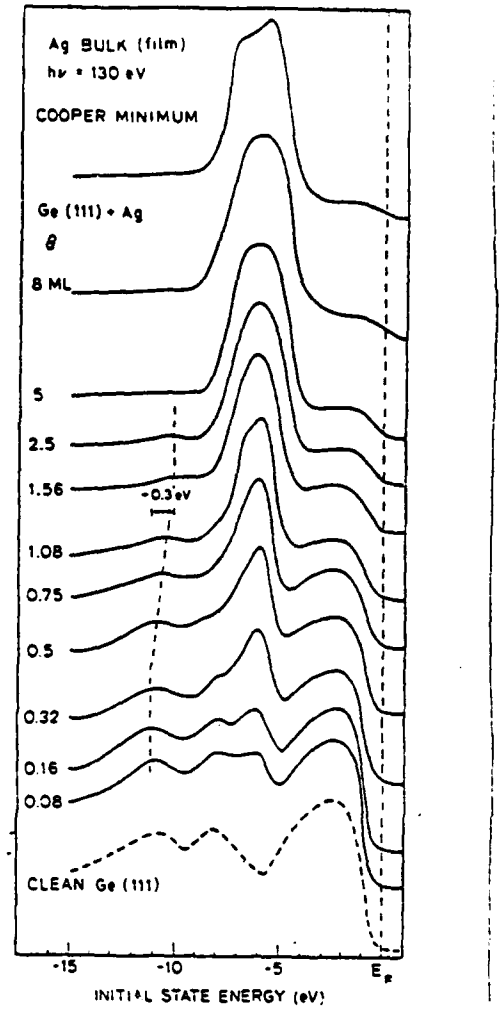

FIG. 2. Angle-integrated EDC's for Ge(111) + Ag and for bulk Ag (film) at the Cooper minimum for the Ag 4*d* photoionization cross section ($h\nu = 130$ eV). The coverages θ are in monolayer units.

inant features are seen in these regions. However, there is no fundamental reason to separate these intervals since the properties of the interface are continuously changing throughout the whole coverage interval investigated.

A. Low-coverage region ($\theta \lesssim 0.3$ ML)

At the very lowest coverages the Ag 4*d* signal is composed of a sharp peak, almost symmetrical in shape, at 6 eV below the Fermi level, i.e., at higher binding energies than in the Ag bulk. This situation is common to all the semiconductors—noble-metal interfaces and is usually explained as a situation where the noble-metal atoms are almost isolated at the substrate-vacuum interface and the photoemission peak is more atomiclike than bandlike.[1,2,5] This also has consequences on the core line binding energies as will be discussed later in Sec. IV D. The 4*d* peak grows in intensity without shifts in energy, within the accuracy of the experiment, up to 0.3 ML as seen in the $h\nu = 80$ eV EDC's of Fig. 1. The Ag 3*d* core lines grow in intensity linearly with the increase in coverage; the

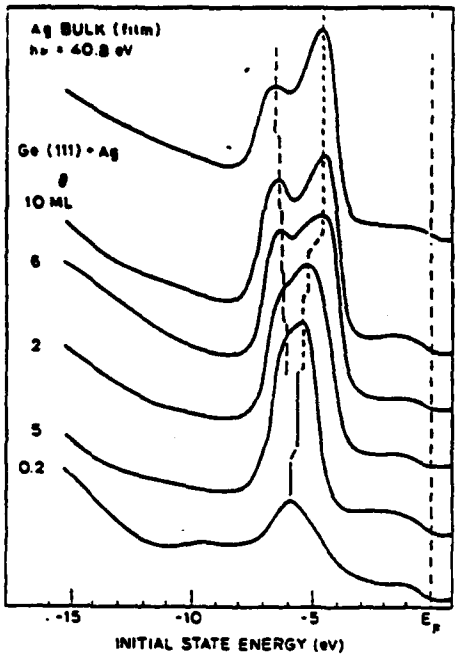

FIG. 3. Angle-integrated EDC's for Ge(111) + Ag and for pure Ag (film) at $h\nu$=40.8 eV. Due to matrix elements effects the evolution of the Ag 4*d* peak shape is much more evident than at the other energies used.

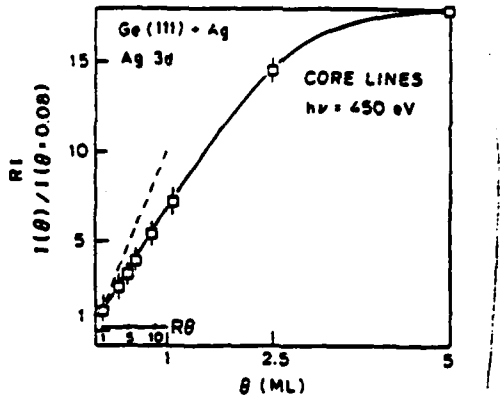

FIG. 5. Intensity profile of Ag 3*d* core line photoemission as a function of the coverage. The reduced intensity (*RI*) [$I(\theta)/I(\theta=0.08)$] is plotted versus the reduced coverage $R\theta$ (θ/0.08 ML) for the submonolayer range. In the submonolayer range, the dashed line shows the expected trend for *RI* vs $R\theta$ in the case of the formation of a uniform monolayer.

decrease of the Ge 3*d* intensity is also linear.

At the Cooper minimum (Fig. 2) it is possible to see the beginning of the Ag signal already at θ=0.08 with no appreciable modifications of the Ge valence band at these coverages. Nothing can be said about the Ge surface states in this range since the photon energies used give very little sensitivity to those states.

The situation in this low-coverage region is quite different from that of the highly reactive interfaces like Si-Pt where dramatic changes in the substrate emission are already seen for 0.1 ML of metal, probably due to a surface disruption mechanism.[17] This confirms the known fact that the interaction between Ag and Si is definitely weaker than in the higher reactive cases.

B. The first monolayer formation (0.3 < θ < 1 ML)

The second region is more interesting because it is possible to see the beginning of a gradual shift

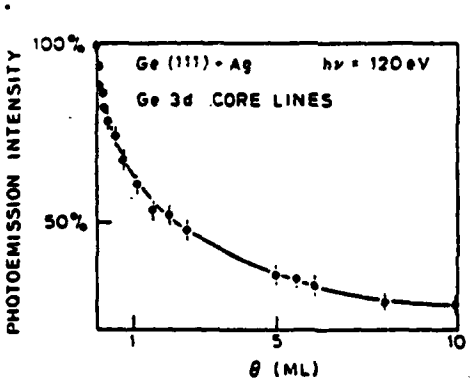

FIG. 4. Intensity profile of Ge 3*d* core line photoemission as a function of the coverage. The intensities are normalized to the clean Ge(111) signal.

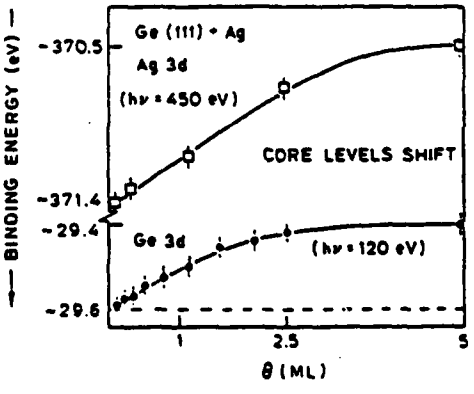

FIG. 6. Binding energy shifts for Ge 3*d* and Ag 3*d* core lies as a function of the coverage θ. The curves are the best fits of the experimental data.

of the Ag 4*d* band towards lower binding energies, i.e., towards a more bandlike situation (see Fig. 1). But the key point in the understanding of the interface growth is seen in the spectra at $h\nu = 130$ eV of Fig. 3, where the shift towards lower binding energies of the deepest structure (10.5 eV below E_F), mostly composed of Ge *s* states, takes place and is almost completed within this interval. In this respect it should be noted that the general trend of this structure is a shift towards lower binding energies whenever the sp^3 configuration, which is known to give the maximum bandwidth,[18] is modified. Thus a shift of this structure towards lower binding energy has been observed in all the elemental semiconductor—*d*-metal reactive interfaces where compounds are formed.[17,19,20] In the present case the shift is thus the first direct spectroscopic evidence of a chemical interaction taking place between Ag and Ge at the interface with the formation of new hybrid orbitals between the two atomic species so that the sp^3 configuration is modified.

The total shift in this case is ~ 0.3 eV, which is less than the analogous shift observed for the Si—transition-metal "reactive" interfaces, where shifts of 1 eV have been detected, e.g., for Si-Pd (Refs. 11 and 19) and Si-Pt.[17] The explanation of this difference can probably be found in the fact that the Ge-Ge covalent bond is weaker than the Si—Si covalent bond and the Ge atomic arrangement is probably less distorted when interacting with Ag than it is in the very reactive cases.[20] We emphasize that the present paper gives the first information on the distortion of the sp^3 configuration in Ge due to the interaction with a metal, and the first set of Cooper-minimum data on a Ge—*d*-metal interface. Thus there are no other data available for comparison.

Photoemission data cannot give structural information, but nevertheless it can be very useful to address the question of the average depth distribution of the Ag atoms in the interface. This can be assessed on the basis of the core lines intensities versus coverage. Plots of the Ag 3*d* core line emission intensities after normalization to the 0.08 ML coverage, and of the Ge 3*d* core line intensities are given in Figs. 4 and 5, respectively. The values of the Ag 3*d* curve up to one monolayer are, in the manner the data are plotted, independent of the absolute calibration of the thickness monitor, and the information is very reliable. One can see that the increase of the Ag 3*d* signal intensity is smaller at the submonolayer coverages than should be expected if a uniform layer were formed. In other words, when the coverage is doubled within these submonolayer coverages, the photoemission intensity of Ag is not doubled; typically 30% of the signal is lost. This provides evidence that Ag must penetrate into the sample, and at least part of it is beneath the first layer.

Our results are qualitatively similar to those recently found by means of surface potential and ion scattering spectroscopy (ISS) (Ref. 21) measurements where the reconstructed $(\sqrt{3}\times\sqrt{3})$ Ag layer was concluded to lie beneath a pure Si surface layer after heating to 400 °C.

It is important to note that this argument is fairly unambiguous for small coverages. An alternative assumption of early Ag agglomeration at < 1 could hardly explain the data. The formation of Ag islands of such large dimensions that a considerable fraction of the signal is lost due to escape depth effects[22] cannot be favored.

Thus a clear result of the present research is that a strong chemical interaction takes place between Ag and Ge, and that the Ge surface is disrupted with the incorporation of Ag in the topmost layer of the substrate. How deep Ag goes into the surface is difficult to assess, but on the basis of escape depth considerations it is possible to conclude that almost all Ag is within the first 2—3 layers of material.

C. The high-coverage interval $(1 < \theta < 10)$

In the high-coverage interval the three most relevant observations are the following:

(i) The valence spectra evolve towards the EDC's typical of pure Ag which is basically reached between 6 and 10 ML (see Figs. 1—3).

(ii) The Ge 3*d* emission intensity, although decreasing, remains considerably high, i.e., about 30% of the signal typical for pure Ge is still present at the high coverages.

(iii) The binding energy shift of the Ge 3*d* core levels reaches a plateau above 2.5 ML.

These experimental results give indications about the growth mechanism of Ag on top of the first intermixed Ge-Ag overlayer. It is also apparent that structural investigation like low-energy electron diffraction (LEED) IV profiles, ISS, and surface extended x-ray absorption fine structure (EXAFS) would be important complements to the present results.

The fact than an almost pure Ag valence band

EDC is obtained for coverages larger than 6 ML is not compatible with the presence of a substantial quantity of Ge (which is obviously present as seen from the intense 3*d* core signal) in a intermixed phase. In fact the valence band for a thick intermixed layer should be dramatically different from that of the pure metal as has been shown, for example, in the case of Si-Au intermixed phases.[1,7] Probably a minor fraction of Ge is still present in the overlayer, as will be discussed later, but the presence of the strong Ge core signal intensity must be thought of as originating from a spatially distinguished region of the surface with respect to that originating the Ag signal.

The presence of an intense Ge 3*d* signal is compatible with two models: the island growth or Stransky-Krostanov (SK) mechanism and the layer-by-layer (Van de Merwe) growth of Ag, with some Ge dissolved, and with Ge segregated to the topmost surface layer. Surface segregation from the substrate has been found in some related systems, Si-Au (Ref. 1) and Si-Cu (Ref. 2) at room temperature, and Si-Pd after annealing.[23]

Our photoemission data cannot be conclusive on this point, but some clear indications are present in the valence-band and core level data. In the case of a Ge surface on top of a Ag-rich layer some spectroscopic evidence of Ge—Ag bonds should be expected. This situation in fact should be similar to that present on the bulk side of the interface when Ag atoms are in contact with the Ge substrate, which has been studied at the low Ag coverages. The presence of strong bonds between a metal-rich phase and a segregated top layer of semiconductor has clearly been found for the annealed Pd-Si interface.[22] From the present data no indications of such a situation are evident so that the alternative model of Ag island formation appears likely. We can explain the photoemission results as a sum of the signal coming from Ag-rich islands and from the uncovered part of the Ge-Ag mixed phase, 2—3 layers thick.

In this case the decrease of peak *C* in the Cooper-minimum spectra of Fig. 2 at increasing coverages can be explained with the gradual decrease of the uncovered area, as more Ag is deposited, and with the smaller emission with respect to the strong Ag signal coming from the islands.

Our data suggest a model of a complex interface with a narrow mixed interface, two or three layers thick, and almost pure Ag islands grown on top of it. This model could also explain the constant value of the Ge binding energy at the high coverages. The Ge atoms are either in the "stable" intermixed region or very diluted in the Ag islands and are not very sensitive to further Ag enrichment. The presence of two different species of Ge is given further support by a slight broadening (~0.1 eV) observed at large θ for the Ge 3*d* core lines.

Further information is obtained analyzing the spectra taken at $h\nu=40.8$ eV (Fig. 3) which are very useful in this high-coverage range. At this photon energy the 4*d* splitting into two peaks is much more evident than at $h\nu=80$ eV where only a shoulder on the higher binding energy side of the peak appears. The splittings has a crystal-field contribution that starts to build up only a relatively high coverages ($\theta=6$) and the bulklike situation is completely reached with 10 ML. This provides evidence that the dimensions of the Ag islands are large enough around 10 ML to produce Ag clusters with a typical bulklike photoemission signal, and indirectly confirms that some Ge is present in the early stage of the Ag island growth, becoming eventually a negligible impurity at the high coverages. It would be premature at the present time to push these arguments further and make a detailed model because of the arbitrariness of several parameters and the lack of more direct structural investigation on this interface.

Thus we will limit ourselves to state that the spectra suggest a qualitative picture for the Ag growth which is basically in agreement with the SK mechanism as proposed by Venables *et al.* for Ag-Si,[24] provided that the actual substrate on which the island growth takes place is not a single Ag chemisorbed layer but a mixed Ge-Ag phase two or three layers thick.

Our picture for the Ge-Ag interface contrasts the one proposed for Si-Ag by McKinley *et al.*[3] In fact, these two silver-elemental semiconductor systems should be very similar, and the model of an atomically abrupt junction is oversimplified as the present results and recent reports on Si-Ag demonstrate.[5,6,21] In this connection we also note that Venables *et al.*[24] have shown that at room temperature, the Stransky-Krostanov and Van der Merwe growths become very similar due to the presence of almost two-dimensional islands so that a clear distinction between the two processes becomes highly speculative, although SK growth was shown to be favored in the Si-Ag case at high coverages.[24]

In summary, our results show that such phenomenology is also applied to Ge-Ag. We are also able to add new information. In particular we demonstrated that the bond between Ag and Ge

has characteristics similar to those of the bands between Si and other *d* metals usually referred as more "reactive."[5] We further showed that the intermediate layer in the SK is a strongly intermixed Ge-Ag phase; and that in the beginning of the nucleation of islands some Ge is still present dissolved with Ag. The presence of this alloyed Ge-Ag phase is probably responsible for the quick convergence towards almost pure Ag overgrowth in the sense that it acts as a membrane against the interdiffusion. The hindrance of an extended intermixing due to this membrane effect is consistent with recent results by Cros *et al.*[25] They prepared a Si-Au-Ag interface with a monolayer of Au deposited onto a Si(111) substrate before growing the Ag film, and observed a strong intermixing of Si and Ag. The interpretation is that the weakening of the Si—Si covalent bond caused by the Si-Au mixed phase makes the Ag-Si interdiffusion easier. Tentatively, transferring this argument to the Ge-Ag case we could say that in absence of *ad hoc* weakening processes the Ag-Ge reaction and intermixing is very quickly saturated. Further studies on the temperature dependence of the excitation of this phase could give more insight on the kinetic of this interface reaction.

V. CONCLUSIONS

A systematic spectroscopic investigation of the Ge-Ag interface at room temperature, making use of the Cooper minimum method and at high surface sensitivity, shows that intermixing takes place at the Ge-Ag interface with the formation of bonds between Ge and Ag atoms in a region extending for 2—3 layers of material. On top of this intermixed region the Ag metal grows in islands with a small amount of Ge dissolved in it. Thus the Ge-Ag interface cannot be considered as a sharp interface and the interpretation of its electronic properties [in particular the very low Schottky barrier height ~0.35 eV (Ref. 26)] cannot rely upon the traditional abrupt junction models[9] but requires the consideration of the role played by the electronic states formed as a consequence of the intermixing processes.

ACKNOWLEDGMENTS

This work was supported by the Gruppo Nazionale di Struttura della Materia of the Consiglio Nazionale della Ricerca, Italy and by the Advanced Research Projects Agency of the Department of Defense under Contract No. N00014-79-C-0072. The experiments were performed at the Stanford Synchrotron Radiation Laboratory which is supported by the National Science Foundation under Grant No. DMR77-27489 in collaboration with the Stanford Linear Accelerator Center and the Department of Energy.

---

*Permanent address: Instituto di Fisica del Politecnico, Milano, Italy.

†Stanford Ascherman Professor of Engineering.

[1]L. Braicovich, C. M. Garner, P. R. Skeath, C. Y. Su, P. W. Chye, I. Lindau, and W. E. Spicer, Phys. Rev. B 20, 5121 (1979).

[2]I. Abbati and M. Grioni, J. Vac. Sci. Technol. 19, 636 (1981).

[3]A. McKinley, R. H. Williams, and A. W. Parke, J. Phys. C 12, 2447 (1979).

[4]I. Abbati, L. Braicovich, and A. Franciosi, Phys. Lett. 80A, 69 (1980).

[5]G. Rossi, I. Abbati, L. Braicovich, I. Lindau, and W. E. Spicer, Surf. Sci. Lett. (unpublished).

[6]G. Rossi, I. Abbati, I. Lindau and W. E. Spicer (unpublished).

[7]R. Weibman, G. Fisher, and K. Müller, Abstract at the ICSFS 2 Conf., Maryland 1981 (in press).

[8]The common definition "reactive *d*-metal—semiconductor interfaces" refers to those systems that give silicidelike or germanidelike compounds, e.g., Si-Pd, Si-Pt, Si-Ni (Refs. 9, 11, 12, and references quoted therein), Ge-Pd, Ge-Ni (Ref. 13). Usually the noble metal—elemental semiconductor interfaces are not termed "reactive," also if considerable intermixing takes place as for Si-Au and Si-Cu, because of the absence of stable stochiometric bulk silicides.

[9]J. Bardeen, Phys. Rev. 71, 717 (1947).

[10]J. M. Andrews and J. C. Phillips, Phys. Rev. Lett. 35, 56 (1975).

[11]G. Rossi, I. Abbati, L. Braicovich, I. Lindau, and W. E. Spicer, Solid State Commun. 39, 195 (1981).

[12]S. Doniach, I. Lindau, W. E. Spicer, and H. Winick, J. Vac. Sci. Technol. 12, 1123 (1975).

[13]F. C. Brown, R. Z. Bachrach, and N. Lien, Nucl. Instrum. Methods 152, 73 (1978).

[14]P. Pianetta, I. Lindau, and W. E. Spicer, in *Quantitative Surface Analysis of Materials, A Symposium Sponsored by ASTM Committee E-42 on Surface Analysis, Cleveland, Ohio, March 1977, Special Technical Publications 643*, edited by N. S. McIntyre (American Society for Testing and Materials, Philadelphia, 1978), pp. 105–123.
[15]H. Gant and W. Mönch, Surf. Sci. 105, 217 (1981).
[16]L. I. Johansson, I. Lindau, M. M. Hecht, and E. Källne, Solid State Commun. 34, 83 (1980).
[17]G. Rossi, I. Abbati, L. Braicovich, I. Lindau, and W. E. Spicer, Abstract in 41st Physical Electronic Conf. program and *Phys. Rev. B* (in press).
[18]J. A. Appelbaum and D. R. Hamann, Rev. Mod. Phys. 48, 479 (1976).
[19]I. Abbati, G. Rossi, L. Braicovich, I. Lindau, and W. E. Spicer, J. Vac. Sci. Technol. 19, 636 (1981); G. W. Rubloff, P. S. Ho, J. F. Freeouf, and J. E. Lewis, Phys. Rev. B 23, 4183 (1981).
[20]I. Abbati, G. Rossi, I. Lindau, and W. E. Spicer, Appl. Surf. Sci. (unpublished).
[21]K. Oura, T. Taminaga, and T. Hanawa, Solid State Commun. 37, 523 (1981); M. Saitoh, F. Shoji, K. Oura, and T. Hanawa, Jpn. Appl. Phys. 19, L421 (1980).
[22]E. Bauer, Proceedings of the ICSFS 2 Conf., Maryland 1981, in Applications of Surface Science (in press).
[23]I. Abbati, G. Rossi, I. Lindau, and W. E. Spicer, J. Appl. Phys. (in press).
[24]D. A. Venables, J. Derrien, and A. P. Janssen, Surf. Sci. 95, 411 (1980).
[25]A. Cros, F. Salvan, and J. Derrien, Phys. Rev. B (in press).
[26]G. Ottaviani, R. N. Tu, and J. W. Mayer, Phys. Rev. Lett. 44, 289 (1980).

D. G. Rossi, I. Abbati, L. Braicovich, I. Lindau, and W. E. Spicer, "The Si(111)/Pt Interface at Room Temperature: An Synchrotron Radiation Photoemission Study," submitted to Physical Review B.

PHYSICAL REVIEW B VOLUME 25, NUMBER 6 15 MARCH 1982

Si(111)-Pt interface at room temperature: A synchrotron radiation photoemission study

G. Rossi, I. Abbati,* L. Braicovich,* I. Lindau, and W. E. Spicer
Stanford Electronics Laboratory, Stanford University, Stanford, CA 94305
(Received 24 August 1981)

We present extensive results on synchrotron-radiation angle-integrated photoemission from Si(111) surfaces onto which increasing amounts of Pt (coverages Θ from 0.07 to 40 monolayers) were deposited. Both core lines (Si $2p$ and Pt $4f$) and valence-band states have been measured. In the latter case we present results taken at a photon energy of $h\nu=80$ eV where the Pt $5d$ contribution is dominant and at $h\nu=130$ eV where the Cooper minimum effect reduces the Pt $5d$ photoemission considerably so that information on the Si contribution to the valence states can be revealed. We show that submonolayer coverages ($\Theta \gtrsim 0.07$) of Pt disrupt the surface sufficiently to introduce considerable changes in the photoemission spectra with respect to that of clean Si(111). An interface with a photoemission spectrum resembling that of a silicide has developed at about 2–10 monolayers. At increasing Θ the region explored with photoemission shows enrichment of the metal, but the situation at $\Theta=40$ is still very far from that of the pure Pt metal, thus indicating a very strong chemical interaction at room temperature on the depth scale of tens of monolayers. Opposite chemical shifts of the Si and Pt core lines are seen (Pt towards lower and Si towards higher binding energies with increasing Θ) and, moreover, the shape of the Si $2p$ core lines is modified towards that typical of a metallic phase. All these results are discussed in terms of the nature of the chemical bond between Si and Pt.
MS code no. BH2100 1977 PACS numbers: 73.40.–c, 79.60.Eq

I. INTRODUCTION

The study of semiconductor–transition-metal interfaces is becoming a central topic in solid-state surface physics both for fundamental and practical reasons. The fundamental interest in these systems lies in the connection between surface chemistry parameters and the electronic properties of the junction[1–6] whose low-barrier (Ohmic) or high-barrier (rectifying) characteristics are not completely understood in terms of the mechanism underlying the formation of different barriers.

A better understanding of the physical chemistry of different semiconductor–d-metal interfaces also provides valuable information of practical use since low- and high-barrier junctions are highly utilized in the production of active devices.[9]

This article presents the first systematic energy-dependent photoelectron-spectroscopy study of the Si-Pt interface at room temperature. Special attention has been given to the low-coverage regime since the very first stage of the interface growth is probably determined by the semiconductor surface disruption caused by the metal adatoms as discussed in an earlier paper.[10] At increasing coverages, we have followed the evolution of the electron states of the Si(111)-Pt interface by taking full advantage of the unique tunability of synchrotron radiation (SR). In addition to extensive core-level spectroscopy data, we present valence-band photoemission spectra at two energies, one ($h\nu=130$ eV) corresponding to the Cooper-minimum region for the Pt $5d$ photoemission ($h\nu=130-160$ eV), so that the information on the Si sp contribution to the energy distribution curves (EDC's) can be revealed. This method, introduced for the first time in an earlier publication,[10] has turned out to be very useful in understanding the nature of the chemical bond between Si and d metals.[11–13] In fact it allows us to make a scheme for the assignment of the Si–d-metal chemical reactions on a pure experimental basis.

The $h\nu$ dependence of the $4d$- and $5d$-electron photoionization cross section which shows a deep minimum in the region between $h\nu=130$ and 160 eV (Cooper minimum) is of great advantage in interface photoemission studies[14] where the density of valence states can be probed, tuning the sensitivity to the d contribution. The presence of Cooper minima in solids has been proved experimentally in a number of recent synchrotron-radiation photoemission works both for pure $4d$ and $5d$ metal[15]

and for *d*-metal compounds.[10–13] A theoretical analysis of the Cooper minima effect for valence-band states is still lacking and possible deviations from the pure atomic levels have not been explored in detail. In this paper we will, therefore, not argue about the Cooper-minimum effect *per se* or try to make quantitative comparisons between our results and the calculated atomic cases because that could only be highly speculative at present and is beyond the purpose of this work on Si—*d*-metal interfaces. Of importance for the present work is that the reduced *d* emission at the Cooper minimum allows a detailed study of the *sp* contributions to the total density of states which are hidden at all the other energies where the *d* emission is the dominant feature in the EDC's.

The Si-Pt junction belongs to the so called Si—transition-metal reactive interfaces as do Si-Pd (Refs. 11, 16, and 17) and Si-Ni (Refs. 18 and 19). One characteristic of the Pt-Si system is that two stable bulk compounds are known: PtSi and Pt_2Si, with the Si-rich silicide formed at higher temperatures.[20] Some spectroscopic information on these two phases of Pt (Ref. 21) as a function of the temperature[22] is already available in the literature.

In general, rather than being characterized by a single stoichiometric reaction product, the nonannealed reactive transition-metal—silicon interfaces present[10–12,16–19,21–23] a broad mixed region where semiconductor-rich and metal-rich phases clamp a silicidelike phase, with concentration gradients defining the boundaries between these phases. A sharp interface has been reported for Si(111)-Pd where a Pd_2Si-like overlayer is formed[11,16,17] as a result of a solid-state reaction, although a concentration gradient is present in the metal-rich side.[11]

This paper adds new information to the previous theoretical and experimental literature on the physical chemistry of the reactive interfaces, which has implications for the Schottky-barrier formation process and for the derivation of the barrier height. Reference to this literature will be made throughout the paper and in particular to the empirical correlations of these properties to such macroscopic observables as the eutectic temperature[7] and the heat of formation of the semiconductor-metal bond.[8]

The paper is organized as follows. An account of experimental techniques is given in Sec. II and the experimental results are collected in Sec. III. The discussion in Sec. IV is carried out with reference to three coverage intervals [in units of monolayers (ML)] which have their own features: section A—low coverages ($\Theta < 0.5$ ML), section B—medium coverages ($0.5 < \Theta < 10$ ML), and section C—high coverages ($\Theta > 10$ ML). In Sec. V, we summarize the main results in connection with the interface growth mechanism.

II. EXPERIMENTAL

Medium-doped (10^{16} atoms/cm^3) *n*-type Si samples were carefully cleaved *in situ* at a working pressure of 4×10^{-11} torr. The cleaves produced highly reproducible angle-integrated valence-band photoemission spectra. This is an important point because the Si(111) photoemission spectra are very surface sensitive at the energies used ($h\nu = 80$ and 130 eV), and the relative intensities of the different valence peaks can vary depending on the quality of the cleaves as will be discussed later. What typically happens for certain qualities of cleaves is that the two deepest structures of the Si(111) valence band are depressed in intensity with respect to the top of the valence band. Examples of these kinds of EDC's can be found in a paper published earlier.[10]

The Pt overlayers were deposited by evaporation from a thin Pt wire wound around a W filament wire. Resistive heating at a power level of about 50 W was necessary for the evaporation. This required a very careful outgassing procedure and a special design of the evaporator assembly, similar to a source for MBE (molecular beam epitaxial) growth. The evaporations were done at a pressure lower than 1.5×10^{-10} torr. The deposition rate was controlled with a quartz oscillator located on the sample carousel and alternatively put in the sample position in order to avoid any geometrical correction factor and any heating from the evaporation filament. Very stable rates, typically 1 Å/min, were easily established and the desired coverages were obtained by operating a shutter in front of the Pt source. The evaporation rate was checked again immediately after the completion of the overlayer preparation. The accuracy of the total coverages should be better than 20% for the lowest coverages and slightly better for the thicker depositions. No traces of contaminants were detected using either x-ray photoemission or core-line *SR* spectroscopy.

The angle-integrated EDC's were taken with a double-pass cylindrical mirror analyzer (CMA) in the retarding mode in an ultrahigh vacuum (UHV)

system described previously. The light source was the 4° beam line at the Stanford Synchrotron Radiation Laboratory (SSRL), equipped with a "grasshopper" monochromator providing intense monochromatic light in the range $h\nu = 65-500$ eV.[24] The surface of the sample was normal to the CMA axis and the light was impinging at grazing incidence (15°). The overall resolution was 0.5 eV which is sufficiently good for the purpose of this study.

III. RESULTS

This section is a summary of the experimental photoemission results which will be discussed in Sec. IV. The main trends in the experimental data are given in representative plots. The valence-band dependence on the Pt coverage (Θ in monolayer units) is summarized in Figs. 1 and 2 for $h\nu = 80$ and 130 eV, respectively. At $h\nu = 80$ eV the Pt $5d$ photoionization cross section is much greater than the Si sp (Ref. 25) so that already at submonolayer coverages ($\Theta > 0.33$ ml), and Pt $5d$ emission is the dominant feature in the EDC's. On the other hand, at $h\nu = 130$ eV the Cooper effect (strong in Pt metal between 130 and 160 eV) reduces the emission and the evolution of the Si valence states are clearly revealed. The photon energy dependence is seen better in Fig. 3 where we contrast, at selected Θ, the EDC's at the Cooper minimum and those with the dominant d contribution.

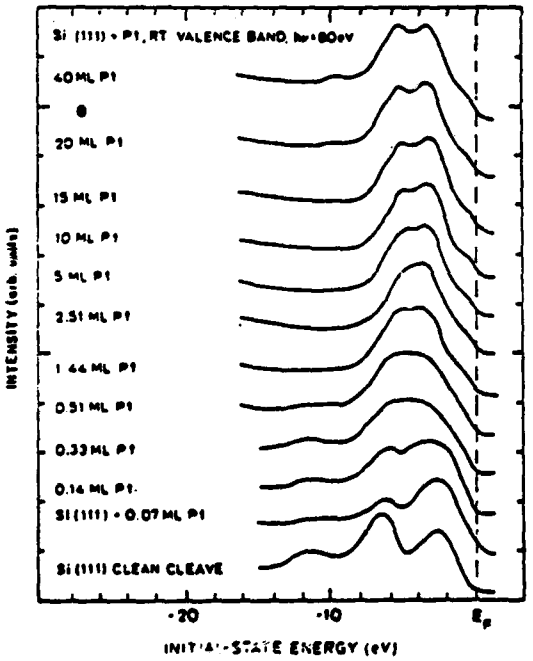

FIG. 1. Angle-integrated photoelectron energy distribution curves (EDC's) at $h\nu = 80$ eV for Si(111) and Pt at increasing coverages at room temperature. The Pt coverages quoted in the figure are in monolayer units where 1 ml $= 7.8 \times 10^{14}$ atoms/cm^2, i.e., the surface density of the Si(111) substrate.

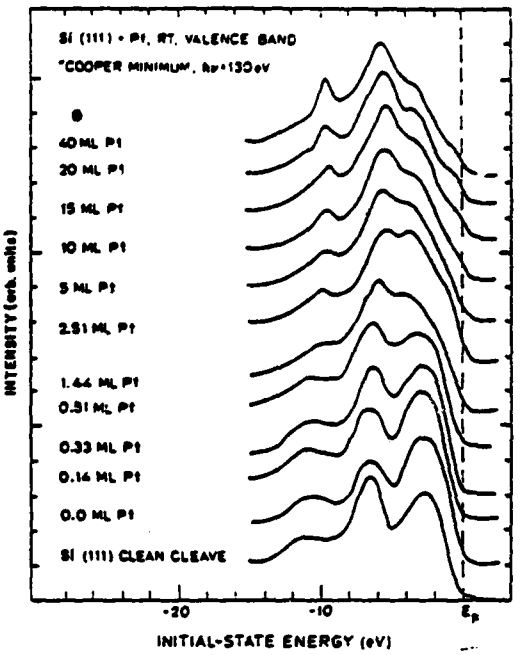

FIG. 2. Angle-integrated EDC's for Si(111) and Pt in the Cooper-minimum region for the Pt $5d$ photoionization cross section ($h\nu = 130$ eV). Coverages in ML.

The Si $2p$ (unresolved doublet) core lines taken at a photon energy of 160 eV are plotted versus Θ (at selected values) in Fig. 4. In the figure, the peaks are normalized to the same height to illustrate the shape modifications as a function of coverage. There is a very pronounced asymmetric broadening of the line towards higher binding energy with increasing coverage. The intensity variations of the Si $2p$ and Pt $4f$ levels versus Θ are given in Fig. 5. From this plot alone, it can be deduced directly that the Si-Pt interface is not atomically abrupt but that some intermixing takes place since the Si and Pt peak intensities change over a much larger coverage interval than the electron escape depth (which is typically 5 Å at these energies.[26] The shift in binding energies for the same Si and Pt core lines as a function of coverage is shown in Fig. 6. The observed chemical shifts are fairly small and in opposite directions for Pt and Si.

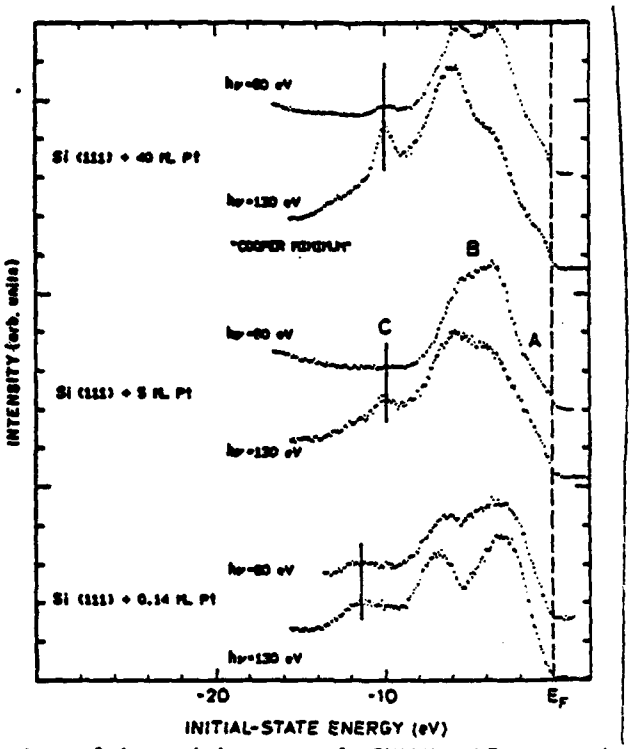

FIG. 3. Photon energy dependence of photoemission spectra for Si(111) and Pt: comparison between $h\nu=80$ eV and the Cooper minimum ($h\nu=130$ eV) at selected low, intermediate, and high coverages (in ML).

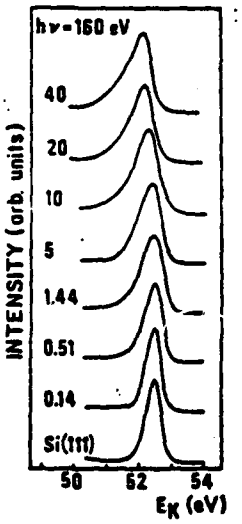

FIG. 4. Coverage dependence of Si 2*p* core-line photoemission (unresolved doublet) at $h\nu=160$ eV. The amplitude of the spectra has been normalized to the same value in order to follow the position and shape evolution. The spectra are plotted vs the kinetic energy of the photoelectrons; in fact, the absolute binding energy is uncertain by a factor of ±0.3 eV because of the monochromator calibration.

It is noteworthy that all the photon energies used for the valence-band and core-level results shown in Figs. 1—4 give similar values for the electron kinetic energies, corresponding to the minimum of the escape depth.[26] This makes the core and valence information directly comparable since they refer to the same sampled depth of the Si-Pt interface (about 5 Å).

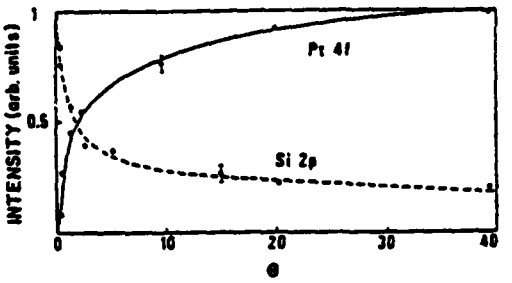

FIG. 5. Intensity profiles of Si 2*p* and Pt 4*f* core lines as a function of the coverage. The intensities are normalized to the maximum value of amplitude of the Si and Pt signals obtained in the experiment [i.e., the clean Si(111) surface and the $\Theta=40$ Pt coverage, respectively].

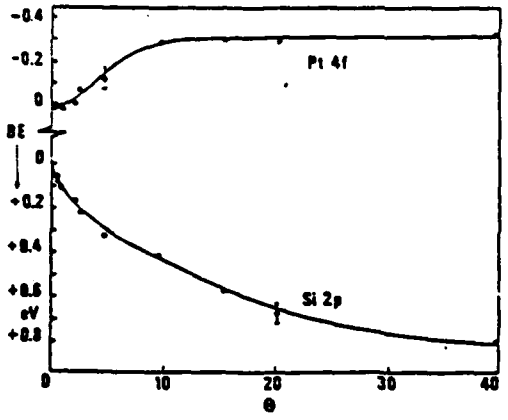

FIG. 6. Binding-energy variations for the Si $2p$ and Pt $4f$ core lines as a function of coverage. The curves are the best fits to the experimental points.

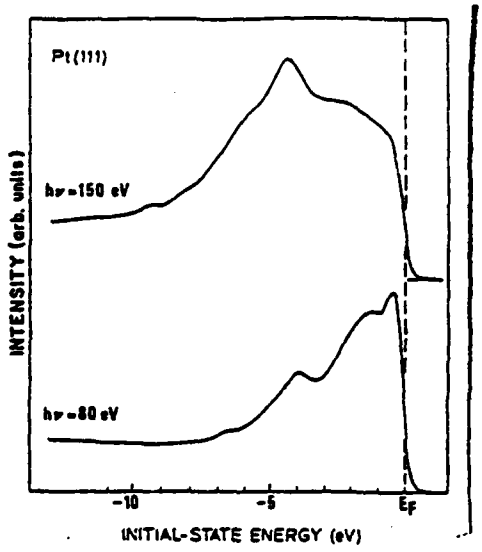

FIG. 7. Valence-band angle-integrated EDC's for pure Pt [Pt(111)] at $h\nu=80$ eV and in the Cooper-minimum region ($h\nu=150$ eV) (Ref. 28). The amplitude of the curves has been normalized to the same value; the counting rate ratio between the spectrum at $h\nu=80$ eV and the spectrum at $h\nu=150$ eV is $I(h\nu=80\ \text{eV})/I(h\nu=150\ \text{eV})=8$.

IV. DISCUSSION

In order to carry out a systematic analysis of the Θ dependence of the spectra, it is important to note some general features present in the spectra of Figs. 1 and 2. The valence spectra never reach the *shape typical of pure* Pt even at the highest coverage ($\Theta=40$) explored in the present research. This is evident by comparing the spectra shown in Fig. 7 for pure Pt (both at and away from the Cooper minimum) with the highest coverage spectrum ($\Theta=40$) of the Si(111)-Pt interface in Figs. 1 and 2. It is clearly seen that even at very high coverages the Si(111)-Pt spectrum is very different with respect to that of pure Pt. This confirms the very strong chemical interaction at the Si(111)-Pt interface which has already been pointed out for lower coverages at room temperature in previous work by Abbati *et al.*[27] The pure Pt measurements were taken in a different run with the same SSRL beam line from a (100)-oriented clean Pt crystal.[28] The scaling factor between the two EDC's (80 and 150 eV) can be directly compared to those of the interface measurements. This comparison provides direct evidence for the reduction of d emission due to the Cooper-minimum effect also for d states involved in bonds with Si; the total counting rate in the spectre at $h\nu=130$ eV is smaller by a factor variable between 10 and 3 with respect to the spectra at $h\nu=80$ eV. It is apparent that relevant contribution from local density of states around Si can be deduced from the results at the Cooper minimum.

It is important to note that, in the intermediate Θ region, the valence-band photoemission is already typically "silicidelike." For example, at $\Theta=1.45$ and 2.50 the valence photoemission at $h\nu=80$ eV is similar to that from Pt_2Si and PtSi at $h\nu=21.2$ eV as reported by Abbati *et al.*[22] Thus, at these coverages, the reaction has proceeded up to a silicidelike situation. This observation suggests a natural way to divide up the coverage regions into three intervals, which will be discussed separately below. In the submonolayer region ($\Theta \lesssim 0.51$) there is not sufficient metal present to develop a silicidelike interface, while at high coverages ($\Theta > 10$) there is a metal-rich phase, although some general features typical of silicides are still present. Of course there is not a clear-cut distinction between the three regions, and the selection of the coverage intervals is somewhat arbitrary; nevertheless, the division is of great help for the discussion.

A. The low-coverage region ($\theta < 0.51$ ml)

In this coverage region the most interesting result is the strong modification of the EDC when a very small quantity of Pt is deposited onto the surface ($\Theta=0.07$). The Pt contribution to the

valence-band emission is very small (3–4 % of the total signal at $h\nu = 80$ eV, as can be deduced by scaling from the high-coverage cases, $\Theta = 20$ and 40). Thus, in the absence of substrate modifications, the EDC is expected to be basically invariant. On the contrary a dramatic modification of the clean Si valence-band contribution is seen in Fig. 1 ($h\nu = 80$ eV) and in Fig. 2 ($h\nu = 130$ eV), mainly in the high-binding energy region of the valence band. This indicates that a small fraction of Pt atoms has a strong effect on the rearrangement of the Si(111) surface, most probably the topmost layer. This observation indicates that the interaction between Si and Pt is very strong to that Pt atoms with surrounding Si from very distorted localized regions which alter the long range properties of the clean Si surface. No systematic low-energy electron diffraction (LEED) studies are available on this subject but would obviously be of great value. The available results by Roth and Crowell[29] confirm that a small amount of several transition metals gives a strong background with a considerable attenuation of the (2×1) pattern. This is consistent with the strong effects seen in the present photoemission study which are direct evidence of a disruption of the Si surface from the very beginning of the interface formation.

As far as the nature of this disruption is concerned we can only present some speculations which should stimulate further research on this interesting problem. A first possibility is that the interaction with Pt induces a partial disordering of the surface. This would be consistent with the decrease of the photoemission intensity from the two deepest valence structures, since a trend of this kind has already been seen in the comparison between crystalline and amorphous Si (Refs. 30 and 31) (generally observed whenever the Si states become more localized). Another possibility is that the interaction with Pt induces changes in the relaxation of the top Si layer with a consequent modification of the surface back bonds which contribute to the deeper region of the valence band.[32] A qualitative comparison to the calculations by Pandey and Phillips[33] for the (1×1) Si surface shows that the modification of our EDC's is in agreement with a strong reduction of the relaxation. In this case the reduction should be originated by the metal atoms interacting with the surface lattice.

Of course the two processes can be present at the same time and further work is needed to assess the problem. In any case, this strong modification is of crucial importance since it creates the surface which interacts with Pt deposited at increasing coverages.

The importance of this disruption mechanism is also confirmed by comparing the present results with our previous work[10] where the clean Si(111) spectrum is very similar to that obtained for 0.07 ml in the present experiment. This is most likely due to a different quality of the cleaves. Imperfections in the cleavage procedure probably have an effect analogous to the disruption induced by the very thin Pt overlayer. With these precautions in mind, there is no contradiction between the present results for the Si(111)-Pt interface and those reported earlier.[10]

When Θ increases beyond 0.07, a small 5*d* contribution is detectable and the deeper-lying Si states are modified, as can be seen from the spectra at the Cooper minimum, Figs. 1 and 2. This is the first evidence for the formation of mixed orbitals between Pt 5*d* and Si *sp* states, which is also confirmed by the progressive chemical shifts of the Si and Pt core lines in opposite directions (see Fig. 6). At these coverages the situation is not yet that typical for silicides, but the chemical shifts of the core lines indicate the presence of a chemical reaction and a starting trend towards a silicidelike situation.

B. The intermediate-coverage region ($\Theta = 1-10$ ML)

The intermediate-coverage region presents a high degree of stability for the shape of the valence-band EDC's both at $h\nu = 80$ and 130 eV and can be characterized as the silicidelike region of the interface. In fact the energy position of the major peak and its width[34] are typical for silicides as already observed in the ultraviolet photoemission spectroscopy (UPS) experiments at $h\nu = 21.2$ eV,[27] and for other reactive Si–transition-metal interfaces such as Si-Pd (Refs. 11, 16, and 17) and Si-Ni.[18] The stability over such a broad interval of coverages is the result of a chemical reaction involving the deposited Pt atoms and the Si substrate, leading to a silicidelike phase several monolayers wide. In fact, for the highest coverages in this region (5 and 10 ML), the unreacted Si surface is at least 10–15 Å beyond the depth sampled by photoemission (5 Å).

Before discussing the details of this coverage regime, we recall the interpretation scheme for the Si–transition-metal bond introduced by Riley

et al.[15] and lately applied to Pd-Si,[10] based both on experimental results and theoretical calculations of the orbital contributions to the various EDC structures. The scheme is in agreement with that obtained independently by Rubloff *et al.*[16] The three main features of the valence states due to a Si—transition-metal bond are (compare Figs. 1 and 2): (i) a structure *A* around 0.5 eV below the Fermi level containing mixed orbital contributions from Si *p* and metal *d* electrons having antibonding character; (ii) the main structure *B* containing dominant Si *p* and Pt *d* hybrid-bonding contributions extending between −0.45 and −2.5 eV, being typical (with respect to the Fermi level) of the silicide bond and having a stronger Pt *d* character in the peak region (−2 eV), and (iii) a deeper structure *C*, less involved in the bonding, due to Si *s* electrons with a minor contribution of metal *d* states. The bonding scheme is discussed in detail by Rossi *et al.*[10] and the reader is referred to this work for further information.

The stability of the bond involving hybridization between Pt *d* and Si *p* states is evident throughout this coverage region as shown by the presence of only minor changes in the EDC shape at $h\nu = 130$ eV (Fig. 2). On the other hand, the details of the valence-band emission at both photon energies, as well as the core-line spectroscopy results, indicate a change in composition of the silicidelike phase as the Pt coverage is increased. The leading peak in the EDC's at $h\nu = 80$ eV shifts towards lower binding energies for increasing Pt coverages. This is consistent with the changes observed for increasing Pt depositions in a silicidelike interface, as reported by Abbati *et al.* in Ref. 34 where temperature-dependent UPS results for Si-Pt were presented.

The analysis of the core-line intensities presented in Fig. 6 shows for this interval a strong decrease of the Si 2*p* emission and an increase in the Pt 4*f* emission. This accounts for a concentration gradient throughout the silicidelike phase. Additional information can be obtained by analyzing the chemical shifts of the core levels. The Pt 4*f* level shift towards lower binding energies is completed within this coverage interval (for $\Theta = 10$), and the shifted peak remains stationary in energy in the high-coverage region, suggesting that the Pt atoms see gradually fewer Si near neighbors and are eventually no longer sensitive to the presence of dilute Si in the high-coverage region. The Si 2*p* core lines, on the other hand, keep shifting towards higher binding energies with increasing Pt coverage which is consistent with a trend towards higher dilution.

It should be noted that the chemical shifts seen in the present system and in related systems are very small. Thus, their interpretation merely in terms of a charge-transfer mechanism is open to difficulties since other processes are also expected to contribute to core-line shifts. Such contributions may come from the change of the atomic configuration due to Si-Pt bond formation, the renormalization of atomic levels due to variations of the volume available per atom, and the variation of relaxation energy as a function of $h\nu$. The discussion of the charge transfer must wait for accurate theoretical accounts of these effects and the present data can constitute a valuable experimental basis for such theoretical work.

Here we note only that a trend of core-line shifts as in Fig. 6 with a monotonic and opposite behavior of Si and Pt levels is not compatible with a model based uniquely on charge transfer.

Another important point in this coverage region is the modification of the Si 2*p* line shape, which broadens gradually and has a growing tail on the high-binding energy side of the unresolved doublet. The broadening can be interpreted as the simultaneous presence in the sampled depth [~6 Å for electron kinetic energies of 55 eV (Refs. 26 and 30)] of Si atoms in slightly different surroundings while the presence of the skewed line shape, much more enhanced in the high-coverage region as discussed in the next section, is related to the metallic nature of the interfacial compounds in which Si is present. We note that this is the first time that the development of the skewing of the Si 2*p* line shape is clearly followed experimentally, step by step, as a function of coverage.

C. High coverages ($\theta > 10$ ml)

When increasing amounts of Pt are deposited onto Si at room temperature, departure from the typical silicidelike situation is observed, and the region explored with photoemission becomes richer in the metal as seen from Fig. 5. It is noteworthy in this case that the EDC never reaches that of pure Pt, thus indicating that the fraction of Si present in the region explored with photoemission is of paramount importance in determining the valence states (compare Figs. 1 and 2 with Fig. 7). Furthermore, it is important to note that the structure *C* (around −10 eV) is still present (Figs.

1–3). This indicates that the gross features of the chemical bond between Si and Pt are basically the same although the system is richer in the metal than at intermediate coverages. This structure increases in intensity when Θ increases and provides evidence that some metal contribution is also present in *C*. This result is analogous to what was seen previously for the Si-Pd interface and is consistent with the Si–Pt and Si–Pd bond calculations by Abbati *et al.*[34] However, this paper provides a new insight, namely that the structure *C* is observed not only at the Cooper minimum, but also at $h\nu = 80$ eV for Θ=40 and thus must contain *d*-electron character as suggested by calculations on silicides.[25,34,35,37].

Another important point is the modification of the EDC shape at increasing Θ. In the *d*-band region the deepest states give a stronger contribution to the photoemission spectra, mainly at the Cooper minimum, than the most shallow ones. This trend is also found in pure Pt (see Fig. 7) where the deeper states give a smaller Cooper effect. In the interface this trend would seem to be enhanced.

The presence of Si in the region explored does not imply that Si is present at constant concentration in the overlayer. Strictly speaking, we cannot exclude that something similar to the Si-Au case[38] takes place, where an intermediate Au-rich layer is found beneath a Si-enriched surface layer. This point deserves further investigation with depth-profiling techniques. But it is very likely that the strong energy gain in the Si-Pt reaction, as compared to the small one for Si-Au, does not lead to a Pt-rich layer with Si segregated on top.

In the metal-rich phase seen at high Θ a strong change is seen in the Si 2*p* emission, both in energy position and in line shape, enhancing the trends already mentioned for the intermediate Θ region in Sec. IV B. The line-shape change is of the Sunjic-Doniach type observed for core levels in metals when hole-pair formation around the Fermi level accompanies the photoemission excitation.[39] Of course we cannot exclude the fact that energy-loss mechanisms can also contribute to the line-shape modification. The skewed line shape (see Fig. 8) for higher coverages (Θ=20) is consistent with the Sunjic-Doniach model, which predicts this will happen with the increase of available states in the E_f region when the system becomes metal rich. The same results have been found for the Si-Pd interface at high coverages.[11] Therefore, it is probably a reliable characteristic of the change from a Si-rich to a metal-rich situation.

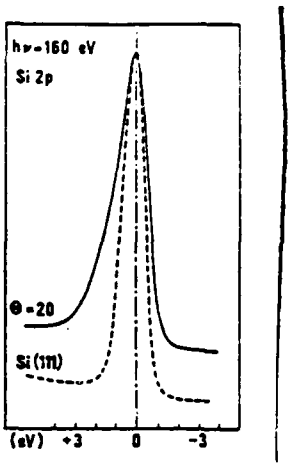

FIG. 8. Si 2*p* core line-shape evolution between the clean Si(111) case and Θ=20 ML of Pt onto Si(111). The peak positions have been aligned in order to demonstrate the broadening and the change in line shape. For the binding-energy shift between Θ=0 and 20, see Figs. 4 and 6.

V. SUMMARY OF INTERFACE GROWTH AND CONCLUSIONS

The current work is the first extensive study of the Si-Pt interface at room temperature by means of the Cooper-minimum photoemission technique. Here we summarize schematically the results concerning the interface growth when increasing amounts of Pt are deposited onto the Si(111) surface.

(1) At submonolayer coverages the major effect is a dramatic change of the relative intensities of the Si(111) valence-band peaks indicating that a very small number of Pt atoms have long-range-order effects on the surface and can change the surface relaxation even before silicidelike bonds are formed.

(2) At increasing coverages the Si-Pt reaction leads to a wide silicidelike interface with a bonding configuration of strong Si *p* – Pt *d* hybridization. This region has a concentration gradient leading gradually to a metal-rich mixed phase. The chemical reaction proceeds with small chemical shifts of the Si 2*p* and Pt 4*f* core levels towards higher and lower binding energies, respectively.

(3) A metal-rich phase, containing diluted Si, is eventually reached at high coverages; this phase still has silicidelike bonding characteristics and a valence band markedly different from pure Pt. In this region the Si 2*p* core lines have a typical asymmetric line shape.

A more detailed analysis of the present data will be possible when theoretical treatments of the Cooper effect in transition-metal compounds and of core lines (both chemical shifts and line shapes) are available together with more experimental structural information. The present paper will hopefully stimulate further work in this direction.

ACKNOWLEDGMENTS

This work was supported by the Advanced Research Projects Agency of the Department of Defense under Contract No. NO0014-79-C-007s and by the Gruppo Nationale di Struttura della Materia of the Consiglio Nationale della Ricerca, Italy. The experiments were performed at the Stanford Synchrotron Radiation Laboratory, which is supported by the National Science Foundation under Grant No. DMR77-27489 in collaboration with the Stanford Linear Accelerator Center and the Department of Energy.

*Permanent Address: Istituto di Fisica del Politecnico di Milano, 20133, Italy.

[1]J. C. Phillips, J. Vac. Sci. Technol. 11, 947 (1974).

[2]S. G. Louie and M. Cohen, Phys. Rev. B 13, 2461 (1976).

[3]H. I. Zhang and M. Schluter, Phys. Rev. B 18, 1923 (1978).

[4]L. J. Brillson, J. Vac. Sci. Technol. 16, 1378 (1979).

[5]J. L. Freeouf, Solid State Commun. 33, 1059 (1980).

[6]J. E. Rowe, G. Margaritondo, and S. B. Christman, Phys. Rev. B 15, 2195 (1977).

[7]G. Ottaviani, R. N. Tu and J. W. Mayer, Phys. Rev. Lett. 44, 284 (1980).

[8]J. M. Andrews and J. C. Phillips, Phys. Rev. Lett. 35, 56 (1975).

[9]E. H. Rhoderick, *Metal-Semiconductor Contacts* (Claredon, Oxford, England, 1978).

[10]G. Rossi, I. Abbati, L. Braicovich, I. Lindau, and W. E. Spicer, Solid State Commun. 39, 195 (1981).

[11]I. Abbati, G. Rossi, L. Braicovich, I. Lindau, and W. E. Spicer, J. Vac. Sci. Technol. 19, 636 (1981).

[12]I. Abbati, G. Rossi, L. Braicovich, I. Lindau, and W. E. Spicer, J. Appl. Phys. (in press).

[13]G. Rossi, I. Abbati, I. Lindau, and W. E. Spicer, Surf. Sci. (in press).

[14]G. Rossi, I. Abbati, L. Braicovich, I. Lindau, and W. E. Spicer, Surf. Sci. (in press).

[15]L. I. Johansson, I. Lindau, M. H. Hecht, and E. Kallne, Solid State Commun. 34, 83 (1980), and references quoted therein.

[16]G. W. Rubloff, P. S. Ho, J. F. Freeouf, and J. E. Lewis, Phys. Rev. B 23, 4183 (1981).

[17]P. S. Ho, P. E. Shmid, and H. Foll, Phys. Rev. Lett. 46, 782 (1981).

[18]I. Abbati, L. Braicovich, V. del Pennino, B. de Michelis, and S. Valeri, in *Proceedings of the Fourth International Conference on Solid Surfaces and the Third European Conference on Surface Science, Cannes 1980*, edited by D. A. Degras and M. Costa (Societe Francaise, du Vide, Paris, 1980), Vol. III, p. 1023.

[19]P. J. Grunthaner, F. J. Grunthaner, and J. W. Mayer, J. Vac. Sci. Technol. 17, 924 (1980).

[20]*Thin Film Interdiffusion and Reactions*, edited by J. M. Poate, R. N. Tu, and J W. Mayer (Wiley, New York, 1978).

[21]L. Braicovich, I. Abbati, J. N. Miller, I. Lindau, S. Schwarz, P. R. Skeath, C. Y. Su, and W. E. Spicer, J. Vac. Sci. Technol. 17, 1005 (1980).

[22]I. Abbati, L. Braicovich, B. de Michelis, V. del Pennino, and S. Valeri, Solid State Commun. 35, 12 (1980).

[23]J. N. Miller, S. A. Schwarz, I. Lindau, W. E. Spicer, B. de Michelis, I. Abbati, and L. Braicovich, J. Vac. Sci. Technol. 17, 920 (1980).

[24]F. C. Brown, R. Z. Bachrach, and N. Lien, Nucl. Instrum. Methods 152, 73 (1978).

[25]I. Abbati, L. Braicovich, B. de Michelis, O. Bisi, C. Calandra, V. del Pennino, and S. Valeri, in Proceedings of the Fifteenth International Conference on the Physics of Semiconductors, Kyoto 1980, edited by S. Tanaka and Y. Toyozawa [J. Phys. Soc. Jpn. 49, Suppl. A, 1071 (1980)].

[26]P. Pianetta, I. Lindau, and W. E. Spicer, in *Quantitative Surface Analysis of Materials, A Symposium Sponsored by ASTM Committee E-42 on Surface Analysis, Cleveland, 1977*, edited by N. S. McIntyre, ASTM Special Technical Publication 643 (Publisher, City, 1978), p. 105.

[27]I. Abbati, L. Braicovich and B. de Michelis, Phys. Lett. (in press).

[28]M. L. Shek, private communication.

[29]J. A. Roth and C. R. Crowell, J. Vac. Sci. Technol. 15, 1317 (1978).

[30]J. O. Joannopoulos and M. L. Cohen, Phys. Rev. 7, 2644 (1973).

[31]W. E. Spicer, in *Proceedings of the Fifth International Conference on Amorphous and Liquid Semiconductors, Garmish-Partenkirchen, 1973*, edited by J. Stuke and W. Brenig, (Taylorand Francis, London, 1974), Vol. II, p. 499.

[32]J. A. Appelbaum and D. R. Hamman, Rev. Mod. Phys. 48, 479 (1976).
[33]K. C. Pandey and J. C. Phillips, Phys. Rev. Lett. 34, 1450 (1975).
[34]I. Abbati, L. Braicovich, B. de Michelis, O. Bisi, and R. Rovetta, Solid State Commun. 37, 119 (1981).
[35]J. D. Riley, L. Ley, D. Azoulay, and T. Terakuta, Phys. Rev. B 20, 776 (1979).
[36]H. Gant and W. Monch, Surf. Sci. 105, 217 (1981).
[37]J. H. Weaver, V. L. Moruzzi, and F. A. Schmidt, Phys. Rev. B 6, 2916 (1981).
[38]L. Braicovich, C. M. Garner, P. R. Skeath, C. Y. Su, P. W. Chye, I. Lindau, and W. E. Spicer, Phys. Rev. B 20, 5131 (1979).
[39]S. Doniach and M. Sunjic, J. Phys. C 3, 285 (1970).

E. G. Rossi, L. Caliari, I. Abbati, L. Braicovich, I. Lindau, and W. E. Spicer, "Photoemission Investigation on the Oxidation of Si(111)-Ag Interfaces and Its Relation to the Interface Structure," submitted to Surface Science.

Submitted to Surf. Sci.

PHOTOEMISSION INVESTIGATION ON THE OXIDATION OF Si(111)-Ag INTERFACES AND ITS RELATION TO THE INTERFACE STRUCTURE

G. Rossi, L. Caliari+, I. Abbati++, L. Braicovich ++, I. Lindau, and W. E. Spicer

Stanford Electronics Laboratories
Stanford University
Stanford, CA 94305

ABSTRACT

We give the first photoemission results on the enhancement of Si reactivity to oxygen when a noble metal (Ag) is present. The tunability of synchrotron radiation (SR) has been used to get high surface sensitivity and to take advantage of cross section energy dependence. We show that when one monolayer of Ag is deposited onto Si(111) the exposure to oxygen (30.10^6L) originates the overgrowth of an oxide phase which is basically SiO_2. This indicates that Ag breaks the sp^3 configuration of Si atoms with a consequent dramatic increase in the Si reactivity. This behaviour rules out the model of Ag adsorbed on top of Si with an atomically abrupt interface.

+ Permanent address: Universita di Trento, Italy

++ Permanent address: Istituto di fisica del Politecnico di Milano, 20133, Italy

One of the crucial problems in the field of semiconductor d-metal interfaces is to establish if intermixing takes place or if the interface is atomically sharp so that it can be used as a test case for available theories which assume such simple geometry [1]. In Si d-metal interfaces a considerable amount of intermixing has been observed in the cases studied spectroscopally in the last few years [2]. Till now the only interface not showing intermixing was thought to be Si(111)-Ag [3-6] but quite recently we have open a controversy by suggesting on the basis of synchrotron radiation photoemission that intermixing does take place for this system [7,8]. The problem of a better understanding of the Si(111)-Ag interface from the point of view of the electron states is thus particularly timely. In particular it is interesting to establish if the (sp^3) configuration of Si atoms is broken upon the deposition of Ag atoms. This problem can be addressed very effectively with an experiment in which the oxidation of the interface is used as a test. We present here the results of such an experiment which is very discriminating between sharp overgrowth of Ag and penetration of Ag into the sample. In the former case (sp^3) configuration of Si needs not to be broken as in the model of [3,4] based on Ag adsorbed on top of surface Si atoms with saturation of the dangling bonds. In this case the Si reactivity to oxygen should decrease whereas it must increase dramatically if sp^3 configuration is broken as it has been clearly shown by the recent results by Cros et al. [11] on Si-Au.

Fresh Si(111) surfaces were prepared in situ by cleavage of n-type ($10^{18}cm^{-3}$) silicon in ultra high vacuum (operative pressure $1x10^{-10}$ torr). The Ag overlayer was obtained by evaporation from a Ag bead on a tungsten filament wire. A careful determination of the Ag coverage, was obtained with the experimental arrangement described in [9]. The estimation of 1 ml

is accurate withing $\pm$ 5 % assuming a unitary sticking coefficient for Ag on Si(111) at RT.

The maximum pressure during the evaporation was 3×10^{-10} torr and the sample surface was more than 10 cm apart from the Ag source so to avoid heating of the surface by irradiation from the evaporator. The oxygen exposures were made using a leak valve with all the hot filaments and voltages in the UHV apparatus turned off to avoid excitation of the oxygen. The O_2 partial pressure was monitored with a cold cathod Redhead gauge. The sample was exposed to 30.10^6 L of unexcited oxygen; this exposure is convenient because it is higher then that required for the saturation of the oxygen uptake at room temperature by clean Si(111) which is a case well studied with photoemission [12].

The difference in the behavior of the clean Si surface and of that treated with Ag is astonishing as it is seen from the core lines of Fig. 1 measured at photon energies which insure a great surface sensitivity (i.e. kinetic energies in the minimum region of the escape depth [10]). Ag 3d were measured at h = 450 eV and Si 2p (unresolved doublet) at h = 160 eV.

The increase of Si reactivity when the surface is treated with Ag is evident. In Si(111) without Ag (point dotted line of Fig. 1b) the oxygen uptake originates in the Si 2p core line spectra the typical shoulder around -2.6 eV below the unoxidized line, in agreement with the literature: the detailed interpretation of this structure is still open to controversies but there is no doubt that it corresponds to a situation very far from SiO_2; as suggested in (12) it is likely that most of the Si atoms are coordinated to two oxygen atoms instead of four as in SiO_2. The surface treated previously with Ag is much more reactive (dashed line in Fig. 1b) as seen from the much

more intense shifted line and from the much higher chemical shift which is ~3.8 eV with respect to the clean surface.

Only a minor amount of broadening is observed on the shifted Si 2p core lines with respect to the residue unshifted peak; this indicates the presence of one dominant oxidation product. The oxidation state as indicated by the chemical shift (3.8eV) is basically that of SiO_2 although the oxide overlayer is so thin, as shown below, that a great fraction of the atoms cannot have the complete coordination as in bulk SiO_2.

As a result of the interaction of the interface with oxygen Ag core line are attenuated (see Fig. 1,2) but not shifted. Thus the oxygen interaction with Ag is negligible and the attenuation of the Ag 3d emission indicates that Ag atoms are certainly below the surface region, possibly intermixed in the SiO_2 overlayer. By taking into account the Ag attenuation, the Si increase and the escape depth values one obtains that approximately 1.5-2 monolayers of oxide have been grown. The residual unoxidized Si 2p emission is due basically to Si atoms at the boundary between the oxide region and that where Ag is present. The small shift (0.3 eV) towards the higher binding energies observed for the unoxidizd Si 2p peak cannot be explained with a change in band bending since this would be also reflected in the Ag core lines which on the contrary remain at constant energy. The explanation of this chemical shift is not unique because several parameters are involved in the chemical and structural change of the oxidized interface. Probably the most important phenomena involved in this shift in binding energy are a charge transfer of the Si atoms in contact with the oxide and a change in relaxation energy due to the new environment of those Si atoms.

The growth of a phase strictly conneted with SiO_2 is also confirmed by valence photoemission colleted in Fig. 2. In the upper part, we give the

photoelectron spectra at $h\nu = 80$ eV where the d-contribution is dominant; the attenuation of the 4d contribution from Ag is clear and is consistent with core line intensities while the oxygen 2p around -6.2 eV from E_F is seen. In the lower part of Fig. 2, we give the results at the Cooper minimum for photoionization of Ag 4d shells ($h\nu = 130$ eV) so that the information from Si (sp) and oxygen p states is emphasized. In particular, O 2p gives a very strong signal in the spectrum of the oxidized intraface. It is interesting to compare this spectrum with that of Si (111) without Ag exposed to oxygen. This last case, a p contribution from Si is clearly seen around 2.2 eV while this region is considerably depleted in the interface treated with Ag; this is another evidence of the growth of a phase closely related to SiO_2 when the Si is pretreated with Ag. (In fact, the highest valence band levels in SiO_2 are the states at $\sim$ - 6 eV.) The above results are relevant in three respects:

(i) They are the first photoemission results on the enhancement of Si oxidation due to the presence of a d-metal; they extend the Auger and electron energy loss results presented recently by Cros et al [11] for Si-Au system and show the usefulness of SR photoemission in the study of these problems.

(ii) They are the conclusive evidence of the fact that sp^3 configuration of Si is broken upon the the arrival of Ag atoms; otherwise such an increase in Si reactivity could not be understood. This point answers the question presented in the introduction and shows that Ag atoms are not adsorbed on top of Si as suggested in [3]; the spectroscopic consequences of this interaction will be discerned in much more detail elsewhere [13]. Here we limit ourselves to state that the present results eliminate the priviligiate position of the Si-Ag interface as a good test case for easy and manageable theories which assume atomically sharp interfaces.

(iii) They show the possibility to modify the Si-SiO_2 interface upon predeposition of a very thin metal layer onto the Si substrate. This point is of great practical importance in device fabrication and applications. In fact the abruptness of the Si-SiO_2 interface and the density of interface states may be substantially modified by the presence of the metal layer which on the other hand is sufficiently thin not to affect the electrical characteristics of the junction.

The present results calls for further structural investigation on the subject and are a strong support in favour of the conjecture presented by Oura et al. [14] and by Rossi et al. [8] on the penetration of Ag beneath the surface. On the basis of this work there must be no more controversy on the occurrence of surface disruption and this calls for a new interpretation of the available LEED results. Another conclusion is the fact that at present no atomically sharp interface between Si and a d-metal is known. Thus, future research should cope both with the problem of developing more sophisticated theories accounting for intermixing and of finding out preparation procedures to minimize the intermixing when this is needed for technological reasons.

Acknowledgment

This work was supported by the GNSM of CNR, Italy and by the Advanced Research Projects Agency of the Department of Defense under Contract No. N00014-70-C-007.

The experiments were performed at the Stanford Synchrotron Radiation Laboratory which is supported by the National Science Foundation under Grant No. DMR 77-27489 in collaboration with the Stanford Linear Accelerator Center and the Department of Energy.

References

1. S. G. Louie and M. Cohen, Phys. Rev. B 13, 2461 (1976).
2. I. Abbati, G. Rossi, L. Braicovich, I. Lindau, and W. E. Spicer, J. Vac. Sci. Technol. 19, No. 4 (1981) and references quoted therein.
3. F. Wehking, H, Beckermann, and R. Niedermoyer, Surf. Sci. 71, 364 (1978).
4. A. McKinley, R. H. Williams, and W. A. Parke, J. Phys. C. Solid State Physics, 12, 2447 (1979).
5. Y. Gotom and S. Ino, Japanese Journal of Applied Physics 17, 2097 (1980).
6. V. Barone, G. Del Re, G. Le Lay, and R. Kern, Surf. Sci. 99, 223 (1980).
7. G. Rossi, I. Abbati, I. Lindau, and W. E. Spicer, to be published in the proceedings of the ICSFS2 Conf., Maryland (1981) on Application of Surface Science.
8. G. Rossi, I. Abbati, L. Braicovich, I. Lindau, and W. E. Spicer, Surf. Sci. Letts., in press.
9. G. Rossi, I. Abbati, L. Braicovich, I. Lindau, and W. E. Spicer, to be published in Phys. Rev. B.
10. H. Gant and W. Monch, Surf. Sci. 105, 217 (1981).
11. A. Cros, F. Salvan, M. Commandre, and . Derrien, Surf. Sci. Letts., 103, L 109, (1981).
12. C. M. Garner, I. Lindau, C. Y. Su, P. Pianetta, and W. E. Spicer, Phys. Rev. B 19, 3944 (1979).
13. G. Rossi, I. Abbati, L. Braicovich, I. Lindau, and W. E. Spicer, to be published.
14. K. Oura, T. Taminaga, and T. Hanawa, Solid State Commun. 37, 523 (1981).

FIGURE CAPTIONS

Figure 1 (a) Ag 3d core lines from Si(111) with 1 monolayer Ag before exposure to oxygen (solid line) and after exposure to $30 \cdot 10^6$ L of unexcited oxygen (dashed line).

(b) Si 2p unresolved doublet from Si (111) with 1 monolayer Ag before exposure to oxygen (solid line) and after exposure to $30\ 10^6$ L of unexcited oxygen (dashed line). The dashed line pertains to Si (111) without Ag with the same oxygen exposure.

The binding energies are referred to the unshifted position. In each section of the figure, the intensities are normalized to the case without oxygen.

Figure 2 Valence photoemission from Si (111) with 1 monolayer of Ag before exposure to oxygen (solid lines) and after exposure to $30 \cdot 10^6$ L of unexcited oxygen (dashed lines). Fig. 2a refers to $h\nu$ = 80 eV and Fig. 2b refers to $h\nu$ = 130 eV. The dot - dashed line at $h\nu$ = 130 eV refers to Si (111) without Ag with the same exposure to oxygen.

In each section of the figure, the intensities are normalized to the case without oxygen.

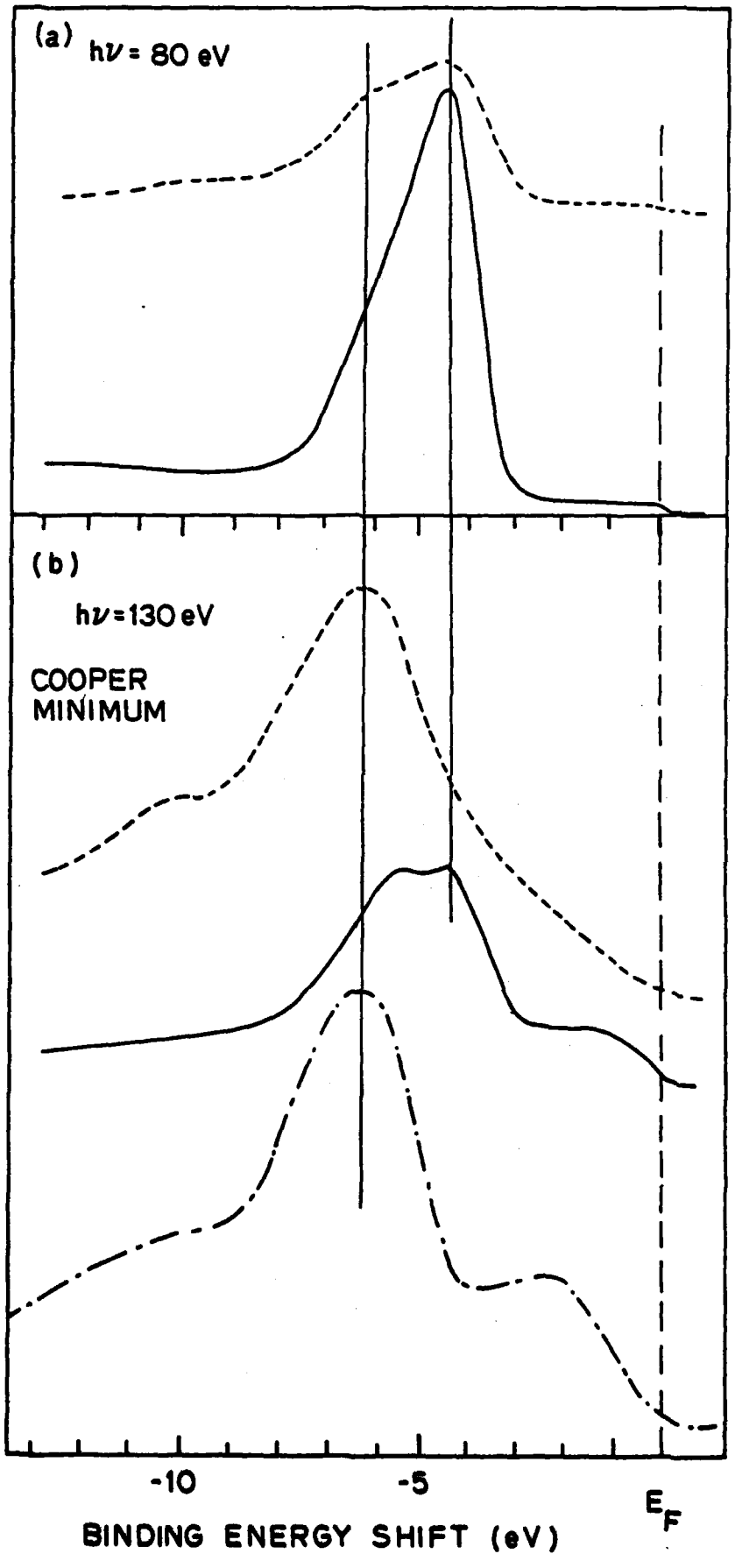
(a)
hν = 80 eV
(b)
hν = 130 eV
COOPER
MINIMUM
-10
-5
E_F
BINDING ENERGY SHIFT (eV)

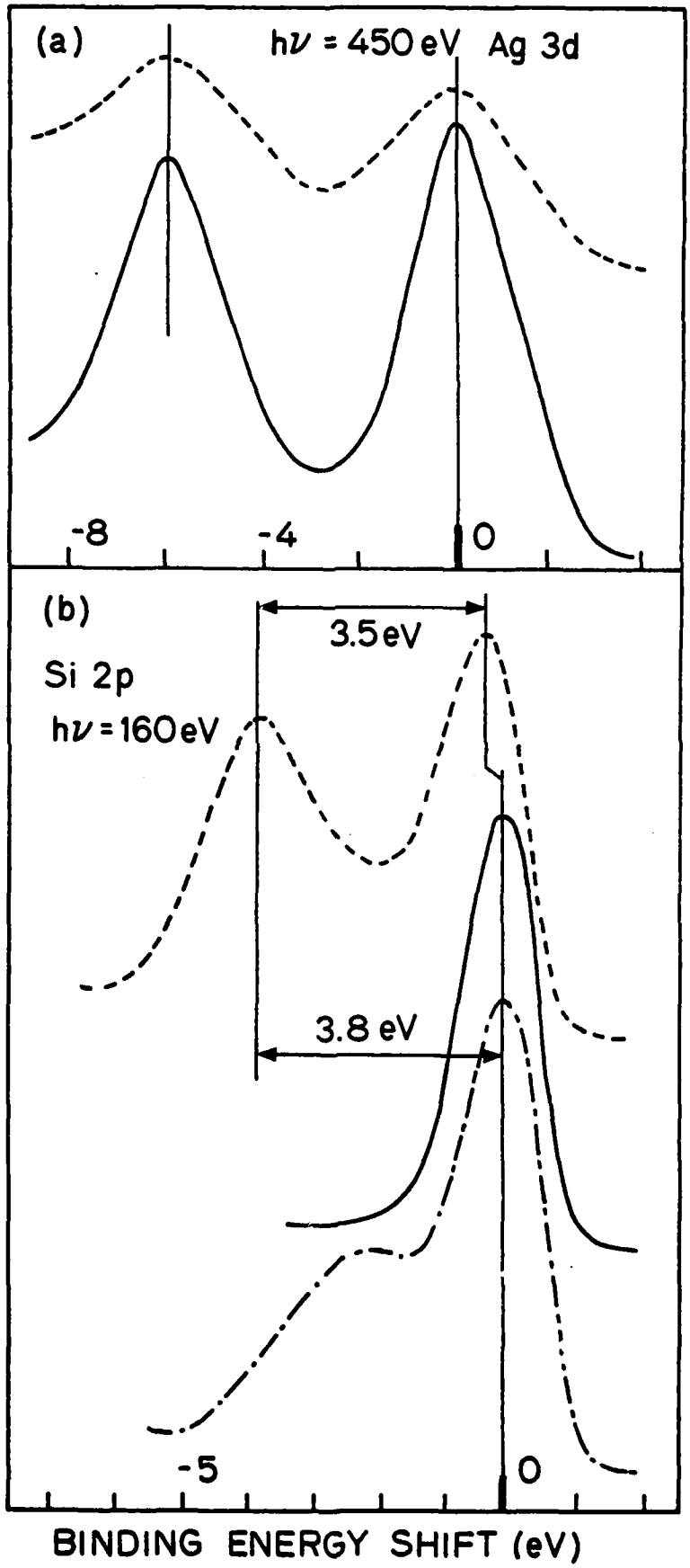
(a)
hν = 450 eV Ag 3d
-8
-4
0
(b)
3.5eV
Si 2p
hν = 160eV
3.8 eV
-5
0
BINDING ENERGY SHIFT (eV)

F. G. Rossi, I. Abbati, I. Lindau, and W. E. Spicer, "Intermixing at the Early Stage of the Si(111)/Ag Interface Growth," *Proc. ICSFS-2* to appear in Applications of Surface Science.

Proc. ICSFS-2, to appear in Appl. Surf. Sci.

Intermixing at the Early Stage of the Si(111)/Ag Interface Growth

G. Rossi, I. Abbati,* I. Lindau, and W. E. Spicerβ

Stanford Electronics Laboratory
Stanford University
Stanford, CA 94305

ABSTRACT

A synchrotron radiation (SR) photoemission investigation of the Si(111) cleaved surface + Ag thin overlayers (0.25 -2.5 monolayers (ML) has been carried out at room temperature with the Cooper Minimum method and at liquid nitrogen temperature (LNT) for a critical coverage (0.5 ML) with the energy dependent escape depth method. The two experiments give independent evidences of intermixing, following chemical reaction, between Ag and Si at the very low coverages, indicating that the very early stage of the Si(111)/Ag junction is not a sharp interface but an intermixed region extended to at least two layers of material.

---

* Permanent Address: Istituto di Fisica del Politecnico di Milano, Milano, 20133 Italy

β Stanford W. Ascherman Professor of Engineering

INTRODUCTION

The Si/Ag interface has been the subject of several investigations, mostly by means of structural methods (LEED, ISS, SRM) because of its apparent singularity with respect to the other Si/d-metal interfaces.[1,3] In fact, while all the Si/d-metal interfaces show, at different degrees, chemical reactivity and intermixing, the Si/Ag junction has been described as an abrupt interface with a weak interaction of Ag atoms positioned in on top sites of the Si(111) surface.[4] In a very recent article,[5] we reported on the presence of a chemical reaction at the Ag/elemental semiconductors interfaces as a result of an investigation on the modifications of the semiconductor density of valence states versus Ag coverage, and core line chemical shifts. The presence of a chemical reaction, however, does not prove per se that a mixed phase is formed at the interface; in fact, the reactivity could be saturated when all the Si surface atoms have reacted with the first monolayer of Ag deposited on top, as assumed in a simple chemisorption model. In the present article we summarize the independent results obtained in two different photoemission experiments regarding the Si/Ag interface at RT with an investigation of the valence EDCs with different sensitivity to the Ag 4d contribution (Cooper Minimum method), the core line intensity profiles of Si 2p and Ag 3d versus coverage, and the thermal evolution of the Si/Ag interface between LNT and RT measuring the valence ECDs with different surface sensitivities. Both experiments give independently the evidence of the formation of an intermixed region extended to at least 2 layers of material which has to be considered the real starting point for the subsequent growth of the Ag overlayers.

EXPERIMENTAL

The experiments were performed with the same UHV apparatus (which has been described in 6) using two different beam lines at Stanford Synchrotron Radiation Laboratory: (1) the 4 degree beam line equipped with a "grasshopper" monochromator for the RT experiments where photon energies of $h\upsilon$=80 eV, $h\upsilon$=130 eV (Ag 4d Cooper Minimum) were used for the valence band and $h\upsilon$=160 eV, $h\upsilon$=450 eV for the core levels, (2) the 8 degree beam line, equipped with a Seya-Namioka monochromator was used for the temperature dependent experiments at photon energies of $h\upsilon$=30 eV and $h\upsilon$=21 eV. In the latter case, the escape depth values are ~7 Å and ~15 Å[7], respectively, and the surface sensitivity is substantially different; whereas all the measurement on the 4° beam line were done with the highest possible surface sensitivity (the kinetic energy of the photoelectrons was in the range 70-120 eV, which corresponds to the minimum of the escape depth for all these measurements, so that the whole set of data refers to the sampled region of the material and are directly comparable. The samples were cleaved in UHV (operative pressure of 7×10^{-11} torr) and the evaporations made from a Ag bead at presures below 1×10^{-10} torr and monitored with a quarz oscillator. The accuracy of the determined coverage was better than 80% for the lowest coverage and better than 95% for the higher coverages as checked independently in situ with XPS core line intensity ratios. The angle integrated photoemission spectra were obtained with a double pass CMA with the sample surface normal to the analyzer axis and the SR beam impinging at grazing incidence.

RESULTS

The results of the present paper are summarized in Figs. 1 and 2 for the coverage dependence of the valence density of states at RT. Fig. 1 shows the series of EDCs taken at $h\nu$=80 eV where the Ag 4d emission is dominant. From this data we can see the evolution of the shape and energy position of Ag 4d band. A total shift of 1 eV towards the Fermi level is observed as well as a broadening of the peak. The peak shape becomes more similar to that of pure Ag with the typical shoulder of deeper d states. We note that the Ag 4d peak position at Θ=2.5 is still deeper for 0.15 eV with respect to the pure Ag case. Fig. 2 shows the same set of samples measured at the Cooper minimum for the photoionization cross section of Ag 4d electrons ($h\nu$=130 eV). At this energy the sensitivity to the sp states of the Si substrate is of the same order of magnitude as that to Ag 4d, so that the evolution of Si contribution to the total DOS is easily followed. Fig. 3 presents the data for the Si(111) + 0.5 monolayers of Ag sample prepared at LNT and then annealed at RT, for two photo energies: $h\nu$=30 eV and $h\nu$=21 eV. All the spectra in this figure were taken with the sample at LNT in order to exclude any possible experimental artifacts due to different conditions of the sample during the measurements; the annealing time at RT was 2 minutes. In Fig. 4, we summarize the core level emission intensities at RT for Si 2p and Ag 3d versus coverage.

DISCUSSION

The evolution of the valence band structure for the Si/Ag interface at RT as seen in Figs. 1 and 2 is typical for the Si/d metal [8] interfaces. In fact the shape of the EDCs and the binding energy values for the peaks

indicate that the main structure is due to metal d-Si p hybrids with an increasing metal contribution when the coverage is increased; in particular the EDC for θ=2.5 cannot be considered as a simple addition of the substrate and the Ag contributions. Furthermore the evolution of the deep structure at 11 eV below the Fermi level (mostly due to Si s electrons) shows a shift towards lower binding energies, as clearly seen in the Cooper minimum spectra of Fig. 2. The shift of the s contribution towards lower binding energies is the spectroscopic fingerprint of the breaking of the tetrahedral co-ordination of Si, due to the chemical reaction with Ag and the rehybridization of the valence states. This fact has been systematically observed for all the Si/d metal "reactive" interfaces, and is widely reported. The important difference in the present case is that the discussed features regard a much smaller coverage range; in fact at θ=2.5 the situation is already converging towards that of pure Ag and for θ=5 ML (not reported here) an almost pure Ag spectra is seen. Contrarywise in the "reactive" cases a high stability of the EDC shape both at $h\upsilon$=80 eV and the Cooper Minimum is observed over a coverage range of several tens of monolayers. This point is of great importance because on the basis of less direct experimental evidence (UPS with conventional light sources and AES) the given interpretation was simply that of a sharp interface.

The first point of the discussion does not solve by itself the problem of the interface growth; in fact the chemical reaction could have been limited to the top layer and the discussed data could in fact be consistent with an atomically sharp interface. However, core line analysis and temperature dependence can provide additional and critically important information. From Fig. 4 we see that at submonolayer coverages the slopes of Ag 3d and Si 2p intensities are different from that expected for a sharp interface. In particular, the Ag

3d intensity does not increase in a geometric way with the coverage. In fact if the Ag atoms were in on top positions on the Si surface we should have expected the Ag signal to double in intensity for doubled coverages. The results of Fig. 4 show on the contrary that 25% of the Ag signal is lost when 1 ML is deposited. This fact is the first evidence that intermixing is taking place at the interface at RT. In fact we can rule out the presence of agglomeration at such low coverages because in order to account for a 25% loss of signal we should hypotise the growth of 3-dimensional islands at least two layers thick which is against the known island formation at low coverages; where, in case of agglomeration, almost two dimensional islands are formed [1]. The attenuation of the Si 2p signal requires assumptions on the exact escape depth. This thus is a less direct determination, nevertheless it seems to give results in agreement with the evidence above accounting for the presence of intermixing in at least the first two layers of materials. The data from the experiment on temperature dependence are given in Fig. 3. The preparation of the interface at LNT was intended to minimize the kinetics of the reaction and the intermixing. A band bending is seen in the spectra at hυ=30 eV, where ~~naturally~~ the Si s structure moves toward higher B. E. with respect to the Fermi level when 0.5 ML of Ag are deposited on the clean Si(111) surface. The evolution of the EDC shape when the smaple was heated is a small broadening of the main structure (Ag 4d) suggesting the presence of different bond situations available for Ag atoms in the reacted interface. But the major result of interest for the present discussion is that a decrease in Ag 4d emission intensity is seen in the sample annealed at RT with respect to the sample prepared at LNT. The fact that the area under the Ag peak is smaller after annealing gives a strong evidence for the activation or the enhancement of intermixing between Ag and Si at RT with respect to LNT and definitly a proof

that intermixing is present at least at RT. As shown in the figure the reduction of Ag 4d signal is different depending on the photon energy used. This result allows us to make an estimation of the intermixing. In fact the 15% attenuation of the Ag signal seen with $h\nu$=30 eV (i.e. with an escape depth of 7 Å) and the 5% attenuation seen with $h\nu$=21 eV, (i.e. with 15 Å of escape depth) are consistent with the assumption of 2 intermixed layers, if we hypotise approximately zero mixing at LNT. This estimation is only indicative and we do not want to over emphasize the absolute value. It is nevertheless noteworthy that a value similar to that deduced from the core line intensities is obtained independently in this way.

An intermixing of two layers seems to agree with the recent results by Oura et al. [10], who on the basis of ISS and surface potential measurements, describe the Ag $\sqrt{3} \times \sqrt{3}$ superstructure on Si(111) as constituted by Ag atoms beneath the surface, which is pure Si. The mobility of Ag atoms in the first few top layers of Si thus seems to be compatible with the presence of well defined Ag reconstructions. Our results therefore consitute an important step forward in the understanding of the Si(111)/Ag interface.

CONCLUSIONS

From two independent experiments we have evidence for intermixing at the Ag/Si(111) interface at RT involving the very top layers (about 2 ML) of the surface. The understanding of the Si/Ag interface growth for an extended coverage interval has to take in account the presence of this narrow reacted and mixed region, which is the actual substrate for the further Ag growth.

Acknowledgment

This work was supported by the Advanced Research Projects Agency of the Department of Defense under Contract No. N00014-79-C-0072.

The experiments were performd at the Stanford Synchrotron Radiation Laboratory which is supported by the National Science Foundation under Grant No. DMR 77-27489 in collaboration with the Stanford Linear Accelerator Center and the Department of Energy.

FIGURE CAPTIONS

Fig. 1 Angle integrated photoelectron energy distribution curves at $h\nu$=80 eV for Si(111)/Ag interfaces at increasing coverage θ (solid curves) compared with the FDC for a clean Si(111) cleaved surface (dashed curve) the coverages are given in monolayer units.

Fig. 2 EDCs at $h\nu$=130 eV, Cooper Minimum for the Ag 4d valence electrons, compared with the cleaved Si(111) valence band EDC at the same h (dashed)

Fig. 3 EDCs at $h\nu$=30 eV and $h\nu$=21 eV for Si(111) = 0.5 ml Ag as prepared at LNT and annealed at RT. The clean substrate [Si(111)] valence bands at the two energies are given for reference (dashed curves).

Fig. 4 Si 2p intensity profile (solid line) versus increasing Ag coverage (monolayer units, and Ag 3d reduced intensity (RI) versus reduced coverage ($R\theta = \theta/0.25$ ML) for the submonolayer interval (solid line).

The dash-dotted line is the result expected in absence of silver-silicon intermixing at the interface.

REFERENCES

1. J. A. Venables, J. Derrien, and A. P. Janssen, Surf. Sci. 95, 411 (1980).

2. J. Derrien, G. LeLay, and F. Salvan, Journal de Physique Letters 39, L287 (1980).

3. Y. Gotom and S. Ino; Japanese Journal of Applied Physics; 17, 2097 (1980).

4. A. McKinley, R. H. Williams and W. A. Parke, J. Phys. C. Solid State Physics 12, 2447 (1979).

5. G. Rossi, I. Abbati, L. Braicovich, I. Lindau, and W. E. Spicer; to be published in the proceeding 3rd Applied Surface Analysis Conference, Dayton 1981, an Application of Surface Science.

6. P. Pianetta, I. Lindau, and W. E. Spicer, in "Quantitative Surface Analysis of Materials, A Symposium Sponsored by ASTM Committee E-42 on Surface Analysis" (N. S. McIntyre, ed.), (Cleveland, Ohio, 2-3 March 1977, ASTM Special Technical Publication 643, pp. 105-123 (1978).

7. H. Gant and W. Monch, Surface Science 105, 217 (1981).

8. G. Rossi, I. Abbati, L. Braicovich, I. Lindau, and W. E. Spicer, Solid State Comm., in press.

   I. Abbati, G. Rossi, L. Braicovich, I. Lindau, and W. E. Spicer, J. Vac. Sci. Tech. 19, No. 4 (1981)

9. L. Braicovich, C. M. Garner, P. R. Skeath, C. Y. Su, P. W. Chue, I. Lindau, and W. E. Spicer, Phys. Rev. B 20, 5131 (1979).

10. K. Oura, T. Taminaga and T. Solid State Comm. 37, 523 (19810.

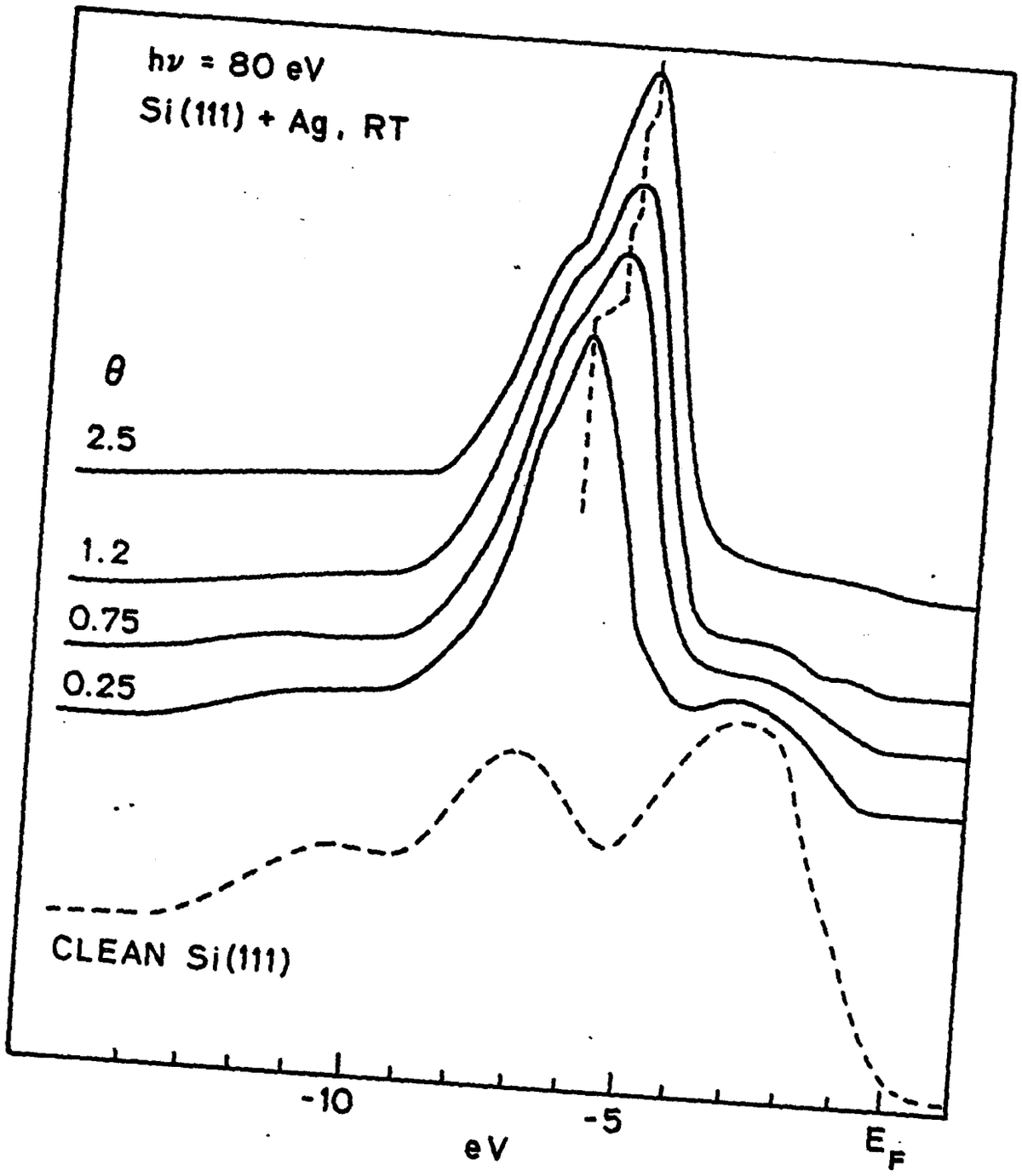

Fig. 1

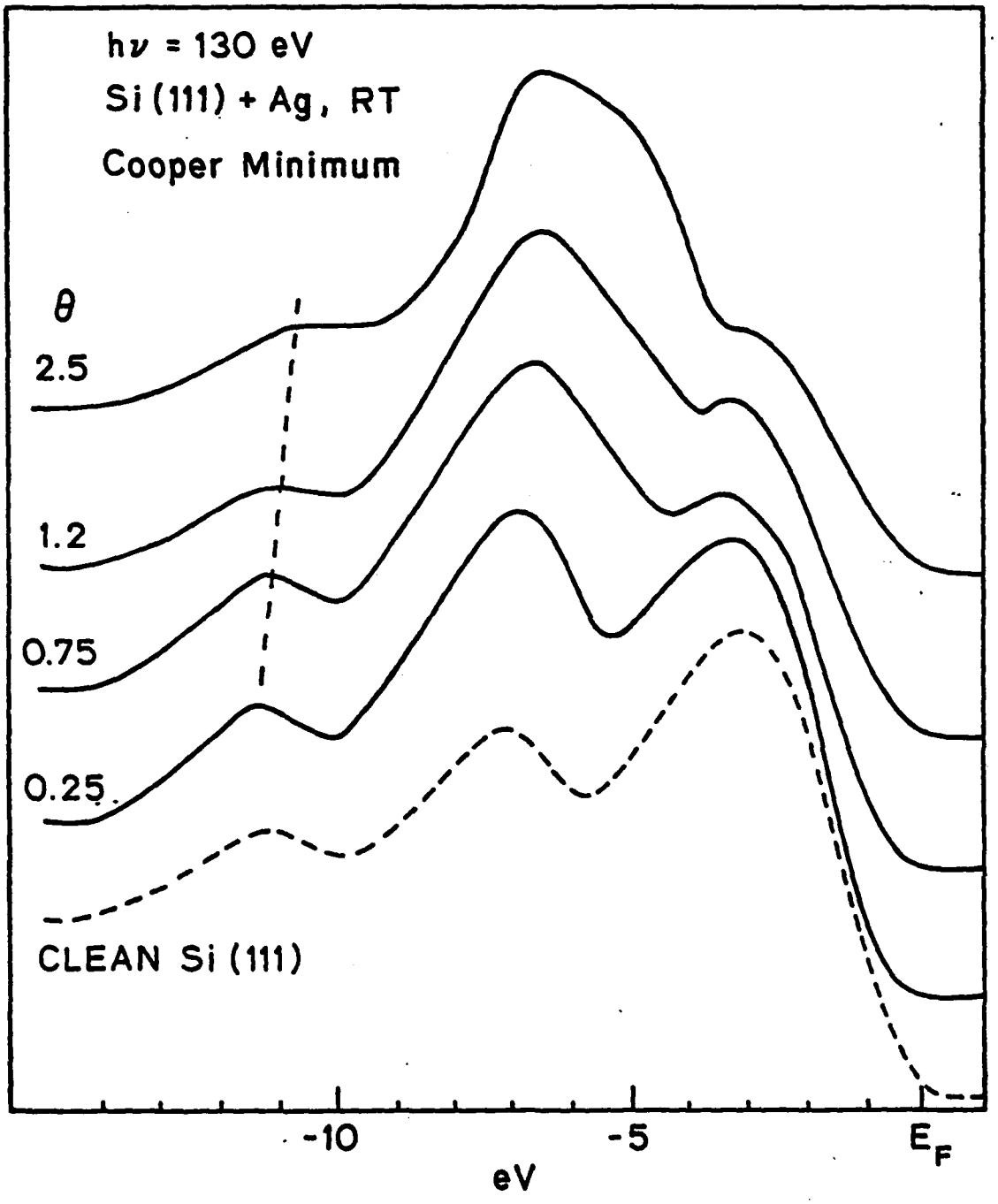
hν = 130 eV
Si (111) + Ag, RT
Cooper Minimum
θ
2.5
1.2
0.75
0.25
CLEAN Si (111)
-10
-5
E_F
eV

Fig 2

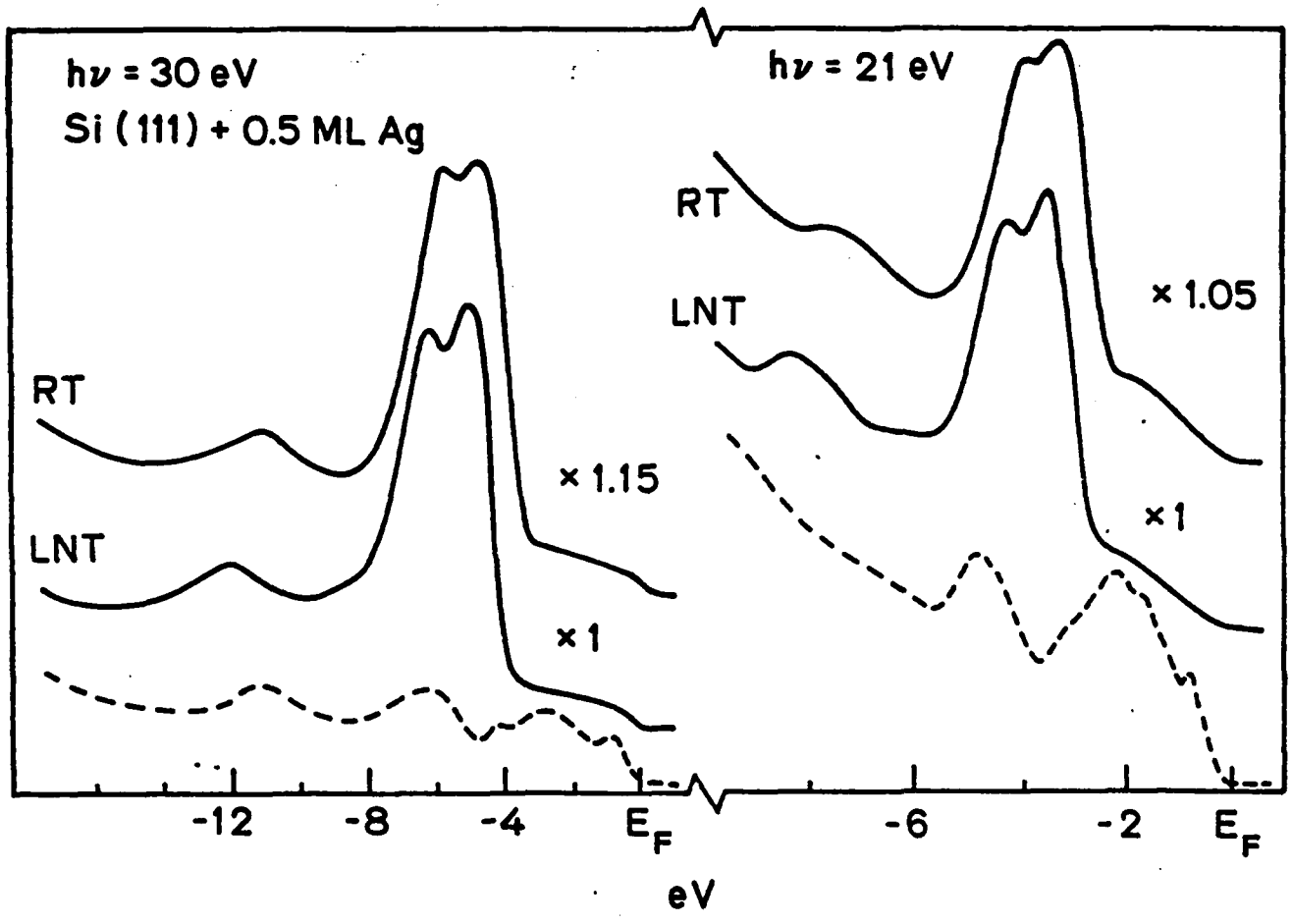
hν = 30 eV
Si (111) + 0.5 ML Ag
RT
LNT
× 1.15
× 1
-12
-8
-4
E_F
hν = 21 eV
RT
LNT
× 1.05
× 1
-6
-2
E_F
eV

Fig 3

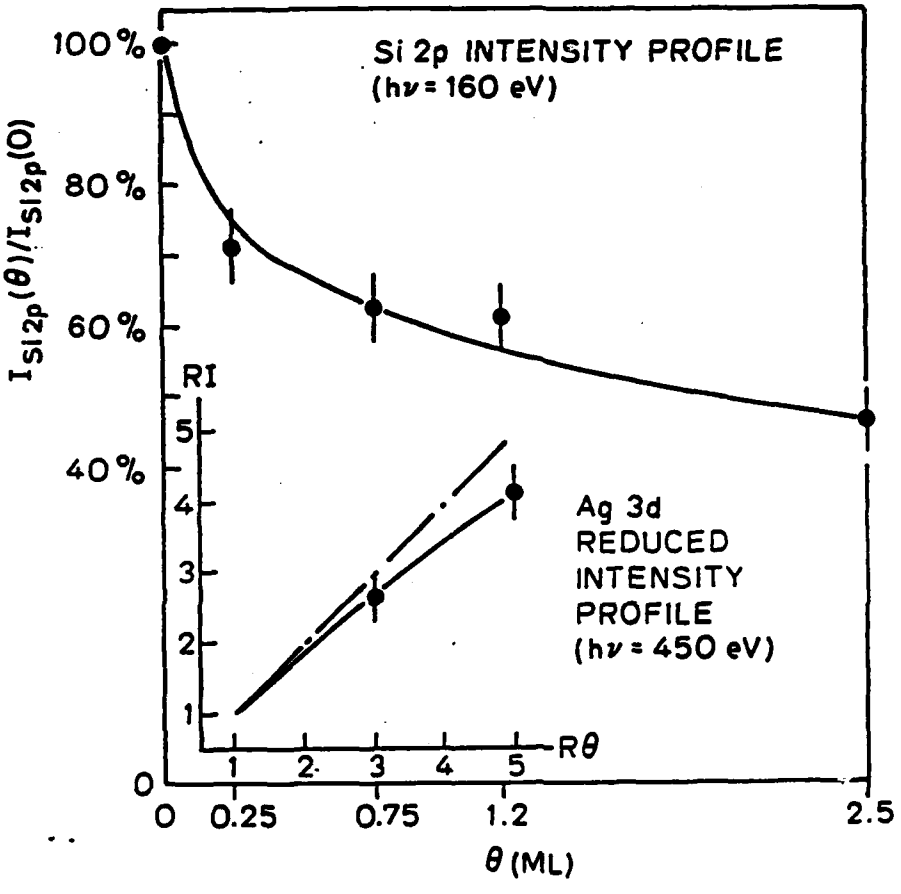
Si 2p INTENSITY PROFILE
(hν = 160 eV)
100%
80%
60%
40%
0
$I_{Si2p}(\theta)/I_{Si2p}(0)$
RI
5
4
3
2
1
Ag 3d
REDUCED
INTENSITY
PROFILE
(hν = 450 eV)
Rθ
1
2
3
4
5
0
0.25
0.75
1.2
2.5
θ (ML)

Fig 4

G. C. Y. Su, I. Lindau, P. R. Skeath, I. Hino, and W. E. Spicer, "Photoemission Studies of As and Its Room Temperature Oxidation," to appear in Surface Science.

To appear in Surf. Sci.

Photoemission Studies of As and Its Room Temperature Oxidation*

C. Y. Su, I. Lindau, P. R. Skeath, I. Hino, and W. E. Spicer**
Electrical Engineering Department
Stanford University
Stanford, California 94305

ABSTRACT

The room temperature adsorption of oxygen on in situ prepared As films has been investigated with photoemission. Direct formation of a disordered As_2O_3 layer is confirmed by comparison of the photoemission spectra of the oxidized As film to those of gas phase As_4O_6 and crystalline As_2O_3. Discussion of the role of s-p Hybridization in determining the electronic structure of As_2O_3 is offered based on the measured photoemission spectra.

---

*Work supported by DARPA through ONR under Contract No. N00014-79-C-0072 and by ONR under Contract No.00014-75-0289. Experiments were performed at the Stanford Synchrotron Radiation Laboratory which is supported by NSF under Grant NO. DMR77-27489 in cooperation with SLAC and DOE.
**Stanford Ascherman Professor of Engineering

INTRODUCTION

Two arsenic chalcogenides, As_2S_3 and As_2Se_3, are known to form stable semiconducting glasses of considerable technological importance as infrared transmitting window materials and as visible-sensitive large area photoconductors. Because of this, the optical properties and transport properties of these glasses, including their crystalline counterparts, have been well studied[1]; efforts to describe the underlying electronic structure with theoretical calculations and photoelectron spectroscopic measurements of the density of valence states (DOVS) have also emerged [2-7]. Similar studies have also been extended to include As_2O_3 [5-7]. There are also a few other reasons to study As_2O_3. As_2O_3 forms layer-lattice compound (claudetite) similar to As_2S_3 and As_2Se_3. However, the intralayer bonding in As_2S_3 and As_2Se_3 is highly covalent, whereas that in As_2O_3 is more ionic. Another property which makes arsenic oxide unique among arsenic chalcogenides is that a molecular compound can be formed with the composition As_2O_3 (arsenolite), whereas molecular compounds with S or Se are formed only with As rich compositions (As_4S_3, As_4S_4 etc.). Measurements of the DOVS of As_2O_3 are also of interest for the extensively investigated problem of oxygen adsorption on GaAs surfaces [8].

Previous photoemission measurements of DOVS of As_2O_3 have been performed on vacuum deposited As_2O_3 films [5-7]. We report here results obtained from exposing clean As films, prepared in ultra high vacuum, to a controlled amount of oxygen.

EXPERIMENTAL

The As film was obtained by flashing As from a GaAs crystal onto an in situ cleaved Si(111) surface in an ultra-high-vacuum preparation chamber connected to the measurement chamber. The GaAs crystal was contained in a quartz crucible held by the heater filament. The crucible and the heater were surrounded by a ~4 inch long stainless steel collimating shield. The ratio of As flux to Ga flux at the exit of the shield was maximumized by not having the crucible in line with the direction of the collimating shield. The GaAs crystal was well outgased before deposition, and mass spectral analyses were carried out to determine the heater current that delivers a negligible amount of Ga. The Si-2p emission from the Si substrate was measured both before and after As deposition by a Mg-Kα x-ray source mounted in the measurement chamber. This emission was completely attenuated after deposition, hence the thickness of the As film should be at least 100 Å. No oxygen contamination was found by checking the O-1s signal. Some Ga incorporation, however, had occurred. The Ga-3d signal was detectable only in the spectrum taken with a photon energy of 30 eV (fig. 1 below); in the Mg-Kα spectrum, the Ga-3d intensity was below the noise level. Assuming approximately equal photoionization cross section for the As valence band and the GaAs valence band, the amount of Ga was estimated to be <u>at most</u> 1% of a monolayer.

Oxygen exposures were made in the measurement chamber (base pressure ~7×10^{-11} torr) by leaking research grade oxygen through a bakable leak valve. Oxygen pressure was monitored by a cold cathode gauge. A hot filament ion gauge operating at 0.4 mA emission current was also present during one exposure in order to speed up the oxygen uptake.

Photoelectrons were energy analyzed with a double pass cylindrical mirror analyzer (CMA) operated in the pre-retarding mode. Light sources used were synchrotron radiation from the 8° line of the Stanford Synchrotron Radiation Laboratory (SSRL). The combined monochromator-analyzer resolution was 0.25 eV for 21 eV spectra and 0.3 eV for 30 eV spectra.

RESULTS AND DISCUSSION

Clean As

Before discussing the DOVS of oxidized As, we briefly examine the spectra of clean As. In fig. 1 we show the valence spectra taken with 21 eV and 30 eV photons. The leading edge of the DOVS of As starts to fall at ~2 eV below the Fermi level and gradually reaches zero intensity at ~0.3 eV below the Fermi level. (The Fermi level is taken as the energy zero in all photoemission spectra below.) The absence of density of states near the Fermi level is in contrast to the spectrum of the substrate Si (the second from top curve, fig. 1), upon which the As was deposited, and the Fermi edge of the spectrum of an in situ evaporated Ag film (the top curve, fig. 1). The peaked feature superposed on the leading edge of the Si spectrum, indicated by an arrow in fig. 1, is due to the now well known surface states of the Si(111)2x1 surface [9]. The comparison to the spectrum of the Ag film suggests that the As film is in a semiconducting state rather than a semimetal state expected for crystalline As. We take this as experimental evidence that the As films studied here are amorphous. (The constrast provided by the surface

states of Si also clearly suggests that no 'extra' states near or above the VBM have to be considered for amorphous As. The conditions for preparing this film are similar to those used by Ley et. al. [10] to prepare amorphous As.)

Other features in the DOVS of As are the two peaks in the 0-6 eV binding energy region, which are primarily bonding p electrons in character. Features expected for the s electrons of As are barely seen above the secondary electron background of the 30 eV spectrum. In the upper two curves of fig. 2 we have indicated in the 21 eV and the 30 eV spectrum smooth, featureless (except a slowly rising step immediately passing the large peaks of primary photoelectrons) backgrounds. The spectra after subtracting the smooth backgrounds can be compared to the XPS spectra of crystalline and amorphous As (see inset) obtained by Bishop and Shevchik [2]. Good agreement can be found in the p-band: the first peak in the p-band is located at 2.3±0.2 eV below the Fermi level, and the splitting in the p-band is 2.2±0.2 eV. The s-like-band cannot be clearly seen in the 21 eV spectrum, because part of the band is close to the work function cutoff. The 30 eV spectrum fully covers these bands; however, the intensity of the s-like-band is drastically suppressed compared to that in the XPS spectra, due to a matrix element effect. The major change in going from crystalline to amorphous As in the XPS spectra, as shown in the inset, is the flattening of the split s-band. Owing to the low intensity of the s-band in the 30 eV spectrum, no clear assessment of the splitting can be made. Nevertheless, we have indicated above the region of the s-band in the 30 eV spectrum the 3.5 eV splitting deduced from the XPS spectrum of crystalline As. It

appears that two features with the right splitting are discernable. It can therefore at least be said that the case of replacement of the doublet with a single peak in amorphous As, as stated by Ley et. al. [10], is not observed here.

Oxidized As

An overview of the DOVS of As subjected to two oxygen exposures, taken wih 30 eV synchrotron radiation, is shown in fig. 3. The changes in the As-3d level, measured with a Mg-Kα source, with oxygen exposures are also shown in the inset of fig. 3. There is no measurable oxygen uptake after exposing to 10^5 L molecular oxygen (i.e., an exposure made without the presence of a hot filament ion gauge or any other source of excitation of the oxygen molecules), as evidenced by the lack of change in either the valence band or the As-3d level. Further exposure to 10^7 L oxygen with the presence of a hot filament ion gauge (emission current=0.4 mA) produced a 3.4±0.2 eV chemical shift in the As-3d level and drastic changes in the valence band region characteristic of oxidized surfaces. Assuming an escape depth of ~30 Å for photoelectrons excited from the As-3d level, the strength of the shifted peak indicates an oxide coverage of only ~0.8 monolayer. The valence band spectra, which are more surface sensitive, however, are dominated by oxygen induced features.

The 3.4 eV shift in the As-3d level is close to the usually quoted binding energy difference between elemental As and As_2O_3, although ambiguity still exists in the literature on how such a value should be obtained. We mention only the result of Holm and Storp [11], who have

measured the As level due to elemental As and that due to As_2O_3 simultaneously on one sample, and found the separation between the two levels to be 3.5 eV. The agreement with the present result is satisfactory.

A more definite signature of the formation of As_2O_3 is found in the DOVS. In the center panels of fig. 4, we present the 21 eV and the 30 eV spectra of oxidized As, with smooth backgrounds of secondary electrons removed. The features in the region of 1 eV to 4 eV BE in the 21 eV and the 30 eV spectra are due to p-band electrons of the underlying As. The dashed extrapolation of the leading edge of the oxygen nonbonding peak (labeled N in fig. 4) provides an approximate representation of the spectra with substrate emission removed. In the lower panel of fig. 4, we have reproduced the He-I spectrum of gas phase As_4O_6 obtained by Cannington and Whitfield [12]. The As_4O_6 molecules were produced by vacuum sublimation of powdered As_2O_3 at 190°C. A comparison of the lower panel and the second lower panel suggests that the spectrum of the oxidized As fits as an <u>envelope</u> over the fine structures of the spectrum of gas phase As_4O_6, or that homogeneous broadening of all fine structures in the spectrum of gas phase As_4O_6 leads to the spectrum of oxidized As. Part of the broadening is instrumental. The energy resolution in the gas phase spectrum is not constant through the spectrum and ranges from 30 meV to 60 meV, whereas the energy resolution used in this work is constant through the whole spectrum and is 250 meV for the 21 eV spectrum and 300 meV for the 30 eV spectrum. Much of the broadening has to come from solid state effects, if there is a true correspondence between the solid spectrum and the gas phase spectrum, because there are features in

the gas phase spectrum separated by more than 1 eV and yet are not resolved in the spectrum of oxidized As. This point will later be further elucidated by comparing with spectra of crystalline As_2O_3 films.

The correspondence between the gas phase spectrum and the spectrum of oxidized As obtained in this work was put on an absolute energy scale by aligninng the most prominent non-bonding oxygen peak in the gas phase spectrum with the peak at 5.4 eV binding energy (referenced to the Fermi level) in the spectrum of oxidized As. The ionization energy of that peak is 11.52 eV (table 1 of reference 12). The work function of As is about 5.1 eV [13]. Hence peak N in the spectrum of oxidized As has a binding energy of 10.5 eV referenced to the vacuum level. This binding energy is ~1 eV lower than the ionization energy of the corresponding peak in the gas phase spectrum, which can be easily accounted for by the additional extra-atomic relaxation energy in solids.

The structural order of the oxide layer can be examined by comparison with the spectra of crystalline As_2O_3. The He-I ($h\nu$=21.2 eV), He-II ($h\nu$=40.8 eV), and Al-Kα ($h\nu$=1486 eV) spectra of crystalline As_2O_3 obtained by Wimmer et al. [5-7] are reproduced in the top panel of fig. 4. In the work of Wimmer et. al., the As_2O_3 film was prepared by high vacuum (10^{-8} torr) in situ evaporation of powdered As_2O_3 onto a stainless steel substrate, and the film was checked by RHEED to be crystalline. There are more features in the crystalline spectra than in the spectra of oxidized As; they are labeled I, II, III, and IV from low binding energy to high binding energy. There is also a strong photon energy dependence of the relative intensities in the features as

expected for a crystalline material. The binding energies given by Wimmer et. al. were referred to the VBM of the As_2O_3 film. Here we have presented these spectra with feature II lined up with peak N in the spectra of oxidized As. This corresponds to a VBM-Fermi level separation of ~2.3 eV in the case of oxidized As. This separation is roughly confirmed by extrapolating the low binding edge of peak N in the spectra obtained in this work. After such alignment, considerable similarity can be seen between the crystalline spectra and the monolayer-oxide spectra. A few differences in details are explained below. The prominent feature IV in the He-II and the Al-Kα spectrum of the crystalline form originate mainly from the 4s level of As. This feature is again suppressed in the 21 and 30 eV spectra of the monolayer-oxide obtained here because of a matrix element effect. Another difference between the spectra of the crystalline form and the monolayer-oxide, however, can be explained only in terms of differences in structural orders. In the 7-11 eV binding energy region, the crystalline spectra show two resolved features, II and III, in good correspondence to the gas phase spectrum, whereas the monolayer-oxide spectra show only one broad feature (band B). This difference cannot be explained by the different energy resolutions used, because the energy resolution used to obtain the Al-Kα spectrum was far poorer (≥1.2 eV [5]) than the resolutions used in this work. The splitting in the 7-11 eV binding energy region in the gas phase spectrum and the crystalline spectra arises from As-O bonding orbitals with opposite symmetries with respect to the plane bisecting the As-O-As angle (i.e., the splitting between the σ and the π component of the As-O-As bonding). A random variation and/or a distortion of the

As-O-As angles tend to flatten out the splitting. The lack of the splitting in our data (center panels of fig. 4) suggests that room temperature adsorption of oxygen on As results in a disordered oxide layer.

It is not clear if the structural arrangement of the disordered monolayer oxide is similar to that of vitreous As_2O_3. There is little direct structural information available for vitreous As_2O_3. Lucovsky and Galeener [14], through detailed interpretation of both Raman spectra and ir reflectance, have proposed that v-As_2O_3 contains local regions characterized by either a layer-like local order or an As_4O_6-like local order. Since the standard free energies of reaction for forming arsenolite (ΔG=-137.6 Kcal/mole) and claudetite (ΔG=-135.9 Kcal/mole) at room temperature are close, the picture described by Lucovsky and Galeener [14] is likely to be also applicable to the monolayer oxide resulting from room temperature oxidation of As. If this is indeed the case, the similarities observed between all spectra in fig. 4 then suggest that the influence of the difference between layer-like and As_4O_6-like order on electronic structures is not important. The essential feature of the electronic structure of As_2O_3 consists of a non-bonding band and a bonding band, whose centers of gravity are separated by ~3.3 eV. This essential feature is largely determined by the $AsO_{3/2}$ pyramids, which are the building units in either layer-like or As_4O_6 structural arrangement.

Another point of interest in studying the electronic structure of A_2B_3 compounds is whether the non-bonding band is purely B-atom derived [1,3]. For powdered crystalline arsenolite, Wimmer et. al. [5-7] have

shown by soft x-ray emission spectra that the As lone pair makes a significant contribution to the non-bonding band. The question can be asked if in different long range structural arrangements (i.e., different ways of connecting $AsO_{3/2}$ pyramids) the relative contribution from As and O lone pairs to the non-bonding band would change. Two extreme pictures can be considered: In one As participates in bonding with three oxygen atoms in p^3 configuration so that all p-like electrons from As are in the bonding band and the lone pair on As has an s^2 configuration [3]. In the other, As assumes sp^3 bonding configuration, and the bonding to three oxygen leaves one sp^3 lone pair [1]. The two pictures predict different non-bonding to bonding p-electrons ratio. Such ratio of p-electrons should be rather uniquely reflected in our spectra of the monolayer As_2O_3, because s-electrons are preferentially suppressed due to a weak matrix element for the photoionization transition. The former picture predicts a non-bonding to bonding p-electron ratio of 3:6, while the latter predicts 4.5:4.5. It is difficult to obtain quantitative assessment of the ratio of the strengths of the bonding and nonbonding bands from the measured spectra, because the bonding band may be broad enough to have substantial overlap with the nonbonding band and the matrix elements for the nonbonding and the bonding orbitals may be different. Nevertheless, the spectra of the oxidized As shown in the center two panels of fig. 4 are suggestive of a nonbonding to bonding band intensity ratio closer to 1:1 than 1:2,, i.e., our results suggest that s-p hybridization to some extent is important even for a disordered layer of As_2O_3. This result should be contrasted to the case of amorphous As_2S_3, where soft x-ray emission experiments [5-7] do not show sig-

nificant contribution from the s lone pair to the non-bonding band. This difference can be explained by the higher ionicity of the As-O bond: The repulsion between the ionic charges on oxygen atoms prevents the O-As-O angle in any $AsO_{3/2}$ pyramid from closing to 90°, and hence prohibits the p^3 configuration.

SUMMARY

In summary, we have shown that room temperature adsorption of oxygen on amorphous As results in direct oxide formation. The electronic structure of oxidized As has been shown to be similar to either that of isolated As_4O_6 molecules, or that of crystalline As_2O_3. The photoemission spectra of the oxidized As film also suggest that As_2O_3 formed in such a way is noncrystalline. The essential features of the electronic structure of the As_2O_3 formed are a non-bonding band and a bonding band separated by ~3.3 eV. The contribution of As lone pairs to the non-bonding band was found to be important in the case of disordered monolayer As_2O_3.

REFERENCES

1. R. Zallen and D. F. Blossey, The Optical and Electrical Properties of Compounds with Layered structures, ed. P. A. Lee (Reidel, Netherlands,1975)

2. S. G. Bishop and N. J. Shevchik, Phys. Rev. B 12, 1567(1975)

3. N. J. Shevchik and S. G. Bishop, Solid State Comm. 17, 269(1975)

4. W. R. Salaneck and R. Zallen, Solid State Commun. 20, 793(1976)

5. E. Wimmer, P. Weinberger, A. Kosakov, and G. Leonhardt, Phys. Stat. Sol (b) 89, 619(1978) and references cited

6. A. Kosakov, H. Neumann, and G. Leonhardt, Phys. Lett. 62A, 95(1977)

7. G. Leonhardt, H. Neumann, A. Kosakov, T. Gotze, and M. Petke, Physica Scripta 16, 448(1977)

8. C. Y. Su, I. Lindau, P. W. Chye, P. R. Skeath, and W. E. Spicer,J. Vac. Sci. Technol. 17, (1980) and references cited

9. L. F. Wagner and W. E. Spicer, Phys. Rev. Lett. 28, 1381(1972)

10. L. Ley, R. A. Pollak, S. P. Kowalczyk, F. R. McFeely, and D. A. Shirley, Phys. Rev. B 8, 641(1973)

11. L. D. Hulett and T. A. Carlson, Appl. Spectroscopy, 25, 33(1971); W. J. Stec, W. E. Morgan, R. G. Albridge, J. R. van Walzer, Inorg. Chem. 11, 219(1972); R. Holm and S. Storp, Appl. Phys. 9, 217(1976); C. D. Wagner and P. Biloen, Surf. Sci. 35, 82(1973)

12. P. H. Cannington and H. J. Whitfield, J. Electr. Spectr. Related Phenom. 10, 35(1977)

13. V. S. Formenko, Handbook of Thermionic Properties, ed. G. V. Samsonov (Plenum, New York, 1966)

14. G. Lucovsky and F. L. Galeener, J. Non-cryst. Solids 37, 53(1980)

FIGURE CAPTIONS

Figure 1: Photoemission spectra of clean As taken at $h\nu$=30 eV (the bottom curve) and $h\nu$=21 eV (the curve second from the bottom). The spectrum of the Si substrate taken at $h\nu$=21 eV prior to the deposition of As is also shown for comparison (the second curve from the top); we notice particularly the feature indicated by an arrow which is attributed to the surface states of Si(111). The top curve is the Fermi edge in the spectrum of a Ag film evaporated in situ.

Figure 2: Photoemission spectra of clean As with the backgrounds due to the secondary electrons being removed (the bottom curves). When compared to the XPS (Al-Kα, $h\nu$=1486 eV) spectra (the inset) of Bishop and Shevchik [2], the s-band in the 30 eV and the 21 eV spectra appear to be drastically suppressed.

Figure 3: Photoemission spectra of clean and oxygen-exposed As taken at $h\nu$=30 eV. The 10^7L exposure was made with excited oxygen (see text). The inset gives the As-3d levels of clean and oxygen-exposed As, obtained with Mg-Kα excitation.

Figure 4: Comparison of spectra of oxidized As film (the center two panels) to the He-I spectrum of gas phase As_4O_6 (the bottom panel) and the spectra of crystalline As_2O_3 (the top panel) obtained with He-I, He-II and Al-Kα excitations [5-7].

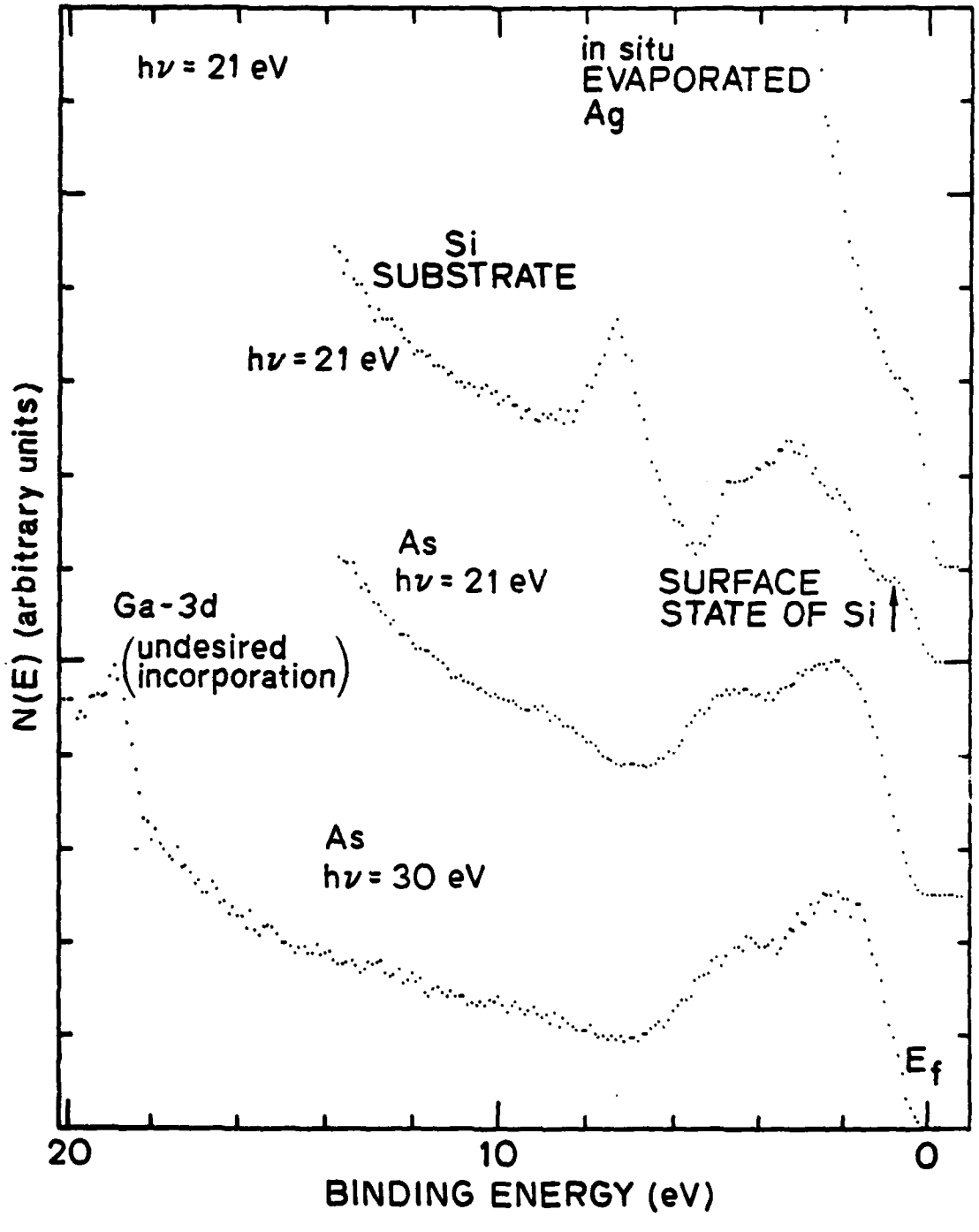
hν = 21 eV
in situ
EVAPORATED
Ag
Si
SUBSTRATE
hν = 21 eV
As
hν = 21 eV
SURFACE
STATE OF Si
Ga-3d
(undesired
incorporation)
As
hν = 30 eV
E_f
N(E) (arbitrary units)
20
10
0
BINDING ENERGY (eV)

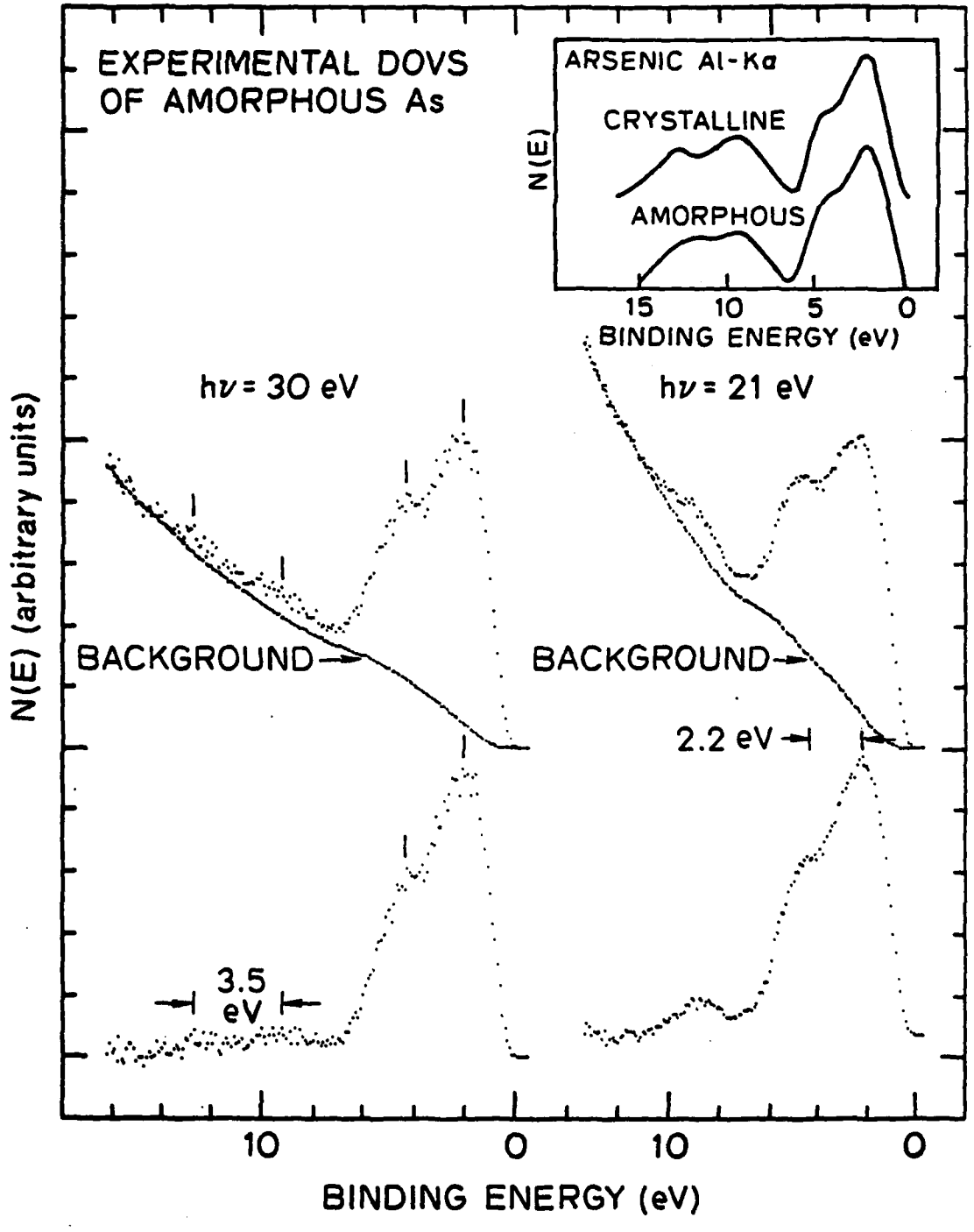
EXPERIMENTAL DOVS
OF AMORPHOUS As
ARSENIC Al-Kα
CRYSTALLINE
AMORPHOUS
N(E)
15
10
5
0
BINDING ENERGY (eV)
hν = 30 eV
hν = 21 eV
BACKGROUND
BACKGROUND
2.2 eV
3.5
eV
N(E) (arbitrary units)
10
0
10
0
BINDING ENERGY (eV)

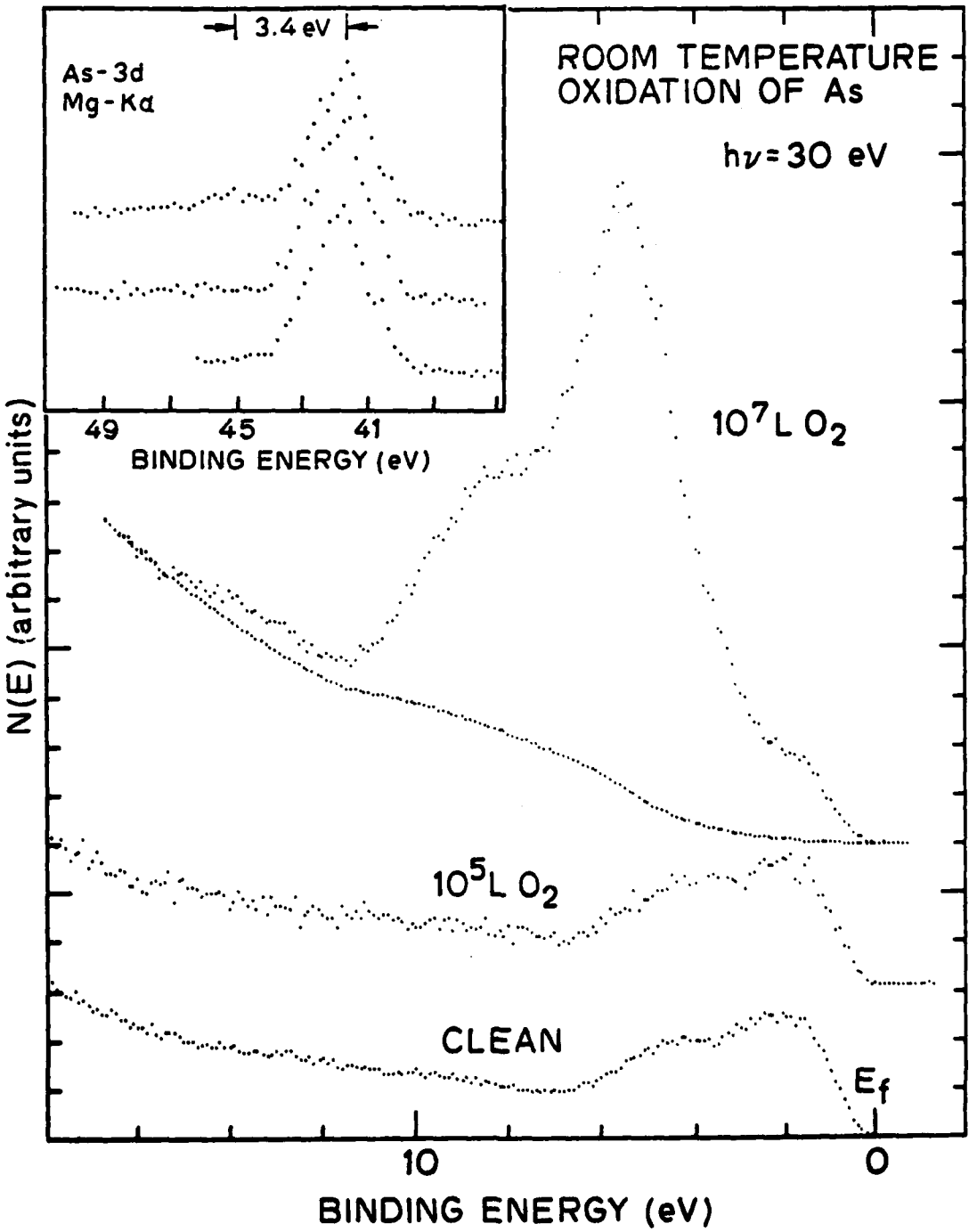
3.4 eV
As-3d
Mg-Kα
49
45
41
BINDING ENERGY (eV)
ROOM TEMPERATURE
OXIDATION OF As
hν = 30 eV
10^7 L O2
10^5 L O2
CLEAN
Ef
N(E) (arbitrary units)
10
0
BINDING ENERGY (eV)

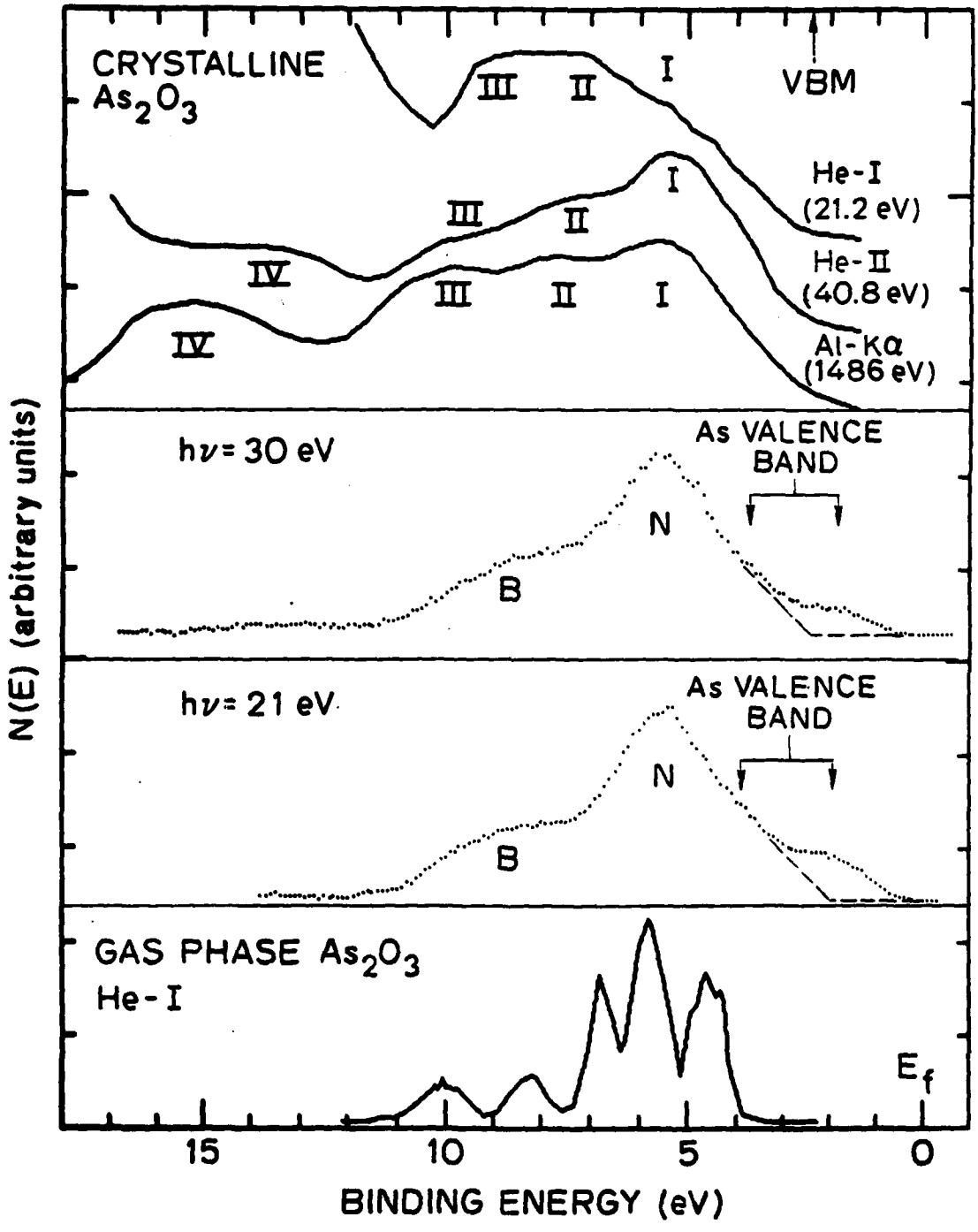
CRYSTALLINE
As2O3
III
II
I
VBM
He-I
(21.2 eV)
He-II
(40.8 eV)
Al-Kα
(1486 eV)
IV
hν= 30 eV
As VALENCE
BAND
N
B
hν= 21 eV
GAS PHASE As2O3
He-I
Ef
N(E) (arbitrary units)
15
10
5
0
BINDING ENERGY (eV)

H. C. Y. Su, P. R. Skeath, I. Lindau, and W. E. Spicer, "Photoemission Studies of Room-temperature Oxidized Surfaces" to be published in Surface Science.

To appear in Surf. Sci.

Photoemission Studies of Room-temperature Oxidized Surfaces

C. Y. Su, P. R. Skeath, I. Lindau, and W. E. Spicer**
Electrical Engineering Department
Stanford University
Stanford, California 94305

ABSTRACT

The oxidation of in situ prepared Ga films at room temperature has been studied with photoemission. Direct formation of Ga_2O_3 has been observed. An interpretation of the valence band spectrum of Ga_2O_3 in terms of the electronic structure of Ga_2O_3 is offered. Correspondence between a donor-like bonding band, due to the interaction between a doubly occupied oxygen lone pair and an empty Ga orbital, an oxygen nonbonding band, and a Ga-O-Ga bonding band and three features in the valence band spectrum of oxidized Ga has been found. Interpretation of the photoemission spectrum of the recently reported chemisorbed-oxygen on Ga metal at 70°K is suggested based on the understanding of the spectrum of Ga_2O_3. The possible existence of an intermediate oxidation state formed by the room temperature oxidation of Ga films is also discussed based on the presence of intermediate chemical shifts ($\Delta E \leq 2.0$ eV) in the Ga-3d level.

---

*Work supported by DARPA and monitored by ONR under Contract No. N00014-79-C-0072 and by ONR under Contract No. N00014-75-0289. Experiments were performed at the Stanford Synchrotron Radiation Laboratory which is supported by NSF under Grant No. DMR77-27489 in coorperation with SLAC and DOE.
**Stanford W. Ascherman Professor of Engineering

INTRODUCTION

The nature of the chemisorbed oxygen produced by room temperature adsorption of oxygen on Al surfaces has been the subject of a large number of studies [1]. It is therefore also interesting to study the interaction of oxygen with Ga, which has an electronic structure similar to that of Al. Recently, Schmeisser et. al. [2] have observed a chemisorption phase of oxygen on Ga metal at ~70°K; interpretation of the O-2p related features in the photoemission spectrum of this chemisorbed oxygen on Ga, however, has been lacking. In this paper we present the experimental spectrum of Ga_2O_3 obtained from room temperature oxidized Ga, and give a detailed interpretation of the photoemission spectrum. Detailed understanding of the electronic structure of Ga_2O_3 can provide a useful reference for understanding the photoemission spectrum of chemisorbed oxygen on Ga; we will indeed see an interesting suggestion, based on the understanding of the electronic structure of Ga_2O_3, made about the nature of the chemisorbed oxygen observed by Schmeisser et. al. [2] and the present authors on sputter-disordered, Ga-rich surfaces [3]. Measurements and interpretation of the density of valence states of Ga_2O_3 is also of interest for the heavily investigated problem of oxygen adsorption on GaAs surfaces [3,4].

EXPERIMENTAL

Experiments were performed in a stainless steel ultra high vacuum chamber with base pressure ~10^{-10} torr. Ga metal was deposited on an *in situ* cleaved GaAs(110) surface. The thickness of the Ga film was about

100 Å, as determined by a quartz crystal thickness monitor. Oxygen exposures were made by leaking in research grade oxygen through a bakable leak valve. Oxygen pressure was monitored by a Redhead cold cathode gauge and a Varian 860 cold cathode gauge. The light source used was synchrotron radiation from the 8° line of the Stanford Synchrotron Radiation Laboratory (SSRL). Photoelectrons were energy analyzed with a double pass cylindrical mirrror analyzer. The combined monochromator-analyzer resolution for 30 eV photon energy is 0.3 eV.

RESULTS AND DISCUSSION

Fig. 1 gives an overview of the spectra, displayed vertically with oxygen exposures indicated with each spectrum. The spectrum of clean Ga shows a featureless valence band and spin-orbit split Ga-3d levels. With 100 L oxygen exposure, only a weak oxygen induced feature is seen in the valence band region and little change occurred to the Ga-3d levels. With 10^4 L exposure, a chemically shifted Ga-3d appeared and strong oxygen induced features appeared in the valence band region. The adsorption of oxygen appears to have saturated at 10^4 L exposure, because no significant change is seen in the spectra of higher exposures (10^5 L and 10^6 L).

Details of the density of valence states (DOVS) of oxidized Ga are shown in fig. 2. The upper curve is a blow-up of the valence band region of the 2×10^6 L spectrum of fig. 1, with the smooth, featureless secondary electron background indicated. The lower curve shows the DOVS after removing the background. There are three features in the DOVS at 5.6, 7.7, and 10.5 eV below the Fermi level (which is the energy zero to

be used throughout this work), in good agreement with the results obtained by Bachrach at 130 eV photon energy [5]. These fetures are labeled I, II and III in fig. 2 in the order of increasing binding energy.

Since the melting point of Ga is near room temperature we expect no long range order and relatively high mobility of the Ga atoms. It is thus not supprising to find the direct formation of Ga_2O_3 by exposing Ga to oxygen at room temperature. As we will see below, this is supported by the fact that the three features in the DOVS of oxidized Ga can be understood by following the tight binding analysis of the electronic structure of Al_2O_3 by Reilly [6]. The α-form (corundum) crystalline Al_2O_3 and Ga_2O_3 are isomorphic. In such a structure [7] each Ga atom is at the center of a distorted octahedron of oxygen atoms, with three oxygen closer to the Ga atom than the other three. Each Ga atom is thus expected to bond strongly with three O's and weakly with three other. Each oxygen atom is surrounded by four Ga's, bonding strongly to two and interacting weakly with the other two. The three oxygen atoms that are strongly bonded to a center Ga can be considered approximately at three corners of a tetrahedron enclosing that Ga. We can thus form sp^3 hybrids on each Ga, with three hybrids participating in bonding to three O's and one hybrid left empty. For an oxygen atom in a Ga-O-Ga bridge-bonding position, only two of the three p-orbitals participate in Ga-O bonding; the third p-orbital which is perpendicular to the plane containing the Ga-O-Ga angle remains non-bonding and forms a doubly-occupied lone pair. The oxygen lone pairs interacts with the empty sp^3 orbital on a nearby Ga atom and lowers its energy. Because the oxygen

lone pair and the Ga empty orbital point to each other at an angle, the interaction is expected to be weak. In addition, not all oxygen lone pairs can find available Ga empty orbitals; only two of the three oxygen atoms in the Ga_2O_3 unit can have such interaction, an oxygen lone pair remains intact on the third oxygen atom. Origins of the three features in the DOVS can now be assigned: feature I, the one with the lowest binding energy, is due to non-bonding oxygen lone pairs, feature II is due to the weak, donor-like interaction between the oxygen lone pair and the empty Ga orbital, and feature III is due to bonding electrons in the Ga-O-Ga bonding unit.

There is one aspect of the DOVS in discordance with the above simplified picture. In that picture, the ratio of non-bonding:weak-bonding:bonding electrons is expected to be 1:2:6. Such a ratio is certainly not indicated by the DOVS in fig. 2. Part of this deviation can be explained by the matrix elements of the photoionization process. Band I is purely p in character, whereas band II and III have considerable s character, it is thus possible to have band I preferentially enhanced at this relatively low photon energy ($h\nu$=32 eV). Another possible explanation is the deviation from the corundum structure. In the ß-form of the gallium sesquioxide [8], Ga atoms occupy two sets of crystallographic nonequivalent sites: half of the Ga atoms occupy ocatahedral sites and the other half occupies tetrahedral sites. Thus the average coordination of Ga atoms in ß-Ga_2O_3 are reduced compared to α-Ga_2O_3. This tends to reduce the interactions between oxygen lone pair and empty Ga orbitals. In fact, detailed structural studies of ß-Ga_2O_3 have shown three nonequivalent oxygen atoms in the Ga_2O_3 unit, and care-

ful examination of the different Ga-O bond lengths has led to the conclusion that only one of the three O's has a bond order greater than two [8]. Namely, only one of the three oxygen lone pairs interacts with empty Ga orbitals and lowers its energy. This brings the ratio of non-bonding, weak-bonding, and bonding electrons to 2:1:6. This ratio is closer to that which can be deduced from the experimental DOVS in fig. 2 than the 1:2:6 ratio (although we recognize the difficulty of extracting such number from the experimental DOVS due to substantial overlap between bands and different matrix elements of photoionization for different bands). Thermodynamic measurements show the β-Ga_2O_3 to be more stable at room temperature [8]. It is thus likely that β-form-like structure was produced by the room temperature oxidation of Ga. It is also possible that we have obtained a disordered oxide layer which contains both β-like and α-like local order. The broad bonding band (band III) in the experimental DOVS also suggests the formation of either β-like or a disordered layer: This is because the bonding band should be split into a σ-band and a π-band if only a single value of Ga-O-Ga angle exists, as is the case for α-form Ga_2O_3; there are, however, three different Ga-O-Ga angles in the β-form Ga_2O_3, and a random variation of the Ga-O-Ga angle may occur in noncrystalline Ga_2O_3, which tend to smear the splitting.

In the inset of fig. 2, we show the experimental DOVS of Al_2O_3 for comparison [9]. The spectrum was obtained by Balzarotti and Bianconi [9] using Al-Kα radiation. There are also three bands in the DOVS. The energy positions of the bands agree semiquantitatively with the tight binding calculation of Reilly [6]. This gives indirect support to the assignments of the origins of the bands in the DOVS of Ga_2O_3. We also

notice the following differences between the spectra of Ga_2O_3 and Al_2O_3 shown in fig. 2: The comparable strength of the donor-like bonding band and the non-bonding band in the XPS spectrum of Al_2O_3, instead of having the nonbonding band stronger than the donor-like bonding band, is caused by the higher crossection for the s-electrons at Al-Kα radiation than at $h\nu$=32 eV. The larger splitting between the non-bonding band and bonding bands in the Al_2O_3 DOVS than that in the Ga_2O_3 DOVS merely reflects the fact that the cohesive energy of Al_2O_3 is higher than that of Ga_2O_3.

The existence of a weak bonding band in addition to a non-bonding band and a bonding band is a unique feature of the oxides of column III metals. This is a direct manifest of the existence of oxygen atoms with bonding order greater than two. It is possible because

1. empty orbitals in the right energy range are available on metal atoms; In contrast, in oxides of column V elements such as As_2O_3, this does not happen because no empty orbitals are available from As. The doubly occupied lone pairs on As in fact interact repulsively with oxygen lone pairs in As_2O_3.

2. high ionicity of the metal-oxygen bond; Once the electronegativity of oxygen is fulfilled through the charge transfer in metal-oxygen bonds, the tendency of oxygen lone pairs to form donor bonds increases. In other words, the splitting between the non-bonding band and the weak-bonding band should scale with the splitting between the non-bonding band and the strong-bonding band. For example, Al-O bond is more ionic than Ga-O bond, hence the splitting between the non-bonding and the metal-O-metal bond-

ing band is bigger in Al_2O_3 (~8.5 eV) than in Ga_2O_3 (~4.9 eV), and the splitting between the non-bonding band and the O-metal dative bonding is also in the same order (4.2 eV in Al_2O_3, 2.1 eV in Ga_2O_3).

Fig. 3 gives details of the Ga-3d level. The upper curve is a blow-up of the Ga-3d part of the 2×10^6 L spectrum in fig. 1, with the smooth, featureless secondary background indicated. The center curve shows the spectrum with background removed. The lower curve is the Ga-3d spectrum of the clean Ga-3d film, with the secondary background removed. The Ga-3d levels of clean Ga-film show a well-resolved spin-orbit splitting of 0.39±0.08 eV, and the binding energy of the Ga-$3d_{5/2}$ is 18.5±0.25 eV below Fermi level. The spin-orbit splitting is lost in the chemically shifted Ga-3d levels of the oxidized Ga. The separation between the apparent peak position of the chemically shifted Ga-3d and the center of gravity of the Ga-3d of the clean surface is 2.0±0.2 eV, in good agreement with the result of Schon [10]. A more careful examination of the center curve of fig. 3, however, suggests the presence of other intermediate chemical shifts. These smaller shifts probably arise from incompletely oxidized Ga, i.e., Ga atoms bond to less than three oxygen atoms. This can occur when the oxidation process becomes diffusion-limitted and a deficiency of oxygen atoms for oxidizing subsurface Ga atoms sets in. A question immediately arising is the influence of these oxygen-deficient bonding complexes on the DOVS which we have just analyzed in terms of complete Ga_2O_3 order. We expect oxygen in these oxygen deficient bonding complexes to assume the same bridge bonding configura-

tion, GA-O-Ga, and hence the approximately same non-bonding-bonding splitting. The weak-bonding or the O-Ga dative bonding band, however, is expected to be missing, due to two possible reasons:

1. an empty Ga orbital, if it exists, cannot find a nearby oxygen lone pair because of the reduced oxygen coordination.

2. no empty Ga orbitals are available in the region of intermediately oxidized Ga. In such regions, Ga atoms bonded to oxygen are also bonded to other Ga atoms. Because the Ga-Ga bond is not as directional as the Ga-O bond, the hybridization of the orbitals of Ga atoms may change in such a way to eliminate any empty Ga orbital with the favorable energy position to form donor-like bond with the oxygen lone pairs.

Oxygen adsorption phases with the donor-like bonding band missing in the DOVS have indeed been observed by Schmeisser et. al. [2] on a Ga metal surface at low temperature (70°K), and by the present authors on disordered, Ga rich GaAs surfaces at room temperature [3]. The postulate of Schmeisser et. al. [2] that such DOVS is due to chemisorbed O_2 molecules appears to be entirely unnecessary. For example, in their case, the low mobility of Ga atoms at low temperature prohibits the formation of Ga_2O_3, and oxygen lone pairs in the surface Ga-O-Ga bonding units point to no Ga empty orbitals so that the donor-like bonding band is suppressed. The absence of any multiplet structure reminisent of the O-O bonding in the photoemission spectra observed by Schmeisser et. al. [2] and by us [3] also argues against the molecular-oxygen assignment.

The observation that the 70°K state oxygen has a higher work function than the room temperature oxygen state is also consistent with the above interpretation of the 70°K state oxygen: the Ga-O-Ga bonding units can be formed with oxygen retaining a position above the surface, whereas formation of Ga_2O_3 requires the O atom to "network" with more than three Ga atoms which can happen only by moving oxygen atoms into or beneath the surface; since oxygen carries net negative charge in forming Ga-O bonding, moving O atoms from outside to inside of the solid surface means reduction of work function. We again see no need to invoke "molecular" state to explain the change in work function. Returning now to the effect of these oxygen-deficient bonding complexes on the experimental DOVS of fig. 2, we believe that the major effect is to make the donor-like bonding band (band II) less prominent than that expected for the true DOVS of Ga_2O_3 [11], by contributing intensities only to the non-bonding band and the bonding band.

SUMMARY

In summary, we have performed high energy resolution photoemission studies of room temperature adsorption of oxygen on Ga metal. At saturation of the adsorption process, both Ga_2O_3 and regions of Ga bonded to less than three oxygen atoms are present. The chemical shift in the Ga-3d level characteristic of Ga_2O_3 has been measured to be 2.0±0.2 eV. Three features in the DOVS at 5.6, 7.7, and 10.5 eV binding energy have been successfully interpreted in terms of the oxygen non-bonding, the O-Ga donor-like bonding, and the Ga-O-Ga bonding band, respectively, of Ga_2O_3.

REFERENCES

1. See, for example, R. P. Messmer and D. R. Salahub, Phys. Rev. B 16, 3415(1977) and references therein

2. D. Schmeisser, K. Jacobi, and D. M. Kolb, Proc. ECOSS 3, Cannes 1980; D. Schmeisser and K. Jacobi, Surf. Sci. 108, 421(1981)

3. C. Y. Su, I. Lindau, P. W. Chye, P. R. Skeath, and W. E. Spicer, Photoemission Studies of the Interaction of Oxygen with GaAs(110), Phys. Rev. B, Feb. 15,1982(in press)

4. C. Y. Su, I. Lindau, P. R. Skeath, P. W. Chye and W. E. Spicer, J. Vac. Sci. Technol. 17, 936(1980) and references therein

5. R. Z. Bachrach, J. Vac. Sci. Technol. 15, 1340(1978)

6. M. H. Reilly, J. Phys. Chem. Solids 31, 1041(1970)

7. R. W. G. Wyckoff, Crystal Structures, 2nd ed., vol. 2 (Wiley, New York, 1964)

8. S. Geller, J. Chem. Phys. 33, 676 (1961)

9. A. Balzarotti and A. Bianconi, Phys. Stat. Sol. 76, 689(1976)

10. G. Schon, J. Electron Spectr. Related Phenom. 2, 75(1973)

11. In one case (reference 7) where we have obtained the spectrum of a thicker Ga_2O_3 film by heavy plasma oxidation of GaAs, the dative-bonding band indeed appeared to be more pronounced than that is shown in fig. 2. The experimental DOVS in that case, however, was taken at 100 eV photon energy, so it is not clear if direct comparison can be made with the present results.

FIGURE CAPTIONS

Figure 1: Photoemission spectra of clean and oxygen-exposed Ga taken at $h\nu$=32 eV.

Figure 2: Blow-ups of the valence band region of the $2x10^6$L spectrum of fig. 1, with the featureless background due to secondary electrons indicated (the center curve). The bottom curve shows the spectrum with the background removed; origins of the features in the spectrum are also indicated. The inset shows the XPS (Al-Kα, $h\nu$=1486 eV) valence band spectrum of Al_2O_3 [9] for comparison.

Figure 3: Blow-ups of the Ga-3d level of clean (the bottom curve) and oxidized (the top and the center curve, respectively with and without the secondary background) Ga. The arrow in the center spectrum point to a region of unresolved chemical shifts in the Ga-3d.

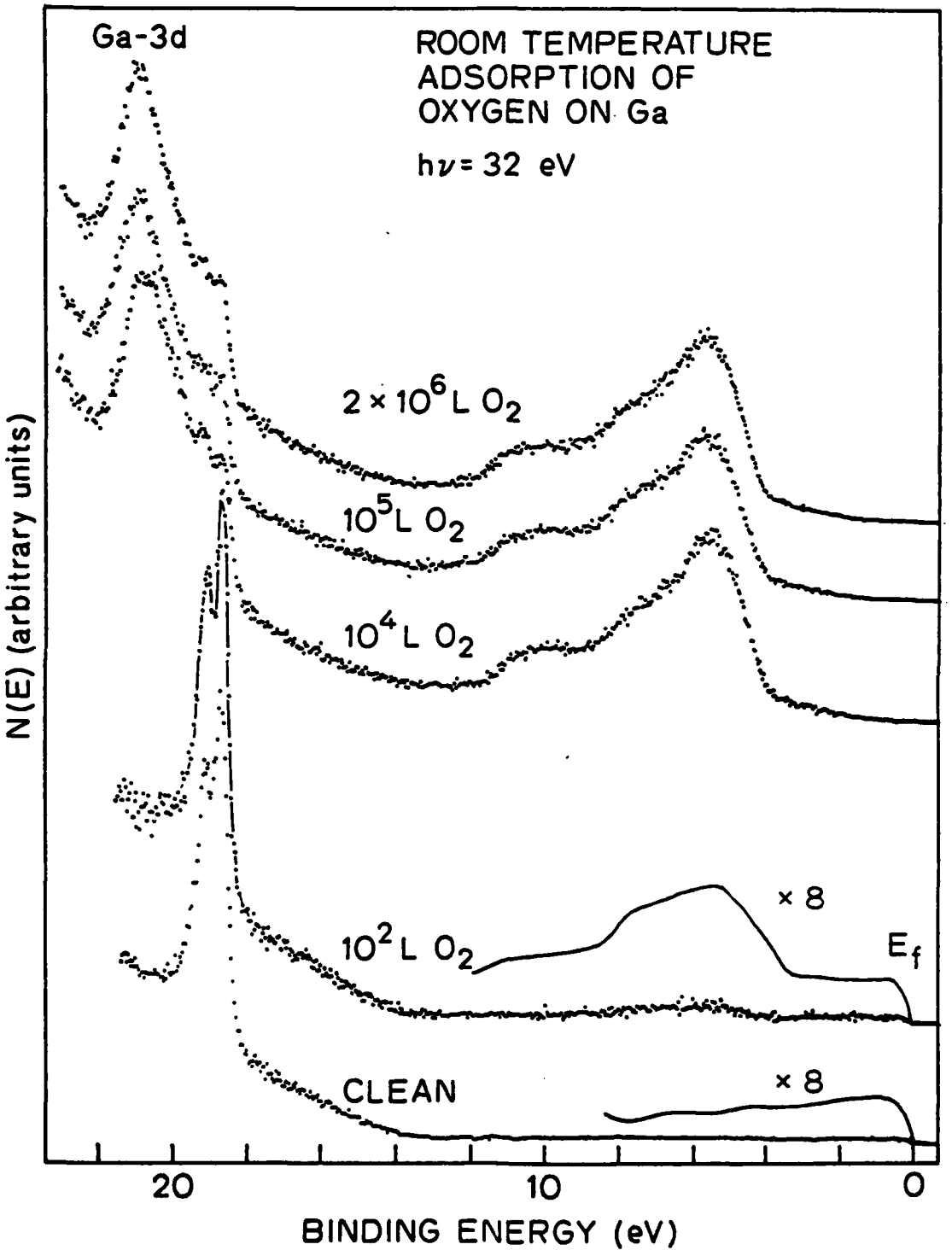
Ga-3d
ROOM TEMPERATURE
ADSORPTION OF
OXYGEN ON Ga
hν = 32 eV
2 × 10^6 L O2
10^5 L O2
10^4 L O2
10^2 L O2
× 8
Ef
CLEAN
× 8
N(E) (arbitrary units)
20
10
0
BINDING ENERGY (eV)

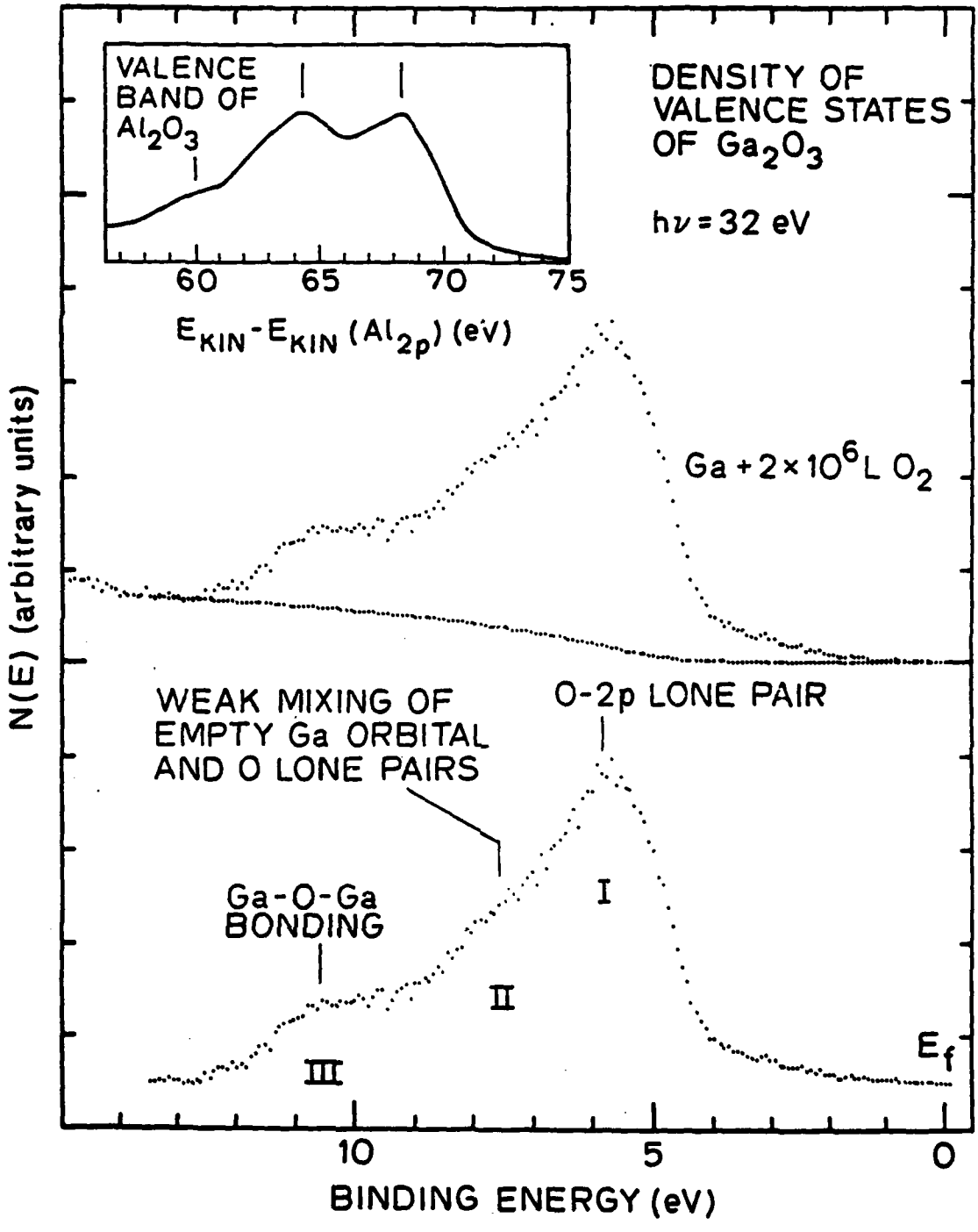
VALENCE BAND OF Al_2O_3
60
65
70
75
$E_{KIN}-E_{KIN}(Al_{2p})$ (eV)
DENSITY OF VALENCE STATES OF Ga_2O_3
$h\nu = 32$ eV
$Ga + 2\times10^6$L O_2
N(E) (arbitrary units)
WEAK MIXING OF EMPTY Ga ORBITAL AND O LONE PAIRS
O-2p LONE PAIR
Ga-O-Ga BONDING
I
II
III
E_f
10
5
0
BINDING ENERGY (eV)

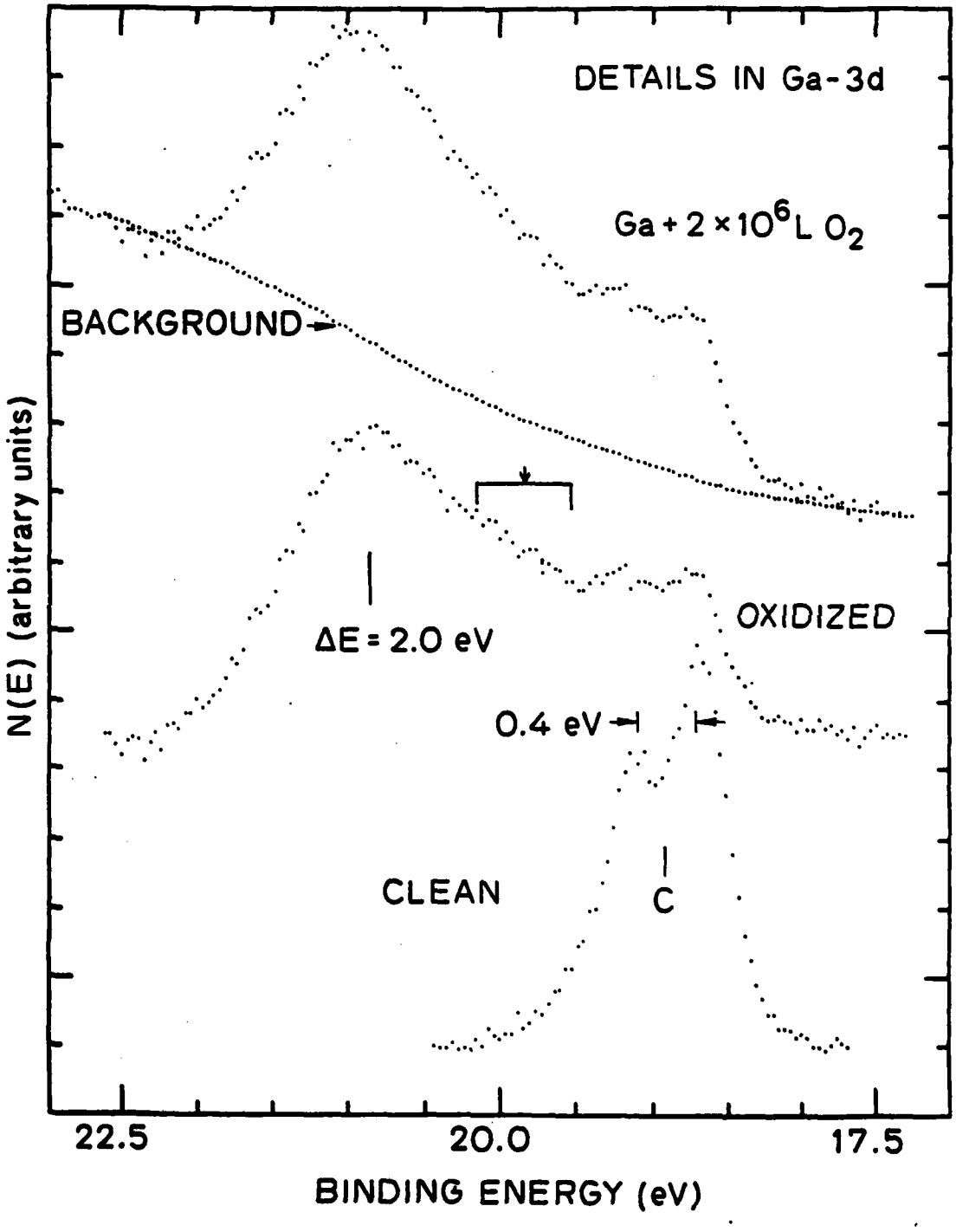
DETAILS IN Ga-3d
Ga + 2 × 10^6 L O2
BACKGROUND
ΔE = 2.0 eV
OXIDIZED
0.4 eV
CLEAN
C
N(E) (arbitrary units)
22.5
20.0
17.5
BINDING ENERGY (eV)

I. W. E. Spicer, S. Eglash, I. Lindau, C. Y. Su, and P. Skeath, "Development and Confirmation of the Unified Model for Schottky Barrier Formation and MOS Interface States on III-V Compounds," 5th Int. Thin Film Conf. (Israel, 1981), to appear in Thin Solid Films.

Thin Solid Films, 89 (1982) 447–460

DEVELOPMENT AND CONFIRMATION OF THE UNIFIED MODEL FOR SCHOTTKY BARRIER FORMATION AND MOS INTERFACE STATES ON III-V COMPOUNDS*

W. E. SPICER, S. EGLASH, I. LINDAU, C. Y. SU AND P. R. SKEATH

Department of Electrical Engineering, Stanford University, c/o Stanford Electronics Laboratory, Stanford, CA 94305 (U.S.A.)

(Received October 15, 1981; accepted October 21, 1981)

The object of the work reported here was to develop an understanding on an atomic basis of the interactions between semiconductors and metal or oxygen overlayers which determine the electronic characteristics of the interface, *e.g.* the Schottky barrier heights and the density and the energy position of states at oxide–semiconductor interfaces.

The principal experimental tool used by ourselves was photoemission excited by monochromatized synchrotron radiation (10 eV < $h\nu$ < 300 eV). Extreme surface sensitivity is obtained by tuning the synchrotron radiation so that the minimum escape depth is obtained for the excited electrons of interest. In this way only the last two or three atomic layers of the solid are sampled. By changing $h\nu$, core levels or valence bands can be studied. The Fermi level position E_{f_s} at the surface can be *directly* determined using a metallic reference.

GaAs, InP and GaSb were studied. On a properly cleaved surface there are no surface states in the semiconductor band gap—thus, no pinning of E_{f_s}. Pinning of E_{f_s} can then be monitored as metal or oxygen is added to the surface, starting from submonolayer quantities. Two striking results are obtained: (1) the pinning position is independent of the adatom, whether it is oxygen or one of a wide range of metals, and (2) the pinning is completed by much less than a monolayer of adatoms. These results cannot rationally be explained by the hypothesis that the pinning is due to the levels produced directly by the adatoms. Rather, they suggest strongly that the adatoms disturb the semiconductor surface indirectly, forming defect levels. This is supported by the appearance of the semiconductor atoms in the metal and by the disordering of the semiconductor surface by submonolayer quantities of oxygen. Since these basic experiments have been reported previously they are only briefly reviewed here.

When metal or oxygen is added under very gentle conditions, the following levels are formed (all energies are relative to the conduction band minimum).

Semiconductor	*Acceptor*	*Donor*
GaAs	0.65 eV	0.85 eV
InP	0.45 eV	0.1 eV
GaSb	0.5 eV	Below VBM

where VBM denotes the valence band maximum.

* Paper presented at the Fifth International Thin Films Congress, Herzlia-on-Sea, Israel, September 21–25, 1981.

0040-6090/82/0000-0000/$02.75

These results explain why Schottky barrier gates will provide useful field effect transistors on n-GaAs but not on n-InP. Likewise they predict that MOS or MIS gates will be practical for n-InP but not for n- or p-GaAs. Studies of the oxygen surface chemistry find the arsenic oxides to be unstable and the phosphorus oxides to be stable, as expected. Some of the new process possibilities opened up by this work are considered.

The work of others is comprehensively reviewed. In general, very satisfactory agreement is obtained.

1. INTRODUCTION

The work which led to the development of the "unified model" has been extensively reported in the literature (see refs. 1–4 and references cited therein) and it would be inappropriate to do more than review that material here. Rather, this paper will have five purposes: (1) to outline briefly the experimental data which led to the development of the unified model; (2) to summarize the unified model briefly; (3) to outline recent work of others, both theoretical and experimental, related to the unified model, and in particular to show how some apparently conflicting data are in fact quite consistent with the data which led to the unified model; (4) to show how critical choices on devices can be made (using present device technology); (5) to point out ways by which the limitations inherent in (4) might be changed by new device processing technology.

2. EXPERIMENTS WHICH RESULTED IN DEVELOPMENT OF THE UNIFIED DEFECT MODEL

The use of synchrotron radiation from the Stanford Synchrotron Radiation Laboratory (SSRL) for UV ($10\ \text{eV} < h\nu < 200\ \text{eV}$) photoemission spectroscopy (UPS) was essential to this work, since the tunability of synchrotron radiation made possible key experiments involving the examination of core and valence levels of the last one or two molecular layers of the semiconductor surface[5,6]. In addition, a range of conventional experimental techniques including low energy electron diffraction[7], Auger electron spectroscopy (its use was minimized because of electron beam damage to the surface) and UPS[8,9] with conventional sources were used in this work.

An absolutely critical technique was the direct measurement of the surface position E_{f_s} of the Fermi level by photoemission[5,6,9]. It should be emphasized that we measured E_{f_s} directly. By contrast, Brillson and coworkers[10] have attempted to measure changes in work function via contact potential techniques; in these experiments the separation of changes in band bending and electron affinity is not obvious. Mönch and coworkers[11,12] have correctly interpreted such contact potential measurements to yield changes in band bending.

On a "well-cleaved"[2] (110) surface of most III–V compounds, E_{f_s} is not pinned since rearrangement of the near-surface atoms moves the intrinsic surface states out of the band gap[1–4], allowing one to start with a surface where E_{f_s} is at the bulk Fermi

level position. Moderately doped n-type and p-type crystals are used so that the Fermi level position on the clean surface is near one of the band edges. Then, by adding foreign atoms such as oxygen or a metal and watching the movement of E_{fs} until it becomes pinned, the new energy levels induced at or near the surface can be determined. In a later section we shall discuss the details of this measurement and of the contact potential measurements[10,11].

The key results from this study were (1) that the E_{fs} pinning position was essentially independent of adatoms, *i.e.* it was at the same position independently of whether the adatom was a metal (cesium, aluminum, indium or gallium) or oxygen, and (2) that the pinning was complete with much less than a monolayer of the adatom. On this basis, the popular theories of Schottky barrier formation[1-4,13] could be discarded (however, the results were in the direction suggested by Anderson and Phillips[14]). Since the adatoms must all induce the same surface or near-surface states, the only reasonable conclusion was that these states were due to a structural defect produced by the perturbation due to the adatom on the surface lattice.

It should be noted that the free surface was highly strained by the rearrangement which moved surface states out of the band gap[15]. It is well established that oxygen adsorption disorders the surface lattice—a process in which defects are expected to be produced[1,15]. With metal adatoms, experiments at SSRL which monitored the core levels of the components of the III–V compounds showed that, on deposition of many monolayers of the metal, the group III and group V constituents of the semiconductors moved into the metal[1-4,13,16]. A detailed mechanism which provides the activation energy for this has been suggested[1-4,13,16].

As will be seen in Section 3, others have since found independent support for the defect model. It is formally titled the "unified defect model", but shortened to unified model for convenience, since it simultaneously explains Schottky barrier formation and the origin of the interface states in MOS or MIS structures as being due to the creation of the same defect states.

Making use of the movement of E_{fs} as a function of adatom deposition[1-3], the defect levels in Fig. 1 have been deduced. The energy positions are considered to be quite firm within the experimental error of ± 0.1 eV. The defect type (acceptor or donor) is also considered quite certain (a donor-like surface defect can donate an electron to the bulk and an acceptor-like surface defect can accept an electron from the bulk). For GaAs and InP the origin of the defect associated with the energy level (*e.g.* an acceptor due to a missing arsenic atom in GaAs) is considered quite tentative. Other suggestions which have been made by Williams and coworkers[19,20] for InP and Harrison[17], Grant *et al.*[18] and Mönch and Gant[12] for GaAs are also indicated in Fig. 1. The identity of the defect for GaSb is thought to be quite certain as it agrees with that for bulk GaSb.

The energy levels shown in Fig. 1 also agree as well as can be hoped with Schottky barrier heights and oxide–semiconductor interface levels found in device structures[1-4,13]. It should be noted that, while all our measurements were made on the (110) cleavage face (the crystals were cleaved *in situ* at 10^{-10} Torr), most of the device structures were made on (111) or (100) faces of III–V materials. The theoretical work of Daw and Smith[21] shows that if the defect levels lie two or more molecular layers beneath the interface they will be characteristic of the bulk and thus

will not depend on the crystal surface. The experimental results mentioned above suggest that this is the case, as do other arguments[1-4,13].

It should be emphasized that the metal adatoms in our experiments were deposited as gently as possible (by evaporation) and that the crystals were not heated during or after deposition. The defect formed may be vacancies or vacancy complexes (*i.e.* "clusters" of two or more defects) as in the case of GaSb [13]. Heating or other subsequent processing may change a vacancy into a complex or change the nature of a complex. However, if this is happening for the defects of interest here, the energy levels are changed by only small amounts (of the order of 0.1 eV), because the Schottky barrier heights and positions of MOS interface states agree so well with results obtained in device processing where the samples are not treated so gently.

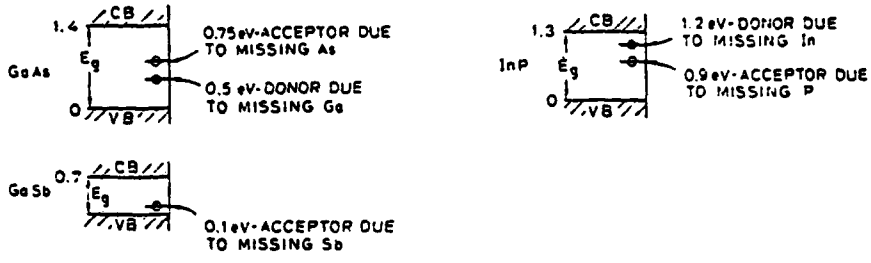

Fig. 1. The surface or interface defect levels obtained in this work. The energies of the levels are considered to be well established (to the experimental accuracy of ± 0.1 eV) as are the acceptor or donor nature of the levels. The identification of the anion or cation is less certain for GaAs and InP. For example, Harrison[17], Grant *et al.*[18] and Mönch and Gant[12] have suggested that both GaAs levels are due to the same defect and associate this with missing arsenic, whereas in InP Williams and coworkers[19,20] associate the 1.2 eV donor with missing phosphorus and the 0.9 eV acceptor with missing indium.

3. CRITICAL DEVICE CHOICES WHICH CAN BE MADE IN THE CONTEXT OF EXISTING PROCESS TECHNOLOGY

An extremely important application of the unified model and the energy levels shown in Fig. 1 is to the choice of the type of gate for field effect transistors (FETs) made with GaAs and InP. Because the energy levels of GaAs lie near midgap, it forms relatively high Schottky barriers and thus provides good Schottky barrier gates for the FET. (Recent work by our group[22] indicates that even larger barrier heights may be possible on n-type GaAs.) However, the depth of the defect levels makes GaAs very unfavorable for MOS device applications. The problem is compounded by the instability of the arsenic oxides[23,24].

Because the position of the defect levels in InP is near the conduction band minimum (CBM) it gives too small a Schottky barrier height for a practical Schottky gate on n-type InP. However, the low activation energy of the interface defect levels on n-type material makes it a good candidate for MOS or MIS devices. Our work[15] has long indicated that the MIS structure should be superior to the MOS for III–V compounds. The fact that there is no instability problem for phosphorus oxides unlike arsenic oxides[24-26] makes the MIS or MOS structures on InP even more attractive. In fact, Wieder[27], Meiners[28] and Fritsche[29] have obtained very promising results with MIS InP devices.

In conclusion, if the results of the unified model are applied to making choices for FET configurations on InP and GaAs using existing device processing, it is clear that GaAs can only be expected to work for Schottky barrier gates and not MOS or MIS gates. This is in agreement with the practical experience on these materials, *i.e.* the success of GaAs Schottky barrier gates and the failure (despite energetic efforts) of GaAs MOS or MIS structures. (It should be remembered that all existing MIS structures have a thin oxide layer on the semiconductor surface before the insulator is deposited.) Conversely, there has been no success with InP Schottky gates but increasing success with InP MIS structures[27–29].

4. NEW DEVICE POSSIBILITIES

Once we know the source of a given problem phenomenon, new techniques can be devised to modify or eliminate that phenomenon. Knowing that Schottky barrier formation and semiconductor–oxide interface states are both due to the same defects opens two closely related avenues. For example, to modify the Schottky barrier pinning position we might alter processing to reduce the defect density and/or add dopants in the surface or interface region in large enough quantities to overcome the effect of the defects.

The work of Farrow *et al.*[30] in which the Schottky barrier height of Ag/InP(100) was studied as a function of the stoichiometry of the (100) face illustrates the reduction in defect density by surface treatment, as given above. When the polar face was saturated with phosphorus before silver deposition, the Schottky barrier height was found to be very small (about 0.1 eV below the CBM) in accord with the donor level shown in Fig. 1. However, when no special treatment was given to the InP face prior to the silver deposition, the normal barrier height of about 0.4 eV was obtained in agreement with the acceptor level in Fig. 1. Apparently, the saturation of the surface with phosphorus inhibits the formation of the level 0.4 eV below the CBM (which we attribute to missing phosphorus) relative to the 0.1 eV level (which we attribute to missing indium).

In Fig. 2 we present what we believe to be the first clear example of a dopant overwhelming the defect levels at the interface of a III–V semiconductor. In previous studies[1–4,13] we found that gold gave a pinning position on n-type GaAs somewhat nearer the valence band maximum (VBM) than oxygen or any of the other metals studied. Therefore, we decided to study gold in more detail. The results of Skeath and coworkers[22] in Fig. 2 give the results in terms of E_{fs} as a function of the amount of gold deposited on an atomically clean GaAs(110) cleavage face. The curve for p-type GaAs is most instructive. At low coverages E_{fs} rises as it typically does for metals on GaAs. However, whereas for metals E_{fs} normally levels off at the final pinning position given by Fig. 1, a reversal takes place with gold, *i.e.* after E_{fs} reaches a maximum it decreases monotonically with increasing gold coverage. This indicates that two competing mechanisms are involved in pinning E_{fs}. At low coverages the defect mechanism dominates; at higher coverages an acceptor level (lying near the VBM) introduced directly by the gold atoms (probably by gold moving into the GaAs) overcomes the defect levels and determines E_{fs}. An important prerequisite for movement of the gold into the GaAs is to have an atomically clean GaAs surface prior to the gold deposition. It appears that even a few layers of oxide

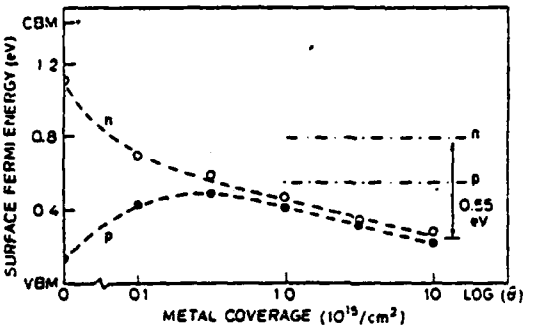

Fig. 2. The Fermi level position E_{f_s} at the surface *vs.* the logarithm of the gold coverage on GaAs(110). From the rise in E_{f_s} for low coverages of gold on the p-type material, it is clear that the defect mechanism is working in that region. The drop in E_{f_s} (above a gold coverage of about 5×10^{14} cm^{-2}) indicates the creation of a new interface level. It is suggested that this is due to a new state that is created by the gold in the GaAs: – – –, gold overlayer; ——, Al/Ga/In overlayer.

greatly inhibit this movement. Such layers are always present in "practical" Schottky barriers made on GaAs surfaces which have been previously exposed to the air. This is believed to be the reason that this effect has not been clearly seen previously.

In the discussion above we give two examples of the methods by which the Schottky barrier height can be changed in real devices. These should be taken as somewhat crude examples, having been discovered without the intention of controlling the barrier height. Making use of techniques such as molecular beam epitaxy, we can begin to design structures giving the desired behavior and then to develop processes to realize it. For example, we might learn methods of heavily doping the last ten or twenty layers of n-type InP with an acceptor, *e.g.* beryllium or zinc, to make it strongly p type. The InP growth would then be terminated with indium and a metal deposited to form a Schottky barrier. This metal may be an alloy containing indium and appropriate heating schedules might be developed. In this way, the formation of donors due to missing indium will be minimized and E_{f_s} will be determined by the beryllium or zinc acceptors which lie near the VBM so that a Schottky barrier height almost equal to the band gap could be obtained on n-type InP—something which has not been possible to date[3,13]. In fact, the inability to form a satisfactorily high Schottky barrier on InP has impeded the practical application of this material greatly.

This gives just one of many configurations which can be envisioned based on the understanding of the fundamentals of Schottky barrier and (III–V)–oxide interface formation as outlined earlier. It should also be noted that certain questions (see Section 2) remain as to the details of the defects involved. These questions need to be answered definitively to give the firmest knowledge possible for the "scientific" engineering of new improved device structures.

5. COMPARISON WITH THE WORK OF OTHERS

As mentioned above, we are in agreement with Williams and coworkers[19,20] for InP except for the assignment of the missing species producing the defect. There

is also agreement with Farrow *et al.*[30] in the location of the InP defect energy levels.

The theoretical work of Daw and Smith[21,31] based on a simple arsenic vacancy gives the observed systematics, as well as insight associated with the vacancy levels as it is moved from the surface into the bulk.

Wieder[32] has studied the Fermi level pinning position by measuring the highest filled level in MIS structures in the system $Ga_xIn_{1-x}As$ (n type) as x is increased from 0 to 1. He found that he could explain his data if he assumed that the pinning was due to an anion vacancy level which was at a fixed height 0.53 eV above the VBM, independent of the composition of the $Ga_xIn_{1-x}As$. The result of a constant vacancy level due to an anion vacancy is in agreement with recent *ab initio* calculations of Daw and Smith[21,31] for the alloy system. Lagowski *et al.*[33], making use of the GaAs–oxide interface states in a "phototransistor" mode, have detected directly the level near 0.7 eV.

Mönch and Gant[12] measured the change in the contact potential of a GaAs surface as a function of temperature and located both GaAs defect levels shown in Fig. 1 in agreement with our energy assignments. Making certain assumptions, they deduce from their data (as indicated in Fig. 1) that the levels shown are both due to the same defect associated with a missing arsenic atom. The defect can accept either an electron or a hole in agreement with the theoretical considerations of Harrison[17] and interpretations of their own data by Grant *et al.*[18] We shall return shortly to the work of Mönch and Gant.

Considerable other work is under way on the defect model. For good collections of articles, the reader is referred to the *Proceedings of the Eighth Conference on the Physics of Compound Semiconductor Interfaces*[34] (and the *Proceedings of the Fifteenth International Conference on the Physics of Semiconductors*[35]). Of particular interest is the theoretical work of Allen and Dow[36] who suggest that surface anti-site defects are responsible for the interface pinning. The calculations of Nishida (ref. 35, p. 1093) and the measurements of Hasegawa and Sawada (ref. 35, p. 1125) should also be noted.

In Fig. 3 we present data on the Fermi level position as a function of metal coverage obtained by ourselves[4,13], using the photoemission methods to be described below, and quite independently by Mönch and Gant[12] by measurement of the contact potential difference as a function of temperature for the indicated metal coverages. Considering the difficulty and different character of the measurements, the agreement is striking. However, the work of Brillson and coworkers appears to be in some disagreement with the model, but this is resolved here. For example, Brillson and Kruger[37] concluded from their data that Fermi level stabilization had not occurred at metal (aluminum) coverages up to 20 Å (15 monolayers), but in a paper published almost simultaneously Brillson *et al.*[38] stated: "... [that portion of] the Fermi level stabilization [that] occurs with less than a few monolayers of metal deposition on ultrahigh-vacuum-cleaved semiconductor surfaces [refs. 10 and 39]". Our purpose in the following paragraphs is to resolve this apparent contradiction. It should be kept in mind that our (photoemission) measurements of the band bending are direct, *i.e.* the surface position of the Fermi level is measured directly with respect to the valence band and or core levels (and thus with respect to the VBM)[1-4]. So, within an uncertainty of ± 0.1 eV, band bending can be measured quite reliably and in a straightforward manner.

The measurements by Brillson and coworkers and Mönch and coworkers often make use of contact potential differences to determine the surface position of the Fermi level. The experimental data consist of plots of the contact potential difference *versus* overlayer coverage. Such plots are included in Fig. 4 for the systems for which data have been published to date[10,11,37]. For Mönch and Gant this is the Ge–GaAs system; for Brillson and coworkers[10,37,38] it is the Al–GaAs system. Both studies show the same characteristic: the curves can be divided into three regions according to coverage[11]. The first region is that in which the contact potential difference changes very rapidly with coverage, and this occurs for coverages below 0.2 monolayers. The next region extends from here to 5 monolayers. In this region the contact potential difference goes through a maximum and then decreases with increasing coverage. In the final region (coverages greater than 5 monolayers), the contact potential difference is constant. Fortunately there have been comprehensive studies[1–4,11,39–45] of overlayers of foreign atoms on semiconductors which allow us to identify the physics taking place in each of these regions. The first is dominated by changes in the band bending, *i.e.* the creation of states which pin the surface (or interface) position of the Fermi level. The second is due to the change in the electron affinity of the semiconductor by the overlayer and the gradual development of

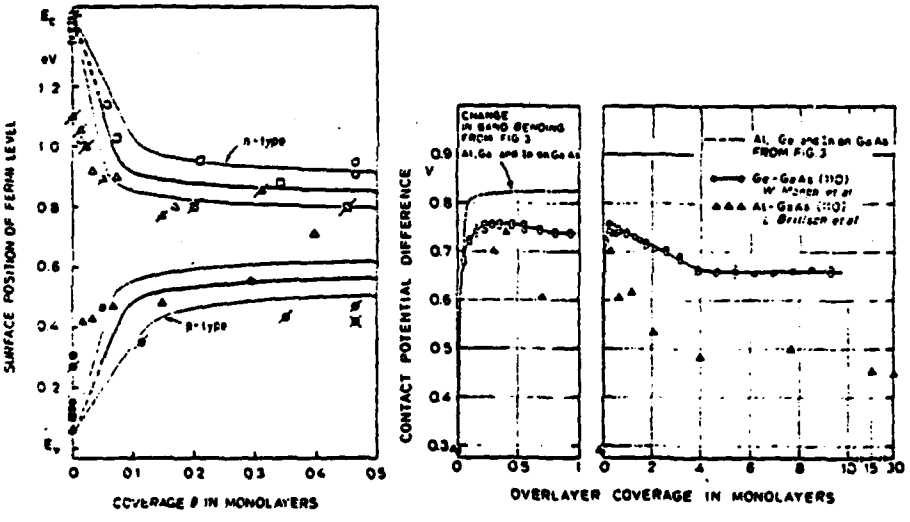

Fig. 3. The Fermi level position E_{f_s} in the energy gap of GaAs as a function of metal coverage on both n-type and p-type samples (GaAs(110), 300 K; $E_{ss}^{A} = E_{CS} - (0.55 \pm 0.05)$ eV; $E_{ss}^{D} = E_{CS} - (0.88 \pm 0.05)$ eV; $N_{ss} = (0.06 \pm 0.04)\sigma_{110}(\theta)$; the data points are from the work of Skeath *et al.*[7] for three different metals (□, ■, aluminum; ○, ●, gallium; △, ▲, indium) obtained by the photoemission technique described in the text and in refs. 5, 8 and 9; ——, results determined by Mönch and Gant[12] for germanium on GaAs by contact potential difference measurement techniques; □, experimental uncertainty of Mönch and Gant.

Fig. 4. The change in contact potential difference (a) that would be expected from the data of Fig. 3 if only the interface position of the Fermi level changed with no change in the electron affinity of the semiconductor and (b) in results obtained by Mönch and coworkers[11] for germanium on GaAs and by Brillson and coworkers[10,37] for aluminum on GaAs. As can be seen, very good agreement is obtained between the results for the surface Fermi level obtained directly from photoemission techniques and the contact potential difference results.

overlayer quantities sufficient to give a contact potential difference that is characteristic of the overlayer itself. The third (constant) region is simply due to the work function of the overlayer, which completely establishes itself for a sufficiently thick layer. As would be expected, region I is missing if the overlayer is deposited on a metal rather than a semiconductor.

For comparison, Fig. 4(a) also includes the result expected from only the change in band bending (*i.e.* the surface Fermi level position E_{fs}) for n-type GaAs. This was obtained from the data of Fig. 3. As can be seen, it is indistinguishable from the contact potential difference for values between 0.3 and 0.65 V (*i.e.* for coverages of less than 0.1 monolayers) and is slightly higher (by about 0.06 eV) than the contact potential difference curves for larger coverages. This difference is due to the reduction in the semiconductor electron affinity with increasing overlayer coverage (see, for example, ref. 43) for coverages less than 0.25 monolayers.

The first region is of key importance since it is here that the change is dominated by the movement of E_{fs}. There is agreement in the literature, except for certain publications[10,37] (although these same researchers also obtain results in agreement with most workers[38]).

Brillson and coworkers introduced an "atomic dipole" to explain the first (low coverage) region of the contact potential difference curves[10], as an integral part of their model[10,37,38]. First we note that all available data, including those in Fig. 4, can be explained without invoking such a dipole. If an opaque electronic barrier is present, as assumed by Brillson and coworkers, it would have caused a greater change in contact potential difference so that the curve would have risen above the curve showing the change in band bending for indium, aluminum and gallium in Fig. 4. There is definitive literature[1-4,39-46] which establishes that for barriers with tunneling probabilities even less than that suggested by Brillson and coworkers[10] there is no contribution to the Schottky barrier height by the "atomic dipole". We illustrate this in Fig. 5, reproduced from Muller and Kamins[46]. We quote from that text[46]:

> "To account for surface effects, the metal–semiconductor contact is treated as if it contained an intermediate region sandwiched between two crystals. The intermediate region is thought to consist of an interfacial layer ranging from several to of the order of 10 atomic dimensions in width. This layer contains the impurities and added surface states. It is too thin to be an effective barrier to electron transfer (which can occur by tunneling)...".

Since the barrier invoked by Brillson and coworkers[10] is not an effective barrier to electron transfer, it will not contribute to the Schottky barrier height as currently measured. This conclusion is well substantiated by the good agreement between work on electron emission over Schottky barriers into vacuum[41-45] and contact potential measurements even when the "atomic" barrier is several electronvolts higher than the threshold for emission and the barrier determined by contact potential differences.

In their photovoltaic studies Brillson and coworkers[10,37] claimed that for certain overlayers the band bending can be measured by "flattening the bands" with radiation of intensity 5×10^{18} photons cm^{-2} s^{-1} and measuring the induced photovoltage. Since their measured photovoltages have consistently been lower than the known barrier heights[10,37,38], they have attributed the difference to the

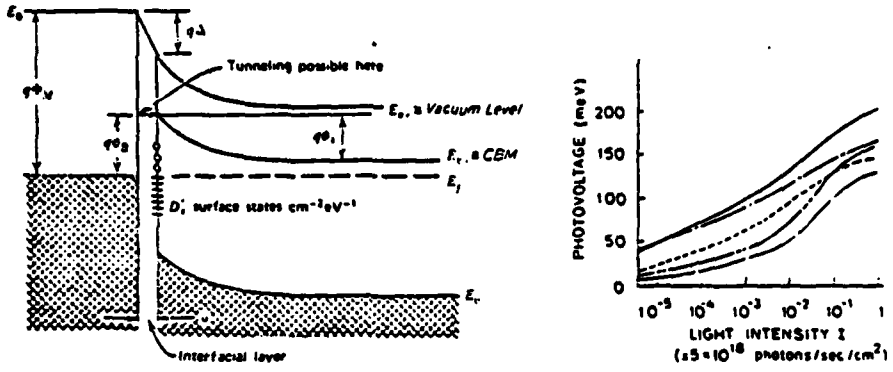

Fig. 5. Band structure near a metal–semiconductor contact. The height of the Schottky barrier is $q\phi_n$. This diagram should be contrasted with the incorrect diagram given by Brillson and coworkers (see, for example, ref. 37, Fig. 3). (From Muller and Kamins[46].)

Fig. 6. The photovoltage data of Brillson and Kruger[37] replotted so that the origin of the vertical scale is the same for all curves. The thickness (Å) of the aluminum overlayer is indicated (we have used 1.4 Å = 1 monolayer, as suggested by Brillson and Kruger[37]). The increase in the low intensity photovoltage between the two thickest samples and the thinner samples should be noted. When these low intensity photovoltages are subtracted from the high intensity photovoltages, no change with aluminum thickness is present in these data: ——, 20 Å; —·—, 6.7 Å; - - -, 2.7 Å; — —, 1.3 Å; —···—, 0.7 Å.

"atomic barrier" discussed above. In addition, they have claimed[37] that the band bending changes with aluminum deposition up to coverages of 15 monolayers.

As McGill *et al.*[47] have pointed out, the maximum photovoltage as a function of light intensity which can be obtained from a Schottky barrier can be predicted from the current–voltage equation for an ideal diode[48]:

$$J = AT^2 \exp\left(-\frac{q\phi}{kT}\right)\left\{\exp\left(\frac{qV}{kT}\right) - 1\right\} \tag{1}$$

where J is the current density, A is a fundamental constant, T is the temperature, ϕ is the Schottky barrier height, k is Boltzmann's constant and V is the applied voltage. In calculating the open-circuit photovoltage of this diode (which is the photovoltage measured by Brillson and coworkers), J is the photocurrent assuming 100% quantum efficiency (the electronic charge multiplied by the photon flux) and V is the photovoltage. The constant of unity subtracted in the braces in eqn. (1) can be ignored for the photon flux density of 5×10^{18} cm^{-2} s^{-1} used by Brillson and coworkers, and the equation can be rewritten as

$$V_{oc} = \phi - \frac{kT}{q} \ln\left(\frac{AT^2}{qI}\right) \tag{2}$$

Here, $V_{oc} = V$ is the open-circuit voltage, I is the incident light flux and q is the electronic charge. It should be noted that we are assuming no loss of photoexcited carriers due to bulk recombination or diffusion; thus eqn. (2) gives us an upper limit to V_{oc}. For the maximum flux (5×10^{18} photons cm^{-2} s^{-1}) reported by Brillson and coworkers (Fig. 6), the second term on the right-hand side is 0.43 eV. Taking the barrier height of 0.7 eV chosen by Brillson and Kruger[37] the maximum value of V_{oc}, the largest possible contact potential difference change due to irradiation, is 0.27 eV.

TABLE I

THE EXPERIMENTAL PHOTOVOLTAGES OBTAINED BY BRILLSON AND KRUGER (REF. 37, FIG. 1) FOR VARIOUS ALUMINUM COVERAGES AT THEIR MAXIMUM AND MINIMUM RADIATION INTENSITIES (SEE FIG. 6 OF THE PRESENT PAPER)

Coverage (monolayers)	*(1), photovoltage with* 5×10^{15} *photons* $cm^{-2} s^{-1}$ (meV)	*(2), photovoltage with* 2×10^{13} *photons* $cm^{-2} s^{-1}$ (meV)	*(3) = (1) − (2), photovoltage difference* (meV)
0.5	140	10	130
1.0	130	10	130
1.5	140	20	120
4.8	160	40	120
15.0	200	40	160

Thus their claim for saturation and flat band conditions, *i.e.* $V_{oc} = q\phi$, even with an incident flux of 5×10^{18} photons $cm^{-2} s^{-1}$, is in error by at least 0.43 eV.

In Table I we have compiled the photovoltages obtained by Brillson and Kruger (ref. 37, Fig. 1). These are replotted in Fig. 6 and are shifted so that the zero of energy is the same for each curve. It should be noted in Fig. 6 that the photovoltage at the lowest intensity measured (approximately 2×10^{13} photons $cm^{-2} s^{-1}$) increases appreciably with increasing overlayer thickness. This cannot be accounted for by the bulk photovoltage equations and is most probably due to a photovoltage produced by exciting carriers out of the interface defect states. Thus, in the last column of Table I, these low intensity photovoltages have been subtracted from those measured at the highest light intensity. The result is plotted in Fig. 7. Since Brillson and Kruger[37] report that "... the band bending can be determined to within 50 meV", the experimental points of Fig. 7 are overlaid by a shaded region 50 meV wide. As can be seen the experimental points fall within this shaded area, *i.e.* within the experimental accuracy. Thus we can draw the following conclusions.

(1) The photovoltage and thus the barrier height are constant and independent of the overlayer thickness for all overlayer thicknesses measured by Brillson and Kruger[37], *i.e.* for coverages greater than 0.5 monolayers. This work of Brillson and Kruger is then found to conform with the rest of the literature including the work by Skeath *et al.*

(2) The simple photovoltage calculation showed that Brillson and Kruger could not have approached saturation with their photon fluxes. Thus, their arguments, based on photovoltage measurements for an "atomic dipole" contribution to the Schottky barrier height, cannot be valid. We note that our arguments do not disprove the presence of the "atomic barriers" proposed by Brillson and coworkers, but such barriers can be observed or verified by contact potential difference measurements.

Thus, all the existing literature is found to be in general agreement with the unified model and the data which led to it. It still remains, however, to identify the actual nature (*i.e.* arsenic or gallium vacancy etc.) of the defect levels.

6. CONCLUSIONS

Since it was formally presented in January 1979 the unified model has

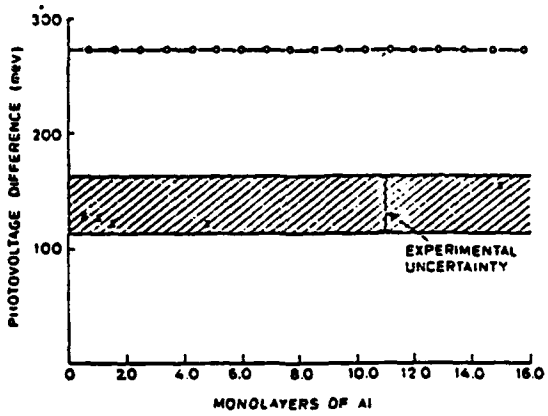

Fig. 7. The difference in photovoltage found by Brillson and Kruger[37] in going from the lowest to the highest intensity light (see Fig. 6 and Table 1): —•—, theoretical upper limit (270 meV) for the photovoltage at 5×10^{18} photons $cm^{-2}\ s^{-1}$ for a real Schottky barrier height of 0.7 eV (see eqn. (2) and text); ×, experimental points of Brillson and Kruger[37]. Within experimental error, the photovoltage is independent of layer thickness, in agreement with the conclusion drawn from Fig. 4.

stimulated considerable interest. At the time it represented a strong break, with one exception[14], from the previous concepts of Schottky barrier formation and, to a lesser extent, the concepts of the formation of MOS interface states. It unified a body of existing data and has stood up well in subsequent investigations by a large and growing group of workers. It has also provided insights for improved "scientific engineering" of device structures.

ACKNOWLEDGMENTS

Extremely fruitful discussions with R. Bauer, T. McGill and W. Mönch are gratefully acknowledged. We are indebted to W. Mönch for making Fig. 3 available before publication and to T. McGill for making the unpublished material cited in ref. 47 available to us.

This work was supported by the Advanced Research Projects Agency under Contract N00014-79-C-0072 and the office of Naval Research under Contract N00014-75-C-0289. Parts of the experiments were performed at the SSRL which is supported by the National Science Foundation under Grant DMR77-27489 in cooperation with the Stanford Linear Accelerator Center and the Department of Energy.

REFERENCES

1 W. E. Spicer, P. W. Chye, P. R. Skeath, C. Y. Su and I. Lindau, *J. Vac. Sci. Technol.*, *16* (1979) 1422. I. Lindau, P. W. Chye, C. M. Garner, P. Pianetta, C. Y. Su and W. E. Spicer, *J. Vac. Sci. Technol.*, *15* (1978) 1332.

2 W. E. Spicer, P. W. Chye, P. R. Skeath, C. Y. Su and I. Lindau, *Inst. Phys. Conf. Ser. 50* (1980) 216, and references cited therein.

3 W. E. Spicer, P. R. Skeath, C. Y. Su and I. Lindau, *Proc. 15th Int. Conf. on Physics of Semiconductors, Kyoto, 1980*, in *J. Phys. Soc. Jpn., Suppl. A*, *49* (1980) 1079–1087.

4 P. R. Skeath, I. Lindau, P. W. Chye, C. Y. Su and W. E. Spicer, *J. Vac. Sci. Technol., 16* (1979) 1143.
5 I. Lindau and W. E. Spicer, in H. Winick and S. Doniach (eds.), *Synchrotron Radiation Research*, Plenum, New York, 1980, Chap. 6, and references cited therein.
6 I. Lindau and W. E. Spicer, *J. Electron Spectrosc. Relat. Phenom., 3* (1974) 409.
M. P. Seah and W. A. Dench, *Surf. Interface Anal., 1* (1979) 2.
7 P. R. Skeath, W. A. Saperstein, P. Pianetta, I. Lindau, W. E. Spicer and P. Mark, *J. Vac. Sci. Technol., 15* (1978) 1219.
8 P. Pianetta, I. Lindau, P. E. Gregory, C. M. Garner and W. E. Spicer, *Surf. Sci., 72* (1978) 298.
9 C. Y. Su, I. Lindau, P. R. Skeath, P. W. Chye and W. E. Spicer, *J. Vac. Sci. Technol., 17* (1980) 936.
10 L. J. Brillson, *Phys. Rev. B, 18* (1978) 2431.
L. J. Brillson, R. Z. Bachrach, R. S. Bauer and J. C. McMenamin, *Phys. Rev. Lett., 42* (1979) 397.
L. J. Brillson and D. W. Kruger, *Surf. Sci., 102* (1981) 518, and references cited therein.
11 W. Mönch, J. J. Clemens, S. Gorlich, R. Enninghorst and H. Gant, *J. Vac. Sci. Technol., 19* (1981) 525.
W. Mönch and H. Gant, *J. Vac. Sci. Technol., 17* (1980) 1094.
12 W. Mönch and H. Gant, *Phys. Rev. Lett., 48* (1982) 512.
13 W. E. Spicer, I. Lindau, P. R. Skeath, C. Y. Su and P. Chye, *Phys. Rev. Lett., 44* (1980) 420, and references cited therein.
14 J. M. Anderson and J. C. Phillips, *Phys. Rev. Lett., 35* (1975) 56, and references cited therein.
15 W. E. Spicer, P. Pianetta, I. Lindau and P. W. Chye, *J. Vac. Sci. Technol., 14* (1977) 885.
16 P. Chye, I. Lindau, P. Pianetta, C. M. Garner, C. Y. Su and W. E. Spicer, *Phys. Rev. B, 18* (1978) 5545.
17 W. A. Harrison, personal communication, February 1980.
18 R. W. Grant, J. R. Waldrop, S. P. Kowalczyk and E. A. Kraut, *J. Vac. Sci. Technol., 19* (1981) 477.
19 R. H. Williams, R. R. Varma and V. Montgomery, *J. Vac. Sci. Technol., 16* (1979) 1418.
20 T. Humphreys, M. H. Patterson and R. H. Williams, *J. Vac. Sci. Technol., 17* (1980) 886.
21 M. S. Daw and D. L. Smith, *Phys. Rev. B, 20* (1979) 5150; *Appl. Phys. Lett., 36* (1980) 690.
22 P. R. Skeath, C. Y. Su, I. Hino, I. Lindau and W. E. Spicer, *Appl. Phys. Lett., 39* (1981) 349.
W. G. Petro, I. A. Babalola, P. R. Skeath, C. Y. Su, I. Hino, I. Lindau and W. E. Spicer, paper presented at *PCSI-9, Asilomar, 1982*, in *J. Vac. Sci. Technol.*, to be published.
23 G. P. Swartz, C. D. Thurmond, G. W. Kammlott and B. Swartz, *J. Vac. Sci. Technol., 17* (1980) 958, and references cited therein.
24 W. E. Spicer, I. Lindau, P. R. Skeath and C. Y. Su, *J. Vac. Sci. Technol., 17* (1980) 1019.
25 P. W. Chye, C. Y. Su, I. Lindau, C. M. Garner, P. Pianetta and W. E. Spicer, *Surf. Sci., 88* (1979) 439.
26 G. Lucovsky and R. S. Bauer, *J. Vac. Sci. Technol., 17* (1980) 946.
27 H. H. Wieder, *J. Vac. Sci. Technol., 17* (1980) 1009.
28 L. G. Meiners, *J. Vac. Sci. Technol., 19* (1981) 373.
29 D. Fritsche, *Inst. Phys. Conf. Ser. 50* (1980) 258.
30 R. F. C. Farrow, A. G. Cullis, A. J. Grant and J. F. Patterson, *J. Cryst. Growth, 43* (1978) 292.
31 M. S. Daw and D. L. Smith, *J. Vac. Sci. Technol., 19* (1981) 508.
32 H. H. Wieder, *Appl. Phys. Lett., 38* (1981) 170.
33 J. Lagowski, T. E. Kazior, J. C. Gatos and J. Sicjka, *J. Vac. Sci. Technol., 19* (1981) 519.
34 *Proc. 8th Conf. on Physics of Compound Semiconductor Interfaces*, in *J. Vac. Sci. Technol., 19* (1981) 279–688.
35 *Proc. 15th Int. Conf. on Physics of Semiconductors, Kyoto, 1980*, in *J. Phys. Soc. Jpn., Suppl. A, 49* (1980) 1079.
36 R. E. Allen and J. D. Dow, *Phys. Rev.*, (1982), in the press.
R. E. Allen and J. D. Dow, *Solid State Commun.*, to be published.
37 L. J. Brillson and D. W. Kruger, *Surf. Sci., 102* (1981) 518.
38 L. J. Brillson, C. F. Brucker, G. Margaritondo, J. Sowik and N. G. Stoffel, *Proc. 15th Int. Conf. on Physics of Semiconductors, Kyoto, 1980*, in *J. Phys. Soc. Jpn., Suppl. A, 49* (1980) 1089.
39 G. Margaritondo, J. E. Rowe and S. B. Christman, *Phys. Rev. B, 14* (1976) 5396.
40 W. Gudat and D. E. Eastman, *J. Vac. Sci. Technol., 13* (1976) 831.
41 G. W. Gobeli, J. J. Lander and J. Morrison, *J. Appl. Phys., 37* (1966) 203.
F. G. Allen and G. W. Gobeli, *Phys. Rev. B, 144* (1966) 558.

42 M. Cardona and L. Ley (eds.), *Photoemission in Solids*, Vol. I, Springer, Berlin, 1978.
43 J. Derrien and F. A. D'Avitaya, *Surf. Sci.*, *65* (1977) 668.
44 R. L. Bell, *Negative Electron Affinity Devices*, Oxford University Press, Oxford, 1973.
45 P. E. Gregory and W. E Spicer, *J. Appl. Phys.*, *47* (1976) 510; *Phys. Rev. B*, *12* (1975) 2370.
46 R. S. Muller and T. Kamins, *Device Electronics for Integrated Circuits*, Wiley, New York, 1977, p. 93, and references cited therein.
47 T. C. McGill, J. O. McCaldin and D. L. Smith, personal communications, February 1979 and August 14, 1981.
48 S. M. Sze, *Physics of Semiconductor Devices*, Wiley, New York, 1969.

J. S. Eglash, W. E. Spicer, and I. Lindau, Reply to "Surface Photovoltage Measurements and Fermi level pinning: comments on 'Development and confirmation of the unified model for Schottky barrier formation and MOS interface states on III-V compounds'" to be published in Thin Solid Films.

Thin Solid Films, 89 (1982) L35–L40

Letter

Reply to "Surface photovoltage measurements and Fermi level pinning: comments on 'Development and confirmation of the unified model for Schottky barrier formation and MOS interface states on III–V compounds'"

S. EGLASH, W. E. SPICER AND I. LINDAU
Stanford Electronics Laboratories, Stanford University, Stanford, CA 94305 (U.S.A.)
(Received March 22, 1982; accepted March 22, 1982)

In a paper appearing elsewhere in this issue our unified model for Schottky barrier formation on III–V semiconductors is reviewed, and some work by Brillson and coworkers is discussed[1]. An accompanying reply by Brillson expresses concern at our treatment of his work[2]. The following response presents a clarification of the issues. We will consider the prototypical example of a column III metal (aluminum, gallium, indium) on n-type GaAs.

The work function of a semiconductor is given by $\phi \equiv E_{vac} - E_f = E_A + qV_B + w_b$, where $E_A = E_{vac} - E_{c,\,surface}$ is the electron affinity, $qV_B = E_{i,\,surface} - E_{i,\,bulk}$ is the band bending, and $w_b = (E_c - E_f)_{bulk}$ is the bulk potential (Fig. 1). Two experimental techniques have been used predominantly to study the evolution of these parameters during Schottky barrier formation. UV photoemission spectroscopy (UPS) samples the energy distribution of valence electrons. This sampling occurs quite close to the surface[3,4]; thus $(E_f - E_v)_{surface}$ and qV_B may be found (Fig. 2)[5]. In particular, changes in the band bending qV_B during adatom deposition may be determined unambiguously. Contact potential difference (CPD) or Kelvin probe measurements determine changes in the work function ϕ of the surface under study. Since we have $\phi = E_A + qV_B + w_b$, measured changes in ϕ can result from changes in electron affinity, band bending and bulk potential. w_b is constant at constant temperature.

Initially, after a "good" cleave, the semiconductor bands are flat; *i.e.* the Fermi level at the surface is unpinned and $qV_B = 0$. After submonolayer metal deposition, both qV_B and E_A may change and contribute to changes in ϕ. Changes in qV_B are due to additional surface state formation and may be measured by UPS. The band bending adjusts so that, if we ignore screening effects, the charge Q_{ss} in the surface states is balanced by the space charge Q_{sc} in the depletion region such that $Q_{ss} + Q_{sc} = 0$. Changes in E_A are due to near-surface (or "interfacial") dipole layers arising from electron transfer between the adatoms and substrate atoms and from local effects such as changes in exchange and correlation. Brillson and coworkers have used the notation $\Delta\chi_0$ to represent the magnitude of the interfacial dipole. The work function changes by the sum of the changes in qV_B and E_A, and its variation may be determined by the CPD (Kelvin probe) technique.

The unified model has been described in detail elsewhere[6–8]. The salient features of our results are that at low adatom coverages (less than a few tenths of a

0040-6090/82/0000-0000/$02.75

monolayer) changes in qV_B dominate the changes in ϕ. In fact, we find that Fermi level pinning is complete for a wide variety of overlayers by about 0.1 monolayer. At thicker coverages E_A changes such that ϕ approaches a value characteristic of surfaces of thick layers of the adatom. This process is generally complete by one to a few monolayers. These conclusions have been reached as a result of direct measurements by ourselves, by calculations from measurements by Mönch and Gant[9], and are consistent with the results of studies of cesium on GaAs by Derrien and d'Avitaya[10], Gregory and Spicer[11] and Allen and Gobeli[12], and silver on GaAs by Palau *et al.*[13]

Since changes in ϕ are due to changes in both qV_B and E_A, there is a need to separate these contributions in a CPD measurement. Mönch and Gant have used the temperature dependence of the CPD to separate these effects. Their results confirm our own (see ref. 1, Fig. 3).

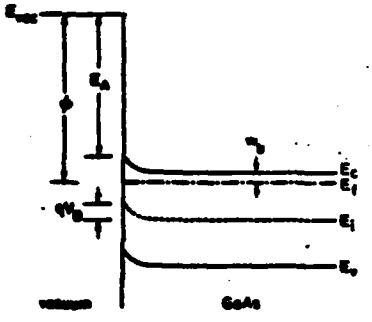

Fig. 1. Relevant energy levels of an n-type semiconductor with Fermi level pinning at the surface. The work function ϕ, electron affinity E_A, band bending qV_B and bulk potential w_b are shown.

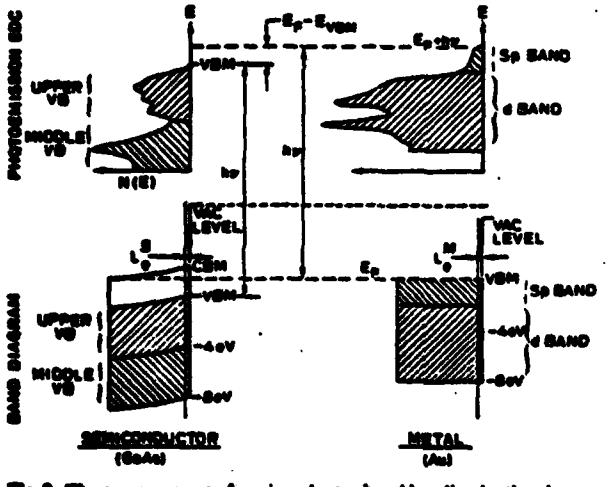

Fig. 2. The measurement of semiconductor band bending by the photoemission technique[3]. In the right-hand panel, determination of the Fermi level by photoemission from a metal is illustrated. In the left-hand panel, the position of the valence band maximum relative to the previously determined Fermi level is shown.

Brillson and coworkers have suggested a different model for Schottky barrier formation in which changes in E_A (due to dipole formation) dominate at low coverages and significant changes in qV_B occur at coverages up to several monolayers[14,15]. CPD measurements were used in their work to determine changes in ϕ. Comparison with data from Mönch and Gant[9] and ourselves[6-8] indicate that changes in ϕ at low coverages arise mostly from changes in qV_B, not E_A as assumed by Brillson and coworkers (see ref. 1, Fig. 4). This assumption is central to their work. Similarly, changes in E_A dominate changes in ϕ at high coverages. Thus, at low coverages surface state production appears to dominate the changes in ϕ, and at high coverages surface dipole formation is dominant.

Brillson and coworkers have based their different interpretation upon surface photovoltage (SPV) measurements. In this technique the difference between ϕ in the dark and under intense illumination is measured. They have interpreted the SPV at high light intensities as the total amount of band bending. This assumes that the incident light flattens the bands completely. This is unlikely, as we show below.

In Fig. 3(a) the equilibrium electron and hole currents toward the surface in the dark are shown. In equilibrium there is no net flow of current. With light of $h\nu > E_g$ incident on the surface, there is at first a net positive current toward the surface (Fig. 3(b)). This is due to the separation of electron–hole pairs created in the space charge region and the subsequent flow of holes to the surface. These holes most likely recombine with electrons in surface states; in any case, the amount of negative charge at the surface is diminished and the amount of band bending decreases.

As the band bending is decreased, the flux of electrons thermionically excited to the surface increases by a Boltzmann factor. The hole flux, however, is approximately constant at a given light intensity. Thus, steady state occurs when the band bending presents just that barrier to the thermionic emission of electrons which is required to make the electron and hole fluxes equal (Fig. 3(c)). This decrease in band bending is the measured SPV; it will be less than the total band bending by a correction factor which has been estimated by McGill *et al.*[16] and presented in detail elsewhere[1]. This correction, in fact, is about 0.4 eV under the conditions for which Brillson and coworkers claim their SPV equals qV_B. Our correction assumes a sufficiently high surface recombination rate, but many studies indicate that surface recombination on GaAs is quite high[17-20].

In his response to our paper[2], Brillson claims our corrections assume "... a Richardson model of the metal as an infinite sink for electrons, [and are] not applicable to the case of [only] a few ångströms of metal on a semiconductor surface"[2]. This is incorrect. Our correction simply assumes that thermionic excitation of electrons from the neutral region of the semiconductor over the band bending barrier occurs. When the band bending is reduced to the point where this electron current balances the drift of photoexcited holes to the surface, steady state occurs. If the surface recombination rate is sufficiently high, as many experiments suggest, this is trivial. However, even if some build-up of carriers at the surface occurs, our correction will not be significantly in error provided the cross sections for electron and hole capture by the surface states are such as to cause the excess electron and hole surface concentrations to be comparable.

Figures 1 and 2 of Brillson's reply purport to show agreement between his work and ours[2]. However, in both figures Brillson plots his value for the semiconductor

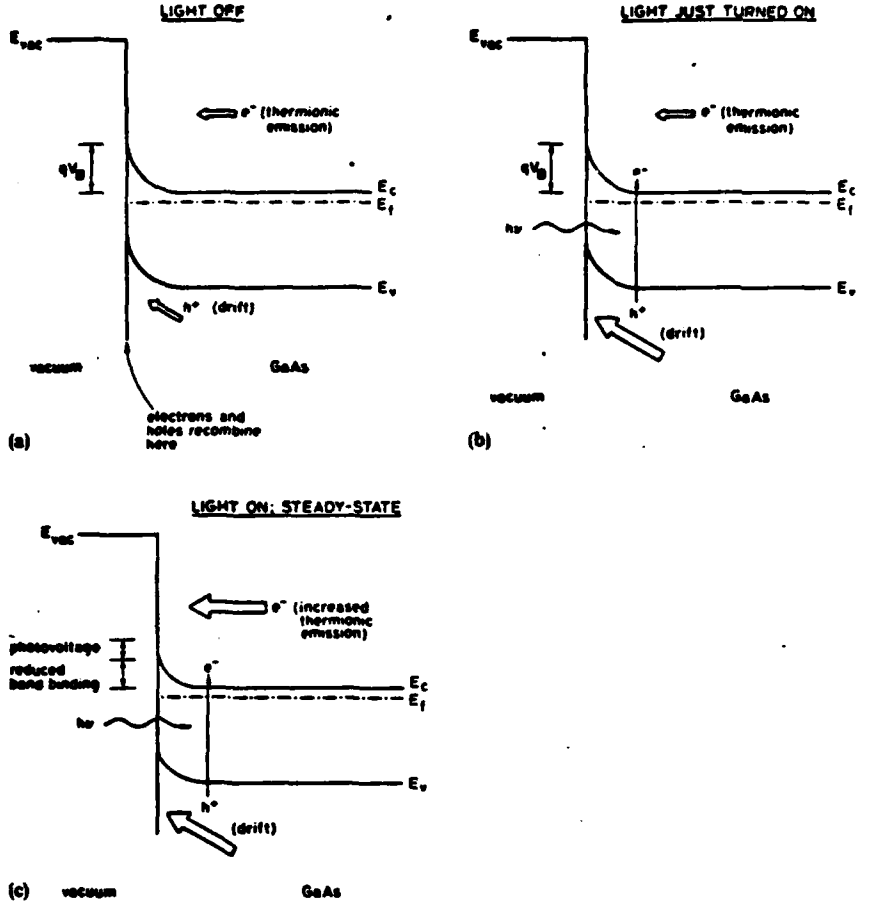

Fig. 3. The evolution in time of the SPV at a semiconductor surface with Fermi level pinning. (a) In thermal equilibrium there is no net flow of current to the surface. The electron current due to thermionic excitation of majority carriers over the barrier is exactly balanced by the drift of minority carriers from the bulk and from generation in the space charge region. (b) When light ($h\nu > E_g$) has been on for a time too short to achieve steady state, there is a net flow of positive current toward the surface. This current will tend to flatten the bands. (c) With the light on, at steady state the band bending has been reduced and the electron current toward the surface correspondingly increased. Now the electron and hole currents toward the surface are equal.

band bending qV_B *plus* the interfacial dipole $\Delta\chi_0$ and compares this with our measured value for the band bending qV_B alone. So the data as plotted in Figs. 1 and 2 of Brillson's reply are in disagreement, unless $\Delta\chi_0$ does not contribute to the barrier. We argue below that the interfacial dipole $\Delta\chi_0$ may contribute to the work function and electron affinity, but not to the barrier height.

Brillson and coworkers have suggested that an Al–GaAs replacement reaction is the origin of this interfacial dipole $\Delta\chi_0$, which they say adds to the barrier height[15,21]. However, our results show that the development and final height of the

barrier is the same for gallium as for aluminum overlayers[1,6-8]. Obviously a replacement reaction has no meaning for gallium overlayers on GaAs. Since we observe identical barrier heights for these two metals, replacement reactions must not be important in determining the barrier heights in these systems. The barrier height is also the same for indium, oxygen, cesium, germanium and antimony overlayers on GaAs(110)[1,6-9].

The resolution of the discrepancy associated with Figs. 1 and 2 of Brillson's reply consists of corrections to the interpretations of Brillson and coworkers. The interfacial dipole $\Delta\chi_0$, even if present, is irrelevant to the barrier heights measured on practical devices. This is because electrons may readily tunnel through such barriers. The tunneling probabilities have been calculated for simple models of the barrier shape by ourselves[1] and Brillson[2]; both groups obtain a probability of about 0.5, which would not contribute significantly to the barrier height. Furthermore, midgap states have been detected by deep level transient spectroscopy at GaAs grain boundaries[22]. In this environment no interfacial dipoles are likely to be present, yet the energy of these states is in accord with the Schottky barrier heights measured on Al/GaAs diodes.

As evidence that these interfacial barriers are an impediment to tunneling, Brillson mentions examples of interfacial oxide layers 20–30 Å thick contributing to measured Schottky barrier heights. However, the tunneling probability depends exponentially on thickness, and these layers are significantly thicker than the interfacial dipoles which are related to electron affinity variations. These dipoles have thicknesses of atomic dimensions, characteristically[14,15] 2–8 Å.

A second correction necessary to resolve the discrepancy in Figs. 1 and 2 of Brillson's reply is to realize that the high intensity light used in the SPV experiment is insufficient to flatten the bands. Thus the values claimed by Brillson and coworkers for the semiconductor band bending are smaller than the actual band bending.

In fact, even the values given by Brillson and coworkers for the semiconductor band bending qV_B in Fig. 3 of their reply are larger than their measured photovoltages published in ref. 14, Fig. 1. We illustrated this in Fig. 6 of our original paper, where we plot Brillson's published photovoltage data. We find it impossible to reproduce the values quoted by Brillson and coworkers for qV_B from their published SPV data.

Brillson in his reply to our paper quotes photovoltages in excess of known barrier heights for gold on n-GaAs(110) as an argument against our corrections to his SPV data. However, recent work by our group shows unusually large barrier heights for this system and suggests that the exact barrier height obtained may depend particularly on the extent of contamination at the interface, the deposition rate and post-deposition heat treatments[23,24]. Gold behaves so differently from the other materials discussed above, it is clear it must be considered separately from, for example, aluminum.

There is also continuing disagreement with regard to the rate of Fermi level stabilization. The phrase "Fermi level stabilization" is ambiguous, because it must be determined from the context whether this includes the surface (or interfacial) dipole or not. The debate actually centers around the rate of *barrier height* stabilization. We attribute the barrier height solely to the band bending qV_B and find that qV_B is essentially constant above a few tenths of a monolayer of adsorbate.

Brillson and coworkers equate $qV_n + \Delta\chi_0$ with the barrier height and find that the barrier height undergoes significant changes up to coverages of eight monolayers. That the barrier height equals qV_n, not $qV_n + \Delta\chi_0$, was argued above. The changes in potentials which Brillson and coworkers see from a few tenths to eight monolayers are changes in the electron affinity and work function, not in the band bending.

In conclusion, Brillson and coworkers have measured changes in the work function ϕ up to several monolayers of aluminum on GaAs, and they attributed the changes in ϕ at higher coverages to changes in the band bending qV_n. However, data from ourselves and others for aluminum, gallium, indium, germanium, antimony, cesium and oxygen overlayers on GaAs show that in all cases the band bending is complete for submonolayer coverages. Brillson and coworkers have also assumed a contribution from interfacial dipole layers to the measured Schottky barrier height. However, electron tunneling through these thin layers precludes such a contribution, as shown in extensive work with cesium overlayers on GaAs. Here, large reductions in electron affinity and work function arising from surface dipoles can only be explained by electron tunneling through the dipole layers[10-12]. If these corrections are taken into account, good agreement between the data of Brillson and coworkers and the rest of the literature can be obtained.

1 W. E. Spicer, S. Eglash, I. Lindau, C. Y. Su and P. Skeath, Development and confirmation of the unified model for Schottky barrier formation and MOS interface states on III–V compounds, *Thin Solid Films*, *89* (1982) 447.
2 L. J. Brillson, Surface photovoltage measurements and Fermi level pinning: comments on "Development and confirmation of the unified model for Schottky barrier formation and MOS interface states on III–V compounds", *Thin Solid Films*, *89* (1982) L27.
3 I. Lindau and W. E. Spicer, *J. Electron Spectrosc. Relat. Phenom.*, *3* (1974) 409.
4 M. P. Seah and W. A. Dench, *Surf. Interface Anal.*, *1* (1979) 2.
5 G. F. Derbenwick, D. T. Pierce and W. E. Spicer, *Methods Exp. Phys.*, *11* (1974) 84.
6 W. E. Spicer, I. Lindau, P. Skeath, C. Y. Su and P. Chye, *Phys. Rev. Lett.*, *44* (1980) 420.
7 W. E. Spicer, P. Skeath, C. Y. Su and I. Lindau, *Proc. 15th Int. Conf. on Physics of Semiconductors, Kyoto, 1980*, in *J. Phys. Soc. Jpn., Suppl. A*, *49* (1980) 1079.
8 W. E. Spicer, I. Lindau, P. Skeath and C. Y. Su, *J. Vac. Sci. Technol.*, *17* (1980) 1019.
9 W. Mönch and H. Gant, *Phys. Rev. Lett.*, *48* (1982) 512.
10 J. Derrien and F. A. d'Avitaya, *Surf. Sci.*, *65* (1977) 668.
11 P. E. Gregory and W. E. Spicer, *Phys. Rev. B*, *12* (1975) 2370.
12 F. G. Allen and G. W. Gobeli, *Phys. Rev.*, *144* (1966) 558.
13 J. M. Palau, E. Testemale and L. Lassabatere, *J. Vac. Sci. Technol.*, *19* (1981) 192.
14 L. J. Brillson and D. W. Kruger, *Surf. Sci.*, *102* (1981) 518.
15 L. J. Brillson, R. Z. Bachrach, R. S. Bauer and J. McMenamin, *Phys. Rev. Lett.*, *42* (1979) 397.
16 T. C. McGill, J. O. McCaldin and D. L. Smith, personal communication, February 1979, August 14, 1981.
17 H. C. Casey, Jr., and E. Buehler, *Appl. Phys. Lett.*, *30* (1977) 247.
18 C. A. Hoffman, H. J. Gerritsen and A. V. Nurmikko, *J. Appl. Phys.*, *51* (1980) 1603.
19 C. A. Hoffman, K. Jarasiunas and H. J. Gerritsen, *Appl. Phys. Lett.*, *33* (1978) 536.
20 G. P. Peka and L. G. Shepl, *Sov. Phys. Semicond.*, *10* (1976) 1140.
21 C. B. Duke, A. Paton, R. J. Meyer, L. J. Brillson, A. Kahn, D. Kanani, J. Carelli, J. L. Yeh, G. Margaritondo and A. D. Katnani, *Phys. Rev. Lett.*, *46* (1981) 440.
22 M. Spencer, *Ph.D. Dissertation*, Cornell University, 1980.
23 P. Skeath, C. Y. Su, I. Hino, I. Lindau and W. E. Spicer, *Appl. Phys. Lett.*, *39* (1981) 349.
24 W. G. Petro, I. A. Babalola, P. Skeath, C. Y. Su, I. Hino, I. Lindau and W. E. Spicer, *PCSI-9, Asilomar, 1982*, in *J. Vac. Sci. Technol.*, to be published.

K. I. Lindau and W. E. Spicer, "The Use of Synchrotron Radiation to Study Oxygen and Metal Overlayers on GaAs (110) Surfaces," in Electron Spectroscopy; Theory, Techniques, and Applications, Ed. C. R. Brundle and A. D. Baker (Academic, 1981), p. 197.

Chapter 4 in "Electron Spectroscopy; Theory, Techniques and Applications," Vol. 4, edited by C. R. Brundle and A. D. Baker, (Academic Press, New York, 1981).

4

The Use of Synchrotron Radiation to Study Oxygen and Metal Overlayers on GaAs (110) Surfaces

I. LINDAU and W. E. SPICER

Stanford Electronics Laboratories, Stanford University, Stanford, California 94305

I. INTRODUCTION

This chapter will deal with the surface electronic structure of the clean GaAs (110) surface and the effects of oxygen and metal overlayers on its properties. Together with silicon, the GaAs surface is without doubt the most studied semiconductor, both from fundamental points of view and from device applications. Our main emphasis will be on the basic properties of the GaAs (110) surface using electron spectroscopy. Particular attention is given to the wealth of information that photoemission spectroscopy has provided during the past few years. The rapid experimental progress is partly due to the development of synchrotron radiation as an excitation source. Much of the material in this review is based on the application of this technique. We have drawn heavily from results obtained in our own group but tried to put these in the context of other experimental and theoretical work. Other articles in this series are closely related to the studies discussed here. A general review of synchrotron radiation as a tool for photoemission studies of surfaces has recently been completed by Lindau and Spicer[114] and C. S. Fadley has reviewed the basic physics and applications of X-ray photoelectron spectroscopy in Volume 3 of this series.

Much of the interest in obtaining a better understanding of the fundamental properties of the GaAs (110) surface has been linked to the role that the empty and filled surface states play for the Fermi-level pinning position and Schottky-barrier height. A comprehensive review of the clean GaAs (110) surface in Section II is therefore followed in Sections III and IV by a detailed account of the effects that oxygen and thin metal overlayers have on the surface electronic structure, Fermi-level pinning position, and Schottky-barrier height. Section V deals with the effects of a thin metal overlayer on the oxidation properties of the GaAs (110) surface. This aspect is important in attempts to achieve better passivation properties. In Section VI a new model for Schottky-barrier formation, based on defect states at or near the oxide/semiconductor interface, is presented. Unfortunately it is not possible to include all aspects of electron spectroscopy studies of the GaAs surface, e.g. the (100) surface, the polar surfaces, thick native oxides, heterojunctions, spin-polarized properties, and photocathodes.

II. THE SURFACE ELECTRONIC STRUCTURE OF THE CLEAN GaAs (110) SURFACE

A. The Energy Location of Filled and Empty Surface States: A Comparison between Theory and Experiment

The electronic and geometrical structure of the clean GaAs (110) surface has been studied extensively both experimentally and theoretically.[1-83] We will not attempt to describe the evolution of different models during the past decade but concentrate on a description of our present understanding of the clean GaAs (110) surface and what the controversial issues still are.

A schematic and pictorial view of the clean GaAs (110) surface is shown in Fig. 1. When a covalent bond is broken on cleavage, each surface atom tends towards its atomic electronic configuration, i.e. p^3s^2 for As and s^2p for Ga. The positions and bond configurations of the surface atoms are determined by achieving the lowest energy. This leads to a geometrical rearrangement of the

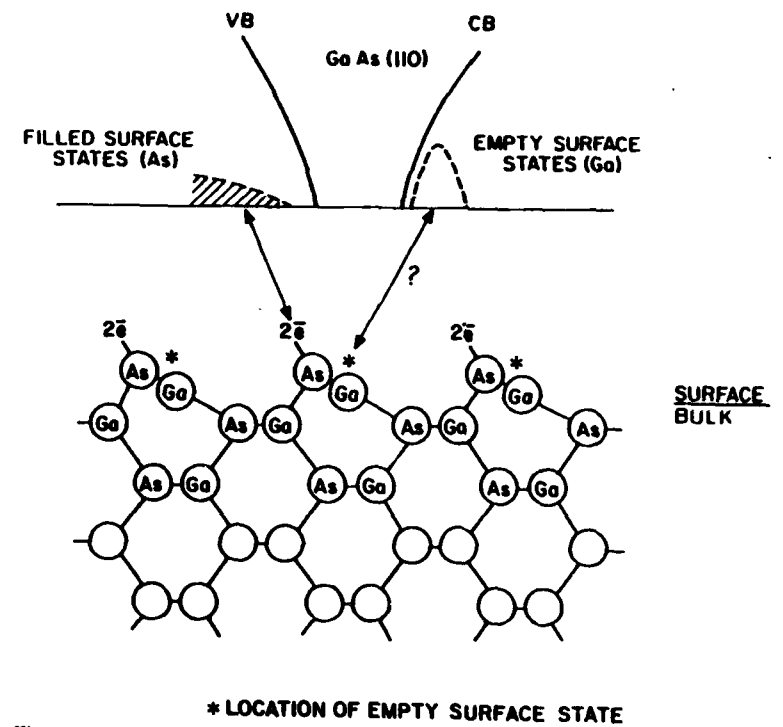

Fig. 1. The GaAs (110) surface. Both the electronic and atomic surface rearrangements are indicated. (From ref. 17)

atoms within the surface lattice with, roughly speaking, the As atoms rotated outwards and the Ga inwards. The geometrical rearrangement will greatly influence the electronic structure at the surface, causing shifts of the surface states of up to as much as 1 eV. The intrinsic filled and empty surface states associated with As and Ga surface atoms, respectively, are thus removed from the band gap (see Fig. 1). There is now general agreement between different experimental and theoretical groups regarding the main features of the geometrical surface rearrangement shown in Fig. 1 and that there are no filled or empty surface states in the band gap. This issue has been discussed extensively in the literature during the past few years.[8, 14, 16]

The pictorial description of the nature and location of the filled and empty surface states in Fig. 1 is, of course, a gross oversimplification. The surface states/resonances are characterized by wave functions that fall off rapidly away from the surface. Their complexity will be illustrated by one state-of-the-art calculation done by Chadi[59] using the tight-binding method. Three different surface models were considered, all involving a raising of the surface As atoms and a lowering of the Ga surface atoms. The input parameters to these different surface relaxation models were mainly obtained from LEED data.[59]

The results for the so-called bond-relaxation model will be shown here.[59] Within this model, the rotation of the As and Ga surface atoms are combined with an interplanar displacement of the atoms in the two top layers. The density of surface states is shown as the solid line in Fig. 2. The notation B_1, B_2, and B_3 is used for filled surface states, and B_1' etc. for empty states. The states S_1 are strongly model dependent and arise in this case from the change in interplanar spacings of the two top surface layers. From Chadi's calculation, the orbital character of the surface states is also obtained.

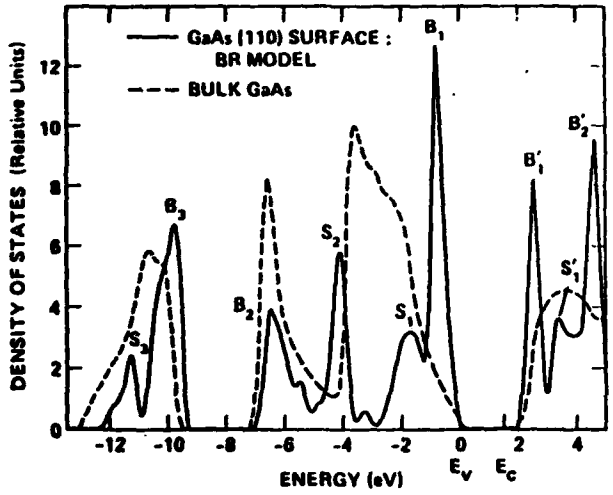

Fig. 2. The local density of states (solid line) for the bond-relaxation model of the (110) surface of GaAs. (From ref. 59)

The common features of the main results of Chadi's calculation, independent of the details of the surface rearrangement, can be summarized as follows.

(1) Surface relaxation removes both filled and empty surface states from the band gap of GaAs. This is true for all surface relaxations where As surface atoms are raised and Ga surface atoms lowered.

(2) The surface relaxation creates new surface states. Not less than five major surface states (filled) are predicted for the valence band region. The exact ordering of the empty and filled surface states closest to the band gap is sensitive to the details of the model parameters

(3) The filled and empty surface states near the band gap are not purely As or Ga derived but contain a mixture of anion–cation character. This aspect will be discussed further in Section C and will be related to experimental data.

Most of the information on the detailed geometrical rearrangements of the GaAs (110) surface has been obtained from LEED intensity studies.[69–79] Angle-resolved photoemission studies, using synchrotron radiation and conventional sources, have recently been done with an encouraging qualitative agreement between theory and experiment for the basic features.[30–33]

A typical angle-resolved spectrum from one of these studies[33] is shown in Fig. 3 for two different polar and azimuthal angles for the emitted photoelectrons. The notations B_1, S_1, S_2, and B_2 refer to the surface states predicted theoretically by Chadi.[59] From a detailed analysis of the angle-resolved data, Huijser *et al.*[33] were able to obtain a fairly detailed picture of the energy dispersion of the surface state bands. A summary of these results is shown in Fig. 4 which also shows the theoretical results by Chadi[59] for the bond-relaxation model discussed above. Fairly good agreement between theory and experiment could be claimed from this comparison. The best fit was obtained for the model where the rotation was combined with interplanar displacements. Angle-resolved photoemission data can thus provide considerable insight into the detailed geometrical rearrangements of the surface lattice and, to some extent, distinguish between different models.

B. The Fermi Level Pinning Position

In this section we will discuss the Fermi-level pinning position for the cleaved GaAs (110) surface and how it is related to filled and empty surface states. The observation by a number of different experimental groups that there are no filled or empty surface states in the band gap was an important

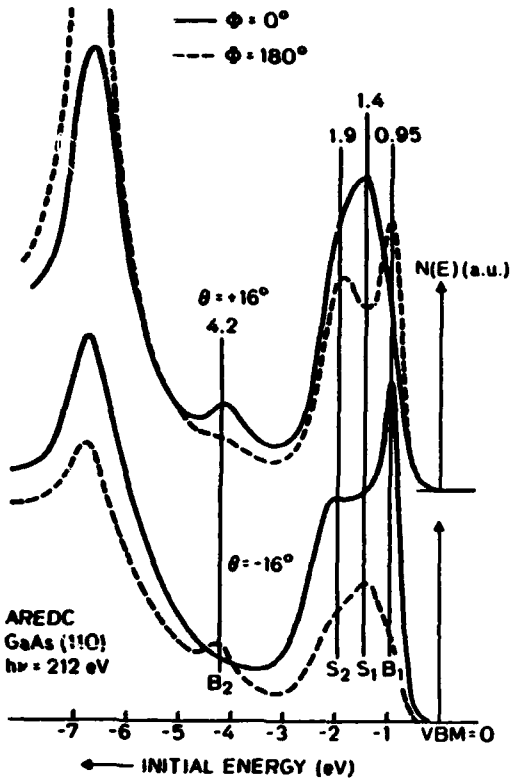

Fig. 3. Angle-resolved photoemission spectra for a few selected angles of the photoemitted electrons. (From ref. 33)

incentive for the theoretical calculations of a relaxed GaAs (110) surface discussed in the preceding section. (Theoretical calculations[48] for the ideal surface predict both filled and empty surface states in the band gap.) Thus there is now general agreement that the Fermi-level position for a high-quality surface of n(p)-type GaAs (110) is just below (above) the conduction (valence) band minimum (maximum), i.e. the surface is unpinned.[8,14,16]

The difficulty in analyzing the existence of intrinsic states in the band gap from Fermi-level pinning measurements is demonstrated in Fig. 5. Data were obtained from ten different cleaves[16,21] made on three different n-type crystals (two from Laser Diode Corp., samples I and II; one from MCP, sample III). The MCP crystal (sample III) was Si-doped (bulk doping $1{\cdot}7 \times 10^{18}\,cm^{-3}$) and the Laser Diode crystals were Te-doped (bulk doping $3 \times 10^{17}\,cm^{-3}$). As can

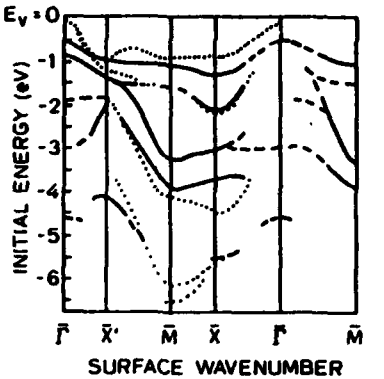

Fig. 4. Energy dispersion relations for the surface bands: (—— –) well resolved and (- - -) weak structure in the angle-resolved spectra; (...) the calculations for the bond-relaxation model by Chadi. (From ref. 33)

be seen, all the cleaves from sample I had no Fermi-level pinning, i.e. the surface Fermi level was at the bulk position. In contrast, sample III had one cleave with the Fermi level at the bulk position and one with the Fermi level pinned 0·6 eV below the bulk position. The inset shows representative valence-band spectra for samples with unpinned and pinned Fermi levels respectively. Surfaces with an unpinned Fermi level always showed sharper valence-band spectra, and Fermi-level pinning always occurred for the more smeared spectra. However, in some cases we observed pinning for surfaces with a valence-band spectrum as sharp as that shown in the inset (bottom curve). Thus, there is not a one-to-one correspondence between the Fermi-level pinning position and the sharpness of the valence-band spectrum.

In Fig. 5 we also indicate how the surface position of E_F varied with oxygen exposure. Note that, for all the surfaces that showed no pinning on cleavage, the surface Fermi level drops rapidly with oxygen exposure. The large changes in Fermi-level pinning are completed by exposures of about 10^5 L. The oxygen coverage at this point is less than 1% of a monolayer. The Fermi-level pinning is affected by the oxygen long before any oxygen-induced emission is observed in the valence-band spectra. A further discussion will be given in Sections C and D

The Fermi-level position undergoes an interesting evolution for cleave B of the MCP crystal. Here E_F is originally pinned 0·6eV below the conduction band minimum. The pinning position rises to the bulk position for exposures between 10 and 10^2 L. For higher exposures, $> 10^3$ L, the oxygen will introduce sufficient extrinsic states in the band gap to cause pinning anew. The unpinning of the Fermi level for low oxygen exposure may be due to a

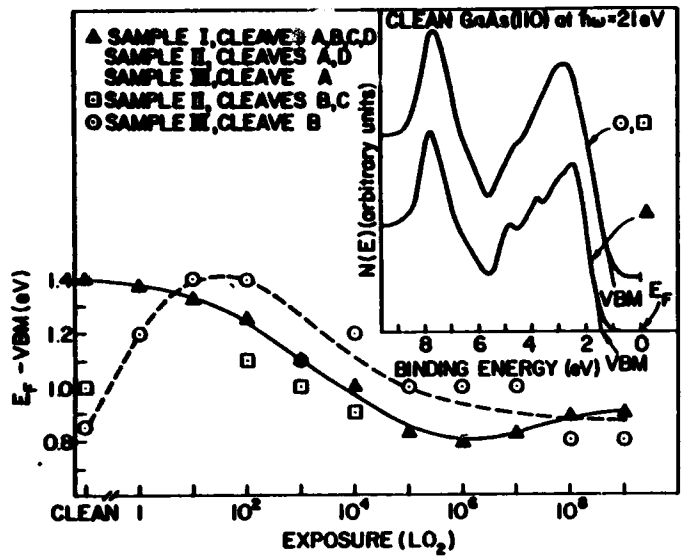

Fig. 5. Fermi-level pinning position on n-type GaAs (110) for various samples and cleaves as a function of oxygen exposure. Inset shows representative valence band spectra for samples with unpinned (▲) and pinned (⊙,⊡) Fermi levels. (From ref. 16)

rearrangement of the surface atoms and relief of strain (probably introduced by the cleavage) within the surface lattice. This occurs for oxygen coverages as low as 1 oxygen per 10^4–10^5 surface atoms, indicating a long-range effect of the oxygen on the surface. The effect of oxygen on the pinning position is also reflected in small changes in the surface electronic structure. This is demonstrated in Fig. 6 for two different crystals and the effects of small amounts of oxygen are also shown.[21] As can be seen from the figure, there are noticeable differences, particularly in the top 4 eV of the valence band, depending on the crystal quality. The curves in the left-hand panel (sample LD1C) show sharp structure in the valence band and an unpinned Fermi level for the clean cleaved surface. Oxygen exposures up to 10^3 L result in a change of pinning position to about mid-gap, but the valence band electronic structure is essentially unchanged. The results for the MCPB sample are drastically different. The structure in the top 4 eV is more smeared for the clean surface but sharpens on oxygen exposure. The effects of oxygen on the surface electronic structure appear before any emission can be seen from the chemisorbed oxygen itself (see Section III.C). The sharpening of the valence band occurs at the same time as the Fermi level is being unpinned (see discussion above), providing evidence that the surface atom arrangement is

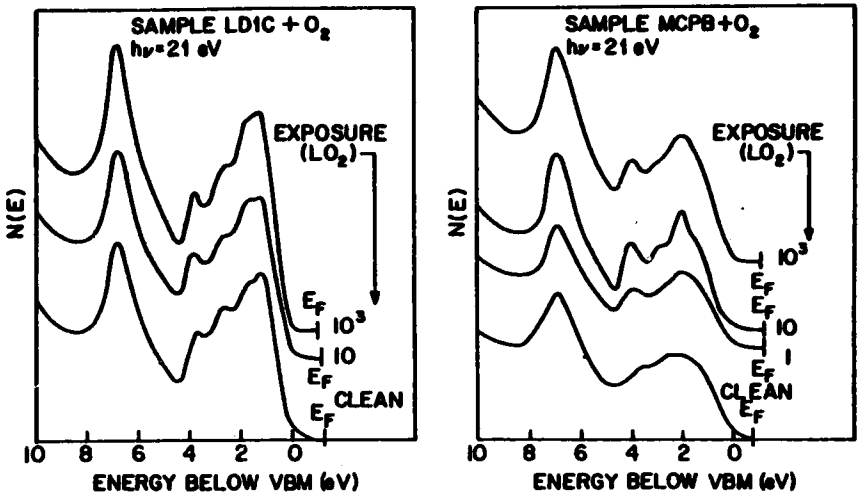

Fig. 6. Photoemission spectra from the upper part of the valence band of two different GaAs (110) crystals. The effects of a small oxygen exposure on the Fermi level and valence band structure are also shown. (From ref. 21)

closer to that described by the calculation for a relaxed surface with no states in the band gap. It should be noted that the structure in the MCPB sample produced after 10 L oxygen exposure is slightly different from that of the cleaved LD1C sample. It is obvious that a detailed comparison with theoretical calculations presents difficulties since the surface electronic structure is very sensitive to the exact geometrical configuration of the surface atoms. Needless to say, this will also make the interpretation of/and correlation to angle-resolved photoemission spectra harder.

C. Probing of Empty Surface States: Constant Final State Spectroscopy

The constant final state spectroscopy (CFS) technique,[84] or partial yield technique, can be used to obtain information on the excitation from an inner core level to the first available empty states above the Fermi level. In principle, CFS is therefore a promising tool to study the location of empty surface states in the band gap and the orbital character of these states (since dipole selection rules apply in the excitation).

CFS results of the excitation from the Ga 3d levels are presented in Fig. 7 for two of the different crystals discussed in the preceding section. The pinning position varies by about 0·5 eV for these two crystals, and the behavior of E_F with oxygen exposure is quite different. The double peak structure in the CFS spectra arises from the 0·5 eV spin–orbit split Ga 3d level ($3d_{5/2}$, $3d_{3/2}$). As can be seen from Fig. 7, the CFS structure is independent of the original pinning

positions on the freshly cleaved surfaces and does not change energy location with oxygen exposure. This provides evidence that the intrinsic surface states are not the cause of the differences in pinning position. An oxygen exposure of 10^6–10^7 L O_2 is required before the sharp double peak structure in the CFS spectra is smeared out. At this exposure the surface is covered with a significant fraction of a monolayer of oxygen, and structure in the valence band spectra is also smeared out (see Section III.D).

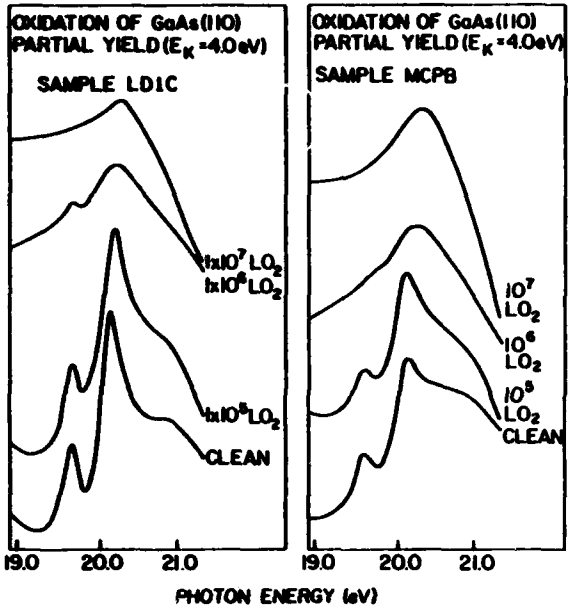

Fig. 7. CFS spectra of GaAs (110) taken at a final state energy of 4 eV. The effects of oxygen exposure are shown for the surfaces originally pinned (right) and unpinned (left). (From ref. 21)

It is now clear that excitonic effects are extremely important in CFS spectra,[34,13,18,35,37–40] and the CFS technique is therefore more limited in determining the exact energy position of the empty surface states than was originally thought. The surface excitons in III–V compounds have a very large binding energy—in the case of GaAs about 0·5 eV. The excitonic nature of the transitions is consistent with the evolution seen for increasing oxygen exposure: no energy shift but a gradual attenuation of the structure as more and more surface atoms are distributed by the oxygen.

Bauer *et al.*[38–40] demonstrated that dipole selection rules could be used to determine the orbital character of the empty surface states. The transitions

seen in Fig. 8 are not present when the excitation is done from the As 3d but are clearly observed for the As 3p core levels. Both the Ga 3d and As 3p transitions are believed to be into the B_1' empty surface state predicted by Chadi.[59] There is thus a distribution of the empty surface states between the anion and cation. From experimental data, Bauer *et al.*[40] estimate the Ga : As distribution to be about 3 : 2, which is consistent with the theoretically derived value.

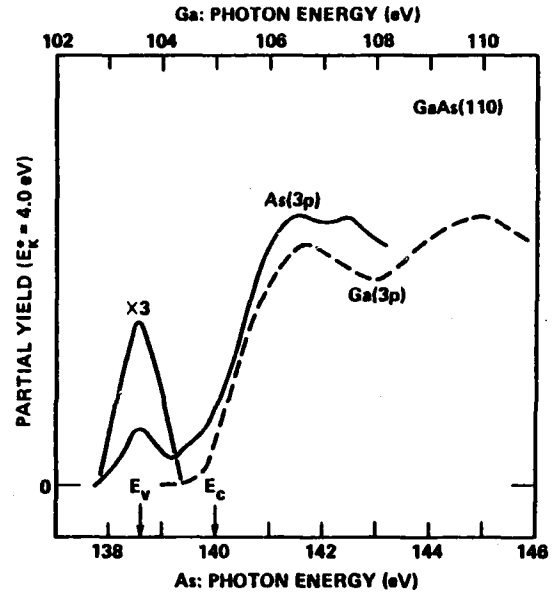

Fig. 8. CFS spectra for the 3p core electrons in GaAs. The transitions assigned to surface states are expanded. (From ref. 40)

D. LEED Determinations of the Surface Atomic Structure

As was mentioned briefly earlier, there has been a large number of LEED investigations and interpretations of the (110) surface of GaAs.[67–83] A schematic of the top and side views of the surface atomic geometry is shown in Fig. 9. A number of investigators now seem to agree that the bond rotation angle between the surface As atoms moving outwards and the surface Ga atoms inwards is about 27° (ω in Fig. 9). The general consensus also appears to be that this rotation is coupled to an interplanar displacement between at least the two topmost surface layers: the As atoms move outward and the Ga atoms inward in the first layer; in the second layer the Ga atoms move outward and

the As atoms inward. The details of this displacement and whether any distortion takes place in the third layer are still being debated.

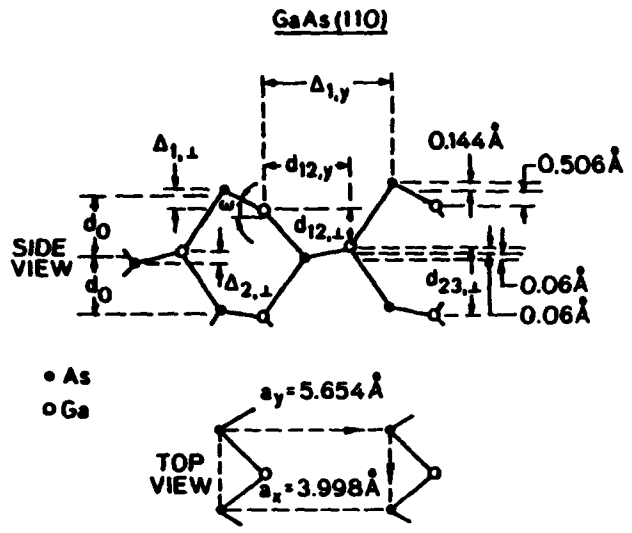

Fig. 9. Schematics of the top and side views of the surface atomic geometry, showing the bond rotation angle ω between As atoms moving outwards and Ga inwards and the interplanar displacements in the top two layers. (From ref. 75)

The detailed analysis of the surface atomic geometry based on LEED intensity measurements is appreciated from Table I, where the results from five recent works are summarized. The table is essentially adapted from the paper by Meyer *et al.*,[75] with the notations given in Fig. 9. The agreement between the different analyses for the basic features of the surface atomic rearrangement is very impressive. At this point it seems clear that photoemission spectroscopy cannot distinguish between the validity of one model or the other. As we pointed out earlier, the angle-resolved photoemission measurements by Huijser *et al.*[33] are consistent with the surface geometries given in Table I; in particular, a direct comparison with the results by Chadi[59] was made. Also, even though the angle-resolved and angle-integrated photoemission data by Eastman *et al.*[28–30] were originally assigned to a 19° bond rotation, it has been pointed out by Meyer *et al.*[75] recently that these photoemission results also seem to be in accord with the models listed in Table I.

TABLE I

Positions of the Atoms in the Uppermost Three Atomic Bilayers for the Reconstructed Surface of GaAs (110) according to Several Investigators (The symbols for the structures are defined in Fig. 9; distances are in Å)

Structure	Layer	As	Ga	$\Delta_{1,\perp}$	$\Delta_{2,\perp}$	$\Delta_{3,\perp}$	$d_{12,\perp}$	$d_{23,\perp}$	$\Delta_{1,y}$	$d_{12,y}$	ω_1	Bond length change (%) Ga_1–As_1	Bond length change (%) Ga_1–As_2
Tong *et al.*[76]	1	↑0·094	↓0·554										
	2	0	0	0·650	0	0	1·452	1·999	4·395	3·313	27·21°	0·06	−2·50
	3	0	0										
Kahn *et al.*[71]	1	↑0·2112	↓0·4888										
	2	↓0·06	↑0·06	0·700	−0·120	0·060	1·450	2·089	4·241	2·827	26·35°	4·01	−13·71
	3	↑0·03	↓0·03										
Miller and Haneman[83]	1	↑0·20	↓0·45										
	2	↓0·05	↑0·04	0·650	−0·09	0·06	1·51	2·080	4·453	3·245	28·51°	−1·22	−0·68
	3	↑0·02	↓0·04										
Meyer *et al.*[75]	1	↑0·144	↓0·506										
	2	↓0·06	↑0·06	0·650	−0·120	0·0	1·434	2·059	4·395	3·313	27·34°	0·08	0·25
	3	0·0	0·0										
Chadi[81]	1	↑0·186	↓0·459										
	2	↓0·06	↑0·07	0·645	−0·13	0·06	1·470	2·109	4·398	3·171	27·25°	−0·08	−2·87
	3	↑0·02	↓0·04										

III. OXYGEN CHEMISORPTION AND THE INITIAL STAGES OF OXIDATION

A. *Introductory Remarks*

Since the clean GaAs (110) surface is perhaps the best understood of all semiconductor surfaces, both experimentally and theoretically, it is also a natural choice for studies of oxygen chemisorption and the initial stages in the oxidation. Also, the problem of the interaction of oxygen with the GaAs (110) has attracted much attention in the past few years.[14-21,26,85-113] The high experimental reproducibility of the cleaved (110) surface has led to a fast advancement in understanding the oxygen interaction with this surface. However, a number of controversial issues remain. In this introductory section we will briefly summarize some of the current issues. We will then give some experimental details in the use of synchrotron radiation for photoemission studies[114-116] of core and valence levels since it has had a profound impact on the understanding of the interaction of oxygen (and metal) overlayers with the GaAs (110) surface (Section B). Section C deals with photoemission results for oxygen exposures in the very low coverage regime, well below 1 monolayer. Valence band studies in the monolayer coverage regime are then discussed (Section D). Core level studies and information from chemical shifts are treated in some length regarding the binding site of oxygen and the surface species formed during the initial oxidation (Sections E–G). Finally, the effect of oxygen exposure on the LEED pattern for the clean surface is described (Section H).

Two major questions for the interaction of oxygen with the GaAs (110) surface are: (1) Is the oxygen bonded to the Ga or the As surface atoms or does it form any other surface complex? (2) Does oxygen chemisorb molecularly or dissociatively? A series of photoemission experiments of the Ga and As 3d core levels addressed the first question. Core level data by Pianetta *et al.*[92] from these first studies showed a 2·9 eV chemically shifted As 3d peak that grows with increasing oxygen exposure and a 0·5 eV broadening in the FWHM of the Ga 3d level only near monolayer coverage. Preferential adsorption on the arsenic sites was therefore favored, with the broadening on the Ga 3d level as due to a secondary effect. On the other hand, energy loss experiments performed on sputter-annealed surfaces exposed to oxygen suggested the involvement of both the surface Ga and As in the chemisorption.[95] A model was then suggested where oxygen atoms bridge all surface Ga–As bonds and form a distorted (111) monolayer of $GaAsO_4$.[95]

The answers to the question on the nature of the adsorbed oxygen species have not been unambiguous either. Lindau *et al.*,[19] by comparing valence band spectra of surfaces subjected to high exposures of unexcited oxygen and surfaces subjected to low exposures of excited oxygen (see experimental section below), first suggested dissociative chemisorption. The same authors,[21] however, also noticed some correspondence between the oxygen-induced structure and the molecular orbital levels of oxygen molecules. More recent studies made with conventional X-ray sources of the O 1s core level by Brundle and Seybold[111] seem to have resolved this controversy in favor of dissociative chemisorption. Recent data by Su *et al.*[112] (see Section C) have provided new insight into the oxygen adsorption at very low exposures.

Results from theoretical investigations are also available.[96-99,113] Using the *ab initio* quantum chemical bond approach, Goddard *et al.*[99] found that atomic oxygen chemisorbed on As sites was the energetically favorable configuration. Tight-binding calculations by Mele and Joannopoulos[96-98] yielded the local density of states of the valence band for all four possible combinations: atomic or molecular oxygen on Ga or As. Also, by comparing with both the energy loss data and the photoemission data,[21] adsorption of molecular O_2 on surface As atoms was concluded.

Brundle and Seybold[111] and Chye *et al.*[110] have recently obtained consistent results regarding the existence of an asymmetrically broadened component on the high binding energy side of the Ga 3d level over the entire adsorption range up to monolayer coverage of oxygen. However, there is still disagreement about the rate of the oxygen uptake and the rates at which the shifted As 3d peak and the broadened Ga 3d component grow. Brundle and Seybold[111] reported the independent growth of the two components and thus favored a model of forming individual oxides of Ga_2O_3 and As_2O_3. Chye *et al.*,[110] however, found that the two components grow at nearly equal rates. The difficulty in interpreting chemical shift data for oxygen adsorption onto GaAs was further emphasized by the calculations by Barton *et al.*[113] who found that As–O bonding induced a chemical shift of 0·8 eV on the Ga 3d level. This would bring back the validity of the simple chemisorption model, discussed earlier, for reconsideration.

B. *Experimental Procedures*

In the following sections we will present a large body of photoemission results obtained by the use of synchrotron radiation at the Stanford Synchrotron Radiation Laboratory.[117] Therefore it may be appropriate to provide some experimental details at this point. For the core level studies in the photon energy region 35–600 eV, the synchrotron radiation is monochromatized by a grazing incidence monochromator (resolution typically 0·2 Å).[118] A schematic is shown in Fig. 10.[106] The monochromator consists of a main mirror which deflects the portion of the spectrum below 1 keV out of the main high-energy X-ray beam and focuses it onto the entrance slit of the monochromator.[118] There is a double focusing mirror after the exit slit of the

monochromator to focus the light onto the sample, which is positioned in the focal spot of a double-pass cylindrical mirror analyzer.

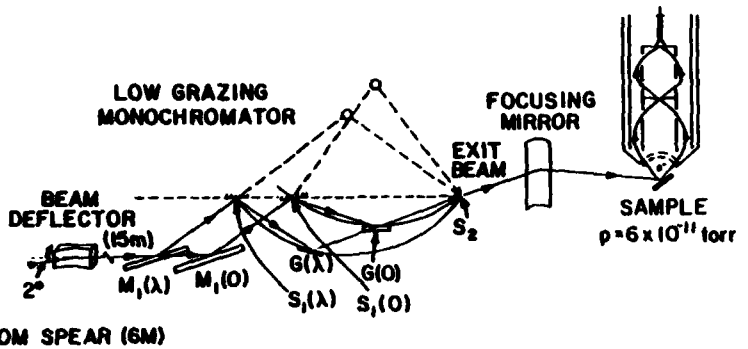

Fig. 10. Schematic of the 4° beam-line monochromator at SSRL showing the main mirror, the monochromator (M_1, $S_{1,2}$, G), the double focusing mixer, the sample, and the energy analyzer. (From ref. 106)

The experimental chamber consists of a stainless-steel ultrahigh-vacuum bell jar with a base pressure $< 1 \times 10^{-10}$ torr (Fig. 11).[106] The chamber contains the double-pass cylindrical mirror analyzer (Physical Electronics), a cleaver, and a sample manipulator capable of holding four samples for cleaving, one sample for heat cleaning ($T_{max} \sim 2000\,^{\circ}C$), and a substrate on which Au or Cu may be evaporated for Fermi-level (and thus binding energy) determinations. For this purpose, an evaporator containing copper and gold beads is also housed in the chamber. The photoemitted electrons are energy analyzed with a typical resolution of 0·2–0·3 eV. The photoemission spectra are recorded with a Tracor Northern signal averager or a PDP 11/34 computer.

Research grade oxygen is admitted into the vacuum system through a bakeable leak valve. For large exposures (pressures up to 750 mm O_2) an auxiliary pumping system is used to return the main chamber to below $\sim 10^{-8}$ torr.

For reasons given below, the gauges and methods to determine the oxygen exposures are described in some detail. Pressures between 10^{-11} and 10^{-5} torr were measured by a Redhead cold-cathode ionization gauge located in the main vacuum system.[92] This pressure range was used for exposures up to 10^4 L (1 L = 10^{-6} torr·s) where the exposure time was no longer than 10^3 s. A hot-filament ionization gauge with thoria-coated iridium filaments (Varian) was also located in the main vacuum system. This gauge was used initially to check the cold-cathode gauge and, more importantly, as a source of excited oxygen (see below) when used during a gas exposure. Pressures between 10^{-5}

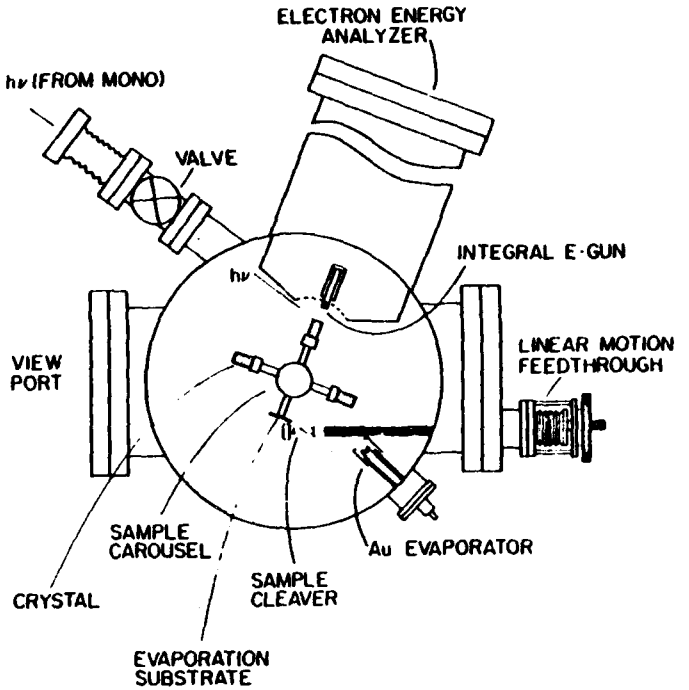

Fig. 11. Schematic of the photoemission spectrometer showing the energy analyzer, sample carousel, gold evaporator, light port, and sample cleaver. (From ref. 106)

and 0·6 torr were measured by a millitorr gauge (Varian) in the auxiliary pumping system. This pressure range gives exposures betweeen 10^4 and $\sim 10^9$ L. A thermocouple gauge (Hasting DV-4), also in the auxiliary pumping system, was used for pressures between 1 and 20 torr, giving exposures between 10^9 and 2×10^{10} L. For larger exposures up to 10^{12} L a mechanical-vacuum gauge (Wallace and Tiernen) was used, measuring pressures up to 800 torr.

The ion gauge and other hot filaments in the sample chamber have a profound effect on the chemisorption and oxidation process. This is probably due to creation of atomic oxygen or molecular oxygen in an excited state.[92] In our discussion we will use the terminology "exposure to excited oxygen" as opposed to "exposure to unexcited molecular oxygen". As will become apparent, it is extremely important to have the state of the used oxygen under control since the reactivity of excited oxygen is several orders of magnitude higher.

The exposures with excited oxygen are performed with the ion gauge in the main chamber turned on.[92] This gauge is out of line of sight of the sample so that the gas molecules must strike at least two surfaces before hitting the sample. However, for the larger exposures it is also possible that the oxygen is deflected to the sample through collisions with other gas molecules since the mean-free path of the molecules is between 1 and 10 cm for the pressures used in the ion-gauge exposures (10^{-3}–10^{-5} torr). Different ion-gauge emission currents are typically used in different exposure ranges, but the relative amount of excited oxygen is not known.

Another important experimental consideration is the choice of reference level (e.g. Fermi level) for the clean and oxygen-exposed surfaces. This point will be discussed in Section IV.A, where the interaction of metal overlayers with the GaAs (110) is presented.

C. *The Effects of Oxygen on the Valence Band Spectra: Low Exposure Regime*

For GaAs (110) surfaces cleaved *in situ* and exposed to unexcited molecular oxygen, there are two qualitatively different exposure regimes: below 10^5 L there is no detectable effect on either the As 3d or the Ga 3d peaks, but the Fermi level is close to fully stabilized (see Section II.B); above 10^7 L exposure there are observable core level shifts on both the Ga 3d and the As 3d levels (see Section E). In this section we will concentrate on the changes observed in the valence band spectra for oxygen exposures in the range 10^5–10^7 L.

The top two curves in Fig. 12 show the photoemission spectra from a clean p-GaAs (110) surface and from the same surface exposed to 10^6 L of oxygen.[112] The Ga 3d level (not shown here) in the 10^6 L spectrum showed no detectable broadening, but there is oxygen-induced structure visible in the valence band region. A comparison with the difference spectrum clearly indicates the existence of four peaks at binding energies $4{\cdot}6 \pm 0{\cdot}2$, $5{\cdot}8 \pm 0{\cdot}2$, $7{\cdot}8 \pm 0{\cdot}2$, and $10{\cdot}4 \pm 0{\cdot}2$ eV. The dip and minimum in the leading part of the difference spectrum may be due to the removal of surface states, as observed by Knapp and Lapeyre[31] in angle-resolved photoemission studies.

The four oxygen-induced peaks can be divided into two groups according to their different rates of growth under increasing oxygen exposures. In Fig. 13 we show the difference spectra of a n-type GaAs (110) surface that undergoes a series of oxygen exposures from 10^5 to 10^7 L. One thing immediately apparent in Fig. 13 is the fast outgrowth of peak 1 over peak 4 in going from 10^5 to 10^7 L. The absolute strength of peak 4 stayed approximately constant with increasing exposures. This is evidenced by the disappearance of intensity at the energy position of peak 4 in the bottom curve of Fig. 13 where we have subtracted the 10^6 L spectrum from the 10^7 L spectrum. Thus, for unexcited oxygen adsorbed on GaAs (110) surfaces, there indeed exist at least two

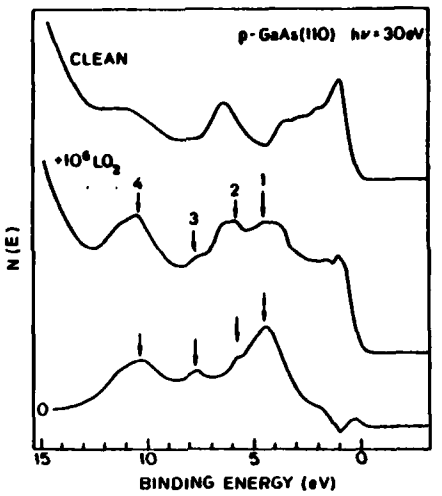

Fig. 12. Photoemission spectra of a clean GaAs (110) surface (top curve) and the same surface exposed to 10^6 L oxygen (center curve), taken at a photon energy of 30 eV. The bottom curve is their difference. (From ref. 112)

different states of oxygen on the GaAs (110) surface, one associated with peak 1 and the other associated with peak 4. In parallel with the work by Ranke and Jacobi[119] the fast growing state is designated β-oxygen and the other state α-oxygen.

The assignments of peaks 2 and 3 are further considered below. The break of slope due to peak 2 on the high binding energy side of peak 1, which is visible at low coverages, becomes overshadowed by the strong emission from peak 1 at higher coverages. This indicates that peak 2 grows at a much lower rate than peak 1 does. There is a barely visible shoulder at the energy position for peak 2 in the 10^7 L difference spectrum, but it disappears in the difference curve between the EDCs of 10^7 and 10^6 L. Thus, although less certain than peak 4, peak 2 can also be assigned as due to α-oxygen. Peak 3 and the energy positions marked by the dashed arrows labeled 3a and 3b should be considered together. We observe the following:

(1) In the 10^6 L curve there are dips at 3a and 3b, while peak 3 has already shown strength comparable to that of peak 4.

(2) In the 10^7 L curve peak 3 *does not* outgrow peak 4 as would be expected if it is associated with peak 1. We also notice that regions under 3a and 3b become filled. This filling could be considered as due to the tail of peak 1 alone before we examine the difference curve between 10^7 and 10^6 L.

(3) In the difference curve between 10^7 and 10^6 L position 3 exhibits a dip compared with the 10^7 L curve. On the other hand, with this dip and the removal of peak 2, emissions are still seen under 3a and 3b; hence they must be features grown together with peak 1. We can therefore, with the same degree of certainty as the assignment for peak 2, separate peak 3 and assign it to α-oxygen, while 3a and 3b are assigned to β-oxygen.

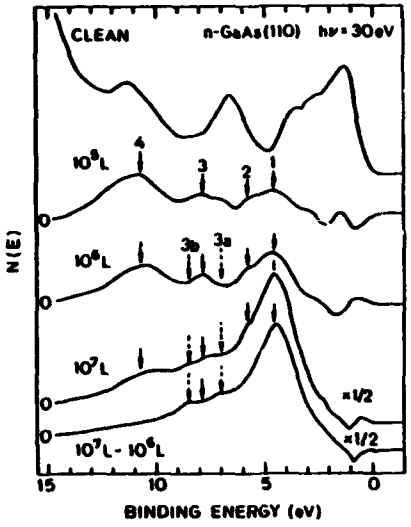

Fig. 13. Photoemission spectrum of a clean GaAs (110) surface and difference spectra of this surface subjected to increased oxygen exposures. The bottom curve is the difference between the spectra for surfaces exposed to 10^7 and 10^6 L of oxygen. Peaks 2, 3, and 4 are associated with α-oxygen, peaks 1, 3a, and 3b with β-oxygen. (From ref. 112)

A few general remarks can be made for α-oxygen before examining the details. The intensity of α-oxygen at 10^7 L is estimated to be 10% of that due to β-oxygen. The oxygen coverage was estimated to be 0·05 monolayer for a surface exposed to 10^7 L oxygen.[20] Thus, the saturation coverage of α-oxygen is approximately 0·005 monolayer. This low coverage, however, is enough to produce surface Fermi-level pinning if one state in the band gap is generated by every adsorbed species. Thus, the observed Fermi-level stabilization around 10^5 L oxygen exposure[21] is consistent with α-oxygen being responsible for the Fermi-level pinning. The Fermi-level pinning may also be correlated with the removal of surface states mentioned earlier, but a detailed study of the behavior of the surface states upon oxygen adsorption still remains to be done. The low saturation coverage also suggests that the adsorption of α-oxygen may be at defect sites.

The bonding of α-oxygen to Ga sites can be suggested from a fingerprinting approach. The center curve in Fig. 14 is obtained by deconvolution of the 10^6 L O_2 + p-GaAs difference curve shown in Fig. 12 into α-oxygen and β-oxygen. The emissions under 3a and 3b are neglected in the deconvolution. The top curve in Fig. 14 is obtained from oxidation of a vacuum deposited Ga metal film in the same experimental setup used for the study of oxidation of GaAs. The Ga 3d level of this film, not shown here, exhibited a clearly resolved 1·6 eV chemical shift which is appropriate for the formation of Ga_2O_3.[120] The three resonance-like structures occurring at binding energies 5·5 ± 0·2, 7·3 ± 0·2, and 10·0 ± 0·2 eV[121] line up almost perfectly with the three peaks of the α-oxygen if a rigid shift of 0·3 eV toward high binding energy is made. The difference in the absolute values of binding energy may be due to difficulties in determining the positions of valence band maxima and/or due to different relaxation shifts on different surfaces. Even the small break in slope on the high binding energy side of peak 4 can be found in the corresponding peak in the spectrum for oxidized Ga. The difference in the weight of the leading peak may be that between small isolated molecules and bulk oxides.

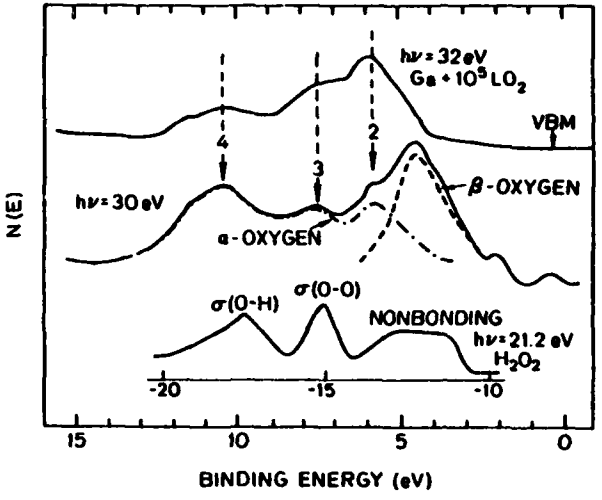

Fig. 14. The top curve shows a photoemission spectrum of oxidized Ga metal. The solid line in the center curve is from a GaAs + 10^6 L O_2 spectrum (reproduced from Fig. 12) deconvoluted into α-oxygen and β-oxygen. The bottom curve is a gas phase spectrum of H_2O_2 from Ref. 122. (From ref. 112)

There is thus strong evidence that α-oxygen is bonded to Ga. If there are defect sites with broken Ga–As bonds the Ga atoms are expected to be more active than As, as was found for sputter damaged surfaces.[110, 111] The

possibility of α-oxygen being adsorbed non-dissociatively cannot be ruled out. To this end it is interesting to note the resemblance between the spectrum of α-oxygen and that of gas phase H_2O_2 (see Fig. 14).[119,122]

The theoretical results of Mele and Joannopoulos[96-98] should be mentioned here. The signature for molecular oxygen adsorbed on GaAs (110) is three peaks at binding energies of 4, 8, and 10 eV in the local density of states of oxygen. These peaks are insensitive to the adsorption site and should thus also be a good approximation for defect sites. Except for the 4 eV peak (which may be obscured by the β-state) there is thus fairly good agreement between the experimental α-oxygen state and the calculation by Mele and Joannopoulos.[96-98] However, this assignment should still be considered very tentative. X-ray photoemission studies of the O 1s core line, as were done by Brundle and Seybold[111] for higher oxygen coverages, should be very valuable for the low exposure regime to distinguish between atomic and molecular oxygen (see Section E).

The identification of the binding form of β-oxygen is not straightforward. It is responsible for the 2·9 eV chemically shifted As 3d peak and the asymmetric broadening of the Ga 3d core level (see Section E). The bottom curve of Fig. 13 should be a good representation for β-oxygen on GaAs. It has very little resemblance to the valence band emission for Ga_2O_3 (Fig. 14). Thus the present valence band spectra do not support the presence of Ga_2O_3 and that β-oxygen is a mixture of Ga_2O_3 and As_2O_3 when the exposure is increased beyond 10^7 L. Instead the simple chemisorption picture or the surface oxide model (see Section A) with only one bonding configuration for oxygen seem more likely. This will be discussed further in Sections E and F.

At present it can only be speculated if the α-oxygen forms stable bonds at defect Ga sites or if it is a precursor state of β-oxygen. The relations between α- and β-oxygen and the adsorption mechanism should be the subject of further studies.

D. The Effects of Oxygen on the Valence Band Spectra: Monolayer Coverage

In Fig. 15 we represent photoemission curves for the valence band over a larger oxygen exposure range (up to 10^9) than in the preceding section.[21] There is little change in the valence band structure up to exposures of about 10^5 L, but between 10^5 and 10^6 L there is an abrupt change and the sharp features at the top of the valence band are replaced by a structureless ramp. The exact oxygen exposure where this change takes place can vary within one order of magnitude, dependent on the cleavage quality, but it is always abrupt. The oxygen uptake also changes abruptly from typically a few per cent coverage at 10^6–10^7 L exposure to 25% at 10^7–10^8 L. The coverage versus oxygen exposure[17] for a typical case is shown in Fig. 16.

As we mentioned earlier, the oxygen uptake is much faster for exposure to excited oxygen. This is illustrated in Fig. 17 where the results are shown for exposure to molecular oxygen (solid line) and excited oxygen (dashed line).

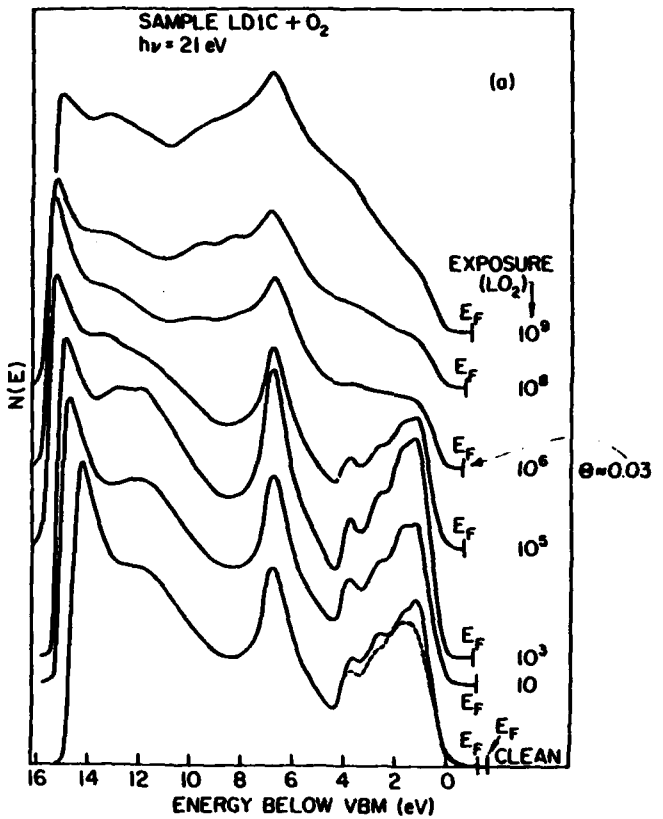

Fig. 15. The change in the valence band spectra for oxygen exposures up to 10^9 L. The spectra were recorded at a photon energy of 21 eV. (From ref. 21)

The dashed curve for 10^5 L O_2 closely resembles the solid curve for 10^7 L O_2, thus reflecting two orders of magnitude difference in the oxygen uptake.[19] This difference can be smaller or larger, depending on the amount of excited oxygen present during exposure. Thus extreme care has to be exercised when oxygen uptake and sticking coefficients are determined for the cleaved GaAs (110) surface.

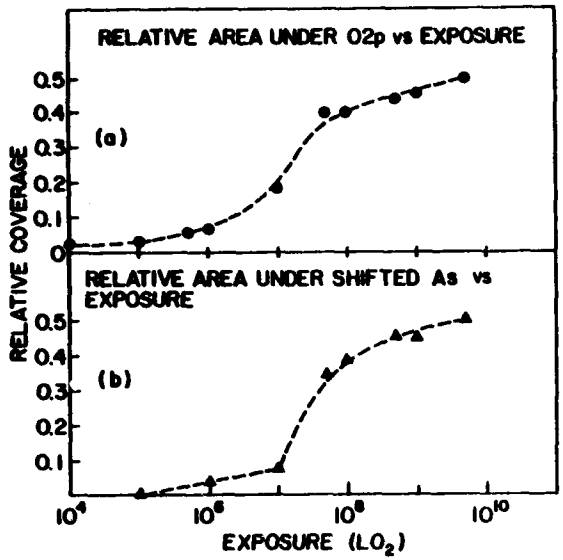

Fig. 16. The coverage of oxygen versus exposure measured by two different methods. Note the abrupt change near 10^6–10^7 L exposure. The saturation coverage is taken to be half a monolayer. (From ref. 17)

E. Core Level Studies of Oxygen Adsorption and Oxidation

In Fig. 18 we show spectra for the clean and oxidized GaAs (110) surface at $h\nu = 100$ eV.[92] The exposures were made with unexcited oxygen. As we expose the surface to oxygen we see a single peak ($E_B = 43{\cdot}7$ eV) growing 2·9 eV below the GaAs As 3d peak ($E_B = 40{\cdot}8$ eV) with a proportionate decrease in the GaAs As 3d intensity. Concurrent with the appearance of the shifted arsenic peak we see the O 2p resonance level at a binding energy of about 5 eV. As we go to higher exposures the shifted As 3d peak and O 2p level grow simultaneously until saturation is reached between 10^9 and 10^{12} L O_2. The Ga 3d peak undergoes a broadening of about 0·5 volt. The oxygen coverage as a function of exposure is shown in Fig. 16.

As a comparison we show the results for the oxidation of GaSb (110) in Fig. 19 for $h\nu = 100$ eV. As in the case of GaAs, all the spectral features of interest can be obtained at the same photon energy and in one spectrum, thus facilitating comparisons.[19] The valence band extends approximately 12 eV below the valence band maximum. The Ga 3d level is at a binding energy of 19·4 eV; the Sb 4d doublet is at 32·1 eV ($4d_{5/2}$) and 33·2 eV ($4d_{3/2}$). We are able to see clearly the spin-orbit splitting in the Sb 4d levels. As we oxidize the

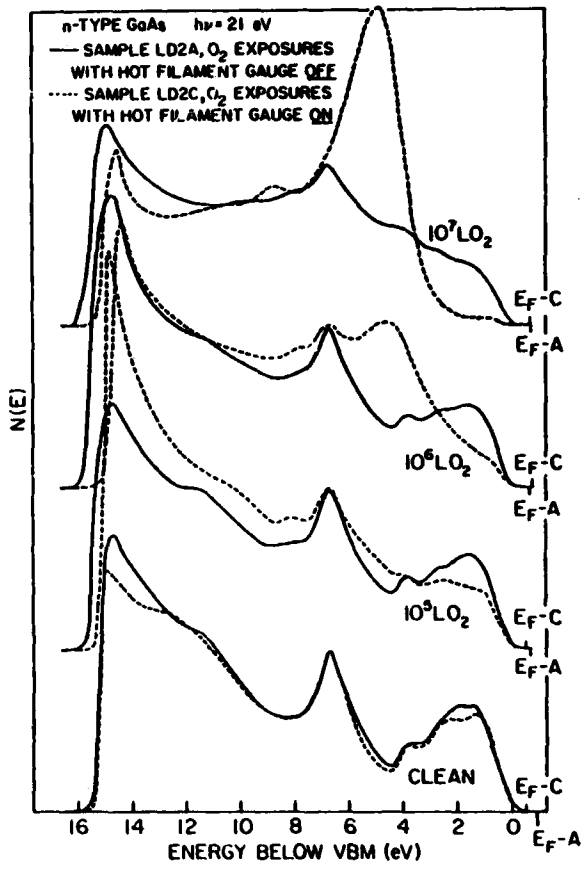

Fig. 17. Photoemission spectra of the valence band of GaAs (110) surfaces exposed to unexcited molecular (solid line) and excited (dashed line) oxygen. Note the rapid growth of the O 2p level for exposure to excited oxygen. (From ref. 19)

GaSb surface we start to see changes in the spectra at about 5×10^5 L O_2. This is about a factor of 2 sooner than with the GaAs. But, more importantly, as we increase the exposure to 5×10^7 L O_2 we start to see a definite broadening of the Ga 3d level toward higher-binding energy. In fact, even by 5×10^8 L O_2 a definite shifted Ga 3d peak is seen ($\Delta E_B = 1{\cdot}1$ eV). Of course, the shifted Sb 4d ($\Delta E_B = 2{\cdot}5$ eV) level has also been growing at the expense of the unshifted level. The shifted peaks for both Sb and Ga completely dominate the unshifted peaks for exposures above 5×10^9 L O_2 and indicate that surface oxides of Ga

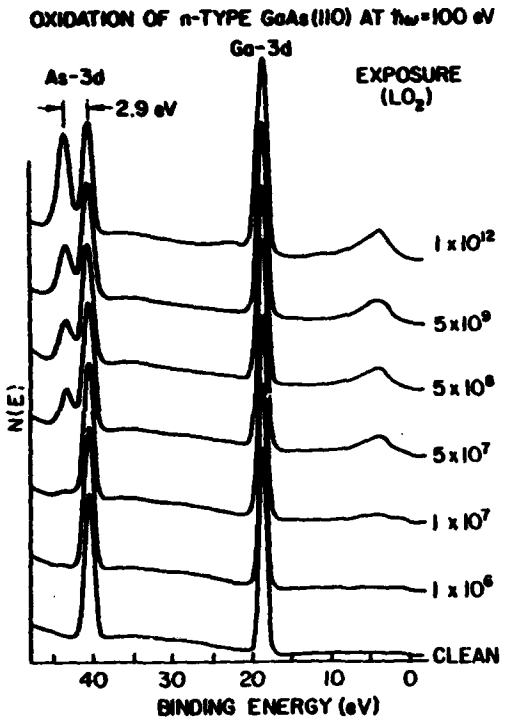

Fig. 18. Photoemission spectra of clean and oxygen exposed GaAs (110), taken at a photon energy of 100 eV. (From ref. 92)

and Sb are now formed. The results for GaSb are thus much easier to understand than those for GaAs.

In Fig. 20 we show the results for GaAs (110) exposed to excited oxygen. The oxygen adsorption is about 10^3 faster and, in addition, there are important differences in the core level data.[92] At an exposure of 5×10^5 L excited oxygen the first shifted peak ($\Delta E_B = 2{\cdot}9$ eV) stops growing and a second shifted peak with a binding energy shift of 4·5 eV starts to grow and soon dominates the first shifted peak. But what is even more striking is that the gallium peak starts to broaden also at 5×10^5 L excited oxygen. At higher exposures we can see that the initial broadening at 5×10^5 L excited oxygen is due to a shifted gallium peak ($\Delta E_B = 1{\cdot}0$ eV) which grows concurrently with the second shifted arsenic peak. This simultaneous growth is very much like what was seen for the oxidation of GaSb in Fig. 19. We also see in these spectra the O 2s at 24 eV and the O 2p at 5 eV below the valence band maximum.

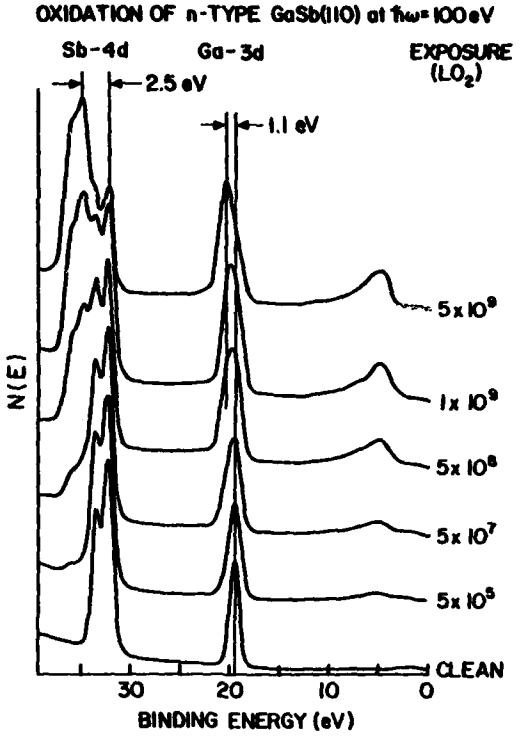

Fig. 19. Photoemission spectra of clean and oxygen exposed GaSb (110), taken at a photon energy of 100 eV. (From ref. 92)

In Fig. 21 we give examples of the effects of very large doses of excited oxygen on the GaAs (110) surface. The top two curves are spectra for clean GaAs (110) and for the clean surface plus 10^{12} L O_2. The spectrum labeled "heavily oxidized" was obtained by exposing the surface, which had previously been exposed to 10^{12} L O_2, to 5×10^5 L excited oxygen. Note that the binding energies of the peaks in this spectrum are the same as those of Fig. 20. There are two oxidation states of As, and there is a shifted gallium peak. The fourth spectrum of Fig. 21 labeled "very heavily oxidized" was obtained by exposing clean GaAs (110) to 5×10^5 L excited oxygen with the emission current of the ionization gauge (IG) set at 4·0 mA (giving a significantly larger amount of excited oxygen than in the previous case). In this case we see no unshifted gallium peak, only the shifted one. There is no unshifted arsenic peak, but there are two other peaks shifted 0·4 and 3·2 eV with respect to the unshifted peak (if it were present). Note the drastic decrease in emission from the arsenic derived

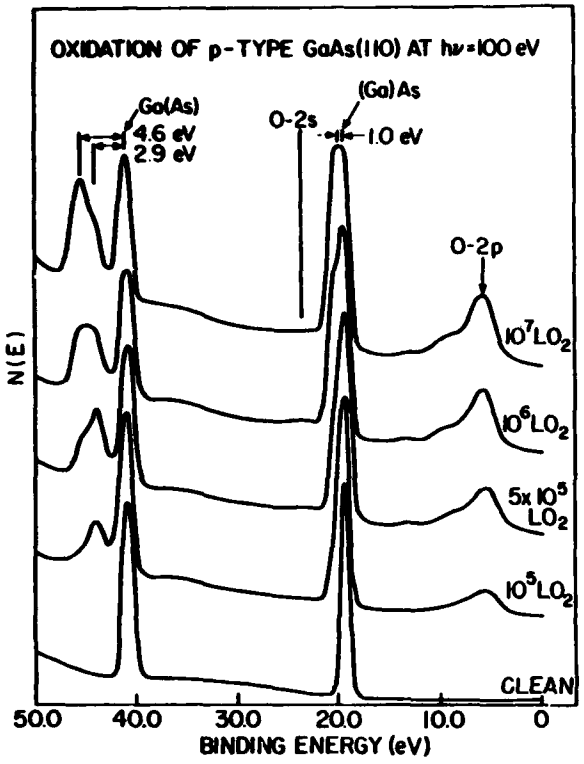

Fig. 20. Photoemission spectra of GaAs (110) exposed to excited oxygen. (From ref. 92)

levels and that the emission from the O 2p and O 2s levels has gone down with respect to that in the second and third spectra.

Pianetta *et al.*[92] performed a ligand shift analysis in trying to understand the chemical shifts observed for the Ga 3d and As 3d core levels. In Table II are presented binding energy shifts for the Ga and As 3d levels in the compounds that will be used as standards in this analysis. These values are taken from the literature, and rather than give absolute binding energies we choose instead to give the binding-energy differences between the levels in the various compounds. This, in effect, avoids many of the problems in choosing an appropriate reference level when comparing the results from several sources. Through the work of Bahl *et al.* [123] we were able to determine the 3d level binding energy shifts for As_2O_5 and As_2O_3 with respect to As. We then calculated the difference between the Ga and As 3d levels of As_2O_3, Ga_2O_3,

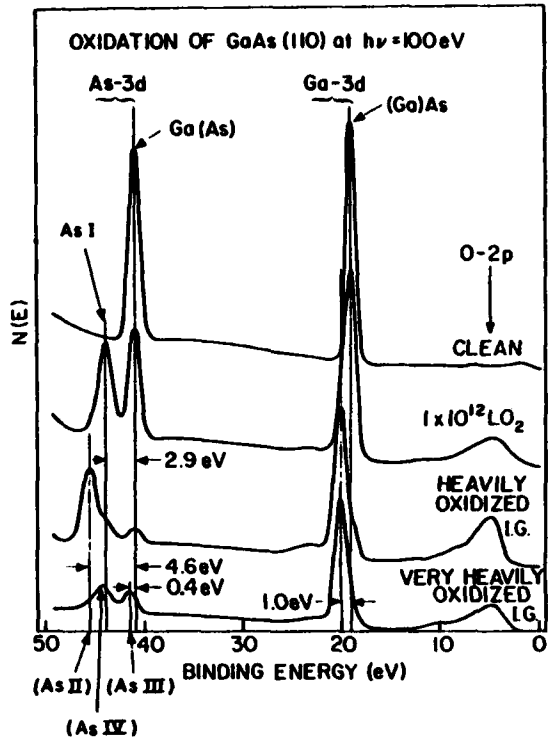

Fig. 21. Photoemission spectra of clean GaAs (110), and GaAs + 10^{12} L of unexcited molecular oxygen and increasing exposures of excited oxygen (heavily oxidized and very heavily oxidized). (From ref. 92)

GaAs, and Ga by referring to the work of Leonhardt *et al.*[124] The Ga_2O_3–Ga shift was found to agree with Schön's measurements to within 0·1 eV.[120]

The ligand shifts for the standard compounds may be calculated from the chemical shifts given in Table II. This is done in Table III, in the first column of which we list the compounds. In the second column we list the shifts of the As or Ga 3d levels in these compounds with respect to their binding energy for the free element. A positive chemical shift is defined as a shift to higher binding energy. Columns four and five give the number and type of ligand for the compounds in the first column. In GaAs each gallium (or arsenic) has four arsenic (or gallium) ligands. As_2O_3 has three oxygen single bonds per arsenic atom. Ga_2O_3 is coordinated by six oxygens. As_2O_5 has three oxygen single bonds and one oxygen double bond per arsenic. $GaAsO_4$ has a quartz-like

structure[128] with the silicon atoms replaced by alternating Ga and As. This results in each gallium and arsenic having four oxygen ligands.

TABLE II

Experimental Binding Energy Differences (eV), from the References Cited, between the Shifted and Unshifted Ga and As 3d Levels for Various Compounds of Ga and As (From ref. 92)

ΔE_B(eV)	As_2O_3[a]	As(GaAs)[b]	As[c]	Ga_2O_3[d]	Ga(GaAs)[e]	Ga[f]
As_2O_5	1·7	4·9	4·3	25·7	26·6	27·0
As_2O_3		3·2	2·6	24·0	24·9	26·0
As(GaAs)[g]			−0·6	20·8	21·7	22·8
As				21·4	22·3	23·4
Ga_2O_3					0·9	2·0
Ga(GaAs)						1·1

[a] Refs 123 and 124. [b] Refs 123, 125, 126, and 127. [c] Refs 123 and 124. [d] Refs 120, 124, and 125. [e] Refs 124, 125, and 127. [f] Refs 120 and 124. [g] See text for the discussion about reliably determining the shifts between the semiconductor compounds and the other compounds in this table.

TABLE III

Experimental Ligand Shifts of the Ga and As 3d Levels for the Compounds whose Shifts were given in Table II (From ref. 92)

Compound	ΔE_s(eV)[a]	ΔE_j(eV)[b]	n_j[c]	Ligand
As_2O_5	4·3	0·87	3	–O
		1·7	1	=O
As_2O_3	2·6	0·87	3	–O
As(GaAs)	−0·6	−0·15	4	–Ga
Ga_2O_3	2·0	0·33	6	–O
Ga(GaAs)	1·1	0·28	4	–As
As($GaAsO_4$)[d]	3·5	0·87	4	–O
Ga($GaAsO_4$)[d]	1·3	0·33	4	–O

[a] ΔE_s is the binding energy shift with respect to the free element.
[b] ΔE_j is the ligand shift referenced to the free element, where $\Delta E_s = n_j \Delta E_j$, summed over all j.
[c] n_j is the number of ligands of the given kind.
[d] These are not experimentally determined shifts; they are calculated for the ideal structures using the ligand shifts given in the rest of the table.

The ligand shifts ΔE_j are the shifts due to the particular ligand j and are obtained most simply by dividing the total shift (column two) by the number of ligands (column four). When there are two types of ligand in the compound in question, such as As_2O_5 which has three —O and one =O, we use another compound, As_2O_3 in this case, to determine one set of the shifts and then we solve for the second. In the last two rows of Table III we have calculated the shifts that we would expect from $GaAsO_4$.

As mentioned in the above discussion, when the GaAs (110) surface is exposed to unexcited oxygen only one shifted arsenic peak, As I, is seen for all coverages. This may imply that only a single site is involved in the chemisorption of unexcited oxygen. Thus, Pianetta *et al.*[92] concluded that the As I peak, with a shift of 2·9 eV with respect to GaAs (2·3 eV with respect to elemental As), is due to one oxygen atom or molecule bonded to a surface arsenic atom. The shift of the As I peak is much larger than the shift due either to a single As–O bond (ΔE_B = 0·87 eV with respect to GaAs) or to an oxygen–arsenic double bond (ΔE_B = 1·7 eV with respect to GaAs). In fact, the experimentally determined shift of 2·9 eV is closer to the shift expected from three oxygens singly bonded to each surface arsenic atom, necessitating the breaking of back bonds. However, this latter situation implies that three, not one, chemically shifted As 3d peaks (ΔE_B with respect to GaAs ~ −0·87, −2·04, and −3·06 eV) should be observed corresponding to the three possible oxidation states which the surface arsenic atoms would then have. We would expect to see the −0·87 and −2·04 eV peaks for low and intermediate coverages and the −3·06 eV peak almost exclusively for the high coverages. This is clearly not what we observe experimentally but, because of the high surface sensitivity of our measurement, we should have been able to see such intermediate states. Therefore, Pianetta *et al.*[92] concluded that the As I peak is due to a single arsenic–oxygen bond that gives a binding-energy shift three times larger than that expected from an As–O bond in an arsenic oxide. In the case of As_2O_3 the oxygens are more electronegative than the arsenic, so there is an equal transfer of charge away from the arsenic along each ligand. In the case of oxygen chemisorbed to the GaAs surface, the gallium back bonds transfer charge to the arsenic so the oxygen is the only ligand in which there is charge transfer away from the arsenic. That is, the single oxygen ligand does not have any competition for the charge on the arsenic. Consequently the oxygen ligand in this case could give a much larger shift than would be predicted by a simple ligand-shift analysis where the different electronegativities of the various ligands have not been taken into account. These same arguments, now used to estimate the shift of the Ga 3d due to a chemisorbed oxygen, would imply that the shift should be less than 0·33 eV (the ligand shift due to a single oxygen ligand in Ga_2O_3). Consequently we would not expect to see a distinct chemically shifted peak for the case of oxygen chemisorption on the surface gallium atoms. We would, however, expect to see an asymmetric broadening of the Ga 3d level. Bonding of oxygen to the surface gallium atoms by breaking back bonds should give an asymmetric broadening of the Ga 3d level along

with intermediate oxidation states of the arsenic atoms, which is not observed experimentally.

The As II peak in the "heavily oxidized" curve of Fig. 21 is shifted 4·6 eV with respect to the arsenic in GaAs (or 4·0 eV with respect to elemental As). This value is bracketed by the experimentally determined value of 4·9 eV (4·3 eV with respect to elemental As) for As_2O_3 and the calculated value of 4·1 eV (3·5 eV with respect to elemental As) for $GaAsO_4$. The average of these two shifts gives 4·5 eV (3·9 eV with respect to elemental As), very close to the value measured in this work. This seemingly fortuitous result may be interpreted within a ligand shift analysis as follows. There are three single bonds and one double bond in As_2O_3, whereas $GaAsO_4$ contains four single bonds. The fact that the shift we measure lies between these two shifts is significant because, first, it indicates that there are four oxygens bound to the As and, secondly, these bonds must have some double-bond character. In the rest of the discussion we will simply refer to this compound as As_2O_5. As mentioned above with reference to Fig. 20, the gallium peak clearly starts to shift as soon as the As II peak appears. The magnitude of the gallium shift is 1 eV, which corresponds to Ga_2O_3. The fact that we start forming oxides of Ga and As at the same time clearly indicates that back bonds are being broken and true oxidation of the surface is occurring.

In the "very heavily oxidized" spectrum of Fig. 21 the gallium peak, Ga I, is still shifted by 1 eV, indicating the presence of bulk Ga_2O_3. But, now, the peak labeled As III is shifted 0·4 eV with respect to the unshifted arsenic peak, As(GaAs). The shift we expect between free arsenic and arsenic in GaAs is 0·6 eV. Thus, this peak could be due to free As or, equally likely, arsenic bound to only one gallium atom [see the Ga ligand shifts in Table III for As(GaAs)]. The latter case would give a shift of about 0·4 eV. Therefore it is likely that this peak is due to either free arsenic or arsenic bound to, at most, one gallium atom. The second arsenic peak in this spectrum, labeled As IV, is shifted 2·6 eV with respect to the As in GaAs. This is exactly the same as the shift observed for bulk As_2O_3 (Table II).

F. Detailed Analysis of the Oxygen Induced Broadening of the Ga 3d Level

We will now return briefly to a more detailed discussion of the observed broadening of the Ga 3d level during exposure to unexcited molecular oxygen.[110] The broadening is displayed in Fig. 22 for exposures between 10^6 and 10^{13} L. The set of Ga 3d levels at various oxygen exposures are normalized to the same peak height (Fig. 22). These are aligned by referencing to the unshifted As 3d with the assumption that BE(As) − BE(Ga) of the unshifted levels remains constant with surface treatment. One notices that with increasing oxygen exposure there is asymmetrical broadening of the line, with a significant amount of broadening to the higher BE side. The amount of broadening may be estimated by deconvolution of the Ga level. Our procedure was to fit the asymmetrical peak with three skewed Gaussian components, one unshifted (which retains the same BE relative to the As 3d as on the clean surface) and two shifted (towards higher and lower BE). We have also tried to fit the Ga 3d using two components, one "unshifted" and one shifted towards higher BE. In this case, however, the position of the "unshifted" component is also permitted to vary in the curve-fitting procedure. The *total* amount of shifted Ga (expressed as percentage of total Ga 3d emission) is roughly the same in the two procedures.

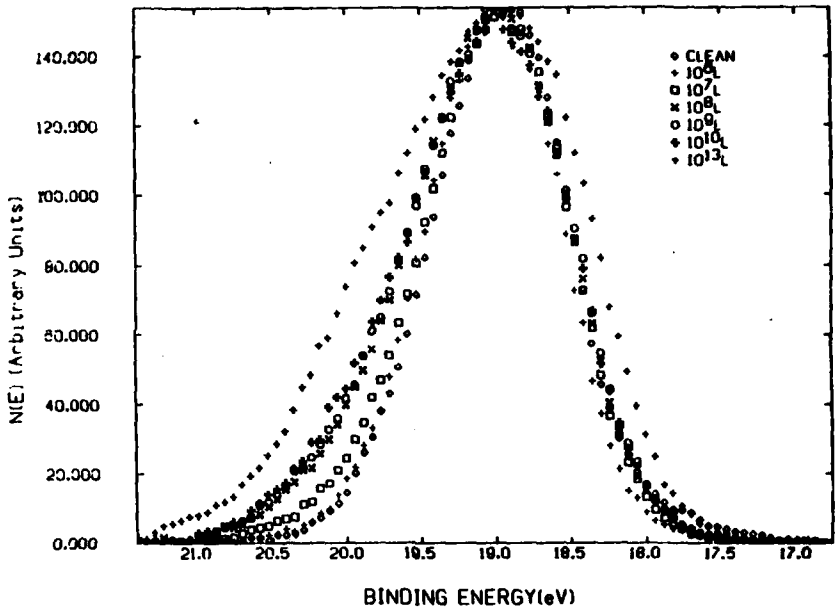

Fig. 22. Detailed display of the Ga 3d core level for GaAs (110) exposed to unexcited molecular oxygen (photon energy = 100 eV) between 10^6 and 10^{13} L. (From ref. 110)

Table IV lists the results of the deconvolution using three components. The amount of shifted As is shown as a percentage of the total As 3d emission (the area under the shifted and unshifted peaks). Also listed is the amount of shifted Ga 3d, expressed as a percentage of the total Ga 3d emission. From this table we observe the following.

(1) For all exposures on the ordered surface with unexcited oxygen the percentage of the total shifted Ga 3d is roughly the same as the As 3d.

(2) For the sputtered surface there is a large shifted Ga 3d component even at 10^9 L (about the same as for 10^{12} L of unexcited oxygen on an ordered surface), but the shifted As 3d is much less than on the unsputtered surface at the same exposure.

The present data show unambiguously that a component shifted (by ~0·9 eV) towards higher BE is present in the Ga 3d when GaAs is exposed to oxygen. However, the nature of this shifted component is not clear. While it is located near the position of Ga 3d in Ga_2O_3, suggesting that Ga_2O_3 or a Ga suboxide is formed, recent calculations by Barton *et al.*[113] show that the expected Ga chemical shift for oxygen chemisorbed on the As is 0·8 eV, so it is possible that oxygen is chemisorbed on the surface As only, with the surface Ga atoms not directly involved. The observed percentage of shifted As 3d is roughly the same as the percentage of shifted Ga at all coverages if the initial surface is undamaged and unexcited oxygen is used. In a chemisorption-on-As picture, each surface As atom (with chemisorbed oxygen) is bonded to three equivalent Ga atoms for very low coverages, much less than 1 monolayer. The percentage of shifted Ga should thus be much larger than the percentage of shifted As unless there is a nucleation mechanism so that the chemisorption occurs in patches. A more definitive test of the simple chemisorption on the As model is to obtain the relative amounts of oxygen and shifted As from the emission intensity of oxygen and As levels after correction for the cross-sections. For simple chemisorption of atomic oxygen on As only, there should be one oxygen for every shifted As. From XPS data Brundle and Seybold[111] estimated the amount of oxygen relative to the shifted As on GaAs (110) exposed to unexcited oxygen and obtained values close to three O for each shifted As. They suggest formation of Ga_2O_3 and As_2O_3. Su *et al*[112] have also made a preliminary estimate of the oxygen/shifted As ratio and obtained values between 3 and 4. If these estimates are correct, simple chemisorption on

TABLE IV

Shift of Surface As and Ga with Oxygen Exposure (From ref. 110)

Treatment	Shifted As (%)	Shifted Ga (%)
10^7 L O_2	9	12
10^8 L O_2	23	22
10^9 L O_2	27	26
10^{10} L O_2	34	28
10^{13} L O_2	52	47
Sputtered surface + 10^9 L O_2	11	48

the surface As alone is not likely. One then would have to invoke bonding to the Ga atoms as well. Possibilities are Ga_2O_3 and As_2O_3, suggested by Brundle and Seybold,[111] although it is difficult to see how these would passivate the surface. Other arguments against this model were given in Section C. Another possibility is $GaAsO_4$. As discussed in Section A, Ludeke[95] has put forward a model suggesting formation of a distorted (111) layer of $GaAsO_4$ which apparently explains the surface passivation and disordering. His model predicts 1·5 monolayers of oxygen at saturation or 3 oxygens per shifted As. The present data are not inconsistent with his model, although he predicted only a 0·2 eV chemical shift on the Ga (compared with the 0·9 eV observed experimentally in our data). However, since Barton *et al.*[113] predict a 0·8 eV shift on the Ga even without direct bonding to the Ga, it is likely that the prediction of the 0·2 eV shift by Ludeke[95] is on the low side.

Once the GaAs (110) surface is disordered by sputtering, the percentage of shifted Ga with oxygen exposure is increased substantially. The opposite is true for the As (see Table IV) although, on an ordered surface, the amount of shifted As with oxygen exposure is about equal to the amount of shifted Ga. This suggests that the As atoms are able to compete strongly for oxygen on an ordered (110) surface because of the structural and electronic rearrangement which places the dangling bond electrons on the As.[3] From the quantitative data in the preceding paragraph it is likely that oxygen bonds to the Ga as well. Thus it appears that bonding of oxygen to the As may perturb the surface sufficiently to promote bonding to Ga sites. On the other hand, once the surface is disordered by sputtering (or has defects produced in other ways) there is much more oxygen bonding to Ga than to As. The arguments based on bulk thermodynamics, namely that Ga oxides form more readily than As oxides, can now be applied.

Mark *et al.*[22,78,129] have suggested that the oxidation of GaAs (110) starts on residual defect sites and produces additional disorder owing to the release of exothermic energy. Thus, as the oxidation progresses, the entire surface becomes disordered. However, the core level results by Chye *et al.*[110] for slightly sputtered surfaces, i.e. surfaces with the right stoichiometry but presumably high disorder, show preferential oxygen adsorption on the Ga sites, whereas the model by Mark *et al.*[22,78,129] would predict roughly equal percentages of shifted As and shifted Ga.

G. The Escape Depth of Photoemitted Electrons

The relative escape depth[130] for electrons with kinetic energies between 20 and 200 eV may be determined from our experimental results on oxygen chemisorption quite simply and elegantly by merely plotting the ratio of the areas under the shifted and unshifted arsenic peaks as a function of photon energy.[92] This curve is given in Fig. 23. The horizontal scale gives the kinetic

energies of the electrons in the crystal. The photon energies that were used for each point are obtained by adding 40 eV (the approximate As 3d binding energy) to the given kinetic energies. The vertical scale on the right gives the actual ratio of the areas of the unshifted to shifted As 3d peaks as measured from the spectra of GaAs(110) + 10^{12} L O_2 (in Fig. 18) for various photon energies. The minimum in the escape depth curve occurs around 60 eV kinetic energy ($h\nu$ = 100 eV) and again demonstrates the extreme surface sensitivity of the photoemission technique in this electron energy region. The error bars associated with the points are due to the uncertainties in measuring the areas under the peaks. The determination of the absolute scale for the escape depth and the source of the error bars are discussed in detail elsewhere.[92]

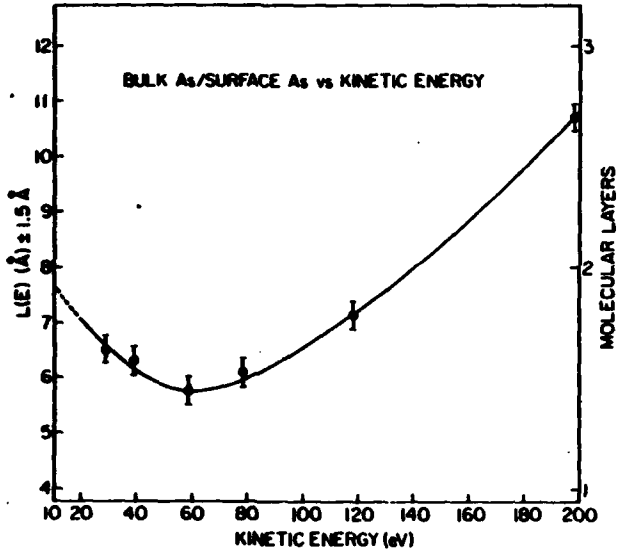

Fig. 23. Plot of the ratio of the unshifted to shifted As 3d levels as a function of electron kinetic energy for the GaAs (110) surface + 10^{12} L O_2. The two other scales give the escape depth in Å and molecular layers. (From ref. 92)

H. LEED Studies of Oxygen Overlayers

There have been fairly few LEED studies of the oxygen interaction with the GaAs (110) surface. Mark *et al.*[22,78,129] reported that oxygen chemisorption on a sputter-annealed surface led to a gradual lowering of the diffracted intensities, followed by the total disappearance of the LEED pattern. The results were interpreted as a growing disorder of the atomic layers close to the surface. A low temperature experiment for the cleaved surface by Russel and Haneman[131] pointed to an ordered oxygen overlayer. However, no analysis of the LEED intensity was performed.

Recently Kahn *et al.*[132] reported on the intensity changes in the LEED pattern when the cleaved surface is exposed to unexcited molecular oxygen at room temperature. Photoemission measurements were made on the same surfaces to correlate changes in the LEED pattern with changes in the valence band. LEED intensity profiles recorded for the clean surface for several beams showed perfect agreement with profiles previously obtained of the clean surface from both cleaved and sputter-annealed surfaces.[133] After exposures to 10^6 and 10^7 L of oxygen the photoemission spectra showed a small oxygen uptake (see Section D) and a slight weakening of the LEED pattern. However, no change in the state of the intensity profiles could substantiate any relaxation of the surface atomic layers. The situation changed drastically after 10^8 L. The photoemission showed a large increase in the oxygen signal and a smearing of the valence band, as discussed in Section D. The LEED pattern changed both quantitatively and qualitatively. The background was considerably larger and the intensity profiles of the diffracted beams were changed. Certain intensity peaks present in the clean surface profiles had totally disappeared or were considerably shifted on the energy scale. The example in Fig. 24 presents intensity profiles taken before and after the exposure. The experimental curves (b) and (d) for the $(\bar{1}\bar{1})$ peak taken before and after the exposure respectively show the transformation of the double peak (129 and 165 eV), associated with the distortion of the first and second atomic layers,[72,73] into a single peak corresponding to the Bragg diffraction from the bulk-like structure. Similar results were obtained for the $(1\bar{2})$ beam. In spite of the increase of the background and the changes in the shapes of the profiles, the diffraction pattern remained extremely sharp, showing no noticeable increase in the spot size. This indicates that the coherent diffraction originates from an extensively ordered periodic structure. The experiment was repeated with increased dosages of oxygen (10^9 and 5×10^{10} L). The UPS spectra showed the expected increase in the oxygen signal. The LEED pattern was not noticeably changed, the sharpness of the spots and their relative intensities remaining the same.

All the diffracted beams showed intensities corresponding to the diffraction from a truncated surface with no atomic displacements after the oxygen exposure. All peaks that had been attributed to the reconstruction of the surface and subsurface atomic layers[73] have been removed (see Section II.D). The facts that the diffracted spots are extremely sharp at all energies and that the background is very high suggest the following model for the surface region. A thin layer, probably monolayer (1–3 Å), highly disordered by the oxidation, covers the GaAs substrate lattice which no longer shows evidence of

atomic displacements. The disordered surface layer produces the strong incoherent background, but it is sufficiently thin (compared with the inelastic mean free path) to allow the emergence of the electrons coherently scattered from the undistorted substrate. This model was tested by kinematic and dynamical computations. The lowering of the intensities by incoherent scattering in the surface area was simulated very crudely in the single scattering computation by increasing the path of the electrons in the absorbing medium.

Intensities produced by an ordered (1 × 1) oxygen overlayer on GaAs (110) have not yet been computed. However, it seems extremely improbable that any ordered overlayer would produce such a high background and, at the same time, intensity profiles corresponding so well to bulk-like diffraction.

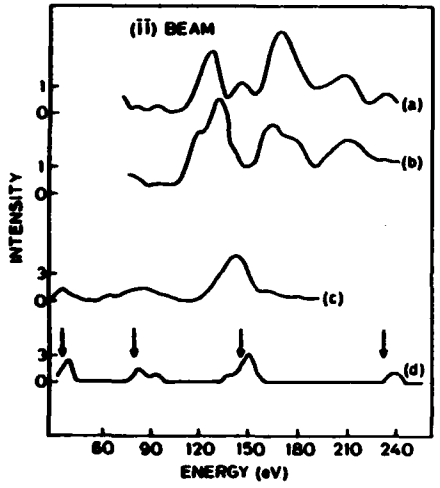

Fig. 24. Experimental and theoretical I–V profiles of the (11) beam. (a) and (c) are dynamical calculations with a two-layer reconstruction and a bulk structure, respectively. (b) and (d) are experimental profiles taken before and after oxygen exposure. The arrows point to the theoretical positions of the single scattering Bragg peaks. The doublet (129 eV, 165 eV) of (b) gives a single peak (145 eV) in (d), which is reproduced in the computation. (From ref. 132)

IV. METAL OVERLAYERS AND THE FORMATION OF SCHOTTKY BARRIERS

A. Introductory Remarks

When a metal is brought into contact with a semiconductor surface a charge transfer takes place between the two materials, giving rise to a space charge layer. The metal and semiconductor are in electronic equilibrium when the

Fermi levels are aligned. The space charge layer lies almost entirely on the more weakly screened semiconductor side of the interface (the Debye length is typically two orders of magnitude smaller for the metal). The necessary potential difference to align the Fermi levels thus occurs almost entirely in the semiconductor, resulting in a potential barrier, the so-called Schottky barrier. The interaction of a metal overlayer with a semiconductor surface is the basis for Schottky-barrier formation and has been the subject of great attention during several decades. Lindau *et al.*[134] have recently reviewed the experimental work on Schottky barriers, mainly summarized in a set of empirical rules, and the large number of theoretical approaches.

In this section we will discuss in some detail experimental results for a few different metal overlayers on the (110) surface of GaAs. We will in particular discuss Au and Al overlayers at some length and elaborate on the changes taking place in Fermi-level pinning, surface electronic structure, interface properties, etc. as the thickness of the metal overlayer is increased from a fraction of one monolayer to several tens of monolayers. In the case of Au overlayers a comparison will be made for the (110) surfaces of GaAs, GaSb, and InP.

Before the experimental results are presented and discussed it may be appropriate to provide some experimental details[134–136] in addition to the discussion in Section III.B. All the (110) surfaces were prepared by cleavage *in situ* in ultrahigh-vacuum environment at a base pressure better than 2×10^{-10} torr. The (110) surfaces exposed to metal overlayers were typically $5 \times 5\ mm^2$ in area. Au deposition was made by rotating the sample through a stream of Au emerging from an evaporator consisting of a shield and a gold bead suspended on tungsten wire. To avoid heating of the sample surface, a shutter was installed in front of the sample and was never left open for more than 20 s (typically 10 s exposures were used). The evaporation rates were monitored by means of a quartz-crystal thickness monitor placed to the side of the evaporator in front of an opening cut in the side of the evaporator shield. This monitor was previously calibrated in a separate pump-down against another placed in front of the evaporator near the sample position. The coverage in monolayers (θ) is then determined from the Å of Au evaporated, with one monolayer defined as one Au atom per surface atom.

In photoemission spectroscopy it is important to be able to establish a meaningful reference level to set the energy scale. Photoemission also has the inherent advantage that changes in the Fermi-level position, for instance due to band bending, can be followed directly and related to an absolute reference level. In these experiments, as well as those for oxygen exposed surfaces, reference spectra were taken from Au evaporated onto a stainless-steel substrate attached to the same sample carousel as the semiconductors and thus in electrical contact with these. The sample carousel is grounded to the

analyzer. The measured electron energy, E_e, is relative to the Fermi energy E_F of the analyzer. The binding energy (BE) relative to E_F is then

$$E_B^F = h\nu - E_e - e\phi_A \quad (1)$$

where $h\nu$ is the photon energy and ϕ_A is the analyzer work function. The location of E_F (and hence ϕ_A) may be found from the Fermi edge of the Au reference. However, in a semiconductor, E_F is not the best reference level since it shifts around in the band gap at the surface owing to changes in band bending and type (n or p) of semiconductor. Nor is the vacuum level a good reference, since electron affinities are not well known and also change with the addition of adsorbates. The BE of a core level in a semiconductor does not change with band bending when measured relative to the valence band maximum (VBM) at the surface, and we shall use this binding energy E_B^{VBM}. However, when the semiconductor dissociates and the individual components become metallic, the meaningful reference level becomes the metal E_F. Thus one needs to be careful in interpreting spectra from mixed metallic and semiconducting states and in comparing BEs made on metals and semiconductors (e.g. Ga metal and Ga in GaAs). It is important to remember that E_B^F in a semiconductor may vary from sample to sample, whereas E_B^{VBM} is constant. Thus the band bending of a semiconductor with small amounts of adsorbates may be followed using the movement of the core level since the work function of the analyzer, ϕ_A, is very stable. That is, from Eq. (1), $\Delta E_B^F = \Delta E_e$. At higher coverages other factors need to be considered, e.g. charge transfer, changes in screening, conversion into metallic form due to dissociation, and so on, which will give extra contributions to ΔE_B^F.

At the lower photon energies, E_F and its position relative to the VBM may be very accurately determined. Our procedure is to use photoelectron energy distribution curves (EDC) at $h\nu \approx 10{\cdot}2$ eV to study E_F movement and locate the VBM. The electron-escape depth is a function of electron kinetic energy[130] and is relatively long (~20 Å) near 10 eV but is short compared with the depletion-layer width of several hundred Å at the doping levels used for the samples in this work. Thus bulk band-structure features remain up to relatively thick coverages of adsorbates. By aligning the bulk peaks, the amount of E_F movement can be measured by locating E_F on the different spectra using the Au reference. The position of E_F relative to the VBM is obtained from the clean sample. We have elaborated in some detail on the methods to determine the energy location of structure in the substrate and the metal overlayer, relative to a reference level, since it is of fundamental importance in interpreting and understanding the spectra.

B. The Interaction with Thin Gold Overlayers

Figure 25 shows the photoemission spectrum of the outer core levels of Au ($4f_{7/2}$, $4f_{5/2}$) and GaAs (Ga 3d, As 3d) as the Au deposition is gradually

increased from 1 to 50 monolayers.[136] As a comparison, the results for GaSb (110) and InP (110) are shown in Figs 26 and 27.[136] These samples were all n-type.

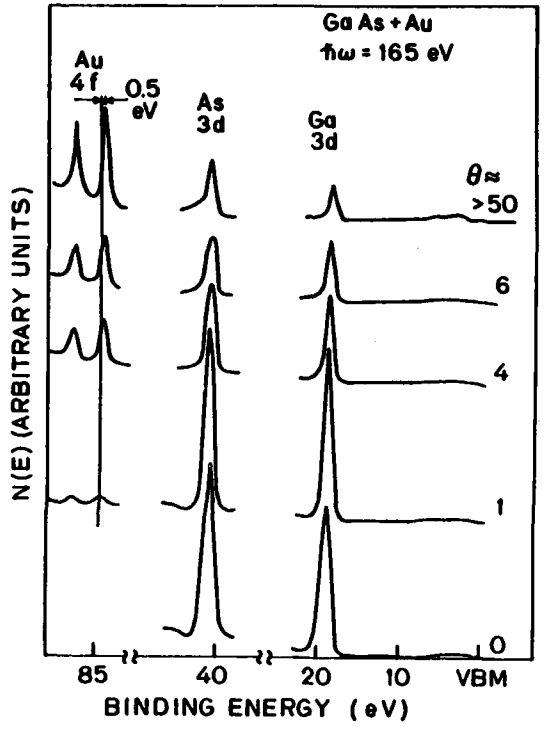

Fig. 25. Photoemission spectra taken at a photon energy of 165 eV for GaAs with different Au coverages. (From ref. 136)

The photon energies used were 165 eV for GaAs, 120 eV for GaSb, and 120 eV for In 4d and 165 eV for P 2p. At 165 eV the cross-section for Au 4f is much larger than at 120 eV, and the escape depth for the photoelectrons[130] is also shorter (4 vs. 10 Å at 120 eV). However, the 4d cross-section is very small at 165 eV—the Cooper minimum;[137] thus it was necessary to use the lower photon energy for studying GaSb. The escape depths of the core levels presented here are all estimated to be between 5 and 10 Å, based on escape depth curves published by Pianetta *et al.*[92] and Lindau and Spicer.[130] Thus SXPS (soft x-ray photoemission) is extremely surface sensitive. [The escape depths here may be compared to those for x-ray photoemission spectroscopy

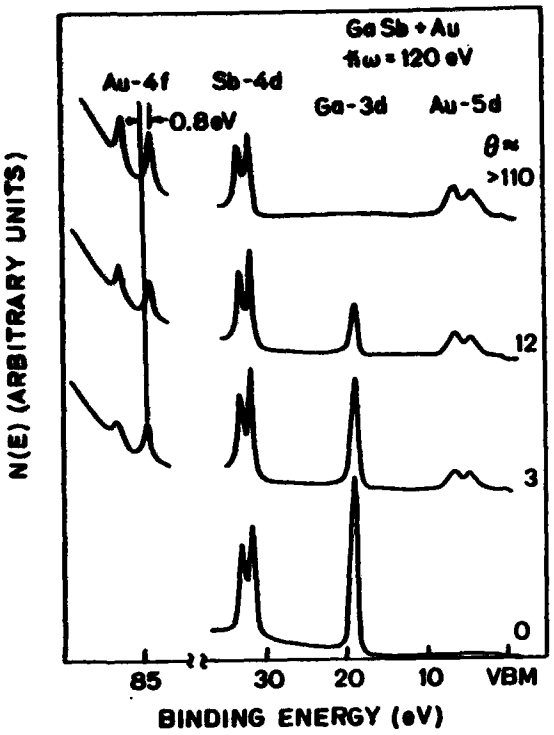

Fig. 26. Photoemission spectra taken at a photon energy of 120 eV for GaSb with different Au coverages. (From ref. 136)

(XPS) which are generally $\gtrsim 20$ Å.] It is immediately obvious from Figs. 25–27 that, while for GaAs and InP both anion and cation core level emissions decrease at roughly the same rate until a residual level is reached, for GaSb the Ga emission is attenuated as Au is deposited and decreases rapidly, while the Sb emission remains strong. This increase in the Sb/Ga ratio is already quite pronounced at a few monolayers coverage.

Chye *et al.*[135,136] interpreted the Au–GaSb spectra as showing selective removal of Sb from the interface such that a layer of Sb "floats" to the surface of the Au. One can give an explanation of this based on known bulk properties. In bulk GaSb it is well known[138–141] that crystals tend to grow non-stoichiometrically with an excess of Ga. Thus segregation of Sb to the surface may be favored. It is also well known from alloy studies[142,143] that the surface composition may be different from the bulk composition in an alloy and that the component with the smallest surface free energy is normally enhanced at the

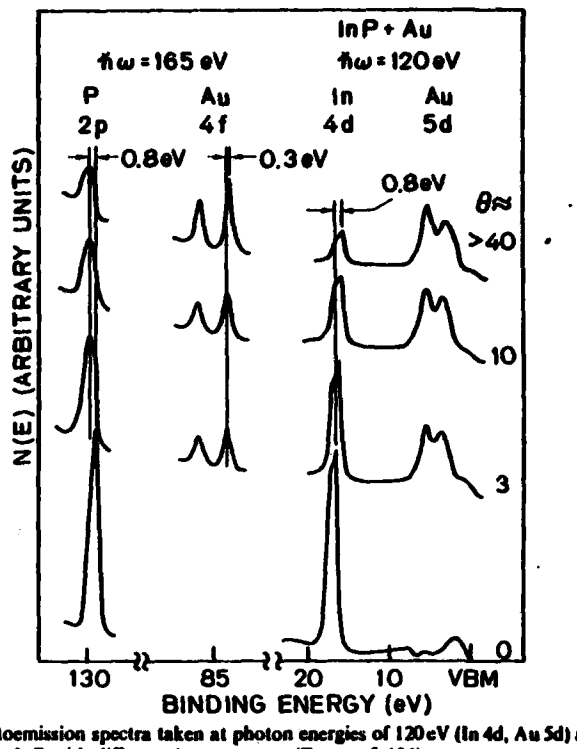

Fig. 27. Photoemission spectra taken at photon energies of 120 eV (In 4d, Au 5d) and 165 eV (P 2p, Au 4f) for InP with different Au coverages. (From ref. 136)

surface. Thus the Sb that the GaSb gave up upon Au deposition moves to the surface since it has the smallest surface free energy. Some caution must be exercised since the system studied here is a very thin film and equilibrium probably has not been attained. Therefore bulk phase diagrams and properties can only serve as rough guides. Semiconductor components are also present on the surface of Au–GaAs and Au–InP and may be there for the same reason of minimizing the surface free energy.

At thick Au coverage there is an apparent enhancement of the As/Ga ratio. This may be due to a preferential removal of As from the semiconductor or may be due to several factors that become important as the Au thickness becomes appreciable. One factor is the relative solubility of the semiconductor elements in the Au layer. Another factor is the relative tendency to form compounds or alloys with the Au. A third factor is the relative diffusion rate. This last factor is quite unlikely here since Ga diffuses rather rapidly in Au.[144] It seems more likely that Ga forms compounds or alloys, thus remaining in the

Au layer. One may conclude from the increase in the As/Ga ratio that dissociation of Ga from As has occurred in certain parts of the surface. It is also important to realize that, on GaSb, the Sb/Ga enhancement is apparent at low coverages when the complicating factors mentioned above are not yet significant. Thus, while it is clear that, on Au–GaSb, Sb is removed preferentially, it is more difficult to tell on GaAs whether preferential removal of the As has taken place. The present data favor near-stoichiometric removal.

In order to study the composition versus depth for the gold overlayers discussed above, ion depth profiles were made on samples onto which a 50–70 Å thick Au layer had been deposited. The results are shown in Figs 28 and 29 for GaSb + Au and GaAs + Au respectively.[136] The ion beam is incident on the surface at a grazing angle near 80°. The ion sputtering rate, calculated from sputtering yields for Au in the literature for 1 keV ions, was 13·4 Å min^{-1} for GaSb + Au and 6·7 Å min^{-1} for GaAs + Au.

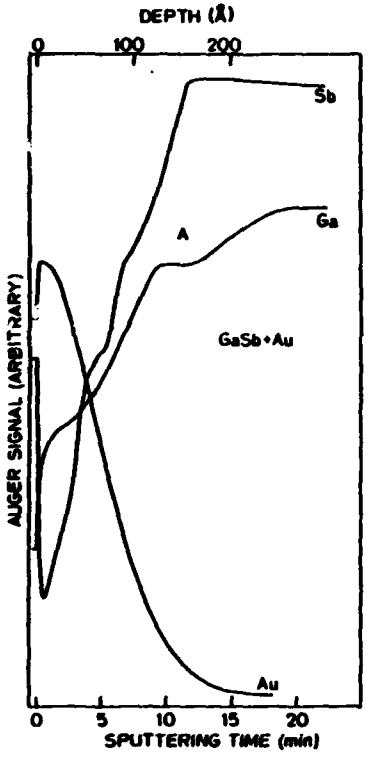

Fig. 28. Compositional depth profile of Au-covered GaSb, obtained using Auger electron spectroscopy in combination with argon ion etching. (From ref. 136)

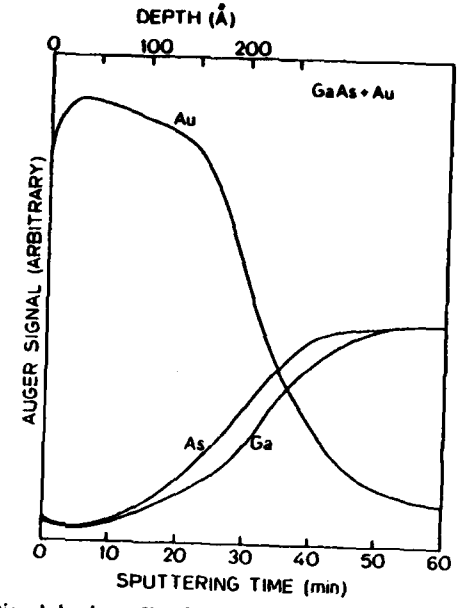

Fig. 29. Compositional depth profile of Au-covered GaAs, obtained using Auger electron spectroscopy in combination with argon ion etching. (From ref. 136)

The profile in Fig. 28 unambiguously shows a layer of Sb forming the top few monolayers. This layer may be in the form of Sb metal, $AuSb_2$, a mixture of the two, or an Sb–Au alloy. Since the increase in Au signal is slight as the top layer is sputtered away, it is likely that Au is present in this top layer. The apparent interface width (90–10% Au) is 110 Å, neglecting broadening factors. Broadening due to finite escape depth is small (< 10 Å) and, at the glancing ion incidence used here, knock-on mixing effects should be less important. In any event, even allowing for a 30 Å broadening due to knock-on, the interface is still quite wide. It is possible that substantial intermixing of semiconductor and Au has occurred at room temperature. One other broadening factor that may be important here is the well known tendency of Au to form islands or to "clump". If the Au film were not of uniform thickness the interface would appear broadened. This clumping may not be very pronounced at room temperature. The existence of region A in Fig. 28 also argues against significant clumping. In this region the Ga signal stays constant while the Sb signal increases steadily. This region also was observed on a second Au–GaSb sample with thicker Au coverage. If there was clumping, one should just observe a steady increase in both the Ga and the Sb signal. (If such a steady increase were observed, as in Fig. 29, one would not be able to distinguish

between broadening by intermixing or by clumping.) In this region, too, non-stoichiometry is likely since one semiconductor component is steadily increasing while the other is constant. This region is roughly 30 Å wide. The depth profile for Au–GaAs shown in Fig. 29 does not exhibit a region similar to A in Fig. 28.

Other workers[145-147] have also studied Au–GaAs depth profiles with various techniques and observed interdiffusion, particularly at high temperatures. In general, more Ga than As was found to be on the surface. For example, Hiraki *et al.*[147] studied Au overlayers on semiconductors and insulators and found that, at room temperature, the surface is Ga-rich with an "alloyed" interface, while for Au–insulator systems the interface is sharp. Figure 29 shows the presence of both Ga and As on the surface, with somewhat more As at the higher coverages. The discrepancy may be explained by differences in initial surface preparation (Hiraki *et al.*[147] used ion-sputter and anneal methods rather than cleaving), by a probable difference in crystal face [which they did not specify but was not likely to be (110)], and possibly by differences in Au evaporation techniques. The most significant thing in their findings is the absence of an alloyed interface on insulators.

A close examination of Figs 25–27 shows that some levels are shifted and some are broadened. The Au-4$f_{7/2}$ level has a BE of 84 eV relative to E_F at thick coverages, in agreement with measurements on bulk Au. However, at low coverages the 4f have a higher BE. This increase is as large as 0·8 eV on GaSb, possibly larger at still lower coverages. The shift is 0·6 eV on GaAs (partly masked by band bending; these spectra are plotted with the VBM aligned) and 0·3 eV on InP. As will be shown below, at low coverages the Au is in a dispersed or "atomic-like" state. Thus it appears that the Au 4f are higher in BE relative to E_F by $>0·8$ eV in the dispersed or atomic-like state and move continuously toward lower BE as more Au is deposited. The shift of a core level may be due to chemical effects such as charge transfer or due to configuration changes or differences in screening and relaxation. Since Au is quite electronegative, shifts due to chemical effects should be towards higher BE as bulk Au is formed, so the observed shift is probably due to changes in screening and relaxation.

On the GaSb cleave of Fig. 26, E_F appears to be pinned near mid-gap after cleaving. While E_F is usually unpinned on n-GaSb, as discussed in Section VI, occasionally extrinsic states cause pinning either over the whole crystal surface or over parts of it. As the Au coverage is increased there is little change in the position of the core peaks relative to VBM. There may be a small shift ($\sim$0·2 eV) of the Sb 4d towards higher BE, but it is difficult to be certain with the present experimental resolution. The full width at half maximum (FWHM) of these levels also shows negligible change. The Sb 4$d_{5/2}$ in metallic Sb has a BE of 32·1 eV (relative to E_F) according to XPS measurements.[148] Here the surface Sb 4$d_{5/2}$ has a BE of 31·9 eV (relative to E_F) and, for clean GaSb, a BE of 31·6 eV (relative to VBM). The difference in BE between XPS and the present measurements is within experimental uncertainties, so it is not possible to tell whether Sb, $AuSb_2$, or an alloy is at the surface. However, the relatively strong intensity of the Au emission and the absence of bulk Au structure favor $AuSb_2$ or an alloy, with perhaps some metallic Sb mixed in. Although the bulk phase diagram[149] for Au–Sb indicates that only Sb + $AuSb_2$ is possible at high concentration of Sb at room temperature, the surface phase diagram is likely to be different. In addition, the present system may not have reached equilibrium.

In GaAs the Ga 3d and As 3d levels are broadened by $\sim$0·5 eV (FWHM) for this particular cleave immediately after cleaving, although most GaAs cleaves do not show this. This is a good example of inhomogeneous band bending over the surface. The inhomogeneity in band bending disappears with the addition of Au since Au causes pinning at the same energy position over the entire surface. Thus the core levels narrow with Au deposition. There is no observable change in the peak position of either core level (relative to VBM) although at thick Au coverage a tail toward higher BE in the As 3d can be clearly seen. This tail falls at the right energy for bulk As 3d, which has slightly higher BE. Once again, since valence band spectra (see below) show that bulk Au is not present at the surface, the surface layer is likely to be As, Ga–Au alloys, or compounds such as $AuGa_2$ or AuGa, and perhaps some free Ga. The surface composition is probably such that the surface free energy is minimized.

For InP the behavior of the P level with Au deposition indicates the possible presence of free P. The P 2p level broadens by $\sim$0·4 eV (FWHM) with the addition of several monolayers of Au, and at thick coverage the peak position has shifted by 0·8 eV towards higher BE. No such broadening is observed in the In 4d level, although a shift by 0·8 eV towards lower BE is observed. Once again, valence band spectra indicate formation of compounds or alloys of Au. These are probably Au–In alloys or compounds such as $AuIn_2$ or AuIn, and the lack of broadening indicates that there is one dominant compound or alloy. However, the broadening of the P 2p indicates the presence of (at least) two different species of P— possibly free P and a Au–P alloy. There is a suggestion of excess P since, even though the P amplitude decreases at roughly the same rate as In, it is broadened. This may be due to a true excess of P removed from the semiconductor since this excess is already observed at several monolayers coverage.

The important conclusions to be drawn from the data shown in Figs 25–29 are:

(1) Au interacts strongly even at room temperature with the semiconductor surface, causing large amounts of intermixing with some surface enhancements.

(2) The semiconductor material removed from the crystal may be partly or totally dissociated and may remain in the free state or form compounds or alloys with Au.

(3) The semiconductor components may be removed non-stoichiometrically, and the excess elements appear to be Sb and (to a lesser extent) P in GaSb and InP, respectively. Ga and As appear to be removed in nearly stoichiometric amounts in GaAs.

Before discussing the valence band spectra, a short remark should be given on the position of E_F in the band gap as a function of Au coverage. This aspect will be discussed in some length in Section VI, where a new model for the mechanism behind the Fermi-level pinning will be discussed. The most important observation is the extreme sensitivity of E_F to Au. It is apparent that, for coverages <0·2 monolayer, E_F has already stabilized near the positions for thick metallic layers of Au on the same cleaved surfaces.[150]

For photon energies larger than 25 eV, the semiconductor valence band matrix elements and the photoelectron-escape depth decrease. On the other hand, the Au 5d matrix elements increase. These factors enable small amounts of Au to be easily observed. It is usually important to know whether the Au is well dispersed on the surface. By following the development of the Au 5d bands, one can gather such information. From photoemission work on Au alloys[151] it is known that, when Au atoms are well dispersed as in a dilute Au alloy, the splitting of the Au 5d peaks is reduced from the bulk value of 2·3 eV until it approaches the value for atomic Au (1·5 eV). In addition, there is a shift towards higher BE of these bands. Therefore the Au distribution may be probed by following the details of the 5d bands. If Au islands of appreciable size form, one would expect to see bulk Au valence bands.

In Figs 30–32 are shown the valence band spectra for different amounts of Au deposited onto GaAs, GaSb, and InP. From Figs 31 and 32 one can see that the splitting for <0·2 monolayer is 1·7 and 1·6 eV for GaSb and InP respectively. The splitting for 0·17 monolayer of Au on GaAs (Fig. 30) is larger (1·9 eV) but still is less than the bulk value. Thus we may conclude that, when E_F has stabilized, the Au on the surface is still well dispersed and has not formed large clumps.

At higher coverages the splitting increases, but the valence bands still do not resemble bulk Au, with the shoulder still absent. This is especially clear in the 21 eV EDCs shown in Fig. 33. This may be explained as due to the formation of compounds or alloys with the semiconductor components, so the Au atoms do not assume the lattice structure of metallic Au.

Another way to determine the dispersion of the Au atoms is to look for non-uniform band bending, i.e. "patch" effects, from the broadening of the Ga or In levels. If Au clumps, pinning will be non-uniform over the surface and the core levels will be broadened. This method works extremely well when E_F changes

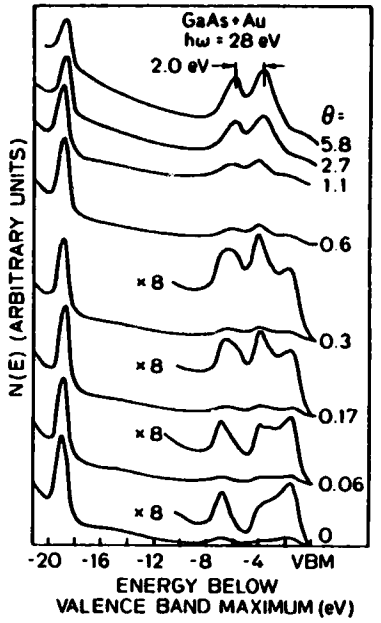

Fig. 30. Photoemission spectra of GaAs at a photon energy of 28 eV as a function of Au coverage. (From ref. 136)

in energy position by large values with deposition of Au. A striking example of the effects of non-uniform band bending is the clean GaSb surface studied here. In Fig. 31 there is a tail on the low BE side of the Ga 3d level (shaded area), due to emission from portions of the surface where E_F is pinned. The deposition of 0·15 monolayer of Au caused the tails to disappear, suggesting that the pinning has become uniform over the surface, once again indicating that the Au is well dispersed over the surface.

Observation of the core levels (Figs 30 and 31) shows that the In 4d level moves upward towards lower BE as Au is added and, at 4·1 monolayers, has shifted up by 0·3 eV, less than the 0·8 eV observed in SXPS at much higher coverage. This possibly is because a more dilute In–Au alloy shows a larger In 4d shift and may indicate formation of a Au–In alloy. The Ga 3d levels on the other two semiconductors appear to have no resolvable shift.

The photoemission measurements were combined with CFS spectroscopy (see Section II.C). At photon energies that cause transitions from the Ga or In d levels, d core holes are created. Recombination of electrons with these holes gives rise to secondary Auger electrons whose final state energy does not

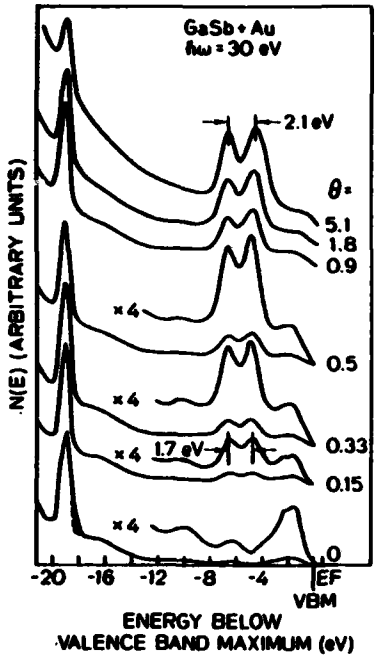

Fig. 31. Photoemission spectra of GaSb at a photon energy of 30 eV as a function of Au coverage. (From ref. 136)

change with photon energy. The final state energy of 4 eV was chosen for the studies reported here.

In Figs 34–36 CFS spectra for GaSb, GaAs, and InP are shown. The double peak structure near 19 eV is believed to be excitonic levels involving transitions from the spin–orbit split anion d core level (Ga 3d and In 4d) and empty states—possibly surface states—above the conduction-band minimum (see Section II.C). The energy necessary to cause a transition into them is lowered by the exciton BE (0·5–1·0 eV). The transition strength is matrix-element dependent.[38] The broad peaks at higher photon energies are due to transitions into the bulk conduction band, reflecting the density of states. The sharp peaks at still higher photon energies in Figs 34 and 36 are due to sweeping of the core d level (primary) photoelectrons through the final state energy of 4 eV.

In Fig. 34 the Ga 3d peak near 28 eV shows the tail (shaded) mentioned earlier. After 0·15 monolayer of Au, the peak shifts by 0·6 eV due to movement of E_F by that amount, and the tail disappears since pinning is now uniform over the surface. Further deposition of Au fails to cause any extra E_F

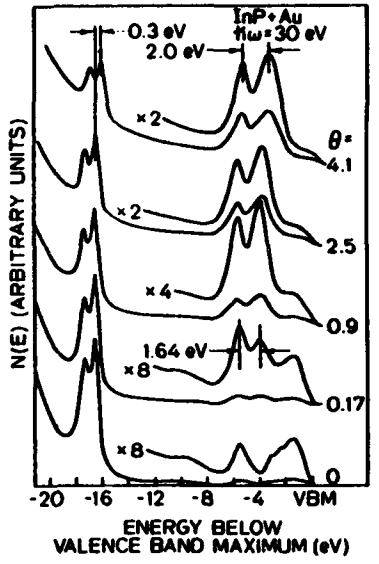

Fig. 32. Photoemission spectra of InP at a photon energy of 30 eV as a function of Au coverage. (From ref. 136)

movement, once again demonstrating that pinning is complete at 0·15 monolayer. Note, however, that even though pinning is complete at 0·15 monolayer the surface excitons are little affected and, in particular, remain at the same energy, showing that the final states are not shifted by the presence of Au. By 0·9 monolayer, however, much of the excitonic structure has disappeared. The coverage for exciton extinction appears slightly higher for the other two semiconductors but, when pinning is complete, the excitons are little affected. Note that in Fig. 36 the shift in the In 4d is due initially to E_F movement, but the shift (0·3 eV) at 4·1 monolayers is due not to E_F movement but to compound or alloy formation.

One question that might be asked is whether the Au creates any new empty levels. The data here show no clear evidence of new levels arising from the deposition of Au. One explanation is that the density of new empty states created (metal-induced states) is low since $< 10^{12}$ states cm^{-2} are sufficient to pin E_F. However, if Au forms covalent bonds with the surface atoms, as suggested for Group III metals on Si (111),[152] one would expect creation of $\sim 10^{15}$ states cm^{-2} and the introduction of new levels into the CFS spectra. The absence of these levels near 1 monolayer suggests that covalent bonding may not be the correct description for the materials studied here. We will

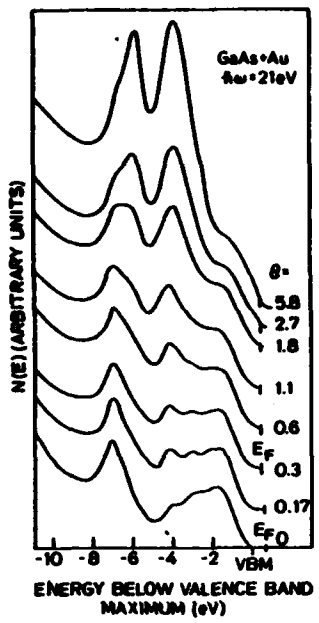

Fig. 33. Photoemission spectra of GaAs at a photon energy of 21 eV as a function of Au coverage. (From ref. 136)

return to this question in the discussion of the electronic structure of Al overlayers on GaAs (110) in Section C.

The final comment will be on the thermodynamics of the Au/III–V compound systems. More details of this will also be discussed in Section VI on the defect states model for Schottky-barrier formation.

When Au is evaporated it is in a higher energy state, with an energy equal to the heat of sublimation (89 kcal mol^{-1} = 3·87 eV atom^{-1}) above the metallic state at room temperature. On arrival at the semiconductor surface the Au atoms go into the lower energy state, releasing large amounts of energy. The amount of energy each condensed Au atom gives up will depend on the strength of binding to the substrate, that is, whether it forms a compound with the semiconductor, chemisorbs, sits interstitially, goes substitutionally into the semiconductor lattice, or bonds weakly to the semiconductor surface or to other Au atoms. This energy will—especially for the first monolayer of Au—be different from the heat of sublimation of Au, since we have seen that bulk Au structure is not obtained until tens of monolayers have been deposited. As an example, it can be mentioned that the initial heat of adsorption of Cs on GaAs (110) is ~60 kcal mol^{-1}, while the heat of sublimation of bulk Cs is ~19

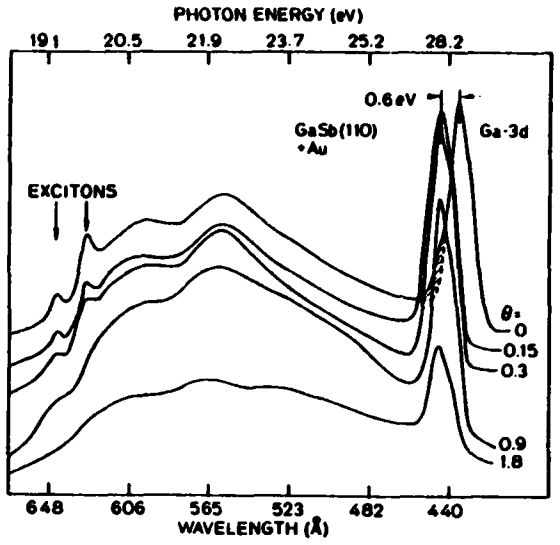

Fig. 34. CFS spectra of GaSb as a function of Au coverage.(From ref. 136)

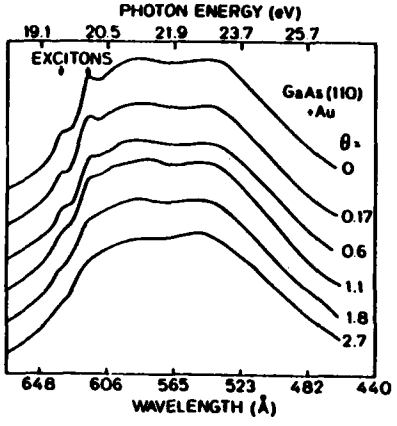

Fig. 35. CFS spectra of GaAs as a function of Au coverage.(From ref. 136)

kcal mol^{-1}.[153] The excess energy carried by the deposited Au is released in a localized volume, thus causing a "thermal spike" that can create defects. Van Vechten[154] has calculated the enthalpies in forming various bulk defects and, for vacancies, the values are typically 2–3 eV for III–V semiconductors. At the surface these values will be reduced because of reduced area in his macroscopic

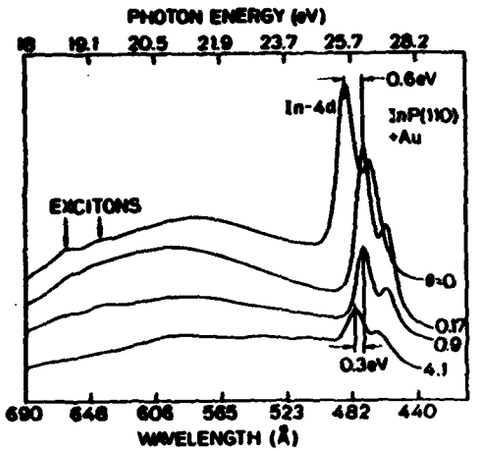

Fig. 36. CFS spectra of InP as a function of Au coverage.(From ref. 136)

"cavity", thus lowering the surface energy. Another way of looking at this is that, at the surface, fewer bonds need to be broken to form a defect. Brillson[155] and Lindau *et al.*[134] have presented plots of the index of interface behavior S versus the heat of formation (HF) of numerous covalent and ionic compounds, and there is a striking relation (see Section VI). The more ionic compounds have high HF and $S = 1$, while the covalent compounds have low HF and small S (indicating weak dependence on ϕ_M). From this one might argue that the defects formed with metal deposition are more numerous when HF is small and that these defects are more important than the particular metal used in determining the pinning, consistent with experimental observations. For more ionic compounds with higher HF, fewer defects are formed, so the dependence on ϕ_M is stronger.

C. The Replacement Interaction with Aluminum

One of the main conclusions from the results for the interaction of Au with the GaAs surface discussed in Section B was that there is a strong perturbation or disruption of the semiconductor lattice at the interface. No evidence was found that chemical reactions, leading to metal–semiconductor compound and/or alloy formation, are necessary for the disruption and intermixing to take place. In this section we will discuss a different case, where experimental evidence suggests that a replacement of Ga by Al takes place in the GaAs (110) surface lattice.[156] The Al metal deposition onto the GaAs surface was done at room temperature in a manner similar to that for Au. Typical deposition rates were 1–2 Å min^{-1}. The GaAs (110) samples were of n-doped material.

The adsorption of Al was begun with submonolayer quantities for correlation of the chemical state of atoms in the interfacial region with the Fermi energy pinning position as the Al coverage was increased in steps (see Fig. 37). Changes in the Fermi energy were measured by the change in energy involved in a rigid shift of all features identified with the semiconductor substrate as discussed previously in Section B. The surface Fermi energy was initially unpinned (Fermi energy near the conduction band minimum for the n-doped samples), but the first deposition of Al (~0·1 monolayer) bent the bands upward by 0·6 ± 0·1 eV, moving the surface Fermi energy toward the middle of the band gap. Further deposition of Al up to approximately 8 Å produced an apparent additional 0·2 ± 0·15 eV shift. It should be noted that the Ga and As core levels were reduced in strength by roughly a factor of 4 at the maximum Al coverage, causing a slightly greater uncertainty in the determination of peak positions.

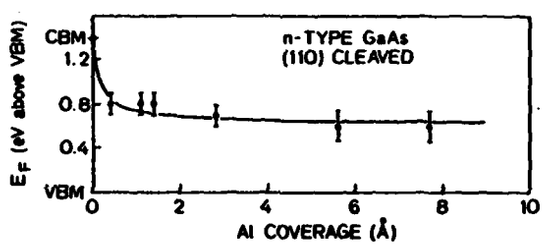

Fig. 37. Fermi-level position in the band gap as a function of Al overlayer thickness. Uncertainty in the Fermi level is indicated with error bars, and the maximum error in the absolute overlayer thickness is about ±50%. (From ref. 156)

As was the case for Au overlayers on GaAs, changes in the core levels (in this case Ga 3d, As 3d, and Al 2p) were monitored to provide insight into the metal–semiconductor interface formation and composition (see Fig. 38). A photon energy of 120 eV was used to excite electrons from the core levels to final states with kinetic energy within the broad escape depth minimum for high surface sensitivity.[130] Beginning with the lowest Al coverage (0·4 Å), a very large shift of the As 3d and Ga 3d core levels toward lower binding energy was observed, corresponding to the bands bending upward, and the pinning of the Fermi energy 0·6 eV below the conduction band minimum. No change in As 3d or Ga 3d peak shape is evident. At this small coverage a very weak emission from the Al 2p core level is observed at an initial state energy of 73·7 ± 0·2 eV. However, after a total deposition corresponding to between 0·5 and 1 monolayer (1·5 Å), the Al 2p peak had grown substantially and shifted 0·3 eV to a higher binding energy (74·0 ± 0·1 eV). These are shifts toward higher binding energy compared with bulk Al and indicate that there is a sequential

formation of two Al states at low coverage, which are distinct from bulk Al metal. A lack of O 2p emission and no evidence for oxygen in AES argue against oxygen contamination as the source of the shifted Al 2p core levels. The As 3d and Ga 3d peaks were attenuated but essentially unchanged except for an increase in emission on the low binding energy side of the Ga 3d peak. At the maximum Al coverage (8 Å) the Al 2p core level is located at 73·1 ± 0·1 eV which corresponds to the observed binding energy for bulk metallic Al.[157] The As 3d peak was further attenuated but no change in peak shape was observed (see Fig. 39). However, a notable increase in emission on the low binding energy side of the Ga 3d peak is quite evident (see Fig. 39) when a comparison is made with the Ga 3d peak from the clean GaAs surface. Subtracting the "clean" Ga 3d peak from the "heavily aluminized" Ga 3d peak yields a difference curve that peaks at 18·4 ± 0·2 eV binding energy, consistent with a binding energy of 18·2 ± 0·2 eV obtained from the literature for metallic Ga.[102] Ga 3d difference curves obtained at lower Al coverages indicated that the free Ga was generated at Al coverages of 1 monolayer or less. However, the position of the free Ga 3d peak at low Al coverage was shifted to higher binding energy (19·0 ± 0·2 eV), which suggests that the free Ga is dispersed across the surface in an "atomic-like" state.[136] This observation is consistent with the results for very thin Au overlayers on III–V compounds, where the binding energy for the 4f levels is larger than for metallic gold (see Figs 25–27).

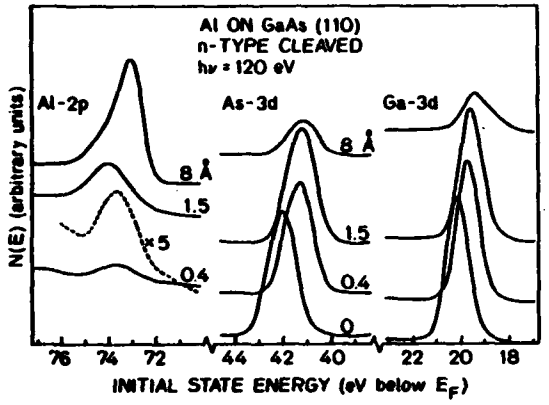

Fig. 38. Al 2p, As 3d, and Ga 3d core level spectra ($h\nu$ = 120 eV) for several Al overlayer thicknesses (given in Å). The rigid shift of the Ga 3d and As 3d after the first deposition of Al is due to band bending at the surface. (From ref. 156)

The present data suggest a very strong chemical interaction between the Al and the GaAs surface. The appearance of free Ga as the semiconductor peaks were attenuated by the Al overlayer is evidence that some disruption of the

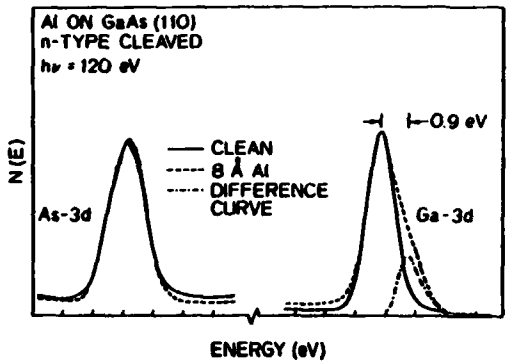

Fig. 39. Detailed analysis of the As 3d and Ga 3d core levels for 8 Å Al coverage. Dashed lines are superposed onto the corresponding peaks from the clean surface (solid lines). The horizontal axis is marked in increments of 1 eV. The peak in the difference curve corresponds to metallic Ga. (From ref. 156)

semiconductor surface is occurring. Since a shifted As 3d peak was not observed, the As most likely remained in the semiconductor surface lattice and Al replaced the Ga which was removed from the lattice.

The Al 2p core level data support this model. The initial Al 2p position observed in this work (73·7 eV) for very low coverages suggests that the Al may be adsorbed onto the surface without penetrating into the lattice. This suggestion is strengthened by the appearance of a further shifted Al 2p peak (74·0 eV) as time elapses (5–7 h), and the coverage is increased to between 0·5 and 1 monolayer which strongly suggests incorporation of Al into the lattice near the surface. Thermodynamically this is quite favorable; the heat of formation of AlAs (28 kcal mol^{-1})[158] is significantly larger than that of GaAs (17 kcal mol^{-1}).[159] The relative heat of sublimation of free Al and Ga on the AlGaAs surface also enters into the energetics of the system, but this is not available (to our knowledge) and an estimate must be made from the elemental heats of sublimation, 75 kcal mol^{-1} for Al on Al and 66 kcal mol^{-1} for Ga on Ga.

The initial stages of the Al reaction described above can be given further interpretation. Chemisorption of Al onto the GaAs surface lattice may be expected to create a local thermal spike. Strong evidence for this was seen, for example, in the disruption of GaAs, GaSb, and InP (110) surfaces following the slow room-temperature deposition of Au onto the semiconductor surface, as discussed in the preceding section. In the case of Au, compound or alloy formation with the semiconductor constituents was thermodynamically unfavorable[159] and therefore was not a driving force for the disruption of the III–V compound lattice. Alloy formation is, however, an additional driving force in the present study, and for this reason it is surprising that the fraction of

deposited Al which is incorporated into the semiconductor surface lattice is not a constant at submonolayer coverages. Instead there is a tendency for the Al to sit on top of the lattice until a coverage of more than 0·7 Å is achieved, after which an increased tendency to replace Ga in the surface lattice is observed.

More than one mechanism may lead to this effect, and some speculative arguments will be presented in this paragraph. From a very rough qualitative argument, surface Ga and As vacancies may be generated by the thermal spike generated when Al chemisorbs on GaAs since the formation energy of a Ga or As vacancy[154] is roughly equal to or less than the energy released upon chemisorption of Al on Al. A similar argument applies to the thermal spike created by a chemisorbed Al atom going into a surface Ga vacancy. The probability of a surface Ga vacancy being replaced by an Al atom before the Ga atom finds its way back into the vacancy increases with the number of Al atoms adjacent to the vacancy site. Thus the probability of Al replacing Ga in the surface lattice increases as the coverage is increased due to the proximity of other Al atoms. A replacement of Ga by Al at one surface Ga site could stimulate replacement reactions at adjacent Ga sites. If the energy released by Al filling a surface Ga vacancy were sufficiently greater than the surface Ga vacancy formation energy, a chain reaction could occur. The Al chemisorption energy, surface Ga vacancy formation energy, and the energy associated with Al filling a surface Ga vacancy will be influenced by rearrangement of the surface lattice due to the Al overlayer. It is therefore likely that both proximity and reconstruction effects give rise to the delayed incorporation of Al into the surface lattice.

The basic conclusion from the photoemission work presented here, namely that a replacement reaction takes place between Al and Ga in the surface lattice, has also been reported by Bachrach *et al.*[160,161] Additional studies, both experimental[162,163] and theoretical,[163,164] of the exchange reaction between Al and Ga have recently been published. In the study by Bachrach *et al.*[160,161] the amount of metallic Ga observed as a result of the replacement reaction was somewhat larger than that observed in our study. A possible explanation may be a higher substrate temperature during the Al deposition. Furthermore, Bachrach *et al.* did not report on the low Al coverage regime, i.e. on the interaction of the Al overlayer with the GaAs substrate before the replacement reaction occurs.

An important observation in the work by Brillson *et al.*[162] is that the LEED pattern of Al on GaAs (110) remains the ordered (1 × 1) structure for coverages up to half a monolayer. This would indicate that the replacement reaction takes place without disturbing the translational symmetry of the clean surface. For larger metal exposures the LEED pattern disappears, consistent with the formation of a disordered Al overlayer on the surface.

Mele and Joannopoulos,[164] using the tight-binding approximation, modeled the exchange reaction theoretically. The results for the densities of states of the valence bands for clean relaxed GaAs (110) and for Al chemisorbed on GaAs (110) in three distinct geometries are shown in Fig. 40. The theoretically calculated densities of states are then compared with the photoemission results by Bachrach *et al.*[161] for clean GaAs(110) and GaAs(110) + 1 monolayer of Al,

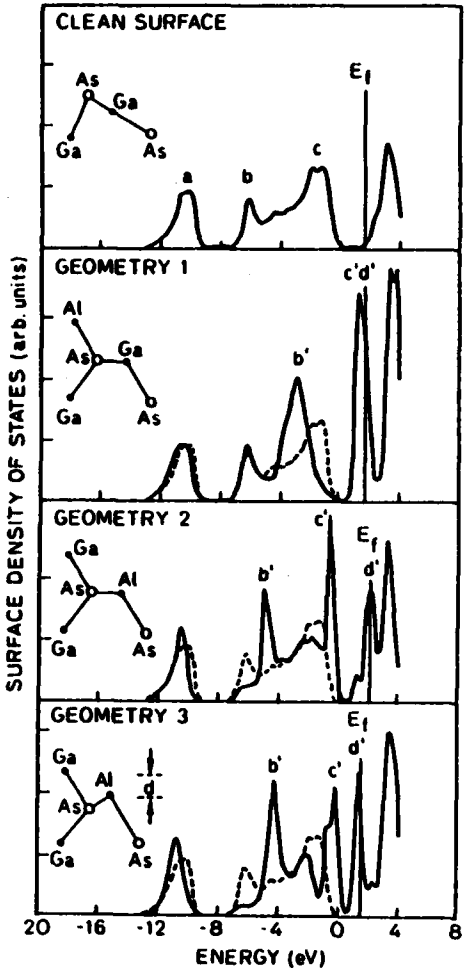

Fig. 40. Theoretical density of states for clean relaxed GaAs (110) (top panel) and for Al chemisorbed in three different configurations. The dashed lines in the lower traces represent the clean spectrum for comparison. (From ref. 164)

shown in Fig. 41. The peaks labeled a, b, and c in Fig. 40 are assigned to the three prominent features in the photoemission data in Fig. 41. After a detailed analysis and comparison, Mele and Joannopoulos[164] concluded that geometry 3 (Fig. 40) gives the best agreement between theory and experiment. Within this model, Al is moved away from the bulk, giving a "counterrelaxed" geometry. However, this model implies that a narrow band of filled states should appear in the band gap, peak d' in Fig. 40. So far this predicted structure has not been reported experimentally.

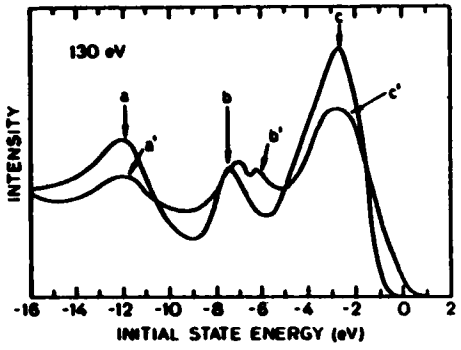

Fig. 41. Experimental photoemission spectra for clean GaAs (110) and GaAs (110) after deposition of ~ 1 monolayer of Al. The main peaks are noted by unprimed (clean) and primed (Al exposed) labels. (From ref. 164)

Chadi and Bachrach,[163] applying a total-energy minimization method to determine the most favorable geometrical configuration for the exchange interaction, argue for a different site geometry—a twofold coordinated position for the Al with the Ga and As substrate atoms in a relaxed position. Thus the interface formation removes the relaxation of the free GaAs surface. As has been discussed in Section II.A, this means that unoccupied states are pulled into the band gap at the replacement interaction. Again, there is not yet any direct experimental observation confirming the existence of these unoccupied states.

D. Additional Aspects of Group III Metal Overlayers

In the preceding section we discussed in some detail the surface electronic structure of GaAs(110)+Al. Quite naturally there is a strong similarity between the predicted effects that Ga and Al overlayers will have on the changes in the surface electronic structure. Thus the theoretical and experimental work by Chadi and Bachrach[163] for Ga overlayers favors a configuration where the Ga atom is in a twofold coordinated site, i.e. forms a bond to a

Ga substrate atom in addition to its bond with the substrate As atom. The main support for this model comes from photoemission studies of the valence band. But, as is the case for Al overlayers, no experimental evidence has been found for the unoccupied states pulled down into the band gap due to removal of the substrate surface relaxation.

In the remainder of this section we concentrate on the effects that Group III metal overlayers (Al, Ga, In) have on the Fermi-level pinning.[165] The physical mechanism behind the pinning and Schottky-barrier formation is discussed in Section VI; the emphasis here will be on generally observed trends for the Fermi-level pinning as a function of metal coverage. In was evaporated from a bead source in the same way as Al (see Section C), while Ga was evaporated from a quartz crucible. Deposition rates were typically about or less than 5 Å min^{-1}. Particular care has to be taken in outgassing the Ga crucible to avoid impurities.

In the following we will study both n- and p-type GaAs (110). An explanatory remark should be made on how the Fermi-level position was determined in these cases (further discussion on the Fermi-level identification was given in Section A). For degenerately doped p-type GaAs there is no band bending and the Fermi level can be determined on an absolute scale to $\pm 0{\cdot}1$ eV relative to the valence band maximum. The flat band condition can be verified by cleaving degenerately doped n-type GaAs without pinning, and noting that the shift of the valence band relative to E_F is equal to the band gap. The basic point in the data and analysis presented below is that we do not have to assume *a priori* that p-type or n-type GaAs is unpinned. This is important since there is considerable confusion in the published literature due to the fact that p-type GaAs was always assumed to be unpinned (see below).

Stepwise deposition of the metal overlayer, beginning with (in most cases) less than 10^{14} atoms cm^{-2}, allowed the evolution of the band bending and electronic states to be observed as the coverage was increased. Photoemission energy distribution curves taken during a series of Ga depositions on n-type GaAs using $h\nu = 21$ eV are shown in Fig. 42 as a typical example for the Group III metals on (110) GaAs. The position of the Fermi energy was determined from a photoemission spectrum taken at the same photon energy of an Au substrate which was electrically shorted to the semiconductor samples, as discussed in Section A. The spectrum of the clean surface shows that the initial degree of band bending is small (~0·1 eV) and that the structure over the entire valence band, which is approximately 14 eV wide, is slightly smeared. This smearing can be due to both strain at the surface and non-uniform pinning (see Section III.C). The structure is typically sharper on well cleaved surfaces of p-type GaAs. The valence band structure had sharpened considerably after deposition of only $0{\cdot}05 \times 10^{15}$ cm^{-2} Ga ($0{\cdot}9 \times 10^{15}$ cm^{-2} = 1 monolayer), indicating that the surface Fermi energy was uniform and the strain reduced

by the metal. An increase of 0·2 eV in the band bending was produced by $0{\cdot}05 \times 10^{15}\,cm^{-2}$ Ga, but emission from states in the band gap was not yet evident. The next Ga deposition increased the total coverage to $0{\cdot}5 \times 10^{15}\,cm^{-2}$ and increased the band bending to 0·5 eV in a continuation of the trends seen after the first deposition. Note that some weak emission is seen from states between the GaAs valence band maximum and the Fermi energy. Further increases in Ga coverage did not produce appreciable changes in the band bending. At 2 monolayers coverage the GaAs valence band structure is somewhat attenuated, and the emission from the states above the GaAs valence band maximum is stronger and resembles emission from Ga metal.

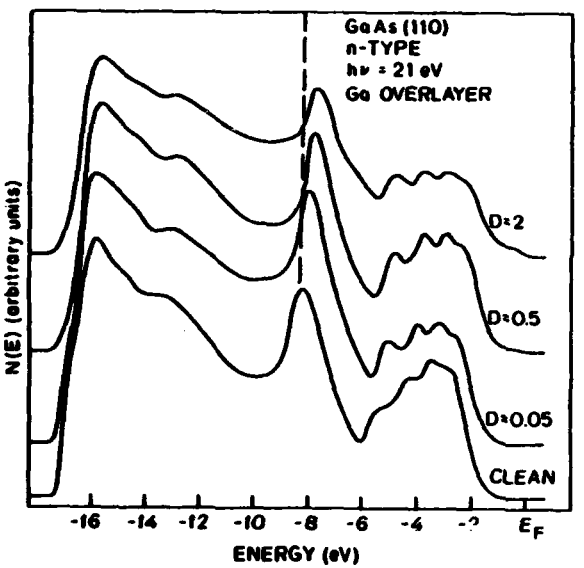

Fig. 42. Valence band photoemission spectra at sequential stages of Ga deposition on n-type GaAs (110). The dosage, D, is given in units of $10^{15}\,cm^{-2}$. (From ref. 165)

CFS spectra were obtained from the same surface (see Fig. 43). The strong peak at $h\nu = 28{\cdot}6$ eV on the clean surface is due to excitation of the Ga 3d core level into the energy window of the CMA, which was centered at 4 eV kinetic energy. The two small peaks at 19·5 and 20·0 eV are produced by excitation of Ga 3d electrons into excitonic levels associated with empty surface or conduction band states, as discussed in Section II.C. The difference in energy of these two peaks (0·5 eV) is just the spin–orbit splitting of the Ga 3d core level. After $0{\cdot}5 \times 10^{15}\,cm^{-2}$ of Ga was deposited on the surface the Ga 3d peak

position shifted by 0·4 eV due to band bending, as seen in the valence band EDCs (Fig. 42). The overlap between the metallic Ga 3d (3/2) and the semiconductor Ga 3d (5/2) makes the Ga 3d peak unreliable for determination of the E_F shift at the highest coverage. The peaks associated with the empty states near the conduction band minimum are of greatest interest here since movement of surface states into the band gap would produce pinning on n-type material. As the Ga overlayer thickness is increased, the excitonic peaks are reduced in amplitude until they are nearly gone at 2 monolayers coverage. However, no movement in energy position of these states is observed. The excitonic states are also stationary in the cases of O_2 and Au, as discussed earlier in Section II.C and above in Section B. However, for O_2 and Au the peaks are eliminated at coverages of less than 1 monolayer Au and at less than

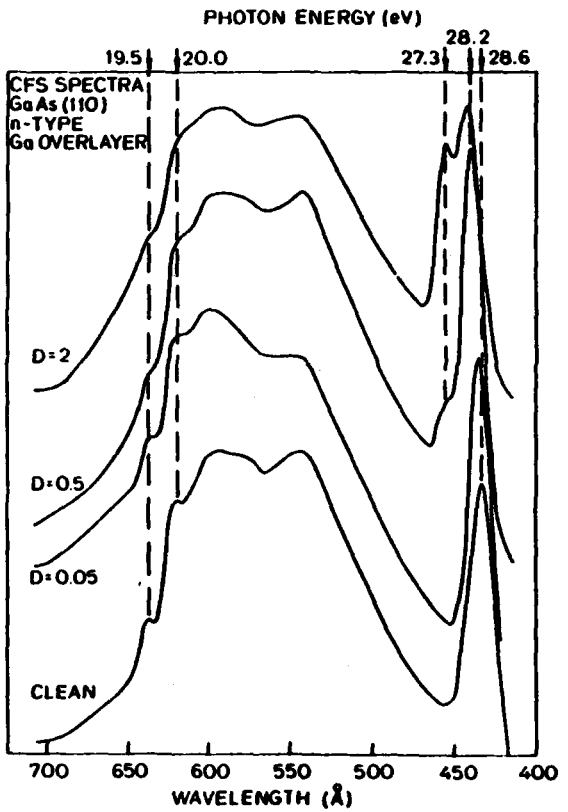

Fig. 43. CFS spectra for the same Ga exposed GaAs surfaces as shown in Fig. 42. The excitonic structure at 19·5 and 20·0 eV is marked with dashed lines. (From ref. 165)

0·5 monolayer O_2. The weak persistence of the excitonic peaks with Group III metal overlayers at about 1 monolayer coverage may be due to a small percentage of uncovered Ga sites or related to the lack of strong disordering (as evidenced by sharp valence band structure) with these overlayers. Future LEED studies would be helpful in clarifying this point.

The variation of E_{VS} at submonolayer coverages is critical to the evaluation of different models for Schottky-barrier formation and is shown in detail in Fig. 44. Here we see that the trend for barrier formation at low coverages is similar for Al, Ga, and In; the pinning is fairly well stabilized by a coverage of $0{\cdot}2 \times 10^{14}\,cm^{-2}$ on both n- and p-type GaAs, and seems to approach a common value for a given bulk doping, regardless of whether the surface was originally unpinned or partly pinned. Some variation is seen in the coverage at which the pinning becomes stabilized, but it is not clear whether any systematic trend in this regard can be extracted from the data. For example, In appears to produce stabilized pinning at a lower coverage than Ga or Al, in general, but also note the large variation of the Ga coverage at which stabilization of the pinning occurs on p-type GaAs. This latter effect may be due to the interaction of Ga with defects produced at the surface by metal deposition.

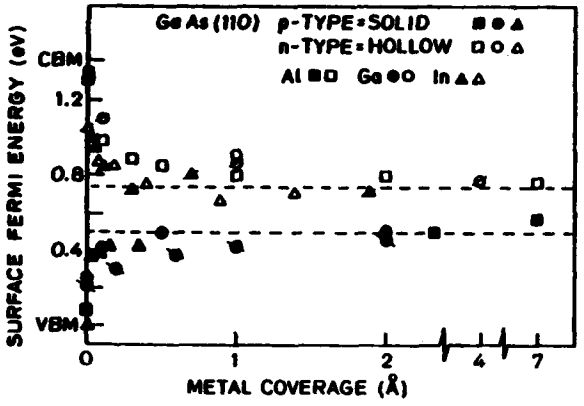

Fig. 44. Variation of band bending as a function of metal coverage of Al, Ga, and In on n- and p-type GaAs (110). Points with a slashed line indicate a second cleave on the same crystal. Note the difference in pinning position on n- vs. p-type samples. (From ref. 165)

A general picture of the sequence of events as the metal coverage is increased from zero can be constructed from these data. At coverages on the order of $0{\cdot}1 \times 10^{13}\,cm^{-2}$, UPS data show that some strain which may be present at the interface is relieved and the pinning becomes fairly uniform across the surface.

Pinning is usually stabilized at or below $0{\cdot}2 \times 10^{13}\,cm^{-2}$ coverage between 0·75 and 0·85 eV on n-type and 0·5 and 0·6 eV on p-type GaAs. As the coverage is increased up to 2 monolayers, EDC structure remains sharp but becomes attenuated, while the excitonic structure in the CFS data almost disappears.

The Fermi energy pinning behavior for Ga on p-type GaAs (110) reported here is not in agreement with the absence of pinning for the same system reported by Bachrach.[160] However, we believe that a closer examination of the photoemission data may help resolve this difference. We note that Ga pins n-type GaAs at 0·8 eV above the valence band maximum (see Fig. 42) and that this corresponds to a separation between metallic and semiconductor Ga 3d core levels of 0·9 eV (see Fig. 43). On p-type GaAs, Ga pins the Fermi level ~0·25 eV closer to the valence band maximum (see Fig. 44), and thus the separation between metallic and semiconductor Ga 3d core levels should also decrease by the same amount to become ~0·65 eV. Bachrach reported that the separation of metallic and semiconducting Ga 3d core levels was 0·6 eV—in excellent agreement with our results and conclusive proof of pinning. His conclusion of no pinning was based on an assumption of an unpinned clean surface and the observation of little or no shift of the Fermi energy as Ga was deposited. Clearly, the assumption of no pinning on the clean surface was not justified and, by examination of core level data, we find that Bachrach[160] and ourselves[165] are in agreement on the pinning position for Ga on p-type GaAs (0·5–0·6 eV above the valence band maximum).

V. OXYGEN ADSORPTION ON SURFACES COVERED WITH THIN Al AND Cs OVERLAYERS

The effects of very thin Al and Cs overlayers on the electronic properties of GaAs surfaces are relevant in a number of technologically important areas, e.g. GaAs passivation, Schottky-barrier formation, negative electron affinity (NEA) photocathodes, and oxidation processes in metals. To study the effect of thin layers, Al (~1 to 4 monolayers) and Cs (~1 monolayer) were deposited onto GaAs (110) surfaces which were then exposed to oxygen at room temperature.[166–168]

Structure in the photoemission energy distribution curves was uniformly attenuated as the Al overlayer thickness increased.[166] Emission from the Ga 3d core level was broadened owing to the presence of metallic Ga, as discussed in Section IV.C (replacement reaction between Ga and Al) (see Fig. 45). The As 3d core level is attenuated without any apparent shift or broadening. The weak valence band emission from the aluminized surface is mainly due to the GaAs substrate.

Exposure of the aluminized surface to unexcited oxygen resulted in the chemisorption of oxygen onto the Al followed by rapid oxide formation,

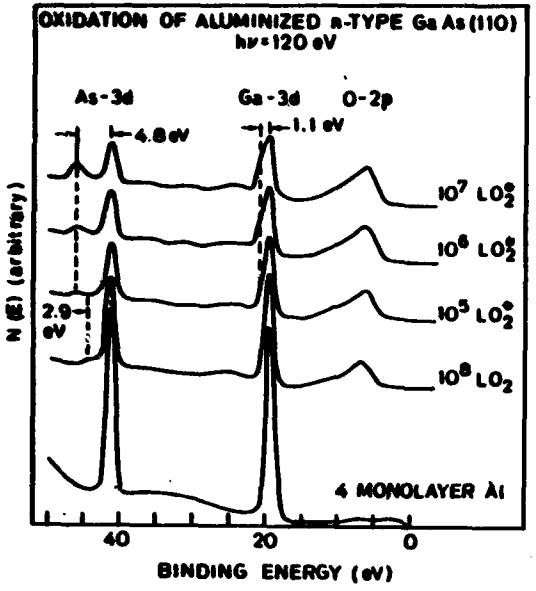

Fig. 45. Photoemission spectra of aluminized GaAs (110) before and after exposure to unexcited molecular oxygen, O_2, and excited oxygen, O_2*. (From ref. 166)

similar to reports in the literature on the oxidation of bulk Al.[169] Oxidation of the Al overlayer was completed between 10^3 and 10^4 L O_2, but the lack of a shifted As 3d peak provided evidence that oxidation of the GaAs had not occurred. Further exposure to unexcited oxygen (up to 10^8 L) resulted in the oxidation of a small amount of Ga, roughly equal to the metallic Ga contained in the Al overlayer. The weak emission which extends to approximately 3 eV beyond the As 3d peak on the high binding energy side is probably due to chemisorption of oxygen on a small fraction of the surface As.

Oxygen exposures were then begun with an ionization gauge operating in the chamber for production of excited oxygen (see Section III.B). At an exposure of 10^6 L excited O_2, a new shifted As 3d peak began to appear and was well established by 10^7 L excited O_2 ($\Delta E = 4{\cdot}8$ eV). This is in good agreement with the shift associated by Pianetta *et al.*[92] with As coordinated by four oxygen atoms (Section III.E).

The Fermi energy, which was near the conduction band minimum (CBM) for the freshly cleaved GaAs surface, was pinned $0{\cdot}8 \pm 0{\cdot}15$ eV below the CBM after the Al deposition (see Fig. 37). The change in band bending following oxidation of the Al was small. At most, there is a ~0·1 eV relaxation following exposure to 10^8 L unexcited oxygen. Similar relaxations were

observed with the other Group III metals: a relaxation of ~0·05 eV at a Ga-covered (~1 monolayer) surface after an exposure to 10^5 L unexcited oxygen and a relaxation of ~0·15 eV at an In-covered (~1 monolayer) surface after an exposure to 3×10^6 L unexcited oxygen.[166]

A typical set of spectra from different oxygen exposures of the bare GaAs (110) surface was shown in Fig. 20. An exposure of 10^7 L O_2 produced only a small shoulder on the As 3d, but 5×10^7 L O_2 resulted in a distinct peak ($\Delta E = 2{\cdot}9$ eV) which has been associated by Pianetta *et al.*[92] with the chemisorption of oxygen on surface As atoms. In the case of the aluminized surface, only 10^4 L unexcited O_2 was required to oxidize the Al overlayer, but a total exposure of 10^8 L unexcited O_2 yielded only a small shoulder on the As 3d core level. This shoulder is probably due to oxygen chemisorption on a small fraction of As at the semiconductor surface. However, at least an order of magnitude greater oxygen exposure was necessary to produce a detectable shifted As 3d peak with the Al oxide overlayer as compared with the bare surface. One likely explanation is that oxygen transport to the semiconductor was impeded by the oxide. Another possibility is that most As dangling bonds at the semiconductor surface were involved in bonding to Al atoms in the oxide overlayer.

A comparison of spectra from the aluminized and the bare surface after exposure to excited oxygen further demonstrates the slower oxidation for the aluminized surface. The excited oxygen spectra in Fig. 45 were obtained from a fresh surface that had not been previously exposed to unexcited oxygen. The oxidation of the bare surface begins with the appearance of a shifted As 3d peak (10^5 L O_2*, $\Delta E = 3{\cdot}1$ eV) similar to that observed using unexcited O_2 (5×10^7 L O_2, $\Delta E = 2{\cdot}9$ eV) but, as the exposure is increased, a second shifted peak ($\Delta E = 4{\cdot}6$ eV) grows and eventually dominates the first shifted As 3d peak, and broadening of the Ga 3d peak is observed. In the model given by Pianetta *et al.*[92] the first shifted As 3d core level corresponds to the chemisorption of oxygen on the surface As, and the second shifted As 3d core level corresponds to the breaking of back bonds and oxide formation. This sequence of events is not the same in the case of the aluminized surface. The only change in the As 3d core level is the appearance of the shifted peak corresponding to oxide formation with As coordinated by four oxygens. This seems to indicate that most of the interfacial As atoms are in sites such that chemisorption of oxygen onto these As atoms cannot occur, i.e. the Al_2O_3 overlayer may be joined to the substrate by interfacial Al–As bonds.

A dramatic change in oxidation behavior of the GaAs (110) surface was seen after cesiation.[167,168] For these studies, a monolayer of Cs was deposited onto a cleaved GaAs (110) surface which was then exposed to different amounts of oxygen in a controlled manner. Photoemission spectra at a photon energy of 120 eV are shown in Figs 46 and 47 for different oxygen exposures between 10

and 10^3 L. A chemically shifted peak appears 2.9 eV below the As 3d peak at 10 L O_2 exposure (Fig. 46). The binding energy position of this shifted peak is identical to that observed for oxygen chemisorbed on the clean GaAs (110) surface. However, the spectrum after 20 L O_2 for the cesiated surface is comparable to the spectrum after 5×10^7 L O_2 for the bare surface. Thus, the rate of oxygen uptake is 10^6–10^7 times larger on the cesiated surface.

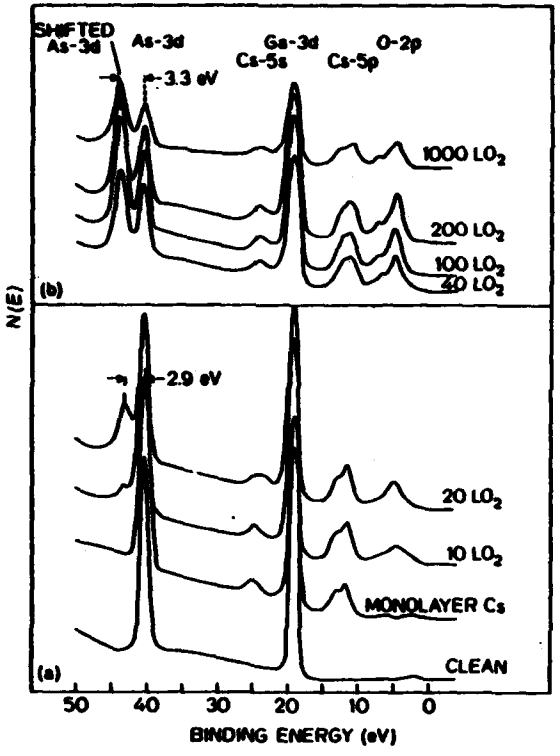

Fig. 46. Photoemission spectra ($h\nu$ = 120 eV) of clean GaAs (110) and of the same surface covered with a monolayer of Cs and then exposed to different amounts of oxygen. (From ref. 168)

As the oxygen uptake is increased, the Cs core-level binding energies decrease (about 0.8 eV—see Figs. 46 and 47), while that of the shifted As 3d level increases (about 0.4—see Fig. 46) up to exposures of 40 L O_2, after which the core levels stay constant in energy position to the highest exposure used (10^3 L). These continuous shifts may be due to interactions between a Cs suboxide layer and the outer GaAs layer containing chemisorbed oxygen.

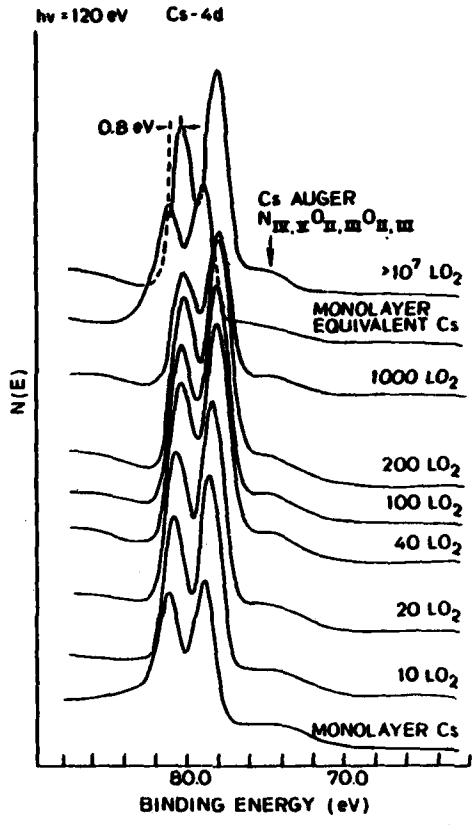

Fig. 47. Photoemission spectra ($h\nu$ = 120 eV) of the Cs 4d core levels for the same surfaces as shown in Fig. 46. The top two curves show the shift caused by a second dose of Cs and then followed by a new O_2 exposure. (From ref. 168)

James *et al.*[170] demonstrated that either the (Cs–O)-vacuum interface or the (Cs–O)-substrate interface could provide the potential barrier which sets the yield threshold of a photocathode. There they attributed the (Cs–O)-substrate interfacial barrier to the heterojunction between the Cs–O layer and the semiconductor substrate. The oxygen chemisorbed on the As of GaAs, as found by the present work, can be another origin of the interfacial barrier because the O–As dipole is oriented in the direction to form barriers for the electrons escaping from the substrate. For a thin Cs–O layer where the (Cs–O)-vacuum interface is important in controlling the threshold, the continuous chemical shift of the Cs peaks reveals that different states of the (Cs–O)-vacuum interface can be reached through the interaction between the

oxidized substrate and the Cs–O layer. Although a definite picture awaits more experiments, we have demonstrated the importance of the chemically active substrate, which has been assumed to be inert in all the existing models for NEA photocathodes.[170–172]

In summary, we can state that exposure of bare and cesiated GaAs (110) surfaces to unexcited oxygen results in the same chemisorption state of oxygen on As, but the oxygen uptake is more than a factor of 10^6 faster for the cesiated surface. On the other hand, aluminization is found to slow the oxygen interaction with the GaAs substrate. As in the case of the aluminized surface, the stabilization of the Fermi energy within the band gap at the cesiated surface was essentially unaffected by oxidation. The similarity in pinning position (within 0·3 eV) of metal and oxide overlayers is another indication that the pinning mechanisms in these two very different situations are very closely related, as will be discussed in Section VI. In the case of aluminized GaAs, the pinning position remained the same within 0·1 eV for the sequential stages of aluminization ($\theta \gtrsim 2$ Å), oxidation of the Al, and further oxygen exposure until oxidation of the semiconductor was accomplished with excited oxygen. The use of Cs instead of Al produced striking changes in the oxidation behavior of the GaAs, yet the pinning position was essentially the same throughout the oxidation.

VI. DEFECT STATES MODEL FOR SCHOTTKY BARRIER FORMATION

In previous sections we have discussed the electronic properties of a metal overlayer interacting with a metal–semiconductor substrate. We have also mentioned briefly how the Fermi-level stabilization (Schottky-barrier height) depends on the thickness and choice of the metal overlayer. The formation of Schottky barriers on semiconductor and insulator surfaces has been the subject of great attention during several decades because of the important applications in practical devices. Therefore we will discuss briefly how these recent results for metal overlayers on semiconductors have led to a new model for Schottky-barrier formation, based on defect states at the interface.[134,173,174]

One common feature for all the metal overlayers on GaAs (110), discussed in previous sections, is that the Fermi-level pinning is essentially completed at a coverage of only 0·1 monolayer. This implies that the important mechanism for the Fermi-level stabilization is not dependent on a continuous bulk-like metal overlayer. Another general observation is that the Fermi-level pinning position is independent of the adatom. This is summarized in Fig. 48 which shows the pinning position for a number of different metals (Cs, Al, Ga, In, Au) and oxygen.[134,173] As a comparison, the results for GaSb and InP are also

shown. It should be noted that the pinning positions for each semiconductor fall in a distinct and separate part of the band gap; for InP in the upper part of the gap, for GaAs in mid-gap, and for GaSb near the valence band maximum. Since the pinning position is independent of the nature of the adatom, it is difficult to rationalize that the produced energy levels are directly related to the adatoms.

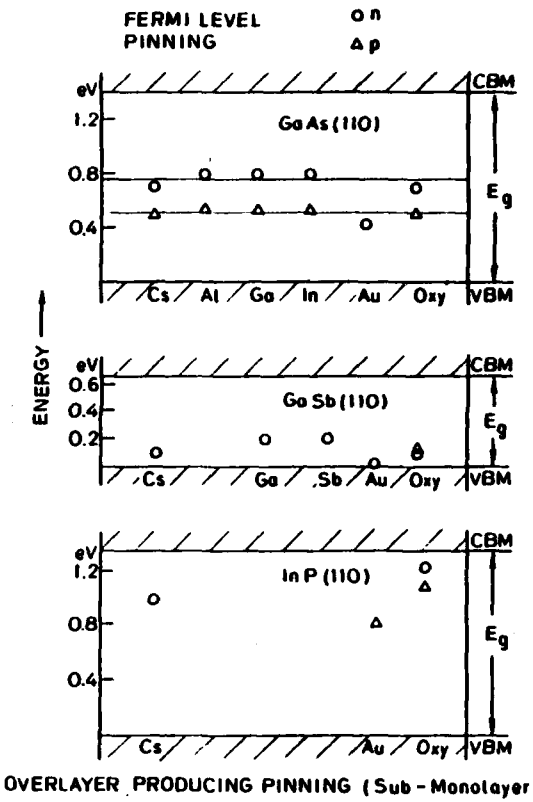

Fig. 48. The Fermi-level positions in the band gaps for GaAs (110), GaSb (110), and InP (110) for a number of different metals and oxygen. (From ref. 173)

The two observations described above—that the barrier height is fully developed at submonolayer coverages, and that the barrier height is to a first approximation independent of the adatom—form the essence of a model where defect levels close to the metal–semiconductor interface are responsible for the Fermi-level pinning. The severe disruption of the III–V semiconductor

surface due to the metal overlayer (see Section IV.B) is further support for the defect states model. Some insight into the driving force behind the disruption can be obtained by plotting the index of interface behavior, S, as a function of the heat of formation (see Fig. 49).[134,150] If the heat of condensation (of the metal) is used to measure the ease of defect formation, it should be noted that the compounds with higher heats of formation ($S = 1$ in Fig. 49) will probably form fewer defects than the more covalent materials ($S \approx 0$). From these arguments, it follows that the influence of defects on the Fermi-level pinning will be stronger for the latter class of materials. As is seen in Fig. 49, the heat of condensation for practically all metals is larger than the heat of formation of GaAs.

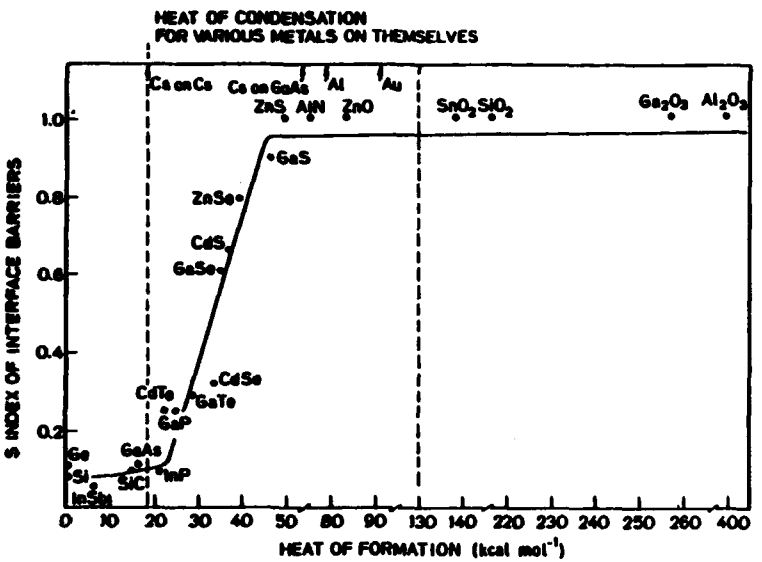

Fig. 49. The index of interface behavior, S, plotted against the heat of formation for various compounds. Also shown is the range of heat of condensation for various metals. (From ref. 134)

Finally, a short comment on the nature of the defects may be appropriate. From the data of Fig. 48 it is apparent that at least two levels at or near the surface are necessary to fit the experimental results for GaAs and InP, whereas one is probably sufficient for GaSb. Where two levels are needed, one must be a donor and the other an acceptor. Figure 50 shows the assigned levels and suggests the defect responsible for each. The level positions were obtained from the final pinning position due to the metal or oxygen adatoms.[174] Also indicated in Fig. 50 is a suggestion as to the simplest source of the defect—a

missing Group III or V atom. This is not to say that the defect is a simple vacancy (it may be more complicated) but that it is the result of a missing atom of the indicated species. Further details of how the assignment of the different defects was obtained can be found elsewhere.[173,174] It is noteworthy, however, that the pinning positions observed here with a method probing the interface on a microscopic scale correlate very well with the barrier heights for device MOS structures. Some further details for GaAs are given in Table V.

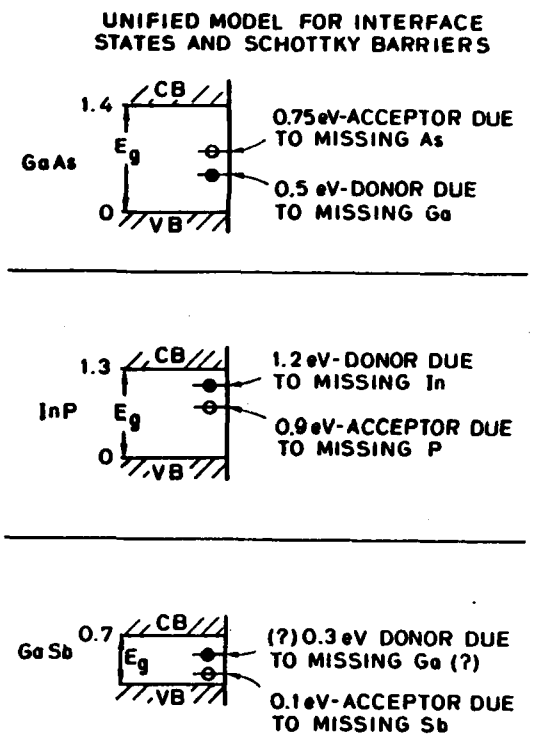

Fig. 50. A model of energy levels for extrinsic states produced near or at the interface. Each level is tentatively associated with a deficit of an anion or cation. However, it is unlikely that the defect is a simple vacancy; it is probably instead an anti-site or a more complicated defect. (From ref. 174)

VII. CONCLUDING REMARKS

This review has attempted to give a fairly detailed description of the surface electronic structure of GaAs (110) and the effects oxygen and metal overlayers have on this surface. A good understanding is now available for the basic

TABLE V

Fermi Energy Pinning Position with Respect to Conduction Band Minimum for n-Type GaAs after Surface Treatment

Thick "device" oxide	Submonolayer of chemisorbed oxygen	Submonolayer to several monolayers of		
		Cs	Al, Ga, In	Au
0·83 (ref. 175) 0·8 (ref. 176) 0·5 (ref. 177)	0·65–0·8 (refs 92 and 178)	0·6–0·8 (ref. 179) 0·7 (ref. 180)	0·6–0·7 (ref. 165)	0·9–1·0 (ref. 136)

The similarity between the Fermi-level pinning position for thick oxides formed by various techniques and that obtained by a fraction of a monolayer of oxygen should be noted. It should also be noted that the pinning position for Schottky barriers is close to that for oxygen.

geometrical configuration of the Ga and As atoms in the surface lattice on the clean (110) surface. More extensive angle-resolved photoemission measurements, using the polarization and tunability of the synchrotron radiation, should be fruitful in determining the energy position, orbital symmetry, and the cation/anion composition of the surface states/resonances. The capability of photoemission to provide information on the geometrical rearrangements of the surface Ga and As atoms has been only partly explored in the past, and further work should be continued. These investigations should be in parallel with further developments of the theoretical work which has been so productive and successful during the past few years.

Much progress has been made in the understanding of the oxygen chemisorption and initial oxidation stages of the GaAs (110) surface, but a number of fundamental issues still remain to be solved particularly regarding the surface species formed under different exposure conditions and in different exposure ranges. Further and extended comparisons with standards (similar to those for oxidation of Ga metal; Section III.C) appear to be crucial in this regard. Another set of critical experiments involves a study of the induced changes in the valence and core levels as the temperature is increased, and comparison of these results at low oxygen exposures with those for high exposures (excited oxygen) at room temperature. A conversion between different surface species, if existing, may be followed in this manner. Very few LEED investigations have been done but it is obvious from Section III.H that future photoemission studies of the oxygen interaction should be combined with LEED intensity measurements.

Characteristic of all the metal overlayers studied on the GaAs (110) surface is the very strong interaction between the metal and substrate, resulting in a non-abrupt interface with intermixing or replacement taking place. The experimental establishment of a non-abrupt interface has already had a profound impact in formulating new models for Schottky barriers. The physical mechanism behind the strong intermixing is, however, not yet well understood, e.g. to what extent the heat of the metal condensation and/or the heat of the alloy/compound formation are the driving mechanisms. Formation of the metal/GaAs(110) interfaces at low temperatures and monitoring of the metal–semiconductor interaction as a function of temperature are extremely important, and such experiments should be initiated. As in the case of oxygen adsorption, the photoemission measurements should be combined with LEED intensity studies, particularly to confirm or refute the theoretical prediction that certain metal overlayers will remove the surface relaxation in the topmost GaAs layer.

It has been emphasized in this review that a thin metal layer (monolayer) will have a dramatic effect on the oxygen interaction with the GaAs substrate. Very few experimental results are available on this important aspect of the passivation properties of the GaAs surface. Future experimental studies are certainly called for.

Strong experimental evidence now exists for the applicability of the defect states model in explaining the Schottky-barrier formation on III–V surfaces. A natural extension in understanding the nature of these defects will involve experiments where the III–V surface is dosed in a controlled manner with anions and cations. Such experiments will be an important first step in engineering Schottky-barrier heights to a predetermined and desired value. The development of theoretical models to describe the defect states will be crucial for future progress in this field.

Acknowledgement

The support from the U.S. Defense Advanced Projects Agency, the Army Office of Research, the National Science Foundation, and the Office of Naval Research is gratefully acknowledged. Part of this work was performed at the Stanford Synchrotron Radiation Laboratory which is supported by the National Science Foundation in cooperation with the Stanford Linear Accelerator Center and the Department of Energy.

REFERENCES

1. J. H. Dinan, L. K. Galbraith, and T. E. Fischer, *Surf. Sci.* **26**, 587 (1971).
2. D. E. Eastman and W. D. Grobman, *Phys. Rev. Lett.* **28**, 1378 (1972).

3. P. E. Gregory, W. E. Spicer, S. Ciraci, and W. A. Harrison, *Appl. Phys. Lett.* 25, 511 (1974).
4. H. Froitzheim and H. Ibach, *Surf. Sci.* 47, 713 (1975).
5. P. E. Gregory and W. E. Spicer, *Phys. Rev.* B13, 725 (1976).
6. J. van Laar and J. J. Scheer, *Surf. Sci.* 8, 342 (1967).
7. A. Huijser and J. van Laar, *Surf. Sci.* 52, 202 (1975).
8. J. van Laar and A. Huijser, *J. Vac. Sci. Technol.* 13, 769 (1976).
9. A. Huijser, J. van Laar, and T. L. van Rooy, *Surf. Sci.* 62, 472 (1977).
10. J. van Laar, A. Huijser, and T. van Rooy, *J. Vac. Sci. Technol.* 14, 894 (1977).
11. D. E. Eastman and J. L. Freeouf, *Phys. Rev. Lett.* 33, 1601 (1974).
12. J. L. Freeouf and D. E. Eastman, *Crit. Rev. Solid State Sci.* 5, 245 (1975).
13. D. E. Eastman and J. L. Freeouf, *Phys. Rev. Lett.* 34, 1624 (1975).
14. W. Gudat and D. E. Eastman, *J. Vac. Sci. Technol.* 13, 831 (1976).
15. W. E. Spicer and P. E. Gregory, *Crit. Rev. Solid State Sci.* 5, 231 (1975).
16. W. E. Spicer, I. Lindau, P. E. Gregory, C. M. Garner, P. Pianetta, and P. W. Chye, *J. Vac Sci. Technol.* 13, 780 (1976).
17. W. E. Spicer, P. Pianetta, I. Lindau, and P. W. Chye, *J. Vac. Sci. Technol.* 14, 885 (1977).
18. P. W. Chye, P. Pianetta, I. Lindau, and W. E. Spicer, *J. Vac. Sci. Technol.* 14, 917 (1977).
19. I. Lindau, P. Pianetta, C. M. Garner, P. W. Chye, P. E. Gregory, and W. E. Spicer, *Surf. Sci.* 63, 45 (1977).
20. I. Lindau, P. Pianetta, W. E. Spicer, P. E. Gregory, C. M. Garner, and P. W. Chye, *J. Electron Spectrosc.* 13, 155 (1978).
21. P. Pianetta, I. Lindau, P. E. Gregory, C. M. Garner, and W. E. Spicer, *Surf. Sci.* 72, 298 (1978).
22. P. Mark, E. So, and M. Bonn, *J. Vac. Sci. Technol.* 14, 865 (1977).
23. F. Meyer and A. Kroes, *Surf. Sci.* 47, 124 (1975).
24. H. Froitzheim and H. Ibach, *Surf. Sci.* 47, 713 (1975).
25. J. E. Rowe, S. B. Christman, and G. Margaritondo, *Phys. Rev. Lett.* 35, 1471 (1975).
26. R. Ludeke and A. Koma, *J. Vac. Sci. Technol.* 13, 241 (1976).
27. G. M. Guichar, C. A. Sebenne, and G. A. Garry, *Phys. Rev. Lett.* 37, 1158 (1976).
28. K. C. Pandey, J. L. Freeouf, and D. E. Eastman, *J. Vac. Sci. Technol.* 14, 904 (1977).
29. K. C. Pandey, *J. Vac. Sci. Technol.* 15, 440 (1978).
30. J. A. Knapp, D. E. Eastman, K. C. Pandey, and F. Patella, *J. Vac. Sci. Technol.* 15, 1252 (1978).
31. J. A. Knapp and G. J. Lapeyre, *J. Vac. Sci. Technol.* 13, 757 (1976).
32. G. P. Williams, R. J. Smith, and G. J. Lapeyre, *J. Vac. Sci. Technol.* 15, 1249 (1978).
33. A. Huijser, J. van Laar, and T. L. van Rooy, *Phys. Lett.* 65A, 335 (1978).
34. G. J. Lapeyre and J. Anderson, *Phy. Rev. Lett.* 35, 117 (1975).
35. P. Thiry, Y. Petroff, R. Pinchaux, J. R. Chelikowsky, and M. L. Cohen, *Solid State Commun.* 20, 1107 (1976).
36. J. L. Freeouf, *Phys. Rev. Lett.* 36, 1095 (1976).
37. R. Del Sole and E. Tosatti, *Solid State Commun.* 22, 307 (1977).
38. R. S. Bauer, *J. Vac. Sci. Technol.* 14, 899 (1977).
39. J. C. McMenamin and R. S. Bauer, *J. Vac. Sci. Technol.* 15, 1262 (1978).
40. R. S. Bauer, D. J. Chadi, J. C. McMenamin, and R. Z. Bachrach, in "Proceedings of the Seventh International Vacuum Congress" and "Proceedings of the Third International Conference on Solid Surfaces" (IAEA, Vienna, 1977), p. A2699.

41. J. A. Appelbaum and D. R. Hamann, *Rev. Modern Phys.* 48, 479 (1976).
42. M. Schlüter, in "Festkorperprobleme XVIII", J. Treusch, ed. (Vieweg, Braunschweig, 1978), p. 155.
43. C. B. Duke, *Crit. Rev. Solid State Mater. Sci.* 8, 69 (1978).
44. J. D. Levine and S. Freeman, *Phys. Rev.* B2, 3255 (1970).
45. S. Freeman, *Phys. Rev.* B2, 3272 (1970).
46. J. D. Joannopoulos and M. L. Cohen, *Phys. Rev.* B10, 5075 (1974).
47. J. R. Chelikowsky and M. L. Cohen, *Phys. Rev.* B13, 826 (1976).
48. S. G. Louie, J. R. Chelikowsky, and M. L. Cohen, *J. Vac. Sci. Technol.* 13, 790 (1976).
49. J. R. Chelikowsky, S. G. Louie, and M. L. Cohen, *Phys. Rev.* B14, 4724 (1976).
50. C. Calandra and G. Santoro, *J. Phys.* C8, L86 (1975).
51. C. Calandra and G. Santoro, *J. Phys.* C9, L51 (1976).
52. C. Calandra and G. Santoro, *J. Vac. Sci. Technol.* 13, 773 (1976).
53. C. Calandra, F. Manghi, and C. M. Bertoni, *J. Phys.* C10, 1911 (1977).
54. N. Garcia, *Solid State Commun.* 17, 397 (1975).
55. E. J. Mele and J. D. Joannopoulos, *Surf. Sci.* 66, 38 (1977).
56. E. J. Mele and J. D. Joannopoulos, *Phys. Rev.* B17, 1816 (1978).
57. D. J. Chadi, *J. Vac. Sci. Technol.* 15, 631 (1978).
58. D. J. Chadi, *J. Vac. Sci. Technol.* 15, 1244 (1978).
59. D. J. Chadi, *Phys. Rev.* 18, 1800 (1978).
60. D. J. Miller and D. Haneman, *Phys. Rev.* B17, 5033 (1978).
61. S. Taugaard, *Phys. Rev.* B18, 3799 (1978).
62. W. Schwalm and J. Hermanson, *Solid State Commun.* 27, 587 (1978).
63. J. R. Chelikowsky and M. L. Cohen, *Solid State Commun.* 29, 267 (1979).
64. E. J. Mele and J. D. Joannopoulos, *Phys. Rev.* B19, 2928 (1979).
65. M. Nishida, *Surf. Sci.* 72, 589 (1978).
66. M. Nishida, *Solid State Commun.* 28, 551 (1978).
67. A. U. MacRae and G. W. Gobeli, *J. Appl. Phys.* 35, 1629 (1964).
68. A. U. MacRae and G. W. Gobeli, in "Semiconductors and Semi-metals", R. K. Willardson and A. C. Beer, eds, Vol. 2, Physics of III-V Compounds (Academic Press, New York, 1966), p. 115.
69. A. R. Lubinsky, C. B. Duke, B. W. Lee, and P. Mark, *Phys. Rev. Lett.* 36, 1058 (1976).
70. C. B. Duke, A. R. Lubinsky, B. W. Lee, and P. Mark, *J. Vac. Sci. Technol.* 13, 761 (1976).
71. A. Kahn, E. So, P. Mark, and C. B. Duke, *J. Vac. Sci. Technol.* 15, 580 (1978).
72. A. Kahn, E. So, P. Mark, C. B. Duke, and R. J. Meyer, *J. Vac. Sci. Technol.* 15, 1223 (1978).
73. A. Kahn, G. Cisneros, M. Bonn, P. Mark, and C. B. Duke, *Surf. Sci.* 71, 387 (1978).
74. G. Cisneros, *J. Vac. Sci. Technol.* 16, 584 (1979).
75. R. J. Meyer, C. B. Duke, A. Paton, A. Kahn, E. So, J. L. Yeh, and P. Mark, *Phys. Rev.* B19, 5194 (1979).
76. S. Y. Tong, A. R. Lubinsky, B. J. Mrstik, and M. A. Van Hove, *Phys. Rev.* B17, 3303 (1978).
77. C. B. Duke, R. J. Meyer, A. Paton, and P. Mark, *Phys. Rev.* B18, 4225 (1978).
78. P. Mark, S. C. Chang, W. F. Creighton, and B. W. Lee, *Crit. Rev. Solid State Sci.* 5, 189 (1975).
79. P. Mark, G. Cisneros, M. Bonn, A. Kahn, C. B. Duke, A. Paton, and A. R. Lubinsky, *J. Vac. Sci. Technol.* 14, 910 (1977).
80. D. J. Chadi, *Phys. Rev. Lett.* 41, 1062 (1978).

81. D. J. Chadi, *Phys. Rev.* **B19**, 2074 (1979).
82. D. J. Miller and D. Haneman, *J. Vac. Sci. Technol.* **15**, 1267 (1978).
83. D. J. Miller and D. Haneman, *Surf. Sci.* **82**, 102 (1979).
84. G. J. Lapeyre, R. J. Smith, J. A. Knapp, and J. Anderson, *J. Physique Colloq.* 39, C4-134 (1978).
85. R. Dorn, H. Lüth, and G. J. Russell, *Phys. Rev.* **B10**, 5049 (1974).
86. R. Dorn and H. Lüth, *Phys. Rev. Lett.* 33, 1024 (1974).
87. H. Lüth and G. J. Russell, *Surf. Sci.* 45, 329 (1974).
88. P. E. Gregory and W. E. Spicer, *Surf. Sci.* 54, 229 (1976).
89. H. Lüth, M. Büchel, R. Dorn, M. Liehr, and R. Matz, *Phys. Rev.* **B15**, 865 (1977).
90. P. Pianetta, I. Lindau, C. M. Garner, and W. E. Spicer, *Phys. Rev. Lett.* 35, 1356 (1975).
91. P. Pianetta, I. Lindau, C. M. Garner, and W. E. Spicer, *Phys. Rev. Lett.* 37, 1166 (1976).
92. P. Pianetta, I. Lindau, C. M. Garner, and W. E. Spicer, *Phys. Rev.* **B18**, 2792 (1978).
93. R. Ludeke, *Phys. Rev.* **B16**, 5598 (1977).
94. P. Pianetta, I. Lindau, C. M. Garner, and W. E. Spicer, *Phys. Rev.* **B16**, 5600 (1977).
95. R. Ludeke, *Solid State Commun.* 21, 815 (1977).
96. E. J. Mele and J. D. Joannopoulos, *Phys. Rev. Lett.* 40, 341 (1978).
97. J. D. Joannopoulos and E. J. Mele, *J. Vac. Sci. Technol.* 15, 1287 (1978).
98. E. J. Mele and J. D. Joannopoulos, *Phys. Rev.* **B18**, 6999 (1978).
99. W. A. Goddard III, J. J. Barton, A. Redondo, and T. C. McGill, *J. Vac. Sci. Technol.* 15, 1274 (1978).
100. H. Iwasaki, Y. Mozokawa, R. Nishitani, and S. Nakamura, *Jap. J. Appl. Phys.* 17, 1925 (1978).
101. H. Iwasaki, Y. Mizokawa, R. Nishitani, and S. Nakamura, *Jap. J. Appl. Phys.* 17, 315 (1978).
102. Y. Mizokawa, H. Iwasaki, R. Nishitani, and S. Nakamura, *J. Electron Spectrosc.* 14, 129 (1978).
103. Y. Mozokawa, H. Iwasaki, R. Nishitani, and S. Nakamura, in Proc. Ninth Conf. on Solid State Devices (Tokyo, 1977), *Jap. J. Appl. Phys.* 17, Suppl. 17-1, 327 (1978).
104. M. Kudo, Y. Nihei, and H. Kamada, *Jap. J. Appl. Phys.* 17, 797 (1978).
105. C. W. Wilmsen and R. W. Kee, *J. Vac. Sci. Technol.* 15, 1513 (1978).
106. P. Pianetta, I. Lindau, and W. E. Spicer, in "Quantitative Surface Analysis of Materials", N. S. McIntyre, ed. A symposium sponsored by ASTM Committee E-42 on Surface Analysis, Cleveland, Ohio, 2–3 March 1977 (ASTM Special Technical Publication 643), pp. 105–123.
107. W. E. Spicer, I. Lindau, P. Pianetta, P. W. Chye, and C. M. Garner, *Thin Solid Films* 56, 1 (1979).
108. W. E. Spicer, P. W. Chye, C. M. Garner, I. Lindau, and P. Pianetta, *Surf. Sci.* 86, 763 (1979).
109. P. W. Chye, C. Y. Su, I. Lindau, C. M. Garner, P. Pianetta, and W. E. Spicer, *Surf. Sci.* 88, 439 (1979).
110. P. W. Chye, C. Y. Su, I. Lindau, P. R. Skeath, and W. E. Spicer, *J. Vac. Sci. Technol.* 16, 1191 (1979).
111. C. R. Brundle and D. Seybold, *J. Vac. Sci. Technol.* 16, 1186 (1979).
112. C. Y. Su, I. Lindau, P. R. Skeath, P. W. Chye, and W. E. Spicer, *J. Vac. Sci. Technol.* 17, 936 (1980).

113. J. J. Barton, W. A. Goddard III, and T. C. McGill, *J. Vac. Sci. Technol.* 16, 1178 (1979).
114. I. Lindau and W. E. Spicer, in "Synchrotron Radiation Research", H. Winick and S. Doniach, eds (Plenum Press, New York, 1980), pp. 159–221.
115. I. Lindau and W. E. Spicer, *J. Electron Spectrosc.* 15, 295 (1979).
116. I. Lindau, in "International College on Applied Physics: Synchrotron Radiation Research" (Alghero, 12–14 September 1976), A. N. Mancini and L. F. Quercia, eds, p. 372.
117. S. Doniach, I. Lindau, W. E. Spicer, and H. Winick, *J. Vac. Sci. Technol.* 12, 1123 (1975).
118. F. C. Brown, R. Z. Bachrach, and N. Lien, *Nucl. Instr. Methods* 152, 73 (1978).
119. W. Ranke and K. Jacobi, *Surf. Sci.* 81, 504 (1979).
120. G. Schön, *J. Electron Spectrosc.* 2, 75 (1973).
121. R. Z. Bachrach, *J. Vac. Sci. Technol.* 15, 1340 (1978).
122. K. Osafume and K. Kimura, *Chem. Phys. Lett.* 25, 47 (1974).
123. M. K. Bahl, R. O. Woodall, R. L. Watson, and K. J. Irgolic, *J. Chem. Phys.* 64, 1210 (1976).
124. G. Leonhardt, A. Berndtsson, J. Hedman, M. Klasson, R. Nilsson, and C. Nordling, *Phys. Status Solidi* **B60**, 241 (1973).
125. Surface Science Laboratories (Palo Alto, Ca.), ESCA Analytical Service Report No. 9-576 (unpublished).
126. J. Hedman, M. Klasson, R. J. Lindberg, and C. Nordling, in "Electron Spectroscopy", D. A. Shirley, ed. (North-Holland, Amsterdam, 1972), p. 681.
127. P. Mark and W. F. Creighton, *Appl. Phys. Lett.* 27, 400 (1975).
128. R. W. G. Wyckoff, "Crystal Structures" (Interscience, New York, 1965), Vols 2 and 3.
129. P. Mark and W. F. Creighton, *Thin Solid Films* 56, 19 (1979).
130. I. Lindau and W. E. Spicer, *J. Electron Spectrosc.* 3, 409 (1974).
131. G. J. Russel and D. Haneman, *Surf. Sci.* 27, 362 (1971).
132. A. Kahn, D. Kanani, P. Mark, P. W. Chye, C. Y. Su, I. Lindau, and W. E. Spicer, *Surf. Sci.* 87, 325 (1979).
133. P. Mark, P. Pianetta, I. Lindau, and W. E. Spicer, *Surf. Sci.* 69, 735 (1977).
134. I. Lindau, P. W. Chye, C. M. Garner, P. Pianetta, C. Y. Su, and W. E. Spicer, *J. Vac. Sci. Technol.* 15, 1332 (1978).
135. P. W. Chye, I. Lindau, P. Pianetta, C. M. Garner, and W. E. Spicer, *Phys. Rev.* **B17**, 2682 (1978).
136. P. W. Chye, I. Lindau, P. Pianetta, C. M. Garner, C. Y. Su, and W. E. Spicer, *Phys. Rev.* **B18**, 5545 (1978).
137. I. Lindau, P. Pianetta, and W. E. Spicer, *Phys. Lett.* 57A, 225 (1976).
138. Y. J. van der Meulen, *Solid State Electron.* 7, 767 (1964).
139. D. Effer and P. J. Etter, *J. Phys. Chem. Solids* 25, 451 (1964).
140. Y. J. van der Meulen, *J. Phys. Chem. Solids* 28, 25 (1967).
141. H. Miki, K. Segawa, and K. Fujibayashi, *Jap. J. Appl. Phys.* 13, 203 (1974).
142. S. H. Overbury, P. A. Bertrand, and G. A. Somorjai, *Chem. Rev.* 75, 547 (1975).
143. G. A. Somorjai and S. H. Overbury, *Faraday Discuss. Chem. Soc.* 60, 279 (1975).
144. V. Simić and Ž. Marinković, *Thin Solid Films* 34, 179 (1976).
145. A. K. Sinha and J. M. Poate, *Appl. Phys. Lett.* 23, 666 (1973).
146. H. B. Kim, G. G. Sweeney, and T. M. S. Heng, *Inst. Phys. Conf. Ser.* 24, 307 (1975).
147. A. Hiraki, K. Shuto, S. Kim, W. Kammura, and M. Iwani, *Appl. Phys. Lett.* 31, 611 (1977).
148. R. B. Shalvoy, G. B. Fisher, and P. J. Stiles, *Phys. Rev.* **B15**, 1680 (1977).

149. M. Hansen, "Constitution of Binary Alloys" (McGraw-Hill, New York, 1958).
150. C. A. Mead and W. G. Spitzer, *Phys. Rev.* 134, A713 (1964).
151. P. W. Chye, I. Lindau, P. Pianetta, C. M. Garner, and W. E. Spicer, *Phys. Lett.* A63, 387 (1977).
152. G. Margaritondo, S. B. Christman, and J. E. Rowe, *Phys. Rev.* B14, 5396 (1976).
153. J. Derrien and F. Arnaud D'Avitaya, *Surf. Sci.* 65, 668 (1977).
154. J. A. Van Vechten, *J. Electrochem. Soc.* 122, 419 (1975).
155. L. J. Brillson, *J. Vac. Sci. Technol.* 15, 1378 (1978).
156. P. R. Skeath, I. Lindau, P. Pianetta, P. W. Chye, C. Y. Su, and W. E. Spicer, *J. Electron Spectrosc.* 17, 259 (1979).
157. S. A. Flodström, C. W. B. Martinsson, R. Z. Bachrach, S. B. M. Hagström, and R. S. Bauer, *Phys. Rev. Lett.* 40, 907 (1978).
158. W. Kischo, *Z. Anorg. Allg. Chem.* 328, 187 (1964).
159. D. D. Wagman, W. H. Evans, V. B. Parker, I. Halow, S. M. Bailey, and R. H. Schumm, National Bureau of Standards Technical Note No. 270-4 (U.S. GPO, Washington, D.C., 1969).
160. R. Z. Bachrach, *J. Vac. Sci. Technol.* 15, 1340 (1978).
161. R. Z. Bachrach, R. S. Bauer, J. C. McMenamin, and A. Bianconi, in "Proceedings of the Fourteenth International Conference on the Physics of Semiconductors", R. A. Stradling, ed. (Plessey, Edinburgh, 1978), p. 1073.
162. L. J. Brillson, R. Z. Bachrach, R. S. Bauer, and J. McMenamin, *Phys. Rev. Lett.* 42, 397 (1979).
163. D. J. Chadi and R. Z. Bachrach, *J. Vac. Sci. Technol.* 16, 1159 (1979).
164. E. J. Mele and J. D. Joannopoulos, *Phys. Rev. Lett.* 42, 1094 (1979).
165. P. R. Skeath, I. Lindau, P. W. Chye, C. Y. Su, and W. E. Spicer, *J. Vac. Sci. Technol.* 16, 1143 (1979).
166. P. R. Skeath, C. Y. Su, P. W. Chye, P. Pianetta, I. Lindau, and W. E. Spicer, *J. Vac. Sci. Technol.* 16, 1439 (1979).
167. C. Y. Su, P. W. Chye, P. Pianetta, I. Lindau, and W. E. Spicer, *Surf. Sci.* 86, 894 (1979).
168. W. E. Spicer, I. Lindau, C. Y. Su, P. W. Chye, and P. Pianetta, *Appl. Phys. Lett.* 33, 934 (1978).
169. S. A. Flodström, R. Z. Bachrach, R. S. Bauer, and S. B. M. Hagström, *Phys. Rev. Lett.* 37, 1282 (1976).
170. L. W. James, G. A. Antypas, J. J. Uebbing, T. O. Yep, and R. L. Bell, *J. Appl. Phys.* 42, 580 (1971).
171. L. W. James and J. J. Uebbing, *Appl. Phys. Lett.* 16, 370 (1970); *J. Appl. Phys.* 41, 4505 (1970).
172. B. Goldstein, *Surf. Sci.* 47, 143 (1975).
173. W. E. Spicer, P. W. Chye, P. R. Skeath, C. Y. Su, and I. Lindau, *J. Vac. Sci. Technol.* 16, 1422 (1979).
174. W. E. Spicer, P. W. Chye, P. R. Skeath, C. Y. Su, and I. Lindau, in "Insulating Films as Semiconductors 1979", Conf. Series No. 50, G. G. Roberts and M. J. Morant, eds (Institute of Physics, Bristol and London, 1979), pp. 216–233.
175. C. C. Chang, P. H. Citrin, and B. Schwartz, *J. Vac. Sci. Technol.* 14, 943 (1977).
176. L. G. Meiners, *J. Vac. Sci. Technol.*, 15, 1402 (1978).
177. A. Shimano, A. Moritani, and J. Nakai, *Jap. J. Appl. Phys.* 15, 939 (1977).
178. P. R. Skeath, W. A. Saperstein, P. Pianetta, I. Lindau, W. E. Spicer, and P. Mark, *J. Vac. Sci. Technol.* 15, 1219 (1978).
179. P. Gregory and W. E. Spicer, *Phys. Rev.* B12, 2370 (1975).
180. J. J. Uebbing and R. L. Bell, *Appl. Phys. Lett.* 11, 357 (1967).

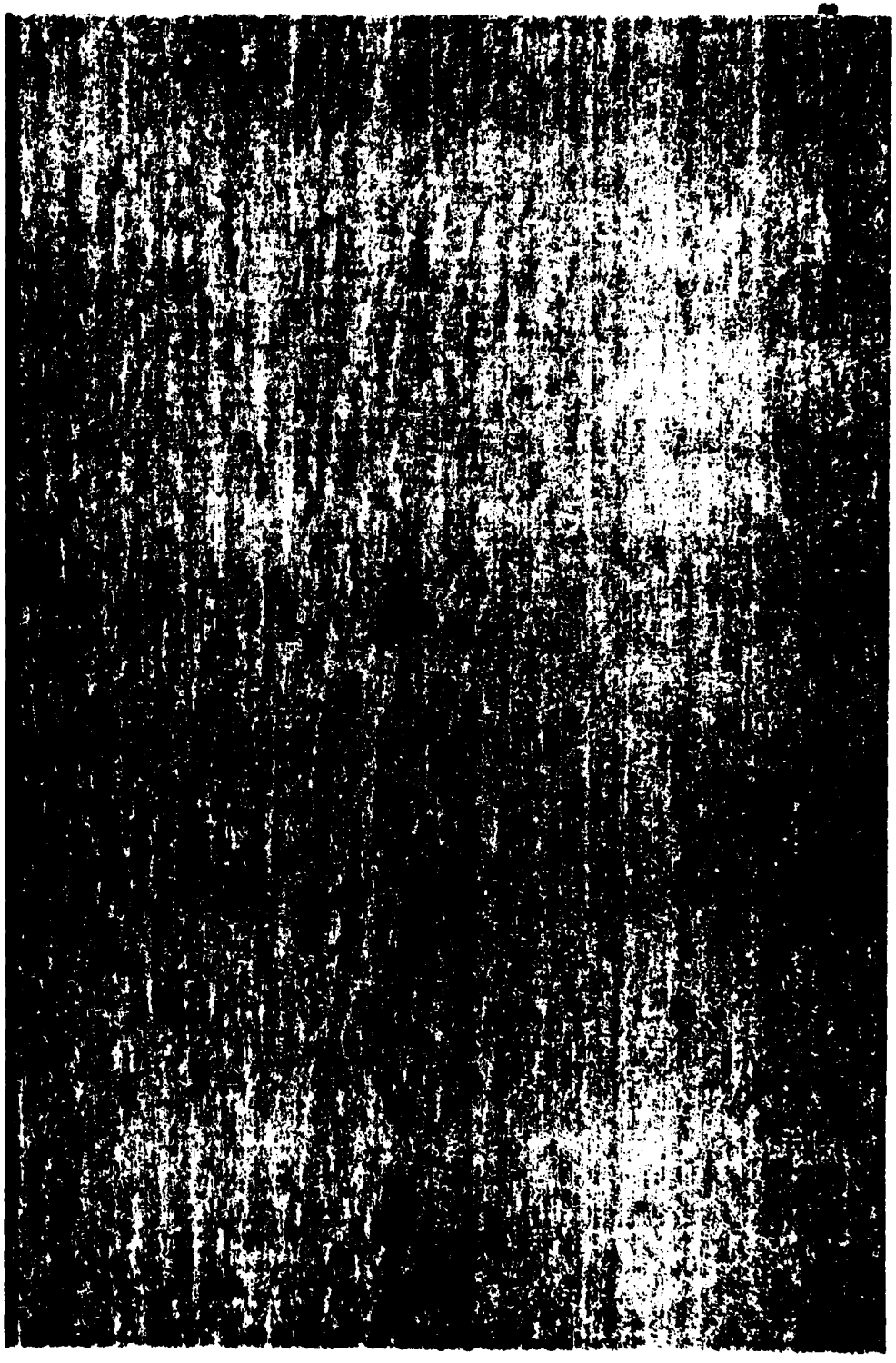

L. Stephen J. Eglash, Shihong Pan, William E. Spicer, and Douglas M. Collins, "Modified Schottky Barrier Heights by Interfacial Doped Layers: MBE Al on GaAs," submitted to Int. Conf. Solid St. Dev. (Tokyo, 1982).

Modified Schottky Barrier Heights by Interfacial Doped Layers: MBE Al on GaAs

Stephen J. Eglash,
Stanford Electronics Laboratories, Stanford University, Stanford, Ca 94305
and
Solid State Laboratory, Hewlett-Packard Laboratories,
1501 Page Mill Road, Palo Alto, Ca 94304
Shihong Pan*, Dang Mo+, and William E. Spicer**,
Stanford Electronics Laboratories, Stanford University, Stanford, Ca 94305
Douglas M. Collins
Solid State Laboratory, Hewlett-Packard Laboratories,
1501 Page Mill Road, Palo Alto, Ca 94304

We report here on progress in optimizing Schottky barrier heights using doped interfacial layers in Al:GaAs diodes grown in a molecular beam epitaxy (MBE) apparatus. It should be emphasized that these contacts were grown entirely in the ultra-high vacuum (UHV) environment of an MBE system, because this allowed us to minimize contamination and control the impurity content at the metal:semiconductor interface.

Schottky diodes are of significant technological importance because of their ease of fabrication and high speed. Their usefulness is limited, however, by the inflexibility of the barrier height: for many semiconductors the barrier height is relatively insensitive to the choice of metal. An early effort on Schottky barrier height modification involved Cu diffusion into n-type CdS[1]. This was followed by an attempt using ion implantation of Sb into p-type Si[2]. The use of doped interfacial layers to modify the barrier height was suggested independently for Schottky barriers on III-V semiconductors by W. E. Spicer et al. as a result of their detailed understanding of the process of Schottky barrier formation on these materials[3].

In this study we have fabricated diodes on n-GaAs epitaxial layers ($n = 5 \times 10^{16}$ cm^{-3}) with Be-doped interfacial layers ($p = 10^{18}$ to 10^{20} cm^{-3}) and epitaxial crystalline Al metal layers (Fig. 1). The GaAs and Al deposition conditions were chosen to yield the most abrupt, "ideal" interfaces. p^+ layer thicknesses, t, from 50 to 360 Å were investigated. The barrier heights, as determined by room temperature I-V measurements, extend from 0.79 eV for Al directly on n-GaAs surfaces, to heights greater than 1.1 eV utilizing a p^+ interfacial layer

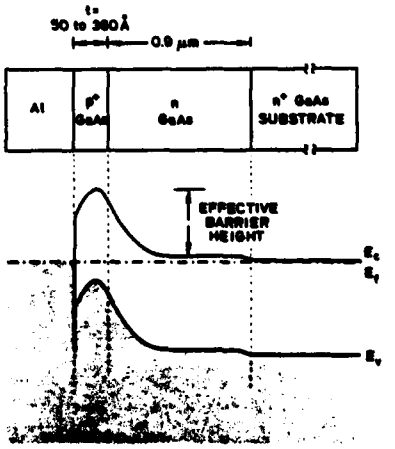

Figure 1. The metal-p^+-n structure used for Schottky barrier height modification in this work, and the corresponding band diagram. The increased barrier height, resulting from the negative space charge in the fully depleted p^+ region, is shown.

(Fig. 2). The ideality factors, n, of these diodes were 1.04 to 1.21. Some increase of n above unity is expected for these structures. The observed increase will be compared with theory.

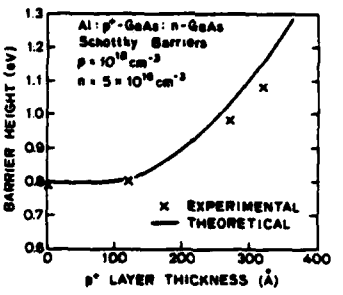

Figure 2. Effective barrier heights, calculated from room temperature I-V measurements assuming a thermionic emission model, for some diodes having the structure shown in Fig. 1. The solid line shows the predictions of our model.

Our theoretical calculation of the barrier height is an improvement upon that of previous workers, and utilizes an understanding afforded by our unified defect model for interface states on III-V semiconductors[3]. The unified model gives detailed insight into the energies and densities of the (defect-induced) interface states that pin the Fermi level. We find good agreement between theory and experiment (Fig. 2). A full calculation of the electrostatics at the interface is under way, but it is evident that the Schottky barrier height on GaAs can be engineered to any desired value over a much broader range than previously thought.

I-V, C-V, internal photoemission, and temperature-dependent measurements have been made. These results were interpreted in conjunction with model charge distributions and electric potentials, and known doping configurations to lend insight to phenomena at metal:semiconductor junctions.

The advantages resulting from engineered Schottky barriers include lower gate currents and reduced noise in GaAs MESFET's, improved performance in solar cell applications, as well as increased flexibility in circuit design with diodes of differing barrier heights. Schottky diodes can be fabricated having large barrier heights approaching those of p-n junctions. Since these are majority carrier devices they should not suffer from the minority carrier charge storage problems which limit the speed of bipolar devices. Diodes can be fabricated that range continuously from majority carrier Schottky devices to recombination dominated p-n junctions. These devices should also facilitate the study of transport mechanisms at rectifying contacts.

Supported in part by ARPA no. N00014-79-C-0072 through ONR, and ONR no. N00014-75-C-0289.

*On leave from Nankai University, Tianjin, Peoples' Republic of China

+On leave from Zhongshan University, Guangzhou, Peoples' Republic of China

**Stanford Aschermann Professor of Engineering

[1]H. K. Bucher, B. C. Burkey, G. Lubberts, and E. C. Wolf, Appl. Phys. Lett. 23, 617 (1973).

[2]J. M. Shannon, Solid St. Electron. 19, 537 (1976).

[3]W. E. Spicer, I. Lindau, P. Skeath, and C. Y. Su, J. Vac. Sci. Technol. 17, 1019 (1980); W. E. Spicer, I. Lindau, P. Skeath, C. Y. Su, and Patrick Chye, Phys. Rev. Lett. 44, 420 (1980).

M. Papers published during this period.

1. Model of Column III and V Elements on GaAs (110): Applications to MBE, P. Skeath, I. Lindau, C. Y. Su, and W. E. Spicer, J. Vac. Sci. Tech., 19, No. 3, Sept./Oct. 1981, pp. 556-560.

2. Exploiting Energy-Dependent Photoemission in Si d-Metal Interfaces: The Si (111)-Pd Case, I. Abbati, G. Rossi, I. Lindau, and W. E. Spicer, J. Vac. Sci. Tech., 19, No. 3, Sept./Oct. 1981, pp. 636-640.

3. Pd_2Si Surfaces Thermally Enriched in Silicon: Evidence of New Si:Pd Bonds, I. Abbati, G. Rossi, L. Braicovich, I. Lindau, W. E. Spicer, and B. de Michelis, J. Appl. Phys. 52 (11), Nov. (1981), 6994-6996.

4. Chemical Reaction at the Ge (111)/Ag and Si(111)/Ag Interface for Small Ag Coverages, G. Rossi, I. Abbati, L. Braicovich, I. Lindau, W. E. Spicer, Surf. Sci. 112, (1981) L765-769.

5. Experimental Determination of the Bonding of Column 3 and 5 Elements on GaAs, Perry Skeath, C. Y. Su, I. Lindau, and W. E. Spicer, J. of Crystal Growth 56, (1982) 505-510.

6. Si(111)-Pt Interface at Room Temperature: A Synchrotron Radiation Photoemission Study, G. Rossi, I. Abbati, L. Braicovich, I. Lindau, W. E. Spicer, Phys. Rev. B 25, No. 6, March 15, (1982).

7. Ge-Ag Interface at Room Temperature: An Energy-Dependent Photoemission Study, G. Rossi, I. Abbati, L. Braicovich, I. Lindau, W. E. spicer, Phys. Rev. B 25, No. 6, Mar. 15, (1982).

8. A Photoemission Study of Clean and Oxidized Nb_3Sn, J. N. Miller, I. Lindau, W. E. Spicer, 88A, No. 2, Physics Letters, Feb. 22, (1982) 97-99.

9. New Considerations of 3-5 MOS and other Device Considerations, W. E. Spicer, I. Lindau, S. Eglash, W. Petro, P. Skeath, C. Y. Su, International Electron Device Meeting (1981), 106-107.

10. Possible Oxygen Chemisorption Configurations on the Si (111) 2 x 1 Surface, C. Y. Su, P. R. Skeath, I. Lindau, and W. E. Spicer, J. Vac. Sci. and Tech. 19, No. 3, Sept./Oct. (1981), pp. 481-486.

11. Use of Photoemission witrh Synchrotron Radiation to Probe Surfaces on and Atomic Scale, W. E. Spicer, SURFACES AND INTERFACES IN CERAMIC AND CERAMIC-METAL SYSTEMS, (1981), Edited by Joseph Pask and Anthony Evans, 51-69.

12. The Surface Electronic Structure of GaAs (110): Effects of Oxygen and Metal Overlayers, I. Lindau and W. E. Spicer, "Electron Spectroscopy: Theory, Techniques, and Applications," Chapt. 4, Vol. 4; Academic Press, New York, (1981) pp. 197-277, edited by C. R. Brundle and A. D. Baker.

13. **The Nature of the 7 x 7 Reconstruction of Si (111): As Revealed by changes in Oxygen Sorption from 2 x 1 to 7 x 7, C. Y. Su, P. R. Skeath, I. Lindau, and W. E. Spicer, Surface Science 107 (1981), L355-L361.**

14. **Possible Oxygen Chemisorption Configurations on the Si(111) 2 x 1 Surface, C. Y. Su, P. R. Skeath, I. Lindau, and W. E. Spicer, J. Vac. Sci. and Tech. 19, No. 3, Sept./Oct. (1981), pp. 481-486.**